LEABHARLANN CHOLÁISTE NA TRÍONÓIDE, BAILE ÁTHA CLIATH | TRINITY COLLEGE LIBRARY DUBLIN
Ollscoil Átha Cliath | The University of Dublin

Terms and Conditions of Use of Digitised Theses from Trinity College Library Dublin

Copyright statement

All material supplied by Trinity College Library is protected by copyright (under the Copyright and Related Rights Act, 2000 as amended) and other relevant Intellectual Property Rights. By accessing and using a Digitised Thesis from Trinity College Library you acknowledge that all Intellectual Property Rights in any Works supplied are the sole and exclusive property of the copyright and/or other IPR holder. Specific copyright holders may not be explicitly identified. Use of materials from other sources within a thesis should not be construed as a claim over them.

A non-exclusive, non-transferable licence is hereby granted to those using or reproducing, in whole or in part, the material for valid purposes, providing the copyright owners are acknowledged using the normal conventions. Where specific permission to use material is required, this is identified and such permission must be sought from the copyright holder or agency cited.

Liability statement

By using a Digitised Thesis, I accept that Trinity College Dublin bears no legal responsibility for the accuracy, legality or comprehensiveness of materials contained within the thesis, and that Trinity College Dublin accepts no liability for indirect, consequential, or incidental, damages or losses arising from use of the thesis for whatever reason. Information located in a thesis may be subject to specific use constraints, details of which may not be explicitly described. It is the responsibility of potential and actual users to be aware of such constraints and to abide by them. By making use of material from a digitised thesis, you accept these copyright and disclaimer provisions. Where it is brought to the attention of Trinity College Library that there may be a breach of copyright or other restraint, it is the policy to withdraw or take down access to a thesis while the issue is being resolved.

Access Agreement

By using a Digitised Thesis from Trinity College Library you are bound by the following Terms & Conditions. Please read them carefully.

I have read and I understand the following statement: All material supplied via a Digitised Thesis from Trinity College Library is protected by copyright and other intellectual property rights, and duplication or sale of all or part of any of a thesis is not permitted, except that material may be duplicated by you for your research use or for educational purposes in electronic or print form providing the copyright owners are acknowledged using the normal conventions. You must obtain permission for any other use. Electronic or print copies may not be offered, whether for sale or otherwise to anyone. This copy has been supplied on the understanding that it is copyright material and that no quotation from the thesis may be published without proper acknowledgement.

SYNTHESIS AND ELECTROCHEMICAL CHARACTERISATION OF POLYPYRROLE AND NOVEL N-SUBSTITUTED POLYPYRROLE CONDUCTING POLYMERS

BY

AILEEN PATTERSON

Thesis Presented to the University of Dublin for the Degree of Doctor in Philosophy

Department of Chemistry,
University of Dublin,
Trinity College.

June 2004

TRINITY COLLEGE
0 8 NOV 2004
LIBRARY DUBLIN
THESIS
7453

DECLARATION

This thesis has not been submitted as an exercise for a degree at any other University. Except where otherwise stated, the work described herein was carried out by the author alone.



Aileen Patterson

DECLARATION

This thesis has not been submitted as an exercise for a degree at any other university. Except where stated, the work described therein was carried out by me alone.

I give permission for the Library to lend or copy this thesis upon request.

Signed: Aileen Patterson

To Ernie, Gloria, Heather

and Paddy

ACKNOWLEDGEMENTS

My greatest thanks go to my supervisor Dr. Mike Lyons for all his help and encouragement along the way. Thanks to Dr. Robin Bedford for his part in helping to design the synthetic strategies employed during the course of this work. To my lab partner, synthetic guru and good friend, Noelle Scully, I extend a special thank you. Thanks to all the crew from the Arches, days that shall not be forgotten easily. Thanks to John O'Brien for the NMR work.

I would also like to thank the Dublin Dental Hospital for providing me with part-time employment, without which I could not have survived. Dr. Mary Kelly deserves a special mention for her mentoring over the past four years. Thank you to the DentEd group who have kept me entertained over the past year and hopefully for a long time to come.

Thank you to my family for understanding the infrequency of my visits to Donegal, I know it must have been difficult. Finally, a big, thank you to Paddy, for keeping me semi-sane during this marathon that is now thankfully at an end.

THANKS

CONTENTS

CHAPTER ONE.	**GENERAL INTRODUCTION**	**1**
1.1	CHEMICALLY MODIFIED ELECTRODES	1
1.2	CONDUCTING POLYMERS	4
1.3	POLY(PYRROLE)	7
1.4	CHARGE TRANSFER IN CONDUCTING POLYMERS	10
1.5	N-SUBSTITUTED POLYPYRROLE FILMS	17
1.6	BIOSENSORS	19
1.7	OBJECTIVES 0F THIS WORK	27
CHAPTER TWO	**SYNTHESIS AND CHARACTERIZATION OF HYBRID MONOMERS**	36
2.1	INTRODUCTION	37
2.2	SYNTHESIS OF FERROCENE DERIVATIVES	39
2.2.1	Preparation of Ferrocenecarboxylic Acid	40
2.2.2	Preparation of 1,1'-Ferrocenedicarboxylic Acid	41
2.2.3	Preparation of Asymmetrically Substituted Ferrocenes	42
2.3	Initial Strategies Employed for the Synthesis of Hybrid Monomers	43
2.4	PREPARATION OF N-SUBSTITUTED PYRROLES	44
2.5	HYBRID FORMATION	61
2.5.1	The Coupling Reaction	61
2.5.2	Intermediate Isolation	69
2.5.3	Disubstituted Ferrocene Hybrid Monomers	70
2.5.4	Asymmetrically Substituted Ferrocenes	75
2.6	CONCLUSIONS	78
2.7	EXPERIMENTAL	79
2.7.1	General Experimental	79
2.7.2	Ferrocene Carboxylic Acids Formation	79
2.7.3	Preparation of ferrocene species **12**	82
2.7.4	Preparation of N-substituted pyrroles	83
2.7.5	Preparation of [N-(Pyrrol-1-yl)alkyl]ferrocene-carboxamide	90
2.7.6	Preparation of disubstituted hybrids	94

2.8 REFERENCES 97

CHAPTER THREE EXPERIMENTAL METHODOLOGIES AND GENERAL THEORY 98

3.1 INTRODUCTION 99
3.2 INSTRUMENTATION 99
3.2.1 BAS 100B Workstation 99
3.2.2 The Potentiostat 100
3.2.3 C2 Cell Stand 104
3.2.4 Low Current Module 105
3.3 THE ELECTROCHEMICAL CELL 106
3.3.1 The Working Electrode 107
3.3.2 The Auxiliary Electrode (Counter Electrode) 108
3.3.3 The Reference Electrode 108
3.3.4 Electrolyte Solutions 110
3.3.5 Reagents 111
3.4 ELECTRODE MODIFICATION TECHNIQUES 111
3.4.1 Electrode pre-treatment 111
3.4.2 Polymer Film Synthesis 112
3.5 EXPERIMENTAL TECHNIQUES 113
3.5.1 Potential Sweep Techniques 113
3.5.2 Cyclic Voltammetry at Microelectrodes 120
3.5.3 Potential Step Techniques 123
3.6 CONCLUSIONS 125
3.7 REFERENCES 126

CHAPTER FOUR ELECTROCHEMICAL PROPERTIES OF HYBRID MONOMER AND POLYMER SPECIES 127

4.1 INTRODUCTION 128
4.2 ELECTROCHEMICAL PROPERTIES OF FERROCENE-PYRROLE HYBRID COMPOUNDS 129
4.2.1 Electrochemical behaviour of compounds of structure **18** 129
4.2.2 Electrochemical behaviour of compounds of structure **20** and **21** 141
4.3 Electropolymerization of hybrid monomers 147

4.3.1	Electropolymerization of compounds of structure **18**	147
4.3.2	Electropolymerization of compounds of structure **20**	160
4.3.3	Electropolymerization of compounds of structure **21**	167
4.4	GLUCOSE OXIDASE IMMOBILIZATION	170
4.5	CONCLUSIONS	172
4.6	REFERENCES	174
CHAPTER FIVE	**HETEROGENEOUS REDOX CATALYSIS AT CONDUCTING POLYMER MICROELECTRODES**	
5.1	INTRODUCTION	176
5.2	MEDIATED ELECTRON TRANSFER AT CONDUCTING POLYMER MICROELECTRODES	176
5.2.1	Preliminary Comments	176
5.2.2	Assumptions	177
5.2.3	"Spill-Over"	179
5.2.4	Development of u- and v- master equations	180
5.2.5	Case by case kinetic analysis	181
5.2.6	Summary of the pertinent rate limiting cases	191
5.2.7	Experimental strategy for determination of specific kinetic case	193
5.3	VOLTAMMETRIC BEHAVIOUR OF THE FERROCYANIDE/ FERRICYANIDE REDOX COUPLE AT PPy/DBS^- MODIFIED MICROELECTRODE	194
5.3.1	Determination of the validity of the model for mediated electron transfer at polymer modified ultramicroelectrodes	194
5.4	CONCLUSIONS	201
5.5	REFERENCES	202

SUMMARY

In this study the synthesis of novel redox substituted pyrrole monomers was achieved. Subsequent investigations into the electrochemical behaviour of the hybrid monomers and polymers were carried out. The study was to examine the use of these chemically modified electrodes as potential sensors for compounds of biological significance. To this end a total of fifteen novel compounds were synthesized, this included seven new monomer species: [4-(Pyrrol-1-yl)butyl]ferrocene-carboxamide, **18** n=4, [5-(Pyrrol-1-yl)pentyl]ferrocene-carboxamide, **18** n=5, [6-(Pyrrol-1-yl)hexyl]ferrocene-carboxamide, **18** n=6 [7-(Pyrrol-1-yl)heptyl]ferrocene-carboxamide, **18** n=7, 1,1'-Bis-[5-(Pyrrol-1-yl)pentyl]ferrocene-1,1'-dicarboxamide, **20** n = 5, 1,1'-Bis-[7-(Pyrrol-1-yl)heptyl]ferrocene-1,1'-dicarboxamide, **20** n=7, and complex **21** were all prepared according to facile, high yielding reaction schemes.

Subsequent work examined the electrochemical reversibilty of the hybrid monomers and results indicated that a one-electron reversible reaction occurs in each of the new hybrid monomer species. The next stage of the study involved the attempted electropolymerization of these compounds. Consequently, a series of novel, reproducible polymers and copolymers have been successfully produced. The electrochemical behaviour of the polymers has been shown to include the reversible redox reaction of the ferrocene group in addition to the conducting matrix of the polypyrrole. Investigations into the the mechanism of electropolymerization of this group of redox conducting polymers have shown that by appropriately functionalizing the second cyclopentadienyl ring of the ferrocene moiety, monomers which are directly electropolymerizable may be created.

In addition, the heterogeneous electrocatalysis at conducting polymer ultramicroelectrodes was to be examined. The modified electrode to be studied was a conducting polypyrrole film, doped with the counter ion dodecylbenzene sulphonate. The mechanism of electrode kinetics for the oxidation of hexacyanoferrate (II) trihydrate and the reduction of hexacyanoferrate (III), was analysed. Results indicated that the kinetic process occurring was governed by an S+E mechanism. The validity of the model being investigated was therefore confirmed experimentally.

Index of Figures, Schemes and Tables

Figures

Figure 1.1:	Structure of some common conducting polymers	6
Figure 1.2:	Possible structures of polypyrrole showing (a) a polaron defect and (b) a bipolaron defect.	11
Figure 1.3:	Band structure of a polypyrrole chain containing: (a) two polarons (b) one bipolaron and (c) two bipolarons.	12
Figure 1.4:	A few representative examples of redox polymers, each contain a polymer backbone with a pendant redox active group	14
Figure 1.5:	Charge propagation by means of quasi-diffusional charge percolation in a redox polymer.	16
Figure 1.6:	Schematic diagram of a biosensor	20
Figure 1.7:	Structure of flavin adenine nucleotide. FAD	21
Figure 1.8:	Graph of the common mediators currently in use	23
Figure 3.1	Block diagram of the BAS 100B/W Workstation	100
Figure 3.2.	Schematic diagram of an operational amplifier.	101
Figure 3.3	Schematic diagram of a circuit for controlling the potential at a fixed point, A.	102
Figure 3.4	Schematic diagram of a simple potentiostat	102
Figure 3.5	Schematic diagram of a full potentiostat based on an adder control amplifier (PC)	103
Figure 3.6	Schematic diagram of BAS 100B/W C2 cell stand	104
Figure 3.7	Block diagram of the Low Current Module(LCM) set up	105
Figure 3.8	Schematic diagram of the electrochemical cell	106
Figure 3.9	Illustration of the linear potential sweep with a triangular waveform, which is applied to the working electrode.	114
Figure 3.10	Transition from reversible to irreversible behaviour of the redox couple due to change of scan rate.	115
Figure 3.11	Cyclic Voltammogram for a model reversible process, $R \Leftrightarrow O + ne^-$.	118
Figure 3.12	The concentration-distance profiles for an electroactive species, R, during various stages of cyclic sweep voltammetry.	118

Figure 3.13 Voltammetric responses at (a) a macroelectrode (b) a micro-electrode at long time and (c) a microelectrode at short time. 122

Figure 3.14 (a) The potential-time profile for a single potential step chrono-amperometric experiment, (b) The resulting current-time transient for the reaction $O + ne^- \Leftrightarrow R$ 124

Figure 4.1 Cyclic voltammogram of **18** n=3 (1mM) at varying scan rates in 0.1M TBAP/ CH_3CN at a Pt disk electrode at 25°C vs $Ag/AgNO_3$ reference electrode. 129

Figure 4.2 Cyclic voltammogram of **18** n=4 (1mM) at varying scan rates in 0.1M TBAP/ CH_3CN at a Pt disk electrode at 25°C vs $Ag/AgNO_3$ reference electrode. 130

Figure 4.3 Cyclic voltammogram of **18** n=5 (1mM) at varying scan rates in 0.1M TBAP/ CH_3CN at a Pt disk electrode at 25°C vs $Ag/AgNO_3$ reference electrode. 130

Figure 4.4 Cyclic voltammogram of **18** n=6 (1mM) at varying scan rates in 0.1M TBAP/ CH_3CN at a Pt disk electrode at 25°C vs $Ag/AgNO_3$ reference electrode. 131

Figure 4.5 Cyclic voltammogram of **18** n=7 (1mM) at varying scan rates in 0.1M TBAP/ CH_3CN at a Pt disk electrode at 25°C vs $Ag/AgNO_3$ reference electrode. 131

Figure 4.6: Cyclic voltammogram of ferrocene at varying scan rates in 0.1M TBAP/ CH_3CN at a Pt disk electrode at 25°C vs $Ag/AgNO_3$ reference electrode. 135

Figure 4.7 Graph of i_p vs $v^{1/2}$ for the oxidation and reduction of the monomers of the structure **18** n=3-7. 137

Figure 4.8: Graph of the variation of current with time of **18** n=5 (1mM) in 0.1M TBAP/ CH_3CN at a Pt disk electrode at 25°C vs $Ag/AgNO_3$ reference electrode 138

Figure 4.9: Graph of i vs $t^{-1/2}$ of **18** n=5 (1mM) in 0.1M TBAP/ CH_3CN at a Pt disk electrode at 25°C vs $Ag/AgNO_3$ reference 138

Figure 4.10 Cyclic voltammogram of **20** n=3 (1mM) at varying scan rates in 0.1M TBAP/ CH_3CN at a Pt disk electrode at 25°C vs $Ag/AgNO_3$ reference electrode 141

Figure 4.11 Cyclic voltammogram of **20** n=5 (1mM) at varying scan rates in 0.1M TBAP/ CH_3CN at a Pt disk electrode at 25°C vs $Ag/AgNO_3$ reference electrode. 142

Figure 4.12 Cyclic voltammogram of **20** n=7 (1mM) at varying scan rates in 0.1M TBAP/ CH_3CN at a Pt disk electrode at 25°C vs $Ag/AgNO_3$ reference electrode. 142

Figure 4.13 Cyclic voltammogram of **21** (1mM) at varying scan rates in 0.1M TBAP/ CH_3CN at a Pt disk electrode at 25°C vs $Ag/AgNO_3$ reference electrode. 143

Figure 4.14 Graph of i_p vs $v^{1/2}$ for the oxidation and reduction of the monomers of the structure **20** n=3, 5, 7.and structure **21**. 145

Figure 4.15: Cyclic voltammogram of repeated cycling of **18** n=4 (10mM) in 0.1M TBAP/ CH_3CN at a Pt disk electrode at 25°C vs $Ag/AgNO_3$ reference electrode. 147

Figure 4.16: Cyclic voltammogram of repeated cycling of pyrrole (10mM) in 0.1M TBAP/ CH_3CN at a Pt disk electrode at 25°C vs $Ag/AgNO_3$ reference electrode. 148

Figure 4.17: Cyclic voltammogram of repeated cycling of **18** n=3 (10mM) in 0.1M TBAP/ CH_3CN at a Pt disk electrode at 25°C vs Ag/AgCl reference electrode. 151

Figure 4.18: Cyclic voltammogram of repeated cycling of **18** n=5 (10mM) in 0.1M TBAP/ CH_3CN at a Pt disk electrode at 25°C vs $Ag/AgNO_3$ reference electrode. 151

Figure 4.19: Cyclic voltammogram of repeated cycling of **18** n=6 (10mM) in 0.1M TBAP/ CH_3CN at a Pt disk electrode at 25°C vs $Ag/AgNO_3$ reference electrode. 152

Figure 4.20: Cyclic voltammogram of repeated cycling of **18** n=7 (10mM) in 0.1M TBAP/ CH_3CN at a Pt disk electrode at 25°C vs $Ag/AgNO_3$ reference electrode. 152

Figure 4.21: Potentiodynamic growth of the copolymer poly(**18** n=3 and pyrrole) in 0.1M TBAP/ CH_3CN, at a Pt disk electrode at 25°C vs Ag/AgCl reference electrode. Scan rate $50mVs^{-1}$ 154

Figure 4.22: Cyclic voltammogram of the copolymer of poly(**18** n=3 and pyrrole) in background electrolyte, 0.1M TBAP/ CH_3CN, at a Pt disk electrode at 25°C vs Ag/AgCl reference electrode 154

Figure 4.23: Potentiodynamic growth of the copolymer poly(**18** n=4 and pyrrole) in 0.1M TBAP/ CH_3CN, at a Pt disk electrode at 25°C vs Ag/AgCl reference electrode. Scan rate $50mVs^{-1}$ 155

Figure 4.24: Cyclic voltammogram of the copolymer of poly(**18** n=4 and pyrrole) in background electrolyte, 0.1M TBAP/ CH_3CN, at a Pt disk electrode at 25°C vs Ag/AgCl reference electrode 155

Figure 4.25: Potentiodynamic growth of the copolymer poly(**18** n=5 and pyrrole) in 0.1M TBAP/ CH_3CN, at a Pt disk electrode at 25°C vs Ag/AgCl reference electrode. Scan rate $50mVs^{-1}$. 156

Figure 4.26: Cyclic voltammogram of the copolymer of poly(**18** n=5 and pyrrole) in background electrolyte, 0.1M TBAP/ CH_3CN, at a Pt disk electrode at 25°C vs Ag/AgCl reference electrode 156

Figure 4.27: Potentiodynamic growth of the copolymer poly(**18** n=6 and pyrrole) in 0.1M TBAP/ CH_3CN, at a Pt disk electrode at 25°C vs Ag/AgCl reference electrode 157

Figure 4.28: Cyclic voltammogram of the copolymer of poly(**18** n=6 and pyrrole) in background electrolyte, 0.1M TBAP/ CH_3CN, at a Pt disk electrode at 25°C vs Ag/AgCl reference electrode 157

Figure 4.29: Potentiodynamic growth of the copolymer poly(**18** n=7 and pyrrole) in 0.1M TBAP/ CH_3CN, at a Pt disk electrode at 25°C vs Ag/AgCl reference electrode. Scan rate $50mVs^{-1}$ 158

Figure 4.30: Cyclic voltammogram of the copolymer of poly(**18** n=7 and pyrrole) in background electrolyte, 0.1M TBAP/ CH_3CN, at a Pt disk electrode at 25°C vs Ag/AgCl reference electrode 158

Figure 4.31 Electropolymerization upon repeated cycling of **20** n=3 (10mM) in 0.1M TBAP/ CH_3CN at a Pt disk electrode at 25°C vs $Ag/AgNO_3$ reference electrode; 20 successive scans between 0 and 0.9V. 162

Figure 4.32: Cyclic voltammogram of poly(**20** n=3) at varying scan rates in 0.1M TBAP/ CH_3CN at a Pt disk electrode at 25°C vs $Ag/AgNO_3$ reference electrode. 162

Figure 4.33 Electropolymerization upon repeated cycling of **20** n=5 (10mM) in 0.1M TBAP/ CH_3CN at a Pt disk electrode at 25°C vs $Ag/AgNO_3$ reference electrode; 20 successive scans between 0 and 0.9V. 164

Figure 4.34: Cyclic voltammogram of poly(**20** n=5) at varying scan rates in 0.1M TBAP/ CH_3CN at a Pt disk electrode at 25°C vs $Ag/AgNO_3$ reference electrode. 164

Figure 4.35: Electropolymerization upon repeated cycling of **20** n=7 (10mM) in 0.1M TBAP/ CH_3CN at a Pt disk electrode at 25°C vs $Ag/AgNO_3$ reference electrode; 20 successive scans between 0 and 0.9V. 165

Figure 4.36: Cyclic voltammogram of poly(**20** n=7) at varying scan rates in 0.1M TBAP/ CH_3CN at a Pt disk electrode at 25°C vs $Ag/AgNO_3$ reference electrode. 165

Figure 4.37 Graph of i_p vs v for the oxidation and reduction potentials of the monomers of the structure **20** n=3, 5, 7. 166

Figure 4.38: Electropolymerization upon repeated cycling of **21** (10mM) in 0.1M TBAP/ CH_3CN at a Pt disk electrode at 25°C vs $Ag/AgNO_3$ reference electrode; 20 successive scans between 0 and 0.9V. 167

Figure 4.39: Cyclic voltammogram of poly(**21**) at varying scan rates in 0.1M TBAP/ CH_3CN at a Pt disk electrode at 25°C vs $Ag/AgNO_3$ reference electrode. 169

Figure 4.40: Graph of i_p vs v for the oxidation and reduction potentials of the monomers of the structure poly(**21**). 169

Figure 4.41: Cyclic voltammogram of a thin film of PPy- co-([5-(Pyrrol-1-yl) -pentyl] ferrocene-carboxamide, **18 n=5** and 200U glucose oxidase] in 0.1M TBAP/ CH_3CN at a Pt disk electrode at 25°C vs $Ag/AgNO_3$ reference electrode. 171

Figure 5.1: Kinetic case diagram 192

Figure 5.2 Graph of j_{cat}^{-1} vs a of PPy/DBS^- layer of 0.03μm thickness in aqueous solutions of various concentrations of $K_4Fe(CN)_6.3H_2O$ and $K_3Fe(CN)_6$. 195

Figure 5.3: Graph of j_{cat}^{-1} vs a of PPy/DBS^- layer of 0.03μm thickness in aqueous solutions of various concentrations of $K_4Fe(CN)_6.3H_2O$ 195

Figure 5.4 Graph of S^{-1} of j_{cat}^{-1} vs a plotted versus concentration of $K_4Fe(CN)_6.3H_2O$. 197

Figure 5.5 Graph of I^{-1} of j_{cat}^{-1} vs a plotted versus concentration of $K_4Fe(CN)_6.3H_2O$. 197

Figure 5.6: Graph of j_{cat}^{-1} vs a of 6mM $K_4Fe(CN)_6.3H_2O$ at bare platinum microelectrodes and at PPy/DBS^- layer of 0.03 thickness. 198

Figure 5.7: Graph of j_{cat}^{-1} vs a of PPy/DBS^- layer of 0.03μm thickness in aqueous solutions of various concentrations of $K_3Fe(CN)_6$. 199

Figure 5.8: Graph of the inverse slope of (j_{cat}^{-1} vs a) Vs concentration of $K_3Fe(CN)_6$. 200

Figure 5.9: Graph of inverse intercept of (j_{cat}^{-1} vs a) Vs concentration of $K_3Fe(CN)_6$. 200

Figure 5.10: Graph of j_{cat}^{-1} vs a of 6mM $K_3Fe(CN)_6$ at bare platinum microelectrodes and at PPy/DBS^- layer of 0.03μm thickness. 201

Schemes

Scheme 1.1: Generally accepted mechanisms of electrochemical polymerisation of polypyrrole. 8

Scheme 1.2: Mechanism of interaction with artificial electron acceptors such as ferrocene and ferrocene derivatives 23

Scheme 2.1: Preparation of Ferrocenecarboxylic Acid 40

Scheme 2.2: Preparation of 1,1'-Ferrocenedicarboxylic Acid 41

Scheme 2.3 Preparation of Asymmetrically Substituted Ferrocenes 42

Scheme 2.4 Preparation of bis Ferrocene species 43

Scheme 2.5 Preparation of N-Substituted Pyrroles 44

Scheme 2.6 The Coupling Reaction 61

Scheme 2.7 Intermediate Isolation 69

Scheme 2.8 Preparation of Disubstituted Ferrocene Hybrid Monomers 70

Scheme 4.1: Structure oh hybrid ferrocene-pyrrole species 128

Scheme 4.2: A proposed mechanism for the passivation process of the hybrid monomers 149

Scheme 4.3: A proposed mechanism for the electropolymerisation of the disubstituted pyrrole amide linked ferrocene hybrid species 161

Scheme 4.4: A proposed mechanism for the electropolymerisation of the disubstituted pyrrole amide linked ferrocene hybrid species 168

Tables

Table 2.1: Yields of the pyrrole derivatives 45

Table 2.2: NMR Spectroscopic details for N- (3-Chloropropyl)pyrrole 46

Table 2.3: NMR Spectroscopic details for N- (3-Cyanopropyl)pyrrole 47

Table 2.4: NMR Spectroscopic details for N- (3-Aminopropyl)pyrrole 48

Table 2.5: NMR Spectroscopic details for N- (4-Chlorobutyl)pyrrole 49

Table 2.6: NMR Spectroscopic details for N- (4-Cyanobuyl)pyrrole 50

Table 2.7: NMR Spectroscopic details for N- (4-Aminobutyl)pyrrole 51

Table 2.8: NMR Spectroscopic details for N- (5-Chloropentyl)pyrrole 52

Table 2.9: NMR Spectroscopic details for N- (5-Cyanopentyl)pyrrole 53

Table 2.10: NMR Spectroscopic details for N- (5-Aminopentyl)pyrrole 54

Table 2.11: NMR Spectroscopic details for N- (6-Chlorohexyl)pyrrole 56

Table 2.12: NMR Spectroscopic details for N- (6-Cyanohexyl)pyrrole 57

Table 2.13: NMR Spectroscopic details for N- (6-Aminohexyl)pyrrole 58

Table 2.14: NMR Spectroscopic details for N- (7-Aminoheptyl)pyrrole 60

Table 2.15: Yields of monomer preparations 63

Table 2.16: NMR Spectroscopic details for [3-(Pyrrol-1-yl)propyl]ferrocene-carboxamide 63

Table 2.17: NMR Spectroscopic details for [4-(Pyrrol-1-yl)butyl]ferrocene-carboxamide 65

Table 2.18: NMR Spectroscopic details for [5-(Pyrrol-1-yl)pentyl]ferrocene-carboxamide 66

Table 2.19: NMR Spectroscopic details for [6-(Pyrrol-1-yl)hexyl]ferrocene-carboxamide 67

Table 2.20: NMR Spectroscopic details for [7-(Pyrrol-1-yl)heptyl]ferrocene-carboxamide 68

Table 2.21: Yields of disubstituted monomer species 70

Table 2.22: NMR Spectroscopic details for 1,1'-Bis-[3-(Pyrrol-1-yl)propyl]-ferrocene-1,1'-dicarboxamide 71

Table 2.23: NMR Spectroscopic details for 1,1'-Bis-[5-(Pyrrol-1-yl)pentyl]-ferrocene-1,1'-dicarboxamide 72

Table 2.24: NMR Spectroscopic details for 1,1'-Bis-[7-(Pyrrol-1-yl)heptyl]-ferrocene-1,1'-dicarboxamide 74

Table 2.25: NMR Spectroscopic details for [3-(Pyrrol-1-yl)propyl]-ferrocene-carboxamide 76

Table 4.1: Estimated Standard Potentials and Diffusion Coefficients for a range of Ferrocene derivatives in 0.1M TBAP/MeCN vs $Ag/AgNO_3$ reference electrode 133

Table 4.2: Cyclic voltammetry and chronoamperometry data corresponding to the redox behaviour of **18** n= 3- 7 in 0.1M TBAP/CH_3CN 139

Table 4.3: Cyclic voltammetry and chronoamperometry data corresponding to the redox behaviour of **20** n= 3, 5, 7 and **21** in 0.1M TBAP/CH_3CN 146

Table 4.4: Surface coverage values for polypyrrole unit and the ferrocene hybrid unit 159

Table 4.5: Surface coverage values for disubstituted ferrocene hybrids 163

Table 5.1: Table of the slopes of the j_{cat}^{-1} vs a for the ferrocyanide/ ferricyanide couple response at varying layer thickness of polymer film 199

CHAPTER ONE
GENERAL INTRODUCTION

1.1 CHEMICALLY MODIFIED ELECTRODES

A chemically modified electrode[1-3] may be defined as an electrode whose surface has been deliberately altered in an attempt to modify, some particular electrode property. More specifically, a particular chemical microstructure, which is capable of performing a specific task, is immobilised on the electrode surface, in an attempt to produce a tailor-made surface. This concept has led to the design, fabrication and application of many modified electrodes over the last thirty years.

Since the conception of chemically modified electrodes many techniques have been developed for the immobilisation of species on the electrode surface.[4-6] For instance, the alteration of an electrode surface may be achieved by adsorption, physical coverage, or by bonding with specific substances, all resulting in obstructing direct access to the electrode surface. The immobilisation technique generally depends on the desired application of the electrode.

Chemisorption was originally the principal method of electrochemical modification. Lane and Hubbard[7] reported one of the earliest examples of the deliberate modification of an electrode surface in 1973. Their work established that the voltammetric behaviour of platinum electrodes could be altered through the incorporation of various unsaturated monomers, such as functionalised olefins, onto the electrode surface *via* chemisorption. Adsorption of different functionalised olefin species resulted in the preparation of a variety of specifically modified electrodes.

The development of a "chiral electrode" by Miller *et al*[8] is considered one of the first examples of a functional modified electrode. This work utilised a carbon electrode, which was directly derivatised by an asymmetric reagent. Acidic surface oxides were bound to optically active amino acids, such as (S)-(-)-phenylalanine methyl ester, via amide bonds. The function of the electrode was to produce one optical isomer over another from a solution of optically inactive reagents. This was accomplished through the reduction of 4-acetylpyridine by the asymmetric component of the electrode. Subsequent work by Murray and Moses[9] illustrated that a more permanent modification of an electrode could be accomplished via the direct covalent linkage between the host electrode and the molecule elected to modify its surface characteristics. This method was

called "covalent anchoring". Initial work involved the use of silane reagents such as chloro- or alkoxysilanes which react with the hydroxyl groups on metal oxide surfaces forming up to two bonds with the surface, this produced the required effect of anchoring the desired species onto the host electrode through covalent bonding. This technique of electrode modification results in either monolayer or multi-layer coatings on the electrode surface, depending on the solvent in which the derivitisation occurs and the nature of the functionality of the silane moiety. Accordingly, most metals oxidise in acidic media and were therefore derivatised with silanes.[10] However, another example of a reagent that may be employed as an anchoring reagent is cyanuric chloride. This compound has been implemented to immobilise quinones and glucose oxidases on host electrode surfaces.[11]

More recently, self-assembled monolayers (SAMs) have been the focus of attention.[12,13] SAMs are ordered molecular assemblies that are one molecule thick and have been adsorbed onto a metal substrate. Typically alkanethiols are utilized in conjunction with a gold electrode/substrate. The thiol groups chemisorb onto the gold surface via the formation of a thiolate bond.[14] Moreover, attractive Van der Waals forces exist between the alkyl chain moieties thereby enhancing the stability and order on the SAM.[15] These highly ordered structures have been investigated extensively as potential matrices for the immobilization of biological components, in particular enzymes. Enzymes have been immobilized via techniques such as cross-linking via glutaraldehyde,[16-18] electrostatic binding,[19,20] and covalent attachment [21-24] to the SAM.

Furthermore, recent research into chemically modified electrodes has been directed towards polymer-modified electrodes[1,25]. This may be credited to various factors such as the simplicity of synthesis and the ease with which multi-layer films are formed. Polymeric coating can be accomplished either through the application of a pre-formed polymeric layer, or through the *in situ* polymerisation of a redox active monomer species and its subsequent deposition onto the electrode surface. The former is attractive in that the polymer may be structurally characterized before immobilization.

In essence, the technique involves the dissolution of the polymer in an organic solvent and the subsequent application of this polymeric solution onto the electrode surface *via* dip or spin coating techniques. The latter technique is usually preferred as it

produces films of more uniform thickness although surface coverage is considered to be less reproducible and it can be difficult to adequately characterize the polymer structure using standard spectroscopic methods.

Spin and drop coating techniques have been employed in producing a range of polymer-modified electrodes, principally ion exchange and redox polymer based systems. Ion exchange polymers[26,27] consist of electrostatically bound redox active groups (such as multivalent metal complex ions) dispersed in an ionomer matrix. Charge percolation in these materials may be ascribed to either physical diffusion (on a local scale) of the electrostatically trapped groups or local electron hopping between neighbouring sites. These materials have been investigated to achieve such ends as device manufacture. This may be attributed to the fact that that almost uniform thick films may be produced in which the extent of loading may be varied, reproducibly. The fabrication mechanism involves two processes: the electrode material with polymeric ion-exchange material is placed in a solution containing the redox active ion, where ion exchange and partition from the solution occurs, this is followed by the counterion binding via coulombic interactions. Poly(4-vinylpyridine)[28] is an example of such a material. When this polymer is placed in a solution of low pH, protonation of the pyridine groups occurs. Consequently, strong electrostatic binding between the now cationic polymer and an anionic analyte occurs, resulting in the incorporation of the latter into the film. This effect has been shown to be common to numerous anionic moieties[29-32]. An example of a cationic exchange polymer has been DuPont's sulfonated fluoropolymer, Nafion[33-35]. Nafion has exhibited a large affinity for hydrophobic cations with typical selectivity coefficients of 10^6 relative to sodium ions. Numerous redox cations have been immobilized in such a manner, these include $Ru(NH_3)_6^{3+}$ and methyl viologen.

Redox polymers may also be deposited *via* the spin or drop coating technique. These polymers contain redox active groups covalently bound to an electrochemically inactive backbone and are localised state conductors. Redox conduction occurs within these polymers through a process of electron transfer between neighbouring redox groups attached to the polymer backbone, (electron hopping). A number of redox

polymers including poly-p-nitrostyrene[36,37] and p-chlorosulfonated polystyrene[38] have been investigated.

As previously mentioned, modification of the electrode may be achieved through the *in situ* polymerization and deposition of the redox active monomer. These three-dimensional electronically conducting materials are easy to fabricate, stable and can be produced to very specific stipulations of formation rate and layer thickness. In addition, these films can be doped to metallic levels of conductivity with the structure thus behaving as an extension of the electrode surface, for example polyacetylene could be made highly conducting ($\sim 10^3 Scm^{-1}$) when exposed to an oxidising agent such as iodine. One of the most investigated electronically conducting polymers has been polypyrrole[39], which will be discussed in more detail in section 1.3.

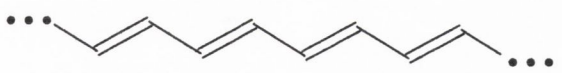
1.2 CONDUCTING POLYMERS

From an electrochemical perspective the most important aspect of conjugated polymers is their ability to act as electronic conductors. The synthesis, characterisation and application of electronically conducting polymers are still major areas of research activity in electrochemistry. The driving force behind this research may be viewed to be the many promising applications in the field of energy storage,[40] electrocatalysis,[41, 42] sensors,[43] bioelectrochemistry,[44] tissue engineering,[45] and corrosion protection.[46]

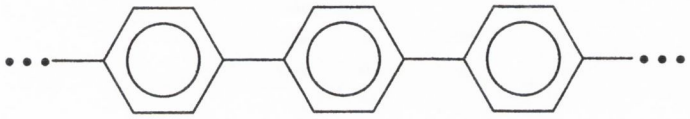
Conducting polymers have been extensively investigated since the successful doping of poylacetylene (PA) with iodine by Heeger and MacDiarmaid[47-50]. This may be attributed to their surprisingly high conductivity in a partially oxidized state. The process endowed the polymer with metallic properties and further encouraged the same scientists to investigate polyacetylene as a rechargeable active battery electrode[51], where they discovered that the polymer would undergo an increase in conductivity of twelve orders of magnitude by oxidative doping. Their promising results led to a wide range of materials being investigated to achieve this end. In the course of this work conducting polymers derived from heterocyclic monomers were discovered. Polypyrrole[39] is one such polymer, however many others exist such as polythiophene[39,52,53] and polyaniline[39,54-59].

The earliest report of the electrochemical synthesis of conducting polymers occurred in 1862 when Letheby[60] discovered that aniline in a solution of dilute sulfuric acid could be anodically oxidised. Subsequent studies led Goppelsroeder[61] to conjecture that "oligomers" were formed through the anodic oxidation of aniline. Work continued with the first electrochemical preparation of polypyrrole being reported by Dall'Olio *et al* in1968[62] However, progress was limited until the late 1970's, when preparations of good quality, continuous films were prepared by Kanazawa and Diaz *et al* [63], using a modification of the pioneering electrochemical technique. Modern work on polypyrrole may be seen to date back to this work of Diaz *et al* [63] who reported the preparation of polypyrrole films in acetonitrile, which exhibited impressive conductivity. Heretofore, investigations into electronically conducting polymers have been the object of a copious amount of studies. In 1982 Tourillon and Garnier[64] demonstrated that anodic oxidation of hetero- and homocyclic monomers produced polythiophene (PTh), polyfuran PFu), polyindole (PIn) and polyazulene (PAz). Projects carried out by other groups[65,66] led to the production of polyparaphenylene (PPP), from the electropolymerization of benzene. Subsequently, numerous substituted heterocyclic compounds have been polymerized and consequently a considerable body of literature now exists.[39]

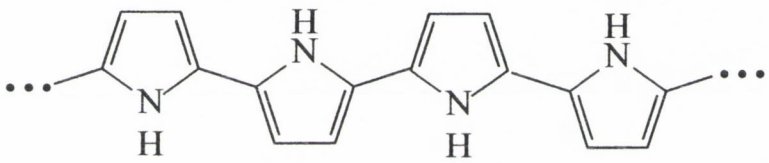
The essential structural characteristic of all conducting organic polymers is the conjugation of the chain-linked electroactive monomeric units as illustrated in figure 1.1. The monomers interact via a π-electron system creating a backbone, which is electronically conducting. It is in this respect that they differ greatly from redox polymers. The simplest possible form of conjugated polymer is polyacetylene (PA). While polyacetylene is too unstable to be of any practical value, its structure constitutes the core of all electronically conducting polymers. Due to its structural and electronic simplicity polyacetylene is well suited to *ab initio* and semi-empirical calculations and has therefore played a crucial role in the discovery of the mechanism of conduction in conjugated polymers. The nature of the conjugated π-electron backbone and how it leads to charge propagation within a conducting polymer film shall be discussed in more detail in section 1.4.



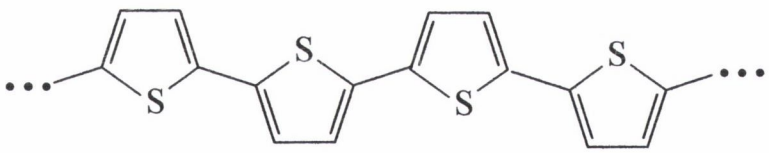
PA



PPP



PPy



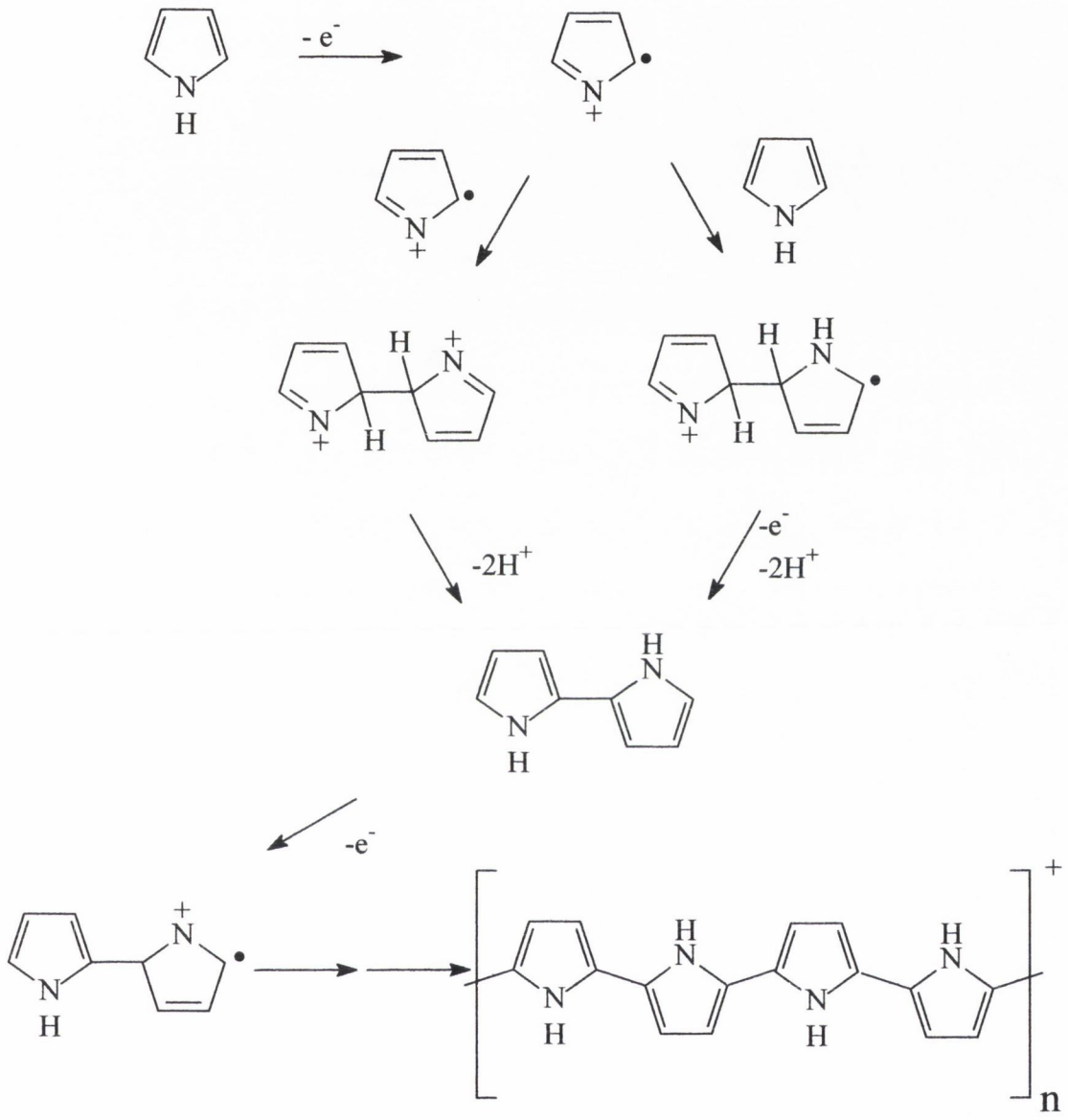
PTh

Figure 1.1: Structure of some common conducting polymers,
PA = polyacetylene, PPP = Polyphenylene, PPy = Polypyrrole and PTh = Polythiophene

1.3 POLY(PYRROLE)

Although a lot of electrically conducting polymers have been synthesized, the polypyrrole film was one of the most extensively studied polymers during the last decade. This may be attributed to its mechanical and chemical stability, its high conductivity and the ease with which it may be electrochemically synthesized. Many investigations[67-70] have been undertaken in order to elucidate the mechanism and kinetics of the electropolymerization process. The generally accepted mechanism of electropolymerization of polypyrrole is the one described by Diaz *et al*[67]. The process is understood to proceed *via* the formation of a radical cation species, which is produced through the oxidation of a pyrrole monomer. The reactivity of the radical cation determines whether the polymerization process will be viable. If the species is relatively stable then it may diffuse into the solution and react with solvent molecules to form soluble products of low molecular weights. Similarly, if the moiety is too unstable then it may react with solvent molecules or anions in the solution to produce low molecular weight, soluble products. However, if the reactivity is between these two circumstances then the radical cation can undergo dimerization reactions. According to Diaz *et al*[67], the radical cation then reacts with a second radical cation producing a dimeric species. The loss of two protons from the dimeric species yields a dimer, which on further oxidation and coupling reactions, under suitable conditions, may propagate to give the required polymer. Eventually, the degree of polymerization exceeds the solubility limit and the polymer precipitates on the electrode surface. However, Pletcher *et al*[69] have proposed that the radical cation instead couples with a neutral monomer to yield a cation dimer. The cation dimer then loses a second electron and two protons to produce a neutral dimer that may undergo further propagation reactions to finally generate poly(pyrrole). Figure 1.2 illustrates both these mechanisms.

Investigations[71,72] have concluded that the electrodeposition of conducting polymers is comparable to that of metal deposition due to its nucleation and growth pathway. In these instances growth may be one, two or three dimensional under instantaneous and progressive nucleation.[52, 53, 58,73-75]



Scheme 1.1: Generally accepted mechanisms of electrochemical polymerisation of polypyrrole.[67, 69]

While the surface structure of the immobilized polymer has not yet been satisfactorily elucidated, it has been observed that pyrroles substituted at either the nitrogen or the 3,4-positions can be polymerized, the generally accepted structure is that the majority of the pyrrole moieties are linked via the α,α'-positions[77] as shown in figure 1.1. It must also be noted that minor cross-linking via α-β' coupling is also possible.

Studies[78-86]have concluded that a number of variables exist which govern the electrochemical and physical properties of the electrodeposited polymer films. Firstly, substrate electrodes such as platinum, glassy carbon, silver, gold, stainless steel, copper, titanium, and iron have all been successfully used for the electrodeposition of polypyrrole.[78] Secondly, electropolymerization in non-aqueous solvents has resulted in the production of a tight film morphology, whereas the same process in aqueous media resulted in the formation of a more porous, open matrix[79]. Thirdly, electropolymerization in aqueous media yields a conducting poly(pyrrole) film when the medium is acidic ,whereas electropolymerization in organic media is dependant on the amount of water present[80]. Finally, the nature of the electrolyte species affects many fundamental properties of the electrodeposited film. These effects are manifested in the chemical and mechanical stability, morphology, redox kinetics and electron transport properties of the poly(pyrrole) film [81-85]. Some examples of inorganic ions utilized as counterion species are perchlorate and tetrafluoroborate[79,81,85] and organic species being toluenesulfonate and dodecylsulfonate.[81,87,88] The counterions may be immobilized within the polypyrrole matrix without affecting the structural integrity of the same due to the strong C-C bond of the polymer backbone and the presence of extensive cross-linking. This feature in addition with its ease of preparation, high conductivity, stability and redox switching properties of the polypyrrole film have all rendered the use of this polymer so attractive.

In summary, the composition of the substrate electrode, the polarity and pH of the solvent system, the nature of the counterion, the concentration of the monomer species in solution and the polymerization method and rate all have profound effects on the physical and spectroscopic characteristics of the consequent polymer film.

1.4 CHARGE TRANSFER IN CONDUCTING POLYMERS

Conducting polymers are of particular importance in the creation of chemically modified electrodes due to their ability to convert between oxidised and reduced states without loss of electroactivity. Accompanying this redox conversion is an alteration of the electrode properties. This reversible transformation from insulating to conducting states is commonly known as redox switching. The redox switching process in a conducting polymer occurs via a potential induced change in the films oxidation state due to the injection or removal of electrons from the electrode/polymer interface. This is accompanied by the ingress or egress of charge compensating counterions. The rates at which these processes occur are controlled by either the rate of electron transport across the various interfaces or the rate of counterion transport within the polymer layer itself.

Charge transfer in solid materials can occur through various mechanisms, such as electron transport in the conduction band (e.g. metals), or electron and hole transport in the conduction and valence band (e.g. semiconductors). The conductivity of metals and semiconductors is well understood. The conductivity mechanisms of electroactive polymer materials are less well understood. However, the precise conductivity mechanism depends on the nature of the electroactive polymer material. For example, in redox polymer materials the electrons hop by transfer or self-exchange between discrete sites known as redox centres which are attached to a non-conductive polymer backbone. In this case maximum conductivity is attained when the mole fraction of oxidized sites is 0.5, otherwise known as the mixed valence condition. This principle does not pertain for electronically conducting polymer films.

An understanding of the conduction processes in electronically conducting materials requires a concept that has been adopted from physics, which involves the idea of the generation and transport of electronic defects such as polarons, bipolarons and solitons. Genies and Pernaut[89] identified that oxidation proceeds through a three-state process involving polaron and bipolaron generation as the level of oxidation increases. These partially delocalized charge carriers are illustrated in Figure 1.2.

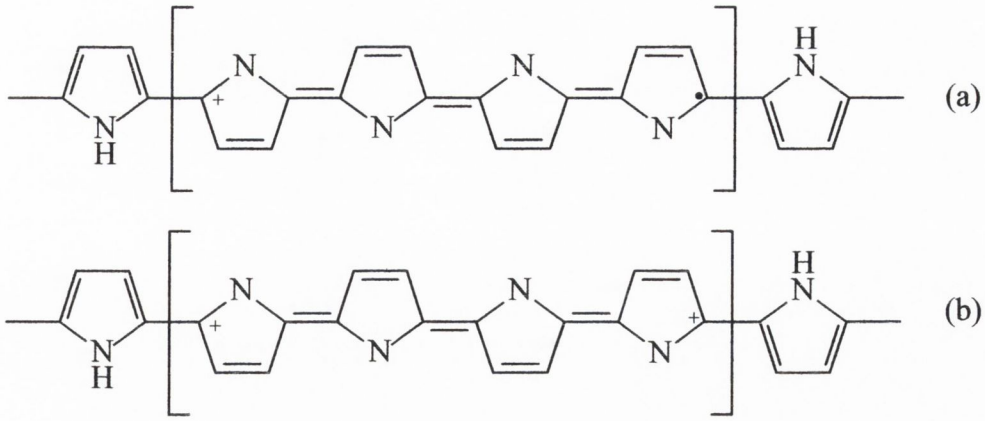


Figure 1.2: Possible structures of polypyrrole showing (a) a polaron defect and (b) a bipolaron defect.

Despite extensive research in attempting to identify the carrier species responsible for electronic conduction in a typical conducting polymer such as polypyrrole, the detailed mechanism of conduction is still debatable. However, it is known that in the absence of dopant ions, two types of π electron energy bands are present, the π-bonding molecular orbitals from the valence band, and the π^*-antibonding molecular orbitals from the conduction band. The energy gap between these two bands is the same as expected for semiconductors. Street *et al* [90,91] have measured a band gap of 3.2 eV for polypyrrole. This figure is relatively high and may explain why undoped polypyrrole acts as an electrical insulator despite its abundance of electron rich double bonds. When an electron is removed from the top of the valence band of a conjugated neutral polymer, such as polypyrrole, *via* a chemical or potential induced oxidation of the polymer chain, a hole or radical cation (polaron) is created which is subject to delocalization over several monomeric units. The energy levels associated with polaron formation are ~0.5eV from the band edges, see figure 1.3(a). If another electron is removed from the already oxidised polymer one of two things can happen: either another independent polaron can form in a different segment of the polymer or, the electron can be removed from the same segment as before to create a bipolaron.

Bredas[92] compared the creation energy of a bipolaron (0.75eV) relative to that of two polarons (0.5eV each) and concluded that one bipolaron is thermodynamically more stable than two polarons. This can be attributed to the fact that the distortion energy to form one bipolaron is roughly equal to that to form two polarons however the decrease in ionisation energy is much more important in the bipolaron case than for two polarons, figure 1.3(b). The final scenario illustrated in figure 1.3(c) presents the case when heavy doping (~33%) is applied, this leads to the overlap of the bipolaron states, which in turn leads to the creation of two bipolaron bands each of which are 0.4eV wide. The fact that bipolaron bands originate from states at the edges of the valence and conduction bands also explains why an increase in E_g is observed from 3.2 to 3.6eV in going from light doping to heavy doping levels.

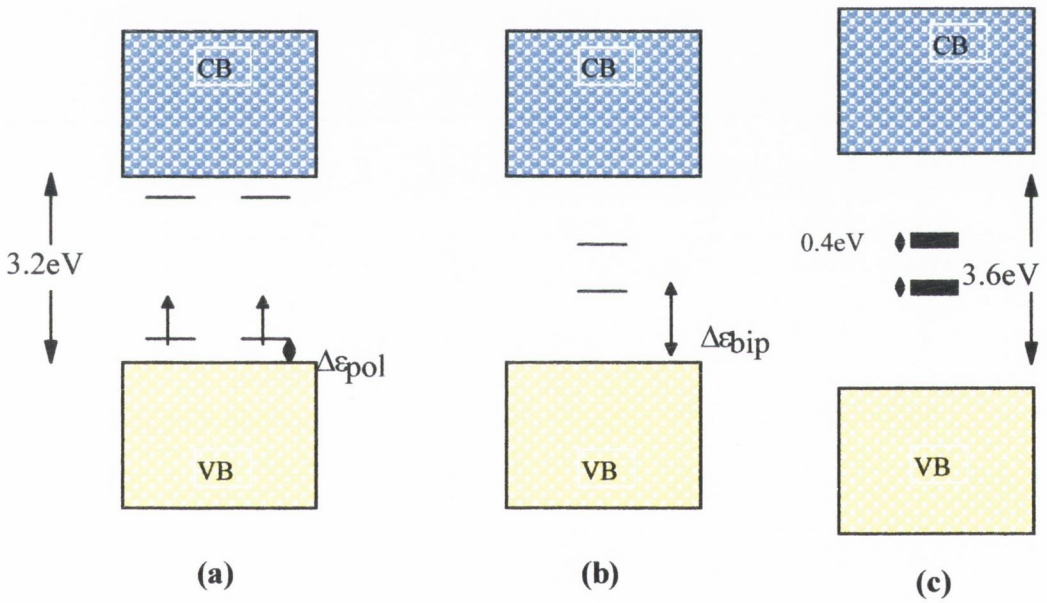


Figure 1.3: Band structure of a polypyrrole chain containing: (a) two polarons (b) one bipolaron and (c) two bipolarons. $\Delta\varepsilon_{pol}$ and $\Delta\varepsilon_{bip}$ denote the decreases in ionisation energy upon formation of the polaron and bipolaron, respectively.

This theory has been established through techniques such as electron spin resonance[93], ESR, and uv-vis spectroscopy[94] that both polaron and bipolaron motion contribute to observed conductivity in polypyrrole. The optical spectrum of polypyrrole at low doping concentrations show three absorption bands below the band gap at 0.7, 1.4 and 2.1eV attributed to the presence of polaron levels. At moderate doping concentrations the 1.4eV absorption band disappears. This band is associated with the transitions between polaron levels and its disappearance points strongly to the disappearance of polarons at higher levels of doping. At very high levels of doping two wide bands emerge giving rise to transitions at 1.0 and 2.7eV, which corresponds to the existence of bipolaron bands. In addition the band gap transition has shifted from 3.2eV to 3.6eV in going from the lightly doped to the heavily doped polymer, this is in excellent agreement with theoretical predictions.[94]

Electron spin resonance, ESR, results also support the degree of polaron and bipolaron formation.[93] In the case of lightly doped polymer the ESR signal increases in accordance with the fact that the polarons have a spin of ½. Upon approaching intermediate doping levels the ESR signal reaches a maximum and then declines. This is consistent with polarons combining to form spinless bipolarons Finally at high levels of doping there is no ESR signal observed, indicating that the charge carriers are spinless bipolarons.

Overall a polymer is generated with an overall positive charge, it is estimated that one positive charge is carried per four pyrrole rings.[95] Studies using cyclic voltammetry techniques have shown that the polymer may be cycled between the conducting (oxidised, doped) and the neutral (reduced, undoped) states. This is achieved through the diffusion of the counter-anions from the electrolyte into and out of the polymer film during the oxidative and reductive processes, preserving electroneutrality as required.

Charge transport at a macroscopic level in conducting polymers may be represented as a mixture of local charge transport mechanisms. These charge percolation processes include intrachain, interchain and interfibre conduction. Various electron hopping and tunnelling models have been proposed to help elucidate these interfibre and interchain conduction processes.[96,97] Consequently, macroscopic conductivity may be

best described in terms of a model of random hopping of charge between localised states of adjacent chain segments on different polymeric strands.

In addition to electronically conducting polymers there also exists a class of conducting polymer, specifically the redox polymers.[98] These polymers as characterized by the presence of specific spatially and electrostatically isolated electrochemically active sites. Electroactivity in the redox polymers is highly localized in contrast to the conducting backbone of the conjugated polymers. Typically, a redox polymer consists of a system where a redox-active transition metal based pendant group is covalently bound to some sort of polymer backbone, which may or may not be electronically conducting. Figure 1.4 illustrates the structure of some well-known redox polymers.

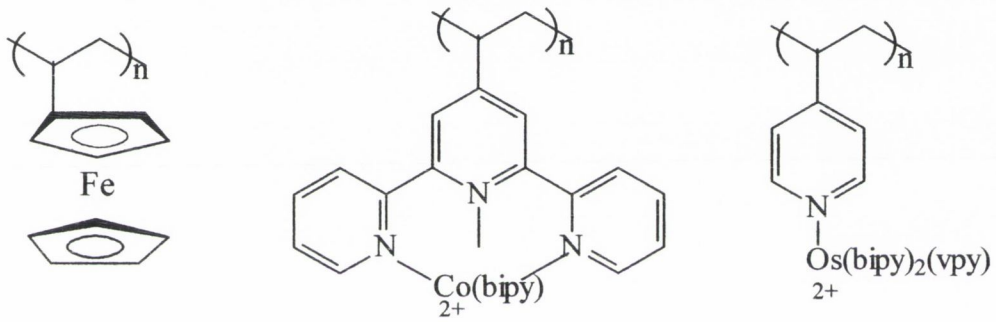


Figure 1.4: A few representative examples of redox polymers, each contains a polymer backbone with a pendant redox active group, where (bipy)= 2,2'-bipyridyl and (vpy) = vinylpyridyl.

These polymers have spurred widespread interest due their applicability in the creation of chemically modified electrodes.[99,100] The process of coating an electrode with such a material produces a chemically modified electrode with very active catalytic properties. The electrocatalyst serves as a mediator, facilitating the transfer of electrons between the electrode and the surface, see Figure 1.5. Electrocatalysis is of great economic importance and the aim of these electrodes is to drive electrochemical reactions selectively and/or at modest potentials, and with better control than would be

possible by the direct interaction between the substrate and the electrode. One such example is the electrocatalytic reduction of O_2, which is of particular interest for fuel cell applications.[100]

In contrast to electronically conducting polymers, redox polymers characteristically exhibit conductivity over a very narrow potential range, with maximum conductivity occurring when the concentrations of oxidised and reduced forms are equal within the film, this is known as the formal potential of the redox centres. This leads to a voltammetric profile where the oxidation and reduction potentials are approximately equal, E_{pa} and E_{pc} respectively, i.e. $\Delta E_p \cong 0$ and where the current produced is proportional to the square root of the scan rate, $i_p \alpha \nu^{1/2}$. The details of charge transport between the electrode and the supported redox sites are a fundamental consideration. It is generally considered that redox conduction in polymers occurs by a process of electron hopping as proposed by Kaufman *et al.*[101,102] This theory suggests that electron transfer proceeds as a process of sequential self-exchange steps between adjacent groups. The rate of self-exchange R_{SE} and electron transfer (ET) processes are connected by the simple relationship:

$$R_{SE} = k_{ET}C_{OX}C_{RED}$$

Where k represents the constant, and C_{OX} and C_{RED} corresponds to the concentration of the oxidised and reduced species respectively.

Within the polymer film where the total amount of redox species must be fixed (i.e. $C_{OX} + C_{RED} = C_{TOT}$) the self-exchange rate will reach a maximum when the concentrations of both the oxidised and reduced species are equal, (i.e. $C_{OX} = C_{RED}$), hence maximum conductivity occurs at E^0. The sequential self-exchanges which gives rise to conductivity through the thickness of the film are depicted in Figure.1.5 In this instance two processes are involved. Firstly, the charge injection at the polymer-electrode interface, which involves redox sites close to the surface occurs (*ca.* 1nm). This is a potential driven process and conforms to Butler-Volmer kinetics. Secondly, the process of charge percolation through the film, which is driven by concentration gradients and is quantifiable as a quasi-diffusional process, takes place. Since electroneutrality in the film must be conserved, the generation of charge at the electrode

and the motion of the charge throughout the polymer must be accompanied by the ingress and motion of counterions. This is an important consideration since redox polymers are in reality mixed conductors, displaying both electronic and ionic conductivity. Often the ionic contribution may be safely discounted, in which case the charge transport diffusion D_{CT} may be attributed entirely to electron diffusion D_e. However, this is not always the case, and electron-hopping rates can be strongly affected by the nature of the counterion. Therefore, full characterization should consider both electronic and ionic conductivities of the material.

Figure 1.5 depicts the electron hopping processes at work in a typical redox active polymer film.[97]

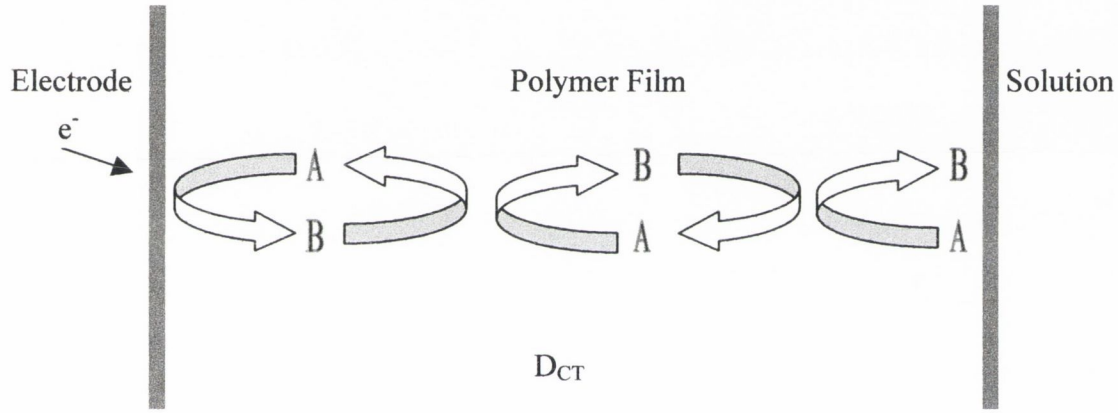


Figure 1.5: Charge propagation by means of quasi-diffusional charge percolation in a redox polymer.[102]

1.5 N-SUBSTITUTED POLYPYRROLE FILMS

The use of organic conducting polymers to chemically modify electrodes has been an area of ongoing research. However, the incorporation of metallic complexes in such films is a relatively new field of research that has attracted a great deal of interest.[103,104] Metallocene-based polymers are one category of such polymers that have attracted increasing interest in the past few years.[105-111] The incorporation of ferrocene into conductive[105-109] and other polymer matrices [111,113] is being actively investigated for a range of applications including biosensors, reference electrodes, electro-optical devices and electrocatalysis.[39,114,115]

In general, two main techniques have been adopted for the synthesis on metallocene-containing polymers. The first strategy involves the chemical polymerisation of a metallocenyl functionalised monomeric species [116,117]. Alternatively, metallocene species may be incorporated within a preformed organic or inorganic conducting polymer film.[118-121] While, this approach represents a facile and versatile method of preparation of novel metallocene-based polymers, problems have been encountered with the "leaching" of the organometallic species out of the polymer film over a given period of time. However, an alternative, less exploited method of synthesis involves the covalent co-ordination of metallocenes to conjugated organic polymeric frameworks[105-111]. The covalent attachment of such a redox moiety onto an organic species results in the formation of a hybrid polymer. The term hybrid is used to denote the fact that the species is comprised of a conducting backbone and a pendant redox active group. Such a material may exhibit conduction characteristics both of redox and electronically conducting materials. Although many organic compounds are suitable for electropolymerization, pyrrole appears to be the most convenient and may be functionalised with transition metal complexes[103, 104]. However, monomers with aniline and phenol substituents have also been investigated. The electropolymerization of pyrrole derivatives allow for the generation of non-passivating polymer films containing active centres (i.e. transition metal complexes).[122] The electropolymerization of pyrrole has been previously described in section 1.3. The electropolymerization of N-substituted pyrrole monomers has proved an excellent method of preparation of polymer films

containing active centres. The result of the N-substitution is to afford a slower polymerisation rate and a marked drop in the conductivity of the poly(pyrrrole) matrix. This may be accounted for by the non-planarity of the polypyrrole chains induced by the substituents[123]. However, the remaining conductivity of the polymeric chain is adequate for the growth of films. Polypyridyl complexes[124], metallic porphyrins[125-129] and other macrocylic compounds[130-135] have all been prepared in this manner. Hybrid films may be synthesised through the electropolymerization of a pyrrole substituted at the nitrogen atom or at the 3,4 positions, Generally, derivatization of the pyrrole monomer with the appropriate ligand, followed by complexation with the desired metal and electropolymerization affords the required complex.

Despite the fact that a wide variety of transition metal complexes with pyrrole groups as ligands have been synthesised, pyrrole monomers containing metallocene moieties remain restricted to a few examples.[105-109, 111] Generally, the only examples of pyrroles functionalised with metallocene redox active centres contain the ferrocene unit Ferrocene is the archetypal organometallic redox compound due to its thermal and photochemical stability and most importantly its reversible redox couple which can be employed in both aqueous and non-aqueous solutions.

Foulds and Lowe[109] reported one of the earliest examples of N-substituted monomers containing redox active ferrocene side chains. Their work investigated the use of such complexes in the design of amperometric enzyme electrodes, or biosensors, and established a basis for future studies employing similar materials. Other studies achieved the synthesis of such monomers, however, only a few are able to form electroactive polymers by direct anodic polymerisation, most requiring copolymerization with the unsubstituted pyrrole. In addition, applications of these novel materials have remained unexplored.

The functionalization of conducting polymer films with metallic complexes for the deliberate modification of electrode surfaces marks the birth of a new field that combines co-ordination chemistry with polymer chemistry and electrochemistry. These "hybrid" moieties have been investigated to achieve applications in areas such as electrocatalysis and sensor devices.[109]

1.6 BIOSENSORS

Biosensors are complex analytical devices, which bridge the boundaries between chemistry, biology, physics, medicine and material science. "Bio" relates to the recognition element within the device, not surprisingly, this is a biological material. "Sensor" corresponds to any technology that has the ability to detect a physiochemical change, for instance; electrical current[136,137], electric potential[136,138,139], capacitance[140,141], mass[136,142,143], electric impedance[144,145], and others[146,147] have all been employed. We may conclude therefore, that a biosensor is an analytical device incorporating a deliberate and intimate combination of a specific biological element (that creates a recognition event) and a physical element (that transduces the recognition event).

Generally, the bioelement is an enzyme or antibody. However, it has been known for the use of whole cells, specific organelles, even sections of animal or plant tissues to be used in biosensors in the hope of reproducing living detection systems, such as olfactory mucosa[147]. However, redox enzymes[148] have proved the most popular to the electrochemical researcher. These moieties catalyse the conversion of a substrate between the reduced and oxidised state, thus allowing detection at the electrode. *In vivo*, enzymes are responsible for the digestion of food substances; they synthesise many of the chemicals required by the organism; they degrade other proteins that have served their purposes, thus recycling the components, in addition to many other functions. Organic synthesis is still playing catch up to the specificity produced by almost 3 billion years of evolution. This specificity of enzymatic action is the basis of enzyme-based biosensors.[149,150] For the purpose of understanding the "workings" of the biosensor, the familiar "lock and key" theory[151] may be adopted, where the sensor consists of an enzymatic species immobilised into a membrane or chemically bound to a surface in contact with the analyte solution. The analyte or substrate and macromolecule react in a specific way that can be monitored by a transducer, (Figure1.6). In the case of an amperometric biosensor, the reaction between the enzyme and substrate produces an electric current, which results in a change of the conductivity of the polymeric material in which the enzyme is immobilized and may subsequently be detected at the electrode.

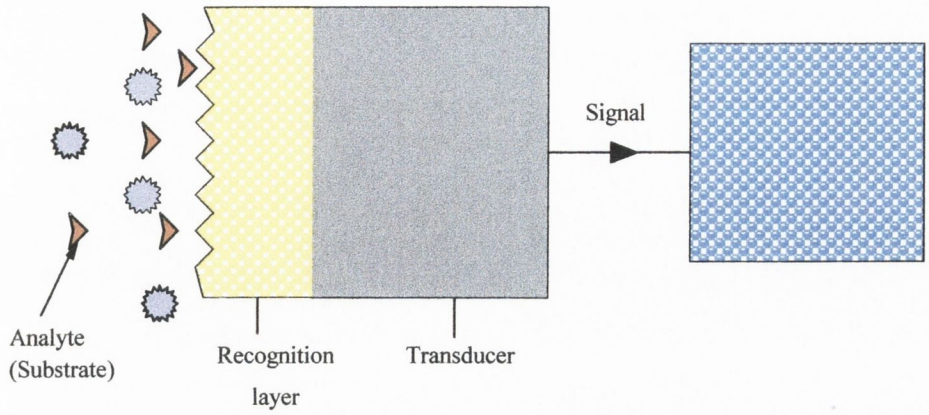


Figure 1.6: Schematic diagram of a biosensor

The first demonstration of an enzyme being incorporated into an electrode to form a biosensor transpired in 1962 when Clark and Lyons[152] investigated the possibility of using membranes containing enzymes to detect urea or glucose concentrations. By 1967, Updike and Hicks[153] had prepared an enzyme electrode by polymerizing gel containing glucose oxidase onto an oxygen electrode. The next landmark in the development of biosensors was the immobilization of more than one enzyme on a single support electrode.[154] The immobilization of cofactors was soon to follow.[155] However, it was not until the discovery of mediators,[121] (synthetic redox molecules which replace the need for oxygen), that it was possible to reoxidise the cofactor thereby preventing the dependence of enzyme sensors on oxygen concentration. Enzyme sensors can also be prepared by the use of field-effect transistors.[156] Such biosensors are constructed by attaching an enzymatic layer to the insulating layer of a semiconductor structure. In addition, optical fibres[157] lend themselves to the construction of biosensors, a suitable biological substance is attached to the tip of the fibre and produces an optical signal when it comes in contact with the system under study. These sensors may use absorption, fluorescence, and bio/chemiluminesence, and may require single or bifurcated fibres. Finally, enzyme biosensors can employ thermal or piezoelectric transducers[158], which detect variations in temperature or mass during an enzymatic reaction. Such biosensors have an extremely rapid response.

Archetypically, the glucose system is studied due to its clinical significance and also the low cost of glucose oxidase.[159] The reaction between glucose oxidase (GOx) and its substrate glucose is shown in equations (1) and (2). In the case of the oxidase enzyme, the electron acceptor is oxygen and is it's primary cosubstrate. GOx, from *Aspergillus niger*, is an example of an oxidase enzyme. This enzyme is rather large with a relative molar mass of ca. 1.86 kDa and a hydrodynamic radius of 4.3 nm. It is a dimeric flavoprotein composed of two polypeptide chains, and is covered with a glycoprotein coat. The enzyme has one flavin adenine nucleotide, FAD, prosthetic centre associated with each monomer. The structure is illustrated in Figure 1.7.

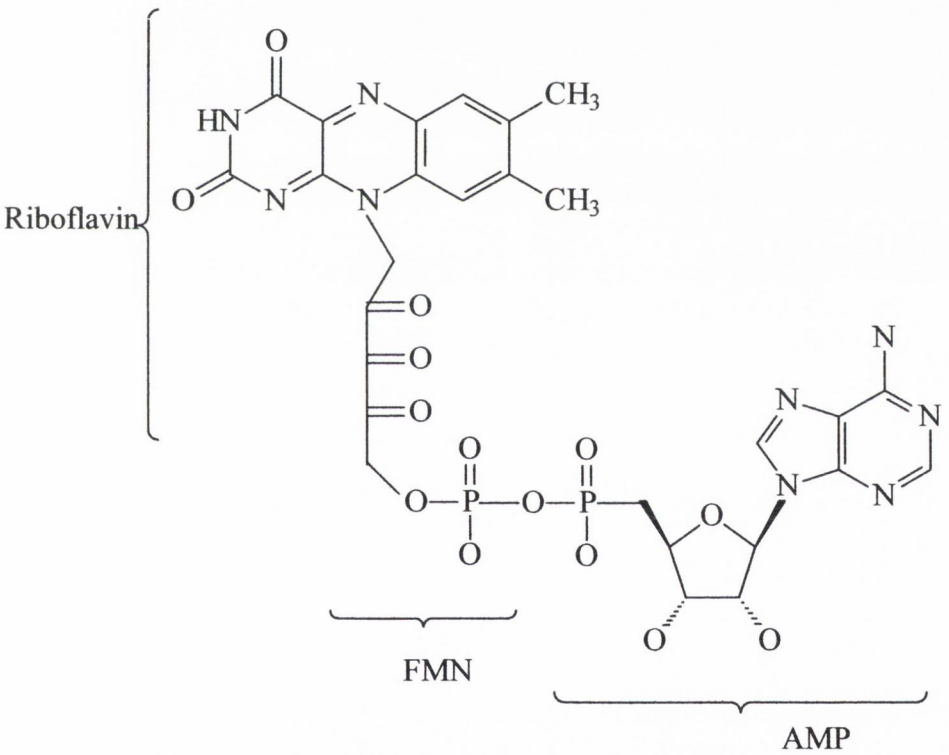


Figure 1.7: Structure of flavin adenine nucleotide. FAD

Direct electron transfer between the enzyme and the bare electrode is poor and suggests the active site is buried deep within the enzyme at a distance beyond which electron tunnelling can easily occur (>1nm). Glucose oxidase, Gox, catalyses the oxidation of glucose, with a subsequent two-electron equivalent reduction of a single

molecule of oxygen, resulting in the production of a single molecule of hydrogen peroxide:

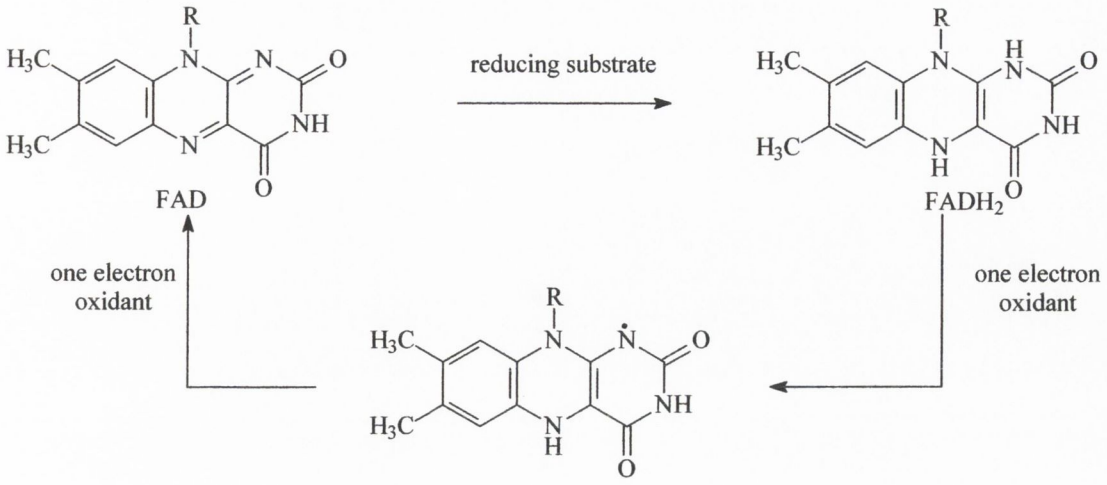
$$\text{glucose} + \text{Gox(OX)} \rightarrow \text{gluconolactone} + \text{Gox(RED)} \qquad (1)$$

$$\text{Gox(RED)} + O_2 \rightarrow \text{Gox(OX)} + H_2O_2 \qquad (2)$$

Glucose sensors may, in principle, monitor any of the oxidised/reduced species of the scheme shown in equations (1) and (2). The most direct approach would be to monitor the current produced by the reduced glucose oxidase. Flavin enzymes have been employed for this purpose; however, unmediated redox reactions of these proteins on solid electrodes have yet to be reported.

Alternatively, measurement of the oxidation current of the hydrogen peroxide produced by the glucose oxidase may be monitored and related back to the amount of glucose present in the sample.[160] Unfortunately, the potential required to oxidise hydrogen peroxide is sufficiently anodic that interfering compounds, e.g. ascorbic acid, are also oxidised and affect the overall measured current response.

Finally, glucose can be measured with the glucose oxidase system using **mediators.**[121] The function of the mediator is to enable amperometric detection of the analyte at less positive potentials. This thereby minimizes the problem of additional currents arising from the oxidation of interfering compounds which would be observed if higher detection voltages are employed. Direct electron transfer from the active sites of enzymes to electrode surfaces, although claimed in some cases,[162] is often obscured by steric effects. This is due to the fact that the active site may be embedded deep within the complex protein structure making electron transfer unfavourable. The fundamental role of a mediator is to facilitate electron transfer between the enzyme and the electrode. As ferrocene and ferrocene derivatives are one-electron acceptors, the electron transfer from the enzyme's prosthetic centre, $FADH_2$ to these compounds takes place in two separate one-electron steps. Scheme 1.2 shows the mechanism involved and the formation of a semi-quinoid intermediate in the reaction. In this case the one electron oxidant is a ferrocene species and the reducing substrate is a glucose molecule.



Scheme 1.2: Mechanism of interaction with artificial electron acceptors such as ferrocene and ferrocene derivatives

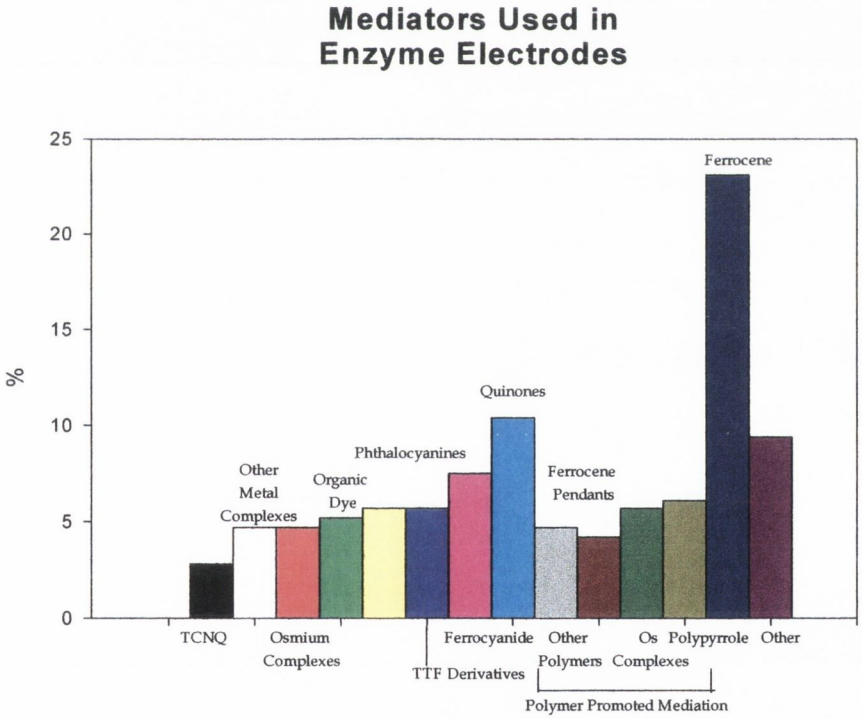


Figure 1.8: Graph of the common mediators currently in use[161]

The use of organic conducting polymers in conjunction with redox species has been well established in the area of biosensors. Immobilisation of an enzyme into the matrix of a hybrid polymer has proved successful in the detection of an appropriate substrate and shall be discussed in more detail later in this section. Hence this technique may be employed to form chemically modified electrodes, which may then be used for analytical purposes. The function of the redox active species is to facilitate electron transfer between an incorporated enzyme and the electrode. Figure 1.8 illustrates the compounds commonly used to fulfil the role of mediator.[161] Typically, ferrocene and its derivatives have been studied and have proved successful in mediating the electron transfer at redox potentials of 100 - 400 mV *vs.* SCE.[162-165] An effective mediator requires the following properties: a good reversible electrochemistry, rapid reaction of one or two electron transfer with active sites in redox enzyme, stable in both oxidised and reduced forms, not prone to autooxidation, to be amenable to chemical substitution, and finally soluble in aqueous and organic media.

Ferrocene, an oxygen insensitive molecule, has a well-behaved redox couple with fast one electron transfer. It is not pH sensitive. However, one property that is of great importance is its ability to be functionalised.[166] This results in the previously mentioned potential window, which may be tuned by modifying the substituents on the ferrocene ring(s). For example, ferrocene monocarboxylic acid possesses good one electron quasi-reversible electrochemistry in the presence of D-glucose.[158] On addition of glucose oxidase a dramatic change occurs and large catalytic oxidation currents are evident. This may be attributed to the reduction of the flavin group by glucose oxidase, see equations (3) and (4).

$$GOD_{RED} + 2FeCp_2R^+ \rightleftharpoons GOD_{OX} + 2FeCp_2R + 2H^+ \quad (3)$$

$$2FeCp_2R \rightleftharpoons 2FeCp_2R^+ + 2e^- \quad (4)$$

The resultant ferricinium ion is then free to reoxidize the reduced enzyme and the ferrocene produced is oxidised at the electrode. On examination of the second order rate constants for a range of ferrocenes it becomes evident that a linear relationship between the half-wave potential, $E_{1/2}$, and the rate constant does **not** exist. This indicates that the charge on the mediator is of importance. Positively charged mediators (2-aminoethlyferrocene) prove to be more efficient than those that are negatively charged (ferrocene dicarboxylic acid). This statement is consistent with the fact that an active site on glucose oxidase is negatively charged and would therefore be more amenable to a positively charged mediator, an important fact to remember when designing these compounds.

Several methods for the immobilization of enzymes within conducting polymer matrices exist. Integration of the enzyme species may be achieved through non-covalent means by using electrostatic, hydrophobic, hydrophilic or affinity interactions.[167-174] Electrostatic interactions between charged surfaces and proteins can result in organized, supramolecular, layered protein interfaces. For example, a mixture of octadecylthiol and dodecyl thiol groups constructed as a self-assembled monolayer on a gold electrode resulted in charged pockets for the immobilization of the enzyme fumarate reductase, which displayed direct electron transfer between the redox site and the electrode surface.[167] Consequently, the bioelectrocatalytic reduction of fumarate enables the modified electrode to be employed as an amperometric fumaric acid sensor. Hydrophobic interactions have been used for the adsorption of proteins such as fibrinogen, pyruvate kinase, and lysosyme onto alkylthiolates on gold electrodes.[168] Similarly, a mixture of hydrophilic and electrostatic interactions allowed for the adsorption of cytochrome c onto monolayer a 16-sulfanylhexadecanoic acid.[169] Affinity interactions refer to the interaction between an enzyme and its substrate or an antibody and its antigen. Glucose oxidase has been immobilized in this manner on a glassy carbon electrode using rabbit IgG antibodies.[170] The antibodies were adsorbed onto a layer of gelatin, a solution of glucose oxidase linked to anti-rabbit IgG antibody was immobilized onto the initial layer of antibodies. This concept has been extended to use biotin-avidin interactions to construct monolayer and multiplayer enzyme electrodes.[171]

The pioneering approach adopted by Foulds and Lowe[109] investigated the use of polypyrrole as a medium to immobilise glucose oxidase and thus measure the glucose analyte directly. As glucose oxidase has an overall negative charge one can see the benefits of the polypyrrole matrix. Overall electroneutrality requires an anion to be incorporated into the polypyrrole medium due to the fact that the growing polymer chain is positively charged; hence the enzyme is immobilised during the film growth process. This entrapment technique has the advantage of promoting proximity between the enzyme active site and the electrode surface. The mechanism by which glucose oxidase is incorporated into the matrix is still uncertain. However, polymer-entrapped glucose oxidase electrodes can be utilised as amperometric glucose sensors in the presence or absence of soluble mediators. The main problem encountered in this approach is due to the position of the redox activity species ($FADH_2$), which is positioned at the centre of the protein, and therefore its oxidation at a solid electrode surface is difficult to achieve. This results in sluggish kinetics for the direct electron transfer between the redox site and the support electrode.

Another technique involves the covalent linkage of proteins to conductive or semiconductive supports. For example, metal oxide materials similar to those discussed in section 1.1 contain surface hydroxyl groups, which may be used for the coupling of organic materials. SnO_2 and TiO_2 have both been used towards this end.[172] Furthermore, carboxylic acid groups or amine moieties attached immediately to the conducting support may be coupled using carbodiimide to complementary amino groups on the lysine residues or carboxylic acid groups of the aspartic acid residues.[173] Finally, cyanuryl chloride, which has been discussed previously, has been extensively investigated to achieve activation of the electrode surface for subsequent immobilization of the enzyme material.[174]

In conclusion, redox mediator substituted pyrrole monomers offer the advantage of a conducting matrix through which electron transfer from the enzyme to the electrode can occur with ease. The recent approach uses N-substituted pyrrole monomers containing ferrocene side chains to produce reagentless glucose electrodes. The redox active side chains are designed to accept electrons from the reduced form of the glucose

oxidase. The electrons may then be shuttled between mediator molecules to the underlying support electrode

1.7 Objectives of this Work

The objectives of this work were to synthesise a range of conducting polymers with redox active side chains and to investigate their use as chemically modified electrodes and examine their use as potential amperometric sensors. Ferrocene modified pyrrole derivatives are to be investigated to this end. The strategy adopted included varying the length of the alkyl unit between the ferrocene and the pyrrole moiety and also asymmetrically functionalising the second cylopentadienyl ring. These variations should affect the polymerisation of such monomers. It was these effects that we were interested in investigating, as they could provide us with an insight into how to design monomers that would produce the required current necessary for the sensing of biological substances.

Firstly, it was believed that by altering the chain length that separated the ferrocene from the pyrrole an optimum chain length could be achieved. This optimum length would encompass both the problem of solubility of these complexes with the increased degrees of freedom experienced by the monomers with higher alkyl groups. Secondly, by varying the substituents on the second cyclopentadienyl ring one could also affect the electronic nature of such compounds. An important factor to note is that the electron donating/withdrawing effects of the substituent group would come into play. In the case of an electron donating group (for example a methyl ester group) electron transfer would be accelerated whereas an electron-withdrawing group would obviously have the direct opposite result.

In addition, the investigation of heterogeneous redox catalysis at conducting polymer ultramicroelectrodes was to be carried out. Examination of the validity of a recent theoretical model which described the behaviour of microelectrodes coated with electroactive polymer thin films was to be achieved through investigations into the redox couple potassium hexacyanoferrate (II) trihydrate/ hexacyanoferrate (III), were to be examined at a polypyrrole/ dodecylbenzoylsulfonate conducting polymer film.

1.8 REFERENCES

1. W.J. Albery and A.R. Hilman, *Ann. Rep. Prog. Chem. Sect. C*, **78**, 377, (1981).
2. A.J. Bard, *J. Chem. Ed.*, **60**, 302, (1983).
3. R.W. Murray, in '*Electroanalytical Chemistry*', ed. A.J. Bard, Dekker, New York, Vol. **13**, (1984).
4. M.D. Ryan, E.F. Bowden, J.Q. Chambers, *Anal. Chem.*, **66**, 360R, (1994).
5. J.L. Anderson, E.F. Bowden, P.G. Pickup, *Anal. Chem.*, **68**, 379R, (1996).
6. J.L. Anderson, L.A. Coury Jr., J. Leddy, *Anal. Chem.*, **70**, 519R, (1998).
7. R.F. Lane and A.T. Hubbard, *J. Phys. Chem.*, **77**, 1401, (1973).
8. B.F. Watkins, J.R. Behling, E. Kariv, L.L. Miller, *J. Am. Chem. Soc.*, **97**, 3549, (1975).
9. P.R. Moses, R.W. Murray, *J. Am. Chem. Soc.*, **98**, 7435, (1976).
10. J.R. Lenhard, R.W. Murray, *J. Electroanal. Chem.*,**78**, 195, (1977).
11. M.A. Fox, F.J. Nobs, T.A. Voynick, *J. Am. Chem. Soc.*, **102**, 4029, (1980).
12. T. Wink, S.J. van Zuilen, A. Bult, W.P. van Bennekom, *Analyst*, **122**, 43R, (1997).
13. K.C. Nirmalya, K. Vijayamohanan, *Biosens. Bioelectron.*, **17**, 1, (2002)
14 F. Ma, R.B. Lennox, *Langmuir*, **16**, 6188, (2000).
15 C.D. Bain, E.B. Troughton, Y.T. Tao, J. Evall, G.M. Whitesides, R.G. Nuzzo, *J. Am. Chem. Soc.*, **111**, 321, (1989).
16. X.D. Dong, J. Lu, C. Cha, *Bioelectrochem. Bioenerg.*, **36**, 73, (1995).
17. S. Campuzano, R. Galvez, M. Pedro, F. J. Manuel de Villena, J.M. Pingarron, *J. Electroanal. Chem.*, **526**, 92, (2002).
18. M. Delvaux, S. Demoustuer-Champagne, *Biosensors and Bioelectronics*, **18**, 943, (2003)
19. J. Li, J. Yan, Q. Deng, G. Cheng, S. Dong, *Electrochim. Acta*, **42**, 961, (1997).
20. J. Hodak, R. Etchenique, E.J. Calvo, K. Singhal, P.N. Bartlett, *Langmuir*, **13**, 2708, (1997).
21. J. Li, G. Cheng, S. Dong, *J. Electroanal. Chem.*, **416**, 97, (1996).

22. I. Willner, V. Heleg-Shabtai, R. Blonder, E. Katz, G. Tao, A.F. Buckmann, A. Heller, *J. Am. Chem. Soc.*, **108**, 10231, (1996).

23. J.J. Gooding, E.A.H. Hall, D.B. Hibbert, *Electroanalysis*, **10**, 1130, (1998).

24. G. Capitani, A.C. Eliot, H. Gutz, R.M. Khomutov, J.F. Kirsh, M.g. Grutter, *Biochim. et Biophys. Acta*, **1647**,55, (2003).

25. A.R. Hillman, in *'Electrochemical Science and Technology of Polymers'*, ed. A. Linford, Elsevier, London, **Vol. 1**, (1987).

26. H. Braun, W. Storck, K. Doblhofer., *J. Electrochem. Soc.*, 1230,4, (1983).

27. P. Mariaulle, F. Sinapi, L. Lamberts, A. Walcarius, *Electrochimica Acta*, **46**, 3543, (2001).

28. N. Oyama, F.C. Anson, *J. Electrochem. Soc.*, **127**,247, (1980).

29. N. Oyama, S. Yamaguchi, Y. Nishiki, K. Tokuda, H. Matsuda, F.C. Anson, *J. Electroanal. Chem.*, **139**, 371, (1982).

30. I. Rubenstein, A.J. Bard, *J. Am. Chem. Soc.*, **103**, 5007, (1981).

31. I. Rubenstein, A.J. Bard, *J. Am. Chem. Soc.*, **102**, 6641, (1980.

32. D.A. Buttry, K.A. Dollard, *J. Am. Chem. Soc.*, **105**, 685, (1983).

33. M.N. Szentirmay, C.R. Martin, *Anal. Chem.*, **56**,1898, (1984).

34. E.L.Ciolkowski, B.R. Cooper, J.A. Janowski, J.W. Jorgenson, M.W. Wightman, *J. Am. Chem. Soc.*, **114**, 2815, (1992).

35. M.E. Rice, C. Nicholson, *Anal. Chem.*, **61**, 1805, (1989).

36. J.B. Kerr, L.L. Miller, *J. Electroanal. Chem.*, **101**, 263, (1979).

37. J.B. Kerr, L.L. Miller, M.H. Van De Mark, *J. Am. Chem. Soc.*, **102**, 10, (1980).

38. C.D. Ellis, T.J. Meyer, *Inorg. Chem.*, **23**, 1748, (1984).

39. *"Handbook of Conducting Polymers"*, ed. T.A. Skotheim, Dekker, New York, **Vol.2**, (1986).

40. K. Gurunathan, A. V. Murugan, r. Marimuthu, U.P. Mulik, D.P. Amalnerkar, *Materials Chemistry and Physics*, **61**, 173, (1999).

41. S. Holdcroft, B.L. Funt, *J. Electroanal. Chem.*, **240**, 89, (1988).

42. A. Malinauskas, *Synth. Metals*, **107**, 75, (1999).

43. M. Gerard, A. Chaubey, B.D. Malhotra, *Biosens. and Bioelectron.*, **17**, 345, (2002).

44. I. Willner, E. Katz, B. Willner, *Electroanalysis*, , **13**, 965-977, (1997).

45. Collier, J.H., J.P. Camp, T.W. Hudson, C.E. Schmidt (2000*). J. Biomed. Mater. Res.*, **50**:574, (1999)

46. R.L. Twite, G.P. Bierwagen, *Progress in Organic Coatings*, **33**, 91, (1998).

47. H. Shirakawa, E.J. Louis, A.G. MacDiarmid, C.K. Chiang, A.F. Heeger, *J. Chem. Soc. Commun.*, **58**, (1977).

48. H. Shirakawa, *Angew. Chem.*, **40**, 2574, (2001).

49. A.G. MacDiarmaid, *Angew. Chem.*, **40**, 2581, (2001).

50. A.J. Heeger, *Angew. Chem.*, **40**, 2591, (2001).

51. C.K. Chiang, Y.W. Park, A.J. Heeger, H. Shirawaka, E.J. Louis, A.G. MacDiarmid, *J. Chem Phys.*, **69**, 5098, (1978).

52. A.R. Hillman, E.F. Mallen, *J. Electroanal. Chem.*, **220**,351, (1987).

53. A. Hammett, A.R. Hillman, *J. Electrochem. Soc.: Electrochemical Science and Technology*, **135**, 10, (1988).

54. R. Noufi, A.J. Nozik, J.White, L.F. Warren, *J. Electrochem. Soc.: Electrochemical Science and Technology*, **129**, 10, (1982).

55. S. Strafstrom, J. C. Bredas, *Synth. Met.*,**14**, 297, (1986).

56. I. Rubenstein, E. Sabatani, J. Rishpon, *J. Electrochem. Soc.: Electrochemical Science and Technology*, **134**, 12 (1987).

57. E.M. Genies, M. Lapowski, C. Santier, E. Vieil, *Synth. Met.*, **18**, 631, (1987).

58. U. Konig, J.W. Schultz, *J. Electroanal. Chem.*, **242**, 243, (1988).

59. G. Zotti, S. Cattarin, N. Comisso, *J. Electroanal. Chem.*, **238**, 387, (1988).

60. H. Letheby, *J. Chem. Soc.*, **15**, 161, (1962).

61. F. Goppelsroeder, *Compt. Rend.*, 82:331, 1392, (1976).

62. A. Dall'Olio, Y. Dascola, V. Varacco, V. Bocchi, *C.R. Acad. Sci. Ser.*, C, **267**, 443, (1968).

63. A.F. Diaz, K.K. Kanazawa, *J.C.S. Chem. Comm.*, 635, (1979).

64. G. Tourillon, F. Garnier, *J. Electroanal. Chem.*, **135**, 173, (1982).

65. M. Delamar, P.C. Laczac,J.Y. Domousseau, J.E. Dubois, *Electrochim. Acta*, **27**, 61, (1982).

66. G. Brilmyer, R. Jasinki, *J. Electrochem. Soc.*, **129**,1950, (1982).

67. E. M. Genies, G. Bidan, A.F. Diaz, *J. Electroanal. Chem.*, **149**, 101, (1983).

68. K.J. Kim, H.S. Song, J.D Kim, *Bull. Korean Chem. Soc.*, **9**, 248, (1988).

69. S. Asavapiriyanont, G.K. Chandler, G.A. Gunawardena, D. Pletcher, *J. Electroanal. Chem.*, **177**, 229, (1984).

70. Y.J. Qiu, J.R. Reynolds, *J. Polym. Sci., Part A: Polym. Chem.*, **30**, 1315, (1992).

71. K.K. Kanazawa, A.F. Diaz, R.H. Geiss, W.D. Gill. J.F. Kwak, J.A. Logan, J.F. Rabolt, G.B. Street, *J.C.S. Chem. Commun*, 854, (1979).

72. B.R. Scharifker, E. Garcia-Pastoriza, W. Marino, *J. Electroanal. Chem.*, **300**, 85, (1991).

73. A. Hammet, A.R. Hillman, *J. Electrochem. Soc.*, **135**, 2517, (1988).

74. T.F. Otero, H. Grande, J. Rodriguez, *J. Electroanal. Chem.*, **394**, 211, (1995).

75. B.R. Scharifker, D.J. Fermin, *J. Electroanal. Chem.*, **365**, 35, (1994).

76. D.J. Fermin, J. Mostany, B.R. Scharifker, *Current Topics in Electrochemistry*, **2**, (1993).

77. A.F.Diaz, A. Martinez, K.K. Kanazawa, M. Salmon, *J. Electroanal. Chem*, **130**, 181, (1981).

78. F. Beck, *Electrochem. Acta*, **33**, 839, (1988).

79. D.J. Walton, C.E. Hall, A. Chyla, *Analyst*, **117**, 1305, (1992).

80. A.S.N Murphy, S. Pal, K.S. Reddy, *J. Mat. Sci. Lett.*, **3**, 745, (1984).

81. M. Salmon, A.F. Diaz, A.F. Logan, M. Krounbi, J. Barfgon, *Mol. Cryst. Liq. Cryst.*, **83**, 265, (1982).

82. L.F. Warren, D.P. Anderson, *J. Electrochem. Soc.: Electrochemical Science and Technology,* **134**, 1 (1987).

83. T.Schimidzu, A. Ohtani, T. Iyoda, K. Honda, *J. Electroanal. Chem.*, **224**, 123, (1987).

84. G.G. Wallace, Y.P. Lin, *J. Electroanal. Chem.*, **247**, 145, (1988).

85. E.L. Kupila, J. Kankare, *Syn. Met.*, **74**, 241, (1995).

86. L.S. Curtin, G.C. Komplin, W.J. Pietro, *J. Phys. Chem.*, **92**, 12, (1988).

87. H. Varela, M. Malta, R.M. Torresi, *J. Power Sources*, **92**, 50, (2001).

88. M.A. De-Paoli, R.C.D. Peres, S. Panero, B. Scrosati, *Electrochim. Acta*, **37**, 7 (1992).

89. E.M Genies and J.M. Pernaut, *J. Electroanal. Chem.*, **191**, 111, (1985).

90. J.L. Bredas and G.B. Street, *Acc. Chem. Res.*, **18**, 309, (1985).

91. G.B. Street, T.C. Clarke, M. Krounbi, K.K. Kanazawa, V. Lee, P. Pfluger, J.C. Scott, G. Weiser, *Mol. Cryst. Liq. Cryst.*, **83**, 253, (1983).

92. J.L. Bredas, *Mol. Cryst. Liq. Cryst.*, **118**, 49, (1985).

93. J.C. Scott, P.Pfluger, M. Krounbi, G.B. Street, *Phys. Rev. B*, **28**, 2140, (1983).

94. J.L Bredas, J.C. Scott, K.Yakushi, G.B. Street, *Phys. Rev. B: Condens. Matter*, **30**, 1023, (1984)

95. J.L Bredas, B. Themans, J.G. Fripiat, J.M. Andre, R.R. Chance, *Phys. Rev. B: Condens. Matter*, **25**, 6761, (1984)

96. J.C. Scott, P.Pfluger, M. Krounbi, G.B. Street, *Phys. Rev. B*, **28**, 40, (1985).

97. M.E.G. Lyons, *Electroactive Polymer Chemistry, Part 1. Fundamentals, Plenum Press, New York*, (1994).

98. H.D. Abruna, *Coord. Chem. Rev.*, **86**, 135, (1988)

99. C. Arana, M. Keshavarz. K.T. Potts, H.D. Abruna, *Inorg. Chim. Acta*, **225**, 285, (1994)

100. H.K. Youssoufi, M.Hmyene, A. Yassar, F. Garnier, *J. Electroanal. Chem.*, **406**, 187, (1996)

101. F.B. Kaufman, E.M. Engler, *J. Am. Chem. Soc.*, **101**, 547, (1979).

102. F.B. Kaufman, A.M. Schroeder, E.M. Engler, S.R. Kramer, J.Q. Chambers, *J. Am. Chem. Soc.*, **102**, 483, (1980).

103. D. Curran, J. Grimshaw, S.D. Perera, *Chem. Soc. Rev.*, **20**, 391, (1990).

104. A. Deronzier, J.-C. Moutet, *Coord. Chem. Rev.*, **147**, 339, (1996).

105. A. Deronzier, J.-C. Moutet, *Acc. Chem. Res.*, **22**, 249, (1989).

106. J.G. Eaves, R. Mirrazei, D. Parker, H.S. Munro, *J. Chem. Soc., Perkin Trans. 2*, 475, (1989).

107. A. Haimerl, A. Merz, *Angew. Chem., Int. Ed. Engl.*, **25**, 180, (1986).

108. A. Merz, A. Haimerl, A.J. Owen, *Synth. Met.*, **25**, 89, (1988).

109. N.C. Foulds, C.R. Lowe, *Anal. Chem.*, **60**, 2473, (1988).

110. I. Cuadrado, C.M. Casado, F. Lobete, B. Alonso, B. Gonzalez, J. Losada, U. Amador, *Organomet.*, **18**, 4960, (1999).

111. J. Chen, C.O Too, G.G. Walace, G.F. Sweigers, B.W. Skelton, A.H. White, *Electrochim. Acta*, **47**, 4227, (2002)

112. J.J. Hickman, D. Offer, C. Zou, M.S. Wrightman, P.E. Laibinis, G.M. Whitesides, *J. Am. Chem. Soc.*, **113**, 1128, (1991).

113. P. Daum, J.R. Lenhard, D. Rolison, R.W. Murray, *J. Am. Chem. Soc.*, **102**, 4649, (1980).

114. J. Heinze, *Top. Curr. Chem.*, **152**, 2, (1990).

115. A.F. Diaz, J.F. Rubinson, H.B. Mark, *J. Adv. Polym. Sci.*, **84**, 113, (1988).

116. M.E.G. Lyons, *Electroactive Polymer Chemistry, Part 1. Fundamentals, Plenum Press, New York*, (1994).

117. I. Manners, *Adv. Organomet. Chem*, **37**, 131, (1995).

118. K.H. Pannell, F. Wang, H.K. Sharma, F. Cervantes-Lee, *Polyhedron*, **19**, 291, (2000)

119. M.J. Green, H.A.O. Hill, *J. Chem. Soc., Faraday Trans.*, **82**, 1237, (1986).

120. A.E.G. Cass, G. Davis, G.D. Francis, H.A.O. Hill, W.J. Aston, I.J. Higgins, E.V. Plotkin, L.D.L. Scott, A.P.F. Turner, *Anal. Chem.*, **56**, 667, (1984).

121. J.E. Frew, H.A.O. Hill, *Anal. Chem.*, **59**, 933, (1987).

122. R.W. Murray, *Ann. Rev. Mater. Sci.*, **14**, 145, (1984).

123. A.F. Diaz, *Chem. Scr.*, **14**, 145, (1981).

124. M. Buda, A. Ion. J.-C. Moutet, E. Saint-Aman, R. Ziessel, *J. Electroanal. Chem.*, **469**, 132, (1999).

125. A. Bettelheim, B.A. White, S.A. Raybuck, R.W. Murray, *Inorg. Chem.*, **26**, 1009, (1987).

126. P.Moisy, F.Bedioui, Y. Robin, J. Devynck, *J. Electroanal. Chem.*, **250**, 191, (1988).

127. A. Deronzier. J.-M. Latour, *J. Electroanal. Chem.*, **224**, 295, (1987).

128. F. Bedioui, M. Voisin ,J. Devynck, C. Bied-Charreton, *J. Electroanal. Chem.*, **297**, 257, (1991).

129. A. Deronzier, R. Devaux, D. Limosin, J.-M. Latour, *J. Electroanal. Chem.*, **324**, 325, (1992).

130. J.-P. Collin, J.-P. Sauvage, *J. Chem. Soc.,Chem. Commun.*, **1075**, 60, (1987).

131. P.N. Bartlett, L.-Y. Chung, P. Moore, *Electrochim. Acta*, **35**, 1051, (1990).

132. E.Sable, M. Handel, M. L'Her, *Electrochim. Acta*, **36**, 15, (1990).

133. C.P. Horwitz, *Chem. Mater.*, 1, 463, 1989

134. A. Deronzier, M.-J. Marques, *J. Electroanal. Chem.*, **370**, 151, (1994).

135. G. Ricciardi, F. Lel, *Polyhedron*, **11**, 2089, (1992).

136. R.S. Sethi, *Biosens. Bioelectron.*, **9**, 243, (1994).

137. P.N. Bartlett, P. Tebbutt, R.C. Whitaker, *Prog. React. Kinet.*, **16**, 55, (1991).

138. R.M. Ianniello, T.J. Lindsay, A.M. Yacynch, *Anal. Chem.*, **54**, 1980, (1982).

139. A.L. Ghindilis, I.N. Kurochkin, *Biosens. Bioelectr.* **9**, 353, (1994)

140. C. Krause, V.M. Mirsky, K.D. Heckmann, *Langmuir,* **12**, 6059, (1996).

141. V.M. Mirsky, C. Krause, K.D. Heckmann, *Thin Solid Films*, **284**, 939, (1996).

142. I. Ben-Dov, I. Willner, E. Zisman, *Anal. Chem.*, **69**, 3506, (1997).

143. A.Bardea, A. Dagan, I. Ben-Dov, B. Amit, I. Willner, *Chem. Commun.*, 839, (1998).

144. D. Athy, M. Ball. C.J. McNeil, R.D. Armstrong, *Electroanalysis*, **7**, 270, (1995).

145. T.M. Nahir, E.F. Bowden, *J. Electroanal. Chem*, **410**, 9, (1998).

146. S.M. Amador, J.M. Pachence, R. Fischetti, J.P. McCAuley, Jr., A.B. Smith, J.K. Blasic, *Langmuir*, **9**, 812, (1994).

147. S. ampuero, J.O. Bosset, *Sensors and Actuators B: Chem.*, **94**, 1, (2003).

148. A. Wiseman, *Handbook of enzyme biotechnology*, London;Elllis Horwood, **3**, (1995).

149. U.J. Krull, M.S. Heimlich, K.M.R. Kallury, P.A.E. Piunno, J.D. Brennan, R.S. Brown, D.P. Nikolelis, *Can. J. Chem.*, **73**, 1239, (1995).

150. I. Willner, E. Katz, B. Willner, R. Blonder, V. Heleg-Shabtai, A.F. Buckmann, *Biosens. Bioelectron.*, **12**, 337, (1997).

151. D. Voet, J.G. Voet, *Biochemistry*, 317, (1999)

152. L. C. Clark, C. Lyons, *Ann. NY Acad. Sci.*, **102**, 29, (1962).

153. S.J. Updike, G.P. Hicks, *Nature*, **214**, 986, (1967).

154. V.V. Sorochinskii, B.I. Kurganov, *Biosens. Bioelectron.*, **11**, 45, (1996).

155. W.J. Albery, P.N. Bartlett, *J. Chem. Soc. Commun.*, **4**, 234, (1984).

156. P. Bergveld, *Trans. Biomed. Eng.*, BME-**19**, 342, (1972).

157. P. Vadgama, P.W. Crump, *Analyst*, **117**, 1657, (1992).

158. F. Benmakroha, T. Boudjerda, R. Boufenar, H. Allag, F. Djerboua, J.J. McCallum, *Analyst*, **118**, 401, (1993).

159. R.M. Ianniello, A.M. Yacynych, *Anal. Chem*, **53**, 20900, (1981).

160. F. Scheller, G. Strand, B. Nellman, M. Kuhn, W. Ostrowski, *J. Electroanal. Chem.*, **104**, 117, (1979).

162. M.J. Green, H.A.O. Hill, *J. Chem. Soc., Faraday Trans.*, **82**, 1237, (1986).

161. www-biol.paisley.ac.uk/macro/enzyme_electrode/chapter1/page4.htm

163. P.N. Bartlett, R.G. Whitaker, *J. Electroanal. Chem.*, **224**, 37, (1987).

164. M.A. Lange, J.Q. Chambers, *Anal. Chim. Acta.*, **175**, 89, (1985).

165. J.E. Frew, M.J. Green, H.A.O. Hill, *J. Chem. Technol. Biotechnol.*, **36**, 357, (1986).

166. R.D.A. Hudson, *J. Organomet. Chem.*, **637**, 47, (2001)

167. K.T. Kinnear, H.G. Monbouquette, *Langmuir*, **9**, 2255, (1993)

168. K.L. Prime, G.M. Whitesides, *J. Am. Chem. Soc.*, **115**, 10714, (1993)

169. M.J. Tarlov, E.F. Bowden, *J. Am. Chem. Soc.*, **113**, 1847, (1991)

170. C. Bourdillon, C. Demaille, J. Moiroux, J.-M. Saveant, *Acc. Chem. Res.*, **29**, 529, (1996).

171. J. Anzai, H. Takeshita, Y. Kobayashi, T.Osa, T. Hoshi, *Anal. Chem.*, **70**, 811, (1998).

172. H.O. Finklea, R. Vithanage, *J. Phys. Chem.*, **86**, 3621, (1982).

173. M.R. Tarasevich, *Electrochemistry of Carbon Materials*, Nauka, Moscow, (1984).

174. R.M. Ianniello, H.J. Wieck, A.M. Yacynych, *Anal. Chem.* **53**, 2090, (1983).

CHAPTER TWO

SYNTHESIS AND CHARACTERISATION OF HYBRID MONOMERS

2.1 INTRODUCTION

The synthetic strategies employed during the course of this work in an effort to prepare hybrid monomers shall be discussed in this chapter. As stated within the aims and objectives of this work a range of conducting polymers with redox active side chains were to be synthesized. More specifically, ferrocene modified pyrrole derivatives were to be prepared and investigated later as potential amperometric sensors. The coupling of a ferrocene carboxylic acid group with an N-(aminoalkyl)pyrrole species through a condensation reaction using a coupling reagent was the procedure favoured. Literature synthesis for the formation of ferrocene carboxylic acid(s) had been well documented.[1-3] However, a novel procedure for the production of the N-(aminoalkyl)pyrrole derivatives needed to be accomplished.

One of the objectives of this work involved varying the length of the alkyl unit between the ferrocene and the pyrrole moiety. This could be accompished through the creation of a series of novel N-(aminoalkyl)pyrrole derivatives, **17**. The formation of N-substituted pyrroles from the ring closure reaction of 2,5-dimethoxyfuran with an alkylamine derivative had been previously reported.[4] It was hoped to extend this synthesis to the production of N-(aminoalkyl)pyrrole species, **17**, using an alkyldiamine species such as 1,6-hexadiamine, **11**. The synthesis proved unsuccessful and another route was investigated which involved coupling one of the amine groups of the 1,6-hexadamine molecule, **11**, to the ferrocene carboxylic acid prior to the ring closure of the pyrrole group. This attempt also proved futile. Finally, a three-step synthetic route was devised for the preparation of the N-(aminoalkyl)pyrroles, **17**, which allowed for the alkyl unit length to be varied with ease, section 2.4 outlines the steps involved.

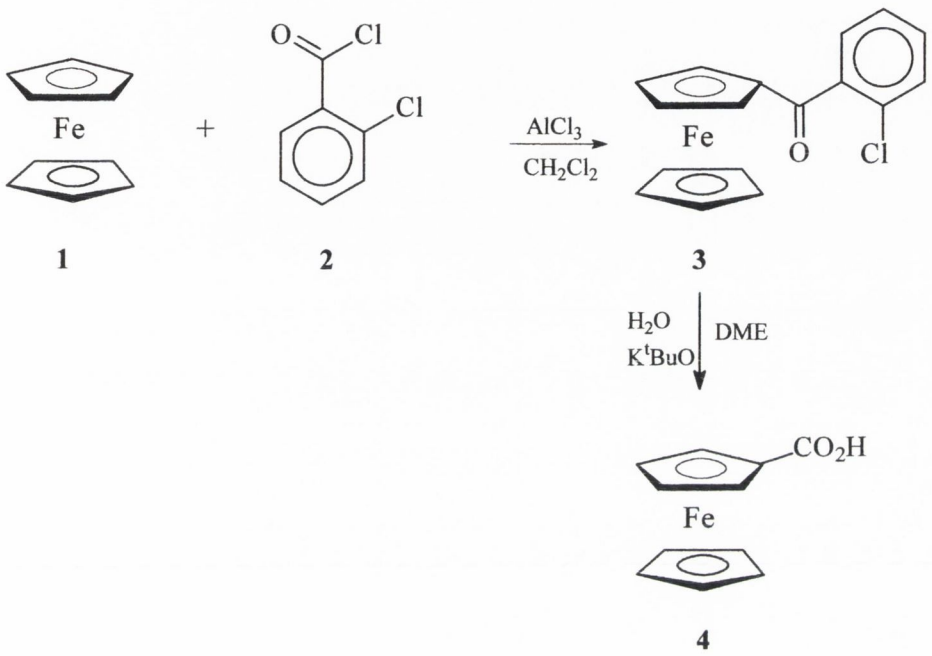
Asymmetrical functionalization of the second cylopentadienyl ring of the ferrocene modified pyrrole was also stated as an objective. Initial endeavours to achieve this included the coupling reaction of one equivalent of the N-(aminoalkyl)pyrrole species, **17**, with one equivalent of 1,1'-ferrocenedicarboxylic acid, **6**. However, disubstitution of the 1,1'-ferrocenedicarboxylic acid, **6**, with the N-(aminoalkyl)pyrrole, **17**, occurred even when the former was used in excess. This led to the serendipitous discovery of a facile route for the production of symmetrically

disubstituted hybrid monomers, **20**. The creation of asymmetrically substituted ferrocenes was achieved through the production of **9** and the subsequent coupling to the N-(aminoalkyl)pyrrole which is described in detail in section 2.1.3.

In conclusion, the synthetic strategies adopted during the course of this work have been described. The synthetic procedures are now reported in more detail beginning with the synthesis of all the ferrocene derivatives, followed by the procedure for the synthesis of the N-(aminoalkyl)pyrrole species. Finally, the coupling reactions of these two moieties to afford the creation of novel ferrocene modified pyrrole hybrid monomers are outlined.

2.2 SYNTHESIS OF FERROCENE DERIVATIVES

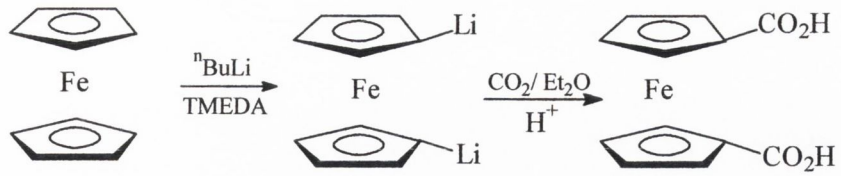
2.2.1 Preparation of Ferrocenecarboxylic Acid[1]



Scheme 2.1

Ferrocenecarboxylic acid, **4**, was prepared by following the literature method of Reeves.[1] Scheme 2.1 illustrates the two-step process involved. The most important and standard method for the preparation of an aryl ketone is a procedure known as Friedel Crafts acylation. The acylation of ferrocene was achieved through the treatment of ferrocene, **1**, with aluminium chloride and 2-chlorobenzoyl chloride, **2**, in dry dichloromethane, DCM, to produce (2-chlorobenzoyl)ferrocene. Subsequently, a potassium tertiary butoxide-water suspension was used as an agent to ensure the fission of the non-enolizable ketone,[5] **3**, produced in the first step. This produced the required ferrocenecarboxylic acid as an air stable yellow powder in an 87% yield, which was comparable with literature results.

2.2.2 Preparation of 1,1'-Ferrocenedicarboxylic Acid[2]



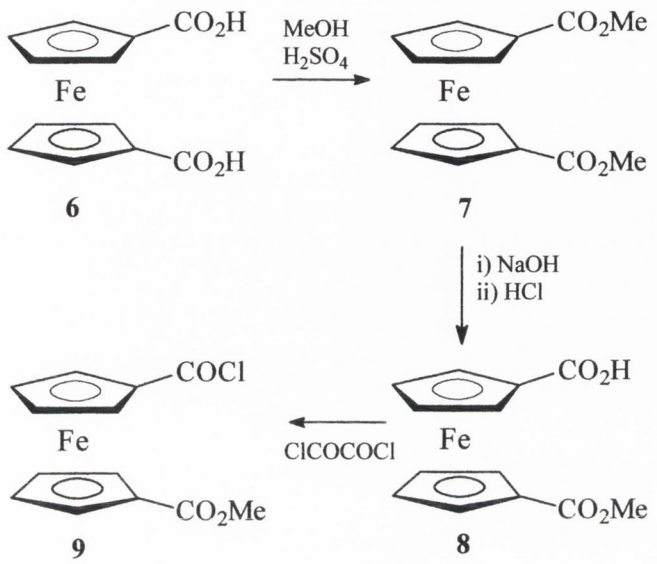
1 **5** **6**

Scheme 2.2

The strategy adopted to produce the asymmetrically substituted ferrocene complexes involved coupling 1,1'- ferrocenedicarboxylic acid to one equivalent of an N-(aminoalkyl)pyrrole derivative through a condensation reaction. To achieve this end 1,1'- ferrocenedicarboxylic acid was prepared through the dilithiation of ferrocene using *n*-butyl lithium and N,N,N',N'-tetramethylethlenediamine as shown in Scheme 2.2. The dilithiated ferrocene species is of a highly explosive nature and a nitrogen atmosphere is maintained at all times. Subsequent to the washing of the dilithiated species with dry petroleum ether it is dissolved in dry diethyl ether and reacted with a flask of finely divided dry carbon dioxide in order to produce the dicarboxy intermediate. Finally, concentrated hydrochloric acid is used to hydrolyze this moiety producing the required diacid derivative. This results in an air stable, orange precipitate in a yield of 67%.

The coupling reaction between the 1,1'- ferrocenedicarboxylic acid, **6**, and the N-(aminoalkyl)pyrrole derivative did not produce the desired asymmetric derivative. The results are described in full later in this chapter in Section 2.5.3. A different approach was assumed, where the precursor ferrocene moiety was asymmetrically substituted prior to the coupling reaction. The following section describes how this was achieved.

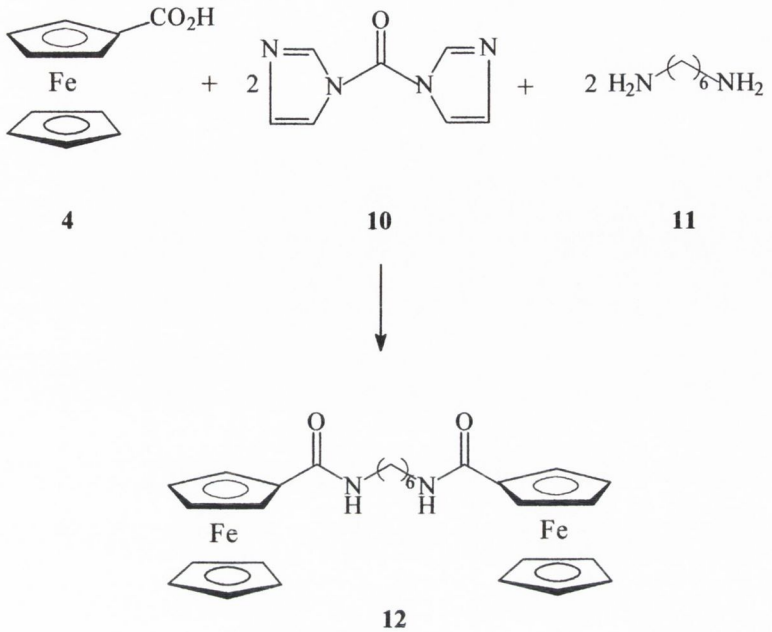
2.2.3 Preparation of Asymmetrically Substituted Ferrocenes[3]



Scheme 2.3

To achieve the preparation of asymmetrically substituted hybrid monomers it was decided to synthesis methyl 1,1'-chloroformylferrocenecarboxylate, **9**. This was achieved according to the preparation carried out by Lorkowski *et al*, as illustrated in Scheme 2.3. Firstly, the esterfication of 1,1'-ferrocenedicarboxylic acid[4], **6**, was achieved by employing methanol as the alcohol and sulfuric acid as the catalyst. This yelded 1,1'-ferrocenedimethoxyester, **7**, as brown crystals in an 83% yield. Following this, 1,1'-ferrocenedimethoxyester, **7**, was treated with aqueous sodium hydroxide in methanol. The acidification of a single ester group was accomplished through the addition of concentrated hydrochloric acid, the outcome being 42% of **8**, as orange crystals and 29% of the starting material, **7**. Finally, the treatment of **8**, with oxalyl chloride in DCM afforded the required complex, **9**, as red crystals in a yeld of 71%. The overall yield achieved from the original ferrocene molecule was 17%. It must be noted that these results did not compare favourably with the published results. Repeated attempts to reproduce the literature synthesis resulted in similar yields, the author did not find any apparent explanation for the deviation of obtained yield from that of the literature.

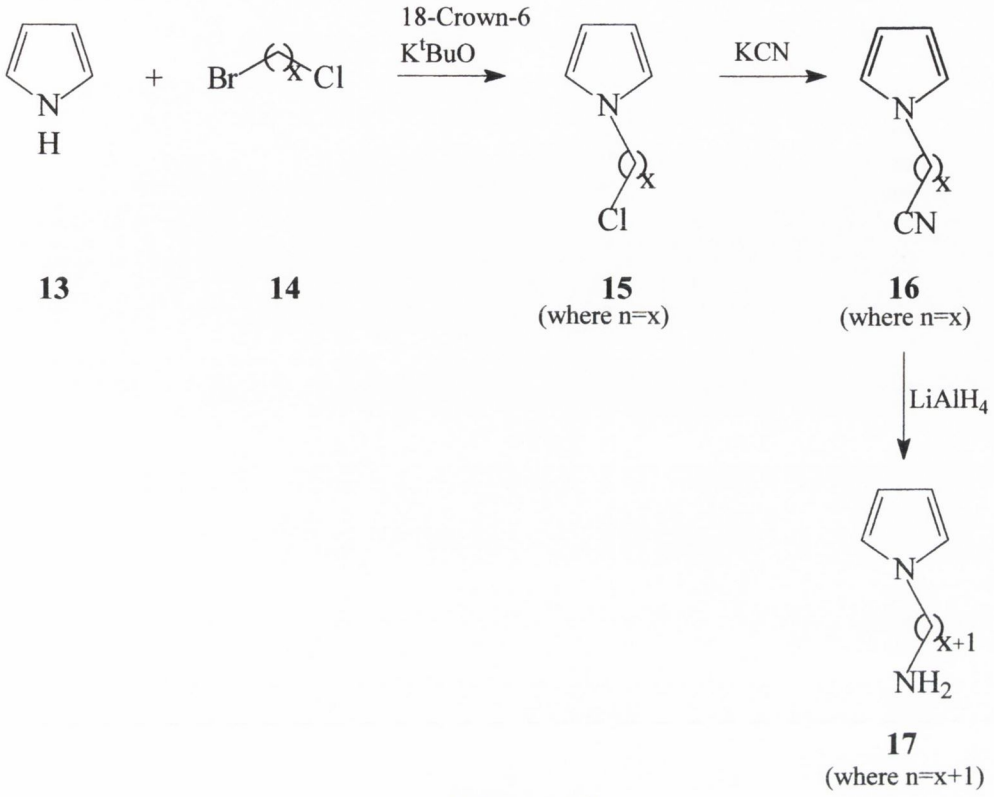
2.3 INITIAL STRATEGIES EMPLOYED FOR THE SYNTHESIS OF HYBRID MONOMERS



Scheme 2.4

In order to synthesise monomers of variable alkyl chain length; it was first necessary to design a synthesis for making N-(aminoalkyl)pyrroles. The formation of N-substituted pyrroles from the reaction of 2,5-dimethoxyfuran has been previously reported. The reaction of primary amines with 2,5-dimethoxyfuran results in the synthesis of the corresponding N-substituted pyrrole. For example, the reaction of glycine with 2,5-dimethoxyfuran to produce pyrroloacetic acid has been achieved using this method. However all attempts to utilize this procedure using 1,6 hexadiamine or similarly substituted diamines proved futile. This may be attributed to the presence of two amine groups on the substrate compared to the literature synthesis, which employed substrates with a single amine group. It was therefore decided to try and couple ferrocene carboxylic acid to one of the amine groups on the diamine moiety and then proceed with the pyrrole formation. This strategy was also unsuccessful. As may have been conceivable the diamine was disubstituted with the ferrocenoyl group, as shown in Scheme 2.4. However, several attempts to remedy this outcome were made and proved unsuccessful with **12** being generated as the only product, this outcome is illustrated in Scheme 2.4. Attempts to overcome this outcome included: using a large excess of amine (10 equivalents); and carrying out the reaction at $-10^{o}C$ with the addition of the diluted ferrocene species over four hours.

2.4 PREPARATION OF N-SUBSTITUTED PYRROLES



13 **14** **15** (where n=x) **16** (where n=x)

17 (where n=x+1)

Scheme 2.5

An alternative approach was adopted in order to synthesise the required N-(aminoalkyl)pyrrole moieties, **17** (n=3-7). This was achieved as outlined in Scheme 2.5. Firstly, the N-(chloroalkyl)pyrrole, **15**, was prepared through the Guida and Mathre method of phase transfer alkylation of pyrrole,**13**, employing 18-Crown-6 as the catalyst and potassium *tert*-butoxide as the base in dry diethyl ether.[6] This procedure proved to be convenient, mild and generally high yielding. Yields for this reaction were found to occur within a range of 92-95%, these were based on the initial pyrrole concentration. Subsequently, the N-(chloroalkyl)pyrrole, **15** was converted to N-(cyanoalkyl)pyrrole, **16**, through an adaptation of the procedure devised by Patterson *et al.*[7] This involved the reflux of the required N-(chloroalkyl)pyrrole, **15**, with potassium cyanide using dimethyl sulfoxide, DMSO, as solvent. Once more this proved to be a high yielding experiment with yields falling in the range of 88-95%. In this case the N-(chloroalkyl)pyrrole was the limiting factor in the reaction. Finally, reduction of the nitrile group to the primary amine to produce the N-(aminoalkyl)pyrrole, **17**, was achieved using lithium aluminium hydride in dry diethyl ether under air and water sensitive conditions as

outlined by Amundsen and Nelson.[8] This resulted in an 83-88% yield of the required complex. There was one exception to this range, the synthesis of N-(6-aminohexyl)pyrrole resulted in a lower yield than usual, the reason for this is believed to have been the condition of the lithium aluminium hydride. This reagent is readily hydrolysed and its activity may reduce over time. Nevertheless, the overall synthesis was found to be very reproducible and compounds N-(4-aminobutylpyrrole), **17** n=4, N-(5-aminopentyl)pyrrole, **17** n=5, N-(5-chloropentyl)pyrrole), **15** n=5, N-(5-cyanopentyl)pyrrole, **16** n=5, N-(6-aminohexyl)pyrrole, **17** n=6, N-(6-chlorohexyl)pyrrole), **15** n=6, N-(6-cyanohexyl)pyrrole **17** n=6, and N-(7-aminoheptly)pyrrole **17** n=7, are novel pyrrole derivatives which may be produced with ease. The individual yields of these reactions are presented in Table 2.1 below.

Table 2.1

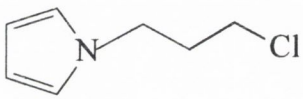
Yields of the pyrrole derivatives

N-substituted pyrrole		Yield, %
N-(3-aminopropyl)pyrrole	**17 n = 3**	87
N-(3-chloropropyl)pyrrole	**15 n = 3**	92
N-(3-cyanopropyl)pyrrole	**16 n = 3**	95
N-(4-aminobutyl)pyrrole	**17 n = 4**	88
N-(4-chlorobutyl)pyrrole	**15 n = 4**	91
N-(4-cyanobutyl)pyrrole	**16 n = 4**	88
N-(5-aminopentyl)pyrrole	**17 n = 5**	83
N-(5-chloropentyl)pyrrole	**15 n = 5**	92
N-(5-cyanopentyl)pyrrole	**16 n = 5**	95
N-(6-aminohexyl)pyrrole	**17 n = 6**	58
N-(6-chlorohexyl)pyrrole	**15 n = 6**	95
N-(6-cyanohexyl)pyrrole	**16 n = 6**	95
N-(7-aminoheptyl)pyrrole	**17 n = 7**	88

The spectroscopic characterisation of compounds **17 n=3** has been previously reported[9] and is in agreement with the key resonances of the compounds described in tables 2.4. Patterson *et al*[7] previously reported the synthesis of compounds **15 n=3, 16 n=3, 15 n=4** and **16 n=4** however no spectroscopic characterisation was carried out at that time (1962). Tables 2.2, 2.3, 2.5-2.14 describe the spectroscopic characterisation of compounds **15 n= 3-6**, **16 n= 3-6** and **17 n= 4-7**. A short discussion of how the peaks were assigned is included.

Table 2.2

NMR Spectroscopic details for *N- (3-Chloropropyl)pyrrole*



15 n=3

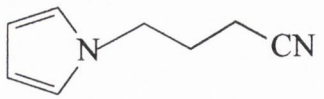
^{13}C (ppm)	^{1}H (ppm)	Multiplicity(^{1}H NMR)	Assignment
CH_2 32.1	2.26-2.29	m	CH_2CH_2Cl
CH_2 41.3	3.53-3.57	t, J = 6.0Hz	CH_2Cl
CH_2 45.6	4.15-4.19	t, J = 6.5Hz	PyrroleNCH_2
CH 108.1	6.28	s	s, 2 x pyrrole CH_α
CH 120.3	6.78	s	s, 2 x pyrrole CH_β

The NMR spectroscopic data obtained for **15 n=3** are summarised in Table 2.2. Key resonances in the ^{1}H NMR spectrum included a multiplet in the range δ_H 2.26-2.29 ppm, which was assigned to the CH_2CH_2Cl group split by the two adjacent CH_2 protons. These adjacent protons are observed as two triplets in the spectrum at δ_H 3.53-3.57 and 4.15-4.19ppm. The former was assigned to the CH_2Cl protons and the latter to the pyrroleNCH_2 protons. These assignments are is consistent with the fact that CH_2Cl protons resonate in the range of δ_H 3.6-3.8ppm, whereas protons adjacent to an aromatic group are shifted downfield due to an increased deshielding effect of the pi electrons of the aromatic ring. Signals for the *CH* protons of the pyrrole group are apparent at δ_H 6.28 and 6.78ppm.

The carbon resonances were assigned with the aid of ^{13}C DEPT and ^{13}C-^{1}H COSY experiments and are described in Table 2.2.

Table 2.3

NMR Spectroscopic details for *N- (3-Cyanopropyl) pyrrole*



16 n=3

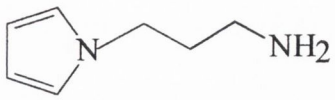
^{13}C (ppm)	^{1}H (ppm)	Multiplicity (^{1}H NMR)	Assignment
CH_2 26.8	2.06-2.09	m	CH_2CH_2CN
CH_2 13.8	2.20-2.24	t, J= 6.5 Hz	CH_2CN
CH_2 47.0	4.01-4.05	t, J= 6.5Hz	PyrroleNCH_2
CH 108. 4	6.24	s	s, 2 x pyrrole CH_α
CH 120.1	6.70	s	s, 2 x pyrrole CH_β
CN 118.5			

The NMR spectroscopic data obtained for **16 n=3** are summarised in Table 2.3. On comparison of the ^{1}H spectrum of **16 n=3** with that of the starting material **15 n=3** it is clear that the characteristic triplet due to the CH_2Cl protons, observed in the spectrum of the chloro derivative, δ_H 3.53-3.57 has shifted to δ_H 2.20-2.24ppm. Other significant signals in the ^{1}H NMR spectrum included a multiplet in the range δ_H 2.06-2.09 ppm, which was assigned to the CH_2CH_2CN group split by the two adjacent CH_2 protons. A triplet observed at 4.01-4.05ppm was assigned to the pyrroleNCH_2 protons. Signals for the *CH* protons of the pyrrole group are apparent at δ_H 6.24 and 6.70ppm.

The carbon resonances were assigned with the aid of ^{13}C DEPT and are described in Table 2.3. It should be noted that a shift in the signal for the *C*CN carbon was apparent. In this instance the shift was from δ_C 41.3 to 13.8ppm. This dramatic shift may be attributed to the fact that the cyano group causes more shielding of the carbon atom and results in the signal being shifted upfield. On comparison with the ^{13}C spectrum of **16 n=3**, a peak was evident at δ_C 118.8ppm and was assigned to the quaternary cyano carbon, this was supported by the disappearance of the peak in ^{13}C DEPT experiments.

Table 2.4

NMR Spectroscopic details for *N- (3-Aminopropyl)pyrrole*



17 n+1=3

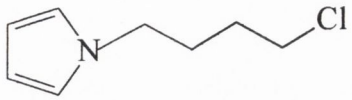
^{13}C (ppm)	^{1}H (ppm)	Multiplicity (^{1}H NMR)	Assignment
CH_2 34.6	1.89–1.96	m	$CH_2CH_2NH_2$
CH_2 38.9	2.71-2.74	t, 6.5Hz	CH_2NH_2
CH_2 46.7	3.97-4.01	t, 6.0Hz	PyrroleNCH_2
CH 107.6	6.16	s	s, 2 x pyrrole CH_α
CH 120.1	6.69	s	s, 2 x pyrrole CH_β

The NMR spectroscopic data obtained for **17 n=3** are summarised in Table 2.4. On comparison of the ^{1}H spectrum of the **17 n=3** with **16 n=3** it is apparent that the characteristic triplet of the CH_2CN, observed at δ_H 2.3 ppm has shifted to δ_H 2.7 ppm, and is now indicative of the CH_2NH_2 protons in the spectrum of **17 n=3**. Other significant signals in the ^{1}H NMR spectrum included a multiplet in the range δ_H 1.89-1.96 ppm, which was assigned to the $CH_2CH_2NH_2$ group split by the two adjacent CH_2 protons. A triplet observed at 3.97-4.01ppm was assigned to the pyrroleNCH_2 protons. Signals for the C*H* protons of the pyrrole group are apparent at δ_H 6.24 and 6.70ppm

The carbon resonances were assigned as previously described with the aid of ^{13}C DEPT and are described in Table 2.3. It should be noted that a shift in the signal for the CNH_2carbon was also apparent. In this instance the shift was fromδ_C 13.8 to 38.9ppm. In this case the shift may be attributed to the decreasing electron density of the amino group at the carbon atom compared to the cyano group of the starting material, hence the increased deshielding effect shifts the signal downfield.

Table 2.5

NMR Spectroscopic details for *N- (4-Chlorobutyl)pyrrole*



15 n=4

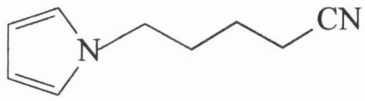
^{13}C (ppm)	^{1}H (ppm)	Multiplicity (^{1}H NMR)	Assignment
CH_2 29.3	1.80-1.84	m	CH_2CH_2Cl
CH_2 28.4	1.98-2.02	m	$CH_2CH_2CH_2Cl$
CH_2 44.0	3.56-3.59	t, J = 6.5Hz	CH_2Cl
CH_2 48.4	3.97-4.00	t, J = 7.0Hz	PyrroleNCH_2
CH 107.8	6.23	s	s, 2 x pyrrole CH_α
CH 120.0	6.72	s	s, 2 x pyrrole CH_β

The NMR spectroscopic data obtained for **15 n=4** are summarised in Table 2.5. Key resonances in the ^{1}H NMR spectrum included two multiplets in the range δ_H 1.80-18.4 and 1.98-2.02 ppm. The latter was assigned to $CH_2CH_2CH_2Cl$ protons; this multiplet is evident in the other spectra of the butyl derivatives and is assigned on the basis that it is not affected by the terminal substituent on the alkyl chain. The former multiplet was assigned to the CH_2CH_2Cl protons. The remaining protons in the aliphatic chain are observed as two triplets in the spectrum at δ_H 3.56-3.59 and 3.97-4.00ppm. The former was assigned to the CH_2Cl protons and the latter to the pyrroleNCH_2 protons. These peaks are in agreement with the previously assigned equivalent peaks of N- (3-cyanopropyl) pyrrole. Signals for the *CH* protons of the pyrrole group are apparent at δ_H 6.23 and 6.72ppm.

The carbon resonances were assigned with the aid of ^{13}C DEPT and ^{13}C-^{1}H COSY experiments and are described in Table 2.5.

Table 2.6

NMR Spectroscopic details for *N- (4-Cyanobutyl)pyrrole*



16 n=4

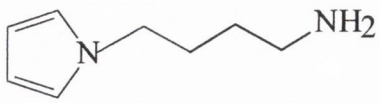
^{13}C (ppm)	^{1}H (ppm)	Multiplicity (^{1}H NMR)	Assignment
CH_2 22.3	1.62-1.66	m	CH_2CH_2CN
CH_2 29.9	1.92-1.96	m	$CH_2CH_2CH_2CN$
CH_2 16.7	2.30-2.31	t, J = 7.0Hz	CH_2CN
CH_2 48.2	3.80-3.97	t, J = 6.5Hz	PyrroleNCH_2
CH 108.0	6.17	s	s, 2 x pyrrole CH_α
CH 119.9	6.65	s	s, 2 x pyrrole CH_β
CN 118.8			

The NMR spectroscopic data obtained for **16 n=4** are summarised in Table 2.6. On comparison of the ^{1}H spectrum of **16 n=4** with that of the starting material **15 n=4** it is evident that the triplet due to the CH_2Cl protons, observed in the spectrum of the chloro derivative, δ_H 3.56-3.59, has shifted to δ_H 2.30-2.31ppm. As stated previously the cyano group results in increased shielding and shifts the signal upfield. This conclusion is also reported for the **n = 3** range of N-substituted alkyl pyrroles. A shift was also observed for the multiplet from δ_H 1.80-1.84 to 1.62-1.66ppm and was assigned to the CH_2CH_2CN. This lesser shift may be attributed to the effect of the cyano group on the protons attached to the second carbon in the chain. A triplet observed at δ_H 3.80-3.97ppm was assigned to the pyrroleNCH_2 protons and a multiplet at δ_H 1.92-1.96ppm, was were assigned to the $CH_2CH_2CH_2CN$ protons.

The carbon resonances were assigned with the aid of ^{13}C DEPT and ^{13}C-^{1}H COSY experiments and are described in Table 2.6. It should be noted that a shift in the signal for the *C*CN carbon was apparent once more. In this instance the shift was from δ_C 44.0 to16.7ppm. In addition, a peak was evident at δ_C 118.8ppm in the ^{13}C spectrum and was attributed to the presence of the quaternary cyano carbon, this was supported by ^{13}C DEPT experiments.

Table 2.7

NMR Spectroscopic details for *N- (4-Aminobutyl)pyrrole*,[8] 17 n=4



17 n=4

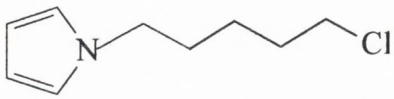
^{13}C (ppm)	^{1}H (ppm)	Multiplicity (^{1}H NMR)	Assignment
CH_2 28.5	1.44-1.49	m	$CH_2CH_2NH_2$
CH_2 30.5	1.80-1.86	m	$CH_2CH_2CH_2NH_2$
CH_2 41.3	2.72-2.75	t, J = 7.0Hz	CH_2NH_2
CH_2 49.0	3.91-3.95	t, J = 7.0Hz	PyrroleNCH_2
CH 107.5	6.19	s	s, 2 x pyrrole CH_α
CH 120.0	6.70	s	s, 2 x pyrrole CH_β

The NMR spectroscopic data obtained for **17 n=4** are summarised in Table 2.7. On comparison of the ^{1}H spectrum of the **17 n=4** with the homologous **16 n=4** it is apparent that the characteristic triplet of the CH_2CN observed at δ_H 2.3 ppm has shifted to δ_H 2.7 ppm, and is now indicative of the CH_2NH_2 in the spectrum of **17 n=4**. This shift is characteristic of the deshielding effects of the NH_2 group. Similarly, a shift is observed in the multiplet assigned for the CH_2CH_2CN protons at δ_H 1.62 ppm to δ_H 1.44-1.49 ppm for the $CH_2CH_2NH_2$ protons. Other significant signals in the ^{1}H NMR spectrum included a multiplet in the range δ_H 1.80-1.86 ppm, which was assigned to the $CH_2CH_2CH_2NH_2$ group split by the two adjacent CH_2 protons. A triplet observed at δ_H 3.91-3.95ppm was assigned to the pyrroleNCH_2 protons.

The carbon resonances were assigned as previously described with the aid of ^{13}C DEPT and are described in Table 2.7. It should be noted that a shift in the signal for the CNH_2 carbon was also apparent. In this instance the shift was from δ_C 16.7 to 41.3ppm. As stated previously, the shift may be attributed to the decreasing electron density of the amino group at the carbon atom, hence the increased deshielding effect shifts the signal downfield.

Table 2.8

NMR Spectroscopic details for *N- (5-Chloropentyl)pyrrole*, 15 n=5



15 n=5

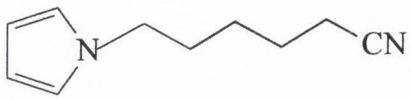
^{13}C (ppm)	^{1}H (ppm)	Multiplicity (^{1}H NMR)	Assignment
CH_2 23.7	1.50-1.52	m	$CH_2CH_2CH_2Cl$
CH_2 30.5, 31.7	1.82-1.87	m	$CH_2CH_2CH_2CH_2Cl$
CH_2 30.5, 31.7	1.82-1.87	m	$CH_2CH_2CH_2CH_2Cl$
CH_2 44.3	3.55-3.58	t, J = 7.0Hz	CH_2Cl
CH_2 48.9	3.92-3.96	t, J = 7.0Hz	PyrroleNCH_2
CH 107.6	6.20	s	s, 2 x pyrrole CH_α
CH 120.0	6.70	s	s, 2 x pyrrole CH_β

The NMR spectroscopic data obtained for **15 n=5** are summarised in Table 2.8. The ^{1}H NMR spectrum included a multiplet in the range δ_H 1.50-1.52ppm and was assigned to $CH_2CH_2CH_2Cl$ as these protons have the most aliphatic environment and are least influenced by the chlorine and aromatic terminal substituents. Consequently they are shifted further upfield. A second multiplet was apparent at 1.82-1.87ppm and integration of this peak indicated the presence of four protons. This was assigned to the CH_2CH_2Cl and the $CH_2(CH_2)_3Cl$ protons on the basis that the latter protons resonated at this frequency for the all propyl and butyl derivatives whereas the former protons for both N- (3-chloropropyl)pyrrole and N- (4-chlorobutyl) pyrrole had a value of approximately δ_H 1.8ppm.The remaining protons in the aliphatic chain are observed as two triplets in the spectrum at δ_H 3.55-3.58 and 3.92-3.96ppm. The former was assigned to the CH_2Cl protons and the latter to the pyrroleNCH_2 protons. These peaks are in agreement with the previously assigned equivalent peaks of N- (3-chloropropyl)pyrrole and N- (4-chlorobutyl) pyrrole. Signals for the CH protons of the pyrrole group are apparent at δ_H 6.20 and 6.70ppm.

The carbon resonances were assigned with the aid of ^{13}C DEPT and ^{13}C-^{1}H COSY experiments and are described in Table 2.8. Carbon peaks at δ_C 30.5 and 31.7ppm were assigned to $CH_2CH_2CH_2CH_2Cl$. Individual assignment of these peaks was not achievable through ^{13}C-^{1}H COSY experiments.

Table 2.9

NMR Spectroscopic details for *N- (5-Cyanopentyl)pyrrole*, 16 n=5



16 n=5

^{13}C (ppm)	^{1}H (ppm)	Multiplicity (^{1}H NMR)	Assignment
CH_2 27.3	1.47-1.48	m	$CH_2CH_2CH_2CN$
CH_2 25.5	1.66-1.68	m	CH_2CH_2CN
CH_2 30.3	1.81-1.85	m	$CH_2(CH_2)_3CN$
CH_2 16.6	2.32-2.35	t, J = 7.0Hz	CH_2CN
CH_2 48.7	3.91-3.94	t, J = 7.0Hz	PyrroleNCH_2
CH 107.7	6.17	s	s, 2 x pyrrole CH_α
CH 120.0	6.67	s	s, 2 x pyrrole CH_β
CN 118.8			

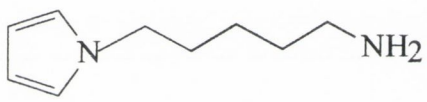
The NMR spectroscopic data obtained for **16 n=5** are summarised in Table 2.9. ^{1}H-^{1}H COSY experiments were carried out but did not aid in the assignment of the signals, it was therefore decided to assign the peaks in accordance with those assigned for the propyl and butyl derivatives. On comparison of the ^{1}H spectrum of **16 n=5** with that of the starting material **15 n=5** it is clear that the characteristic triplet due to the CH_2Cl protons observed in the spectrum of the chloro derivative, δ_H 3.55-3.58 has shifted to δ_H 2.32-2.35ppm in the spectrum of the cyano moiety. A shift was also observed for the multiplet from δ_H 1.82-1.87 to 1.66-1.68ppm and was assigned to the CH_2CH_2CN. This is consistent with the shifts observed for the propyl and butyl derivatives. A second multiplet, apparent at δ_H 1.81-1.85ppm, was assigned to the $CH_2(CH_2)_3$CN protons on the basis that these protons had a shift of approximately δ_H 1.8ppm for all other N-subsituted pyrrole derivatives. The multiplet at δ_H 1.47-1.48ppm was assigned to the $CH_2CH_2CH_2$CN protons and agrees with that

found for the $CH_2CH_2CH_2Cl$ protons of **15 n=5**. A triplet observed at δ_H 3.91-3.94ppm was assigned to the pyrroleNCH_2 protons.

The carbon resonances were assigned with the aid of ^{13}C DEPT and ^{13}C-^{1}H COSY experiments and are described in Table 2.9. It should be noted that a shift in the signal for the *C*CN carbon was apparent once more. In this instance the shift was from δ_C 44.3 to 16.6ppm. In addition, a peak was evident at δ_C 118.8ppm in the ^{13}C and was attributed to the presence of the quaternary cyano carbon, this was supported by the disappearance of the peak in ^{13}C DEPT experiments.

Table 2.10

NMR Spectroscopic details for *N- (5-Aminopentyl)pyrrole*, 17 n=5



17 n=5

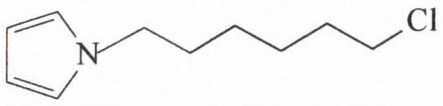
^{13}C (ppm)	^{1}H (ppm)	Multiplicity (^{1}H NMR)	Assignment
CH_2 26.7	1.32-1.36	m	$CH_2CH_2NH_2$ **or** $CH_2CH_2CH_2NH_2$
CH_2 32.8	1.44-1.48	m	$CH_2CH_2NH_2$ **or** $CH_2CH_2CH_2NH_2$
CH_2 30.9	1.79-1.82	m	$CH_2(CH_2)_3NH_2$
CH_2 41.5	2.68-2.72	t, J = 7.0Hz	CH_2NH_2
CH_2 49.5	3.88-3.91	t, J = 7.0Hz	PyrroleNCH_2
CH 107.4	6.15	s	s, 2 x pyrrole CH_α
CH 120.0	6.66	s	s, 2 x pyrrole CH_β

The NMR spectroscopic data obtained for **17 n=5** are summarised in Table 2.10. ^{1}H-^{1}H COSY experiments were carried out but did not aid in the assignment of the signals, it was therefore decided to assign the peaks in accordance with those assigned for N- (5-Chloropentyl)pyrrole, **15 n=5**, and N- (5-Cyanopentyl)pyrrole, **16 n=5**. On comparison of the ^{1}H spectrum of the **17 n=5** with the homologous **16 n=5** it is apparent that the characteristic triplet of the CH_2CN observed at δ_H 2.3 ppm has shifted to δ_H 2.7 ppm, and is now indicative of the CH_2NH_2 in the spectrum of **17 n=4**. Other significant signals in the ^{1}H NMR spectrum included a multiplet in the range δ_H 1.79-1.82 which was assigned to the $CH_2(CH_2)_3NH_2$ protons on the basis that these protons had a shift of approximately δ_H 1.8ppm for all other N-substituted pyrrole derivatives. The remaining multiplets at δ_H 1.32-1.36 and 1.47-1.48ppm could not be assigned conclusively. However, it is believed that the latter signal is due to the $CH_2CH_2CH_2NH_2$ protons and agrees with that found for the $CH_2CH_2CH_2Cl$ protons of **15 n=5** and the $CH_2CH_2CH_2CN$ protons of **16 n=5**. A triplet observed at δ_H 3.88-3.91ppm was assigned to the pyrroleNCH_2 protons. Signals for the C*H* protons of the pyrrole group are apparent at δ_H 6.15 and 6.66ppm

The carbon resonances were assigned as previously described with the aid of ^{13}C DEPT and ^{13}C-^{1}H COSY experiments and are described in Table 2.10. It should be noted that a shift in the signal for the *C*CN carbon was also apparent. In this instance the shift was from δ_C 16.6 to 41.5ppm.

Table 2.11

NMR Spectroscopic details for *N- (6-Chlorohexyl)pyrrole*, 15 n=6



15 n=6

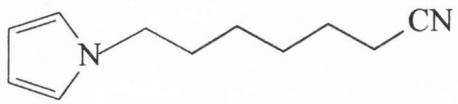
^{13}C (ppm)	^{1}H (ppm)	Multiplicity (^{1}H NMR)	Assignment
CH_2 24.8	1.30-1.35	m	$CH_2(CH_2)_2Cl$ **or** $CH_2(CH_2)_3Cl$
CH_2 25.2	1.49-1.53	m	$CH_2(CH_2)_2Cl$ **or** $CH_2(CH_2)_3Cl$
CH_2 30.8, 31.2	1.81-1.92	m	$CH_2(CH_2)_2CH_2CH_2Cl$
CH_2 44.2	3.55-3.57	t, J = 7.0Hz	CH_2Cl
CH_2 49.1	3.92-3.94	t, J = 7.0Hz	PyrroleNCH_2
CH 107.6	6.18	s	s, 2 x pyrrole CH_α
CH 120.0	6.68	s	s, 2 x pyrrole CH_β

The NMR spectroscopic data obtained for **15 n=6** are summarised in Table 2.11. The ^{1}H NMR spectrum included a multiplet at 1.81-1.92ppm and integration of this peak indicated the presence of four protons. This was assigned to the CH_2CH_2Cl and the $CH_2(CH_2)_4Cl$ protons on the basis that the latter protons resonated at this frequency for the all propyl, butyl and pentyl derivatives whereas the former protons for both N- (3-chloropropyl)pyrrole, N- (4-chlorobutyl) pyrrole and N- (5-chloropentyl) pyrrole had a value of approximately δ_H 1.8ppm. The remaining two multiplets in the range δ_H 1.30-1.35ppm and δ_H 1.49-1.53ppm were assigned to $CH_2CH_2CH_2Cl$ and $CH_2(CH_2)_3Cl$, ^{1}H-^{1}H COSY experiments were carried out but did not aid in the differentiation of these signals. The remaining protons in the aliphatic chain are observed as two triplets in the spectrum at δ_H 3.55-3.57 and 3.92-3.94ppm. The former was assigned to the CH_2Cl protons and the latter to the pyrroleNCH_2 protons. Signals for the CH protons of the pyrrole group are apparent at δ_H 6.20 and 6.70ppm.

The carbon resonances were assigned with the aid of ^{13}C DEPT and ^{13}C-^{1}H COSY experiments and are described in Table 2.11.

Table 2.12

NMR Spectroscopic details for *N- (6-Cyanohexyl)pyrrole*, 16 n=6



16 n=6

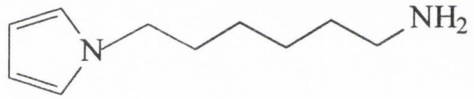
^{13}C (ppm)	^{1}H (ppm)	Multiplicity (^{1}H NMR)	Assignment
CH_2 26.3	1.31-1.37	m	$CH_2(CH_2)_2CN$ **or** $CH_2(CH_2)_3CN$
CH_2 27.1	1.47-1.53	m	$CH_2(CH_2)_2CN$ **or** $CH_2(CH_2)_3CN$
CH_2 31.0	1.66-1.70	m	CH_2CH_2CN
CH_2 33.3	1.77-1.81	m	$CH_2(CH_2)_4CN$
CH_2 16.8	2.35-2.41	t, J = 7.0Hz	CH_2CN
CH_2 49.1	3.87-3.91	t, J = 7.0Hz	PyrroleNCH_2
CH 107.4	6.17	s	s, 2 x pyrrole CH_α
CH 120.0	6.67	s	s, 2 x pyrrole CH_β
CN 118.7			

The NMR spectroscopic data obtained for 16 n=6 are summarised in Table 2.12. On comparison of the ^{1}H spectrum of **16 n=6** with that of the starting material **15 n=6** it is clear that the characteristic triplet due to the CH_2Cl protons observed in the spectrum of the chloro derivative, δ_H 3.55-3.57 has shifted to δ_H 2.35-2.41ppm in the spectrum of the cyano moiety. A shift was also observed for the multiplet from δ_H 1.81-1.92 to 1.66-1.70ppm and was assigned to the CH_2CH_2CN. This lesser shift may be attributed to the effect of the cyano group on the protons attached to the second carbon in the chain. Moreover, these shift are in agreement with the shifts observed for the propyl, butyl and pentyl derivatives. A second multiplet, apparent at δ_H 1.77-1.81ppm, was assigned to the $CH_2(CH_2)_4CN$ protons on the basis that these protons had a shift of approximately δ_H 1.8ppm for all other N-substituted pyrrole derivatives. The remaining two multiplets in the range δ_H 1.31-1.37ppm and δ_H 1.47-1.53ppm were assigned to $CH_2(CH_2)_2CN$ and $CH_2(CH_2)_3CN$, ^{1}H-^{1}H COSY experiments were carried out but did not aid in the differentiation of these signals. A triplet observed at δ_H 3.87-3.91ppm was assigned to the pyrroleNCH_2 protons.

The carbon resonances were assigned with the aid of ^{13}C DEPT and ^{13}C-^{1}H COSY experiments and are described in Table 2.12. It should be noted that a shift in the signal for the *C*CN carbon was apparent once more. In this instance the shift was from δ_C 44.2 to 16.7ppm. In addition, a peak was evident at δ_C 118.7ppm in the ^{13}C and was attributed to the presence of the quaternary cyano carbon, this was supported by the disappearance of the peak in ^{13}C DEPT experiments.

Table 2.13

NMR Spectroscopic details for *N- (6-Aminohexyl)pyrrole*, 17 n=6



17 n=6

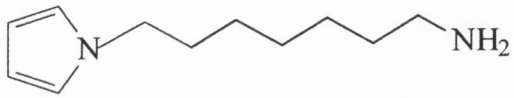
^{13}C (ppm)	^{1}H (ppm)	Multiplicity (^{1}H NMR)	Assignment
CH_2 26.0, 26.1	1.31-1.38	m	$CH_2CH_2NH_2$ **or** $(CH_2)_2(CH_2)_2NH_2$
CH_2 33.2	1.43-1.47	m	$CH_2CH_2NH_2$ **or** $(CH_2)_2(CH_2)_2NH_2$
CH_2 31.0	1.77-1.81	m	$CH_2(CH_2)_4NH_2$
CH_2 41.6	2.68-2.71	t, J = 7.0Hz	CH_2NH_2
CH_2 49.1	3.87-3.91	t, J = 7.0Hz	PyrroleNCH_2
CH 107.4	6.17	s	s, 2 x pyrrole CH_α
CH 120.0	6.67	s	s, 2 x pyrrole CH_β

The NMR spectroscopic data obtained for **17 n=6** are summarised in Table 2.13. On comparison of the ^{1}H spectrum of the **17 n=6** with the homologous **16 n=6** it is apparent that the characteristic triplet of the CH_2CN observed at δ_H 2.4 ppm has shifted to δ_H 2.7 ppm, and is now indicative of the CH_2NH_2. in the spectrum of **17 n=6**. This shift is in accordance with those reported for the propyl, butyl and pentyl derivatives. Other significant signals in the ^{1}H NMR spectrum included a multiplet in the range δ_H 1.77-1.81 which was assigned to the $CH_2(CH_2)_4NH_2$ protons on the basis that these protons had a shift of approximately δ_H 1.8ppm for all other N-substituted pyrrole derivatives. The remaining two multiplets in the range δ_H 1.31-1.38ppm and δ_H 1.43-1.47ppm were assigned to $(CH_2)_3CH_2CN$, ^{1}H-^{1}H COSY experiments were carried out but did not aid in the differentiation of these signals. Integration of the latter peak indicated the presence of four protons A triplet observed at δ_H 3.87-3.91ppm was assigned to the pyrroleNCH_2 protons. Signals for the CH protons of the pyrrole group are apparent at δ_H 6.15 and 6.66ppm

The carbon resonances were assigned as previously described with the aid of ^{13}C DEPT and ^{13}C-^{1}H COSY experiments and are described in Table 2.13. It should be noted that a shift in the signal for the *C*CN carbon was also apparent. In this instance the shift was fromδ_C 16.7 to 41.6ppm.

Table 2.14

NMR Spectroscopic details for *N- (7-Aminoheptyl)pyrrole*, 17 n=7



17 n=7

^{13}C (ppm)	^{1}H (ppm)	Multiplicity (^{1}H NMR)	Assignment
CH_2 26.2, 26.3	1.21-1.25	m	$(CH_2)_4NH_2$
CH_2 28.5, 33.3	1.43-1.46	m	
CH_2 31.0	1.76-1.80	m	$CH_2(CH_2)_4NH_2$
CH_2 41.7	2.67-2.70	t, J = 7.0Hz	CH_2NH_2
CH_2 49.1	3.86-3.90	t, J = 7.0Hz	PyrroleNCH_2
CH 107.3	6.15	s	s, 2 x pyrrole CH_α
CH 119.9	6.66	s	s, 2 x pyrrole CH_β

The NMR spectroscopic data obtained for **17 n=7** are summarised in Table 2.14. On comparison of the spectra with those obtained for **17 n = 3, 4, 5 and 6** it was apparent that the triplet observed at 2.67-2.70 corresponded to CH_2NH_2, in addition the triplet observed at δ_H 3.86-3.90ppm was assigned to the pyrroleNCH_2. Furthermore, a multiplet in the range δ_H 1.76-1.80 was assigned to the $CH_2(CH_2)_5NH_2$ protons on the basis that these protons had a shift of approximately δ_H 1.8ppm for all other N-substituted pyrrole derivatives. Other significant signals in the ^{1}H NMR spectrum included two multiplets in the range δ_H 1.21-1.25 and 1.43-1.46ppm were assigned to the $(CH_2)_4CH_2NH_2$ protons, it was not possible to distinguish individual assignments in this case. Integration of the both these peaks indicated the presence of four protons. Signals for the *CH* protons of the pyrrole group are apparent at δ_H 6.15 and 6.66ppm

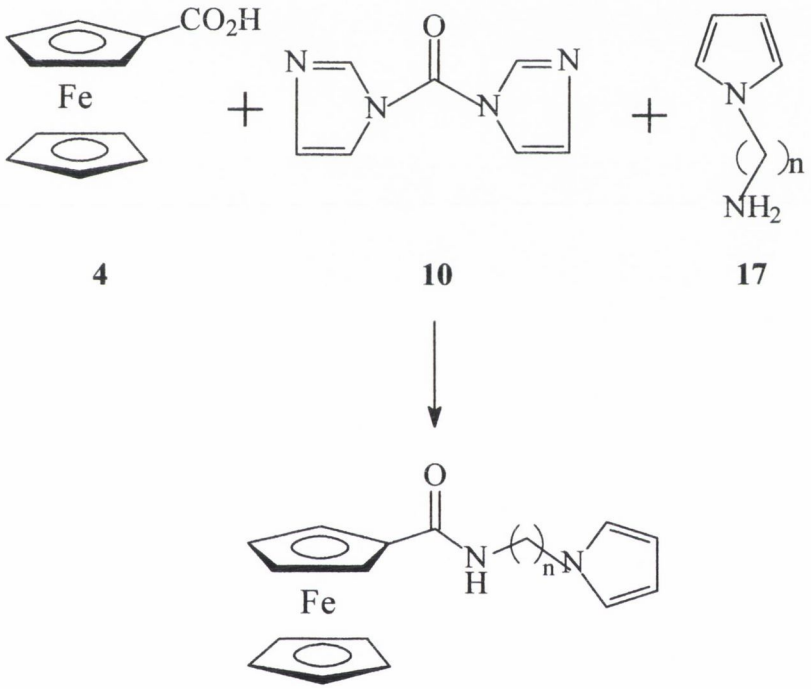
The carbon resonances were assigned as previously described with the aid of ^{13}C DEPT and ^{13}C-^{1}H COSY experiments and are described in Table 2.14.

2.5 HYBRID FORMATION

2.5.1 The Coupling Reaction

The procedure employed for the preparation of the hybrid monomers is illustrated in Scheme 2.6. [3-(Pyrrol-1-yl)propyl]ferrocene-carboxamide, **18** n = 3, was prepared by reacting 1,1'-carbonyldiimidazole[10-13], **10**, with ferrocenecarboxylic acid, **4**, in dry tetrahydrofuran, THF and stirring overnight at room temperature. This was followed by the addition of N-(3-aminopropyl)pyrrole, **17** n=3, and further stirring for another 24hours. Purification of the black residue afforded the required product, [3-(Pyrrol-1-yl)propyl]ferrocene-carboxamide, **18** n=3, as an orange solid in an 87% yield. It should be noted that this was an improvement of 63% on the literature yield. Yields were calculated using ferrocene carboxylic acid, **4**, as the limiting reagent in all of the coupling experiments. Difficulties were encountered when following the literature synthesis.[14] However, these were overcome by employing a number of modifications. Firstly, the solvent system adopted was THF, as opposed to dichloromethane, DCM. Secondly, alternative purification techniques were adopted. These included the extraction of the product into DCM followed by the use of column chromatography instead of recrystallisation from methanol. It is thought that these modifications may account for the increased yield. The initial extraction of the product into DCM caused the separation of the imidazole by-products into the water phase. The ferrocene modified pyrrole moieties were slightly soluble in water and therefore this stage was done with great speed at room temperature. Not all the imidazole by-products could be eliminated in this manner without having a detrimental effect on the yield of product obtained. Drying over magnesium sulfate, filtration and evaporation to dryness resulted in an impure, orange solid being produced. Consequently, column chromatography techniques were employed to complete the purification process, the solvent system used in each case was 2:1 ethyl acetate: hexane. The preparation of [3-(Pyrrol-1-yl)propyl]-ferrocene-carboxamide was used to optimise the yield of the reaction and serve as a template for the preparation of the homologous hybrid monomers.

With the N-(aminoalkyl)pyrrole compounds, **17**, and the optimisation results in hand the coupling reactions were undertaken. [4-(Pyrrol-1-yl)butyl]ferrocene-carboxamide, **18** n=4, [5-(Pyrrol-1-yl)pentyl]ferrocene-carboxamide, **18** n=5, [6-(Pyrrol-1-yl)hexyl]ferrocene-carboxamide, **18** n=6, and [7-(Pyrrol-1-yl)heptyl]ferrocene-carboxamide, **18** n=7, were prepared in a similar manner with yields in the range of 80-87%, these are represented in tabular form, see table 2.15.



18
n = 3, 4, 5, 6 and 7

Scheme 2.6

Table 2.15

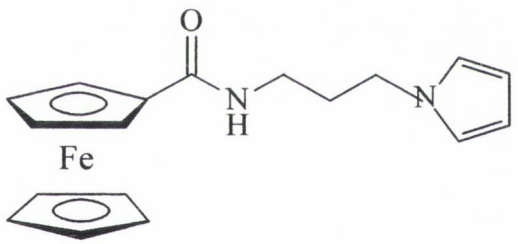
Yields of monomer preparations

Monomer		Yield (%)
[3-(Pyrrol-1-yl)propyl]ferrocene-carboxamide	**18 n =3**	87
[4-(Pyrrol-1-yl)butyl]ferrocene-carboxamide	**18 n =4**	80
[5-(Pyrrol-1-yl)pentyl]ferrocene-carboxamide	**18 n =5**	81
[6-(Pyrrol-1-yl)hexyl]ferrocene-carboxamide	**18 n =6**	75
[7-(Pyrrol-1-yl)heptyl]ferrocene-carboxamide	**18 n =7**	82

The spectroscopic characterization of the hybrid monomers of structure **18** is described in tables 2.16 to 2.20.

Table 2.16

NMR Spectroscopic details for *[3-(Pyrrol-1-yl)propyl]ferrocene-carboxamide]*



18 n=3

^{13}C (ppm)	**^{1}H (ppm)**	**Multiplicity (^{1}H NMR)**	**Assignment**
CH_2 31.2	2.04- 2.10	m	$CH_2CH_2CH_2$
CH_2 37.0	3.42- 3.47	dd, J = 6.0, 6.5	CH_2NH
CH_2 47.6	4.02- 4.05	t, J = 6.5Hz	PyrroleNCH_2
CH 69.2	4.19	s	Cp
CH 69.8	4.33	s	2(H_β-Cp-amide)
CH 67.6	4.60	s	2(H_α-Cp-amide)
	5.44	bs	N*H*
CH 108.3	6.25	s	s, pyrrole CH_α
CH 120.0	6.75	s	s, pyrrole CH_β
C=O 169.8			

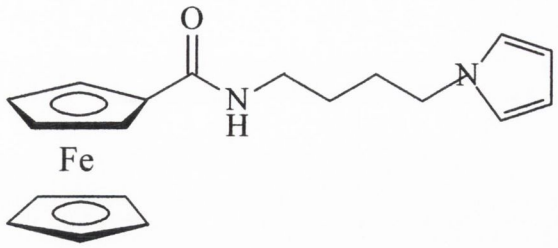
The NMR spectroscopic data obtained for **18 n=3** are summarised in Table 2.16. Key resonances in the ^{1}H NMR spectrum included a multiplet in the range δ_H 2.04-2.10ppm, which was assigned to the $CH_2CH_2CH_2$ group split by the two adjacent CH_2 protons. These adjacent protons are observed as a doublet of doublets and a triplet in the spectrum at δ_H 3.42-3.47 and 4.02-4.05ppm. The former was assigned to the CH_2NH protons and the latter to the pyrroleNCH_2 protons. The presence of a broad singlet at δ_H 5.44ppm was attributed to the amide proton. Other significant signals included three singlets at δ_H 4.19, 4.33 and 4.60ppm. These peaks integrated to show the presence of 5, 2 and 2 protons respectively. The peak at δ_H 4.19 was attributed to the cyclopentadienyl ring, Cp, and is accordance with values reported for the Cp ring of ferrocene carboxylic acid, δ_H 4.28ppm. The remaining two signals were assigned in accordance with their proximity to the CC=O group. The protons closest to this group, H_α-Cp-amide, are shifted more downfield to 4.60ppm whereas the final two protons, H_β-Cp-amide, have an environment closer to that of the unsubstituted Cp ring. Signals for the C*H* protons of the pyrrole group are apparent at δ_H 6.28 and 6.78ppm.

The carbon resonances were assigned with the aid of ^{13}C DEPT and ^{13}C-^{1}H COSY experiments and are described in Table 2.16. A significant signal was evident at δ_C 169.8ppm in the ^{13}C and was attributed to the presence of the quaternary carboxyl carbon, this was supported by the disappearance of the peak in ^{13}C DEPT experiments.

The remaining monomers of structure **18** showed similar peaks at approximately δ_H 4.19, 4.33, 4.60, 5.44, 6.25 and 6.75ppm.These were assigned as for **18** n = 3 and will not be discussed further in tables 2.17 to 2.20. Furthermore, the quarternary carbonyl carbon peak was evident in all spectra in the range δ_C 169.6-169.8ppm. The discussion will centre on the assignments of the alkyl chain protons and carbons. Microanalysis of all compounds was carried out and is shown in experimental section 2.75.

Table 2.17

NMR Spectroscopic details for *[4-(Pyrrol-1-yl)butyl]ferrocene-carboxamide],*



18 n=4

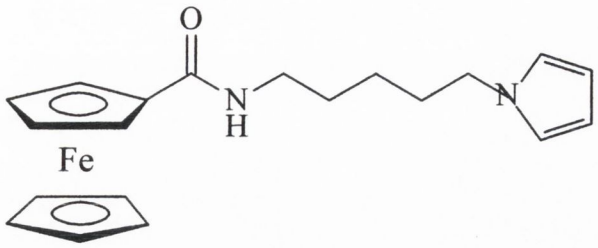
^{13}C (ppm)	^{1}H (ppm)	Multiplicity (^{1}H NMR)	Assignment
CH_2 26.8	1.55-1.62	m	CH_2CH_2NH
CH_2 28.4	1.84-1.91	m	$CH_2CH_2CH_2NH$
CH_2 38.5	3.34-3.42	dd, 6.5,7.0Hz	CH_2NH
CH_2 44.3	3.95-3.98	t, J = 7.0Hz	pyrroleNCH_2
CH 69.2	4.19	s	Cp
CH 69.8	4.33	s	2(H_β-Cp-amide)
CH 67.6	4.60	s	2(H_α-Cp-amide)
	5.68	bs	N*H*
CH 108.3	6.17	s	s, pyrrole CH_α
CH 120.0	6.68	s	s, pyrrole CH_β
C=O 169.8			

The NMR spectroscopic data obtained for **18 n=4** are summarised in Table 2.17. Key resonances in the ^{1}H NMR spectrum included two multiplets in the range δ_H 1.55-1.62 and 1.84-1.91ppm, these were assigned to the CH_2CH_2NH and the $CH_2CH_2CH_2NH$ groups respectively, both split by the two adjacent CH_2 protons. The latter peak is in agreement with the series of N-substituted pyrrole compounds, where the protons on the carbon adjacent to the pyrroleNCH_2 group had a shift of approximately δ_H 1.8ppm. The CH_2NH protons are observed as a doublet of doublets at δ_H 3.34-3.42ppm and the pyrroleNCH_2 protons as a triplet in the spectrum at δ_H 3.95-3.98ppm. The presence of a broad singlet at δ_H 5.68ppm was attributed to the amide proton.

The carbon resonances were assigned with the aid of ^{13}C DEPT and ^{13}C-^{1}H COSY experiments and are described in Table 2.17.

Table 2.18

NMR Spectroscopic details for *[5-(Pyrrol-1-yl)pentyl]ferrocene-carboxamide*



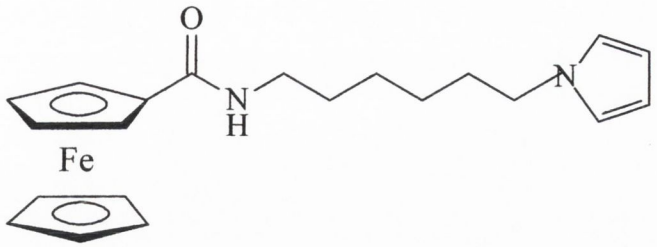
18 n=5

^{13}C (ppm)	^{1}H (ppm)	Multiplicity (^{1}H NMR)	Assignment
CH_2 23.6	1.35-1.43	m	$CH_2(CH_2)_2NH$
CH_2 29.1	1.58-1.65	m	CH_2CH_2NH
CH_2 30.6	1.82-1.89	m	$CH_2(CH_2)_3NH$
CH_2 38.8	3.35-3.40	dd, 6.5,7.0Hz	CH_2NH
CH_2 48.9	3.91-3.94	t, J = 7.0Hz	PyrroleNCH_2
CH 69.2	4.20	s	Cp
CH 69.8	4.35	s	2(H_β-Cp-amide)
CH 67.6	4.66	s	2(H_α-Cp-amide)
	5.64	bs	N*H*
CH 107.5	6.17	s	s, pyrrole CH_α
CH 120.0	6.68	s	s, pyrrole CH_β
C=O 169.7			

The NMR spectroscopic data obtained for **18 n=5** are summarised in Table 2.18. Key resonances in the ^{1}H NMR spectrum included a multiplet in the range δ_H 1.35-1.43ppm which was assigned to the protons in the most aliphatic environment with least influence from the amide and aromatic substituents, $CH_2(CH_2)_2NH$. The multiplet at δ_H 1.58-1.64 was assigned to the CH_2CH_2NH group and the final multiplet at δ_H 1.82-1.89 to $CH_2(CH_2)_3NH$. This is in agreement with the previously assigned peaks of [4-(Pyrrol-1-yl)butyl]ferrocene-carboxamide, **18** n = 4. The CH_2NH protons are observed as a doublet of doublets at δ_H 3.35-3.40ppm and the pyrroleNCH_2 protons as a triplet in the spectrum at δ_H 3.95-3.98ppm. The carbon resonances were assigned with the aid of ^{13}C DEPT and ^{13}C-^{1}H COSY experiments and are described in Table 2.18.

Table 2.19

NMR Spectroscopic details for *[6-(Pyrrol-1-yl)hexyl]ferrocene-carboxamide*



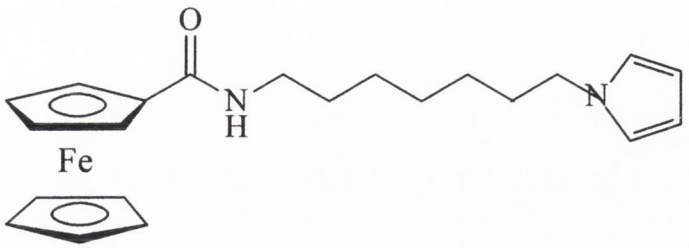
18 n=6

^{13}C (ppm)	^{1}H (ppm)	Multiplicity (^{1}H NMR)	Assignment
CH_2 26.0, 26.1	1.39-1.42	m	$(CH_2)_2(CH_2)_2NH$
CH_2 29.5	1.54-1.60	m	CH_2CH_2NH
CH_2 31.0	1.79-1.83	m	$CH_2(CH_2)_4NH$
CH_2 38.9	3.35-3.40	dd, 6.5,7.0Hz	CH_2NH
CH_2 49.0	3.88-3.91	t, J = 7.0Hz	pyrroleNCH_2
CH 69.2	4.21	s	Cp
CH 69.8	4.35	s	2(H_β-Cp-amide)
CH 67.6	4.66	s	2(H_α-Cp-amide)
	5.64	bs	N*H*
CH 107.4	6.16	s	s, pyrrole CH_α
CH 120.0	6.66	s	s, pyrrole CH_β
C=O 169.6			

The NMR spectroscopic data obtained for **18 n=6** are summarised in Table 2.19. Key resonances in the ^{1}H NMR spectrum included a multiplets in the range δ_H 1.39-1.42 which was assigned to the protons in the most aliphatic environment with least influence from the amide and aromatic substituents, $(CH_2)_2(CH_2)_2NH$. Integration of this peak showed the presence of four protons. The next multiplet at δ_H 1.54-1.60 was assigned to the CH_2CH_2NH group and the final multiplet at δ_H 1.79-1.83 to $CH_2(CH_2)_3NH$. This is in agreement with the previously assigned peaks of [4-(Pyrrol-1-yl)butyl]ferrocene-carboxamide, **18** n = 4 and [5-(Pyrrol-1-yl)pentyl] - ferrocene-carboxamide, **18** n = 5. The CH_2NH protons are observed as a doublet of doublets at δ_H 3.35-3.40ppm and the pyrroleNCH_2 protons as a triplet in the spectrum at δ_H 3.95-3.98ppm. The carbon resonances were assigned with the aid of ^{13}C DEPT and ^{13}C-^{1}H COSY experiments and are described in Table 2.19.

Table 2.20

NMR Spectroscopic details for *[7-(Pyrrol-1-yl)heptyl]ferrocene-carbo*xamide



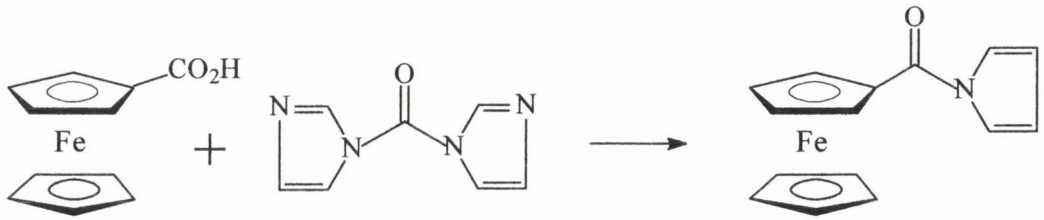
18 n=7

^{13}C (ppm)	^{1}H (ppm)	Multiplicity (^{1}H NMR)	Assignment
CH_2 26.2, 26.4, 28.4	1.28-1.39	m	$(CH_2)_3(CH_2)_2NH$
CH_2 29.5	1.59-1.64	m	CH_2CH_2NH
CH_2 31.0	1.75-1.83	m	$CH_2(CH_2)_5NH$
CH_2 39.0	3.35-3.40	dd, 6.0, 7.0Hz	CH_2NH
CH_2 49.1	3.87-3.91	t, 7.0Hz,	pyrroleNCH_2
CH 69.2	4.21	s	Cp
CH 69.8	4.36	s	2($H\beta$-Cp-amide)
CH 67.5	4.66	s	2(H_α-Cp-amide)
	5.65	bs	N*H*
CH 107.4	6.15	s	s, pyrrole CH_α
CH 120.0	6.66	s	s, pyrrole CH_β
C=O 169.6			

The NMR spectroscopic data obtained for **18 n=7** are summarised in Table 2.20. Key resonances in the ^{1}H NMR spectrum included a multiplets in the range δ_H 1.28-1.39, integration of this peak showed the presence of six protons. The multpilet was assigned to $(CH_2)_3(CH_2)_2NH$. The next multiplet at δ_H 1.59-1.64 was assigned to the CH_2CH_2NH group and the multiplet at δ_H 1.75-1.83 to $CH_2(CH_2)_3NH$. This is in agreement with the previously assigned peaks of [4-(Pyrrol-1-yl)butyl]ferrocene-carboxamide, **18** n = 4 and [5-(Pyrrol-1-yl)pentyl] -ferrocene-carboxamide, **18** n = 5 and [6-(Pyrrol-1-yl)hexyl]ferrocene-carboxamide **18** n = 6 The CH_2NH protons are observed as a doublet of doublets at δ_H 3.35-3.40ppm and the pyrroleNCH_2 protons as a triplet in the spectrum at δ_H 3.87-3.91ppm. The presence of a broad singlet at δ_H

5.68ppm was attributed to the amide proton. The carbon resonances were assigned with the aid of ^{13}C DEPT and ^{13}C-^{1}H COSY experiments and are described in Table 2.20.

2.5.2 Intermediate Isolation

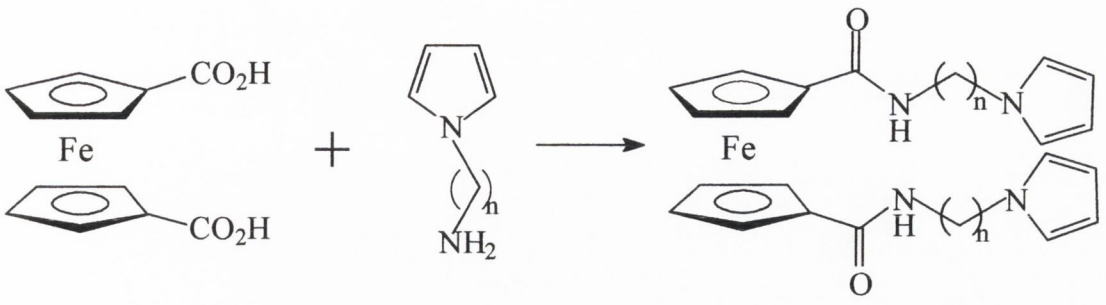


4 **10** **19**

Scheme 2.7

The initial reaction between ferrocene carboxylic acid, **4**, and 1,1'-carbonyldiimidazole, **10**, is shown above, Scheme 2.7. The intermediate, **19**, was also isolated when the coupling reaction was carried out. It was hoped that synthesis of this intermediate moiety, **19**, directly could produce a more efficient means of synthesizing modified ferrocene species. Therefore, it was decided to carry out the reaction shown in Scheme 2.7, i.e. without the addition of the N-(aminoalkyl)pyrrole. This resulted in the intermediate being isolated in a 38% yield. However, NMR analysis showed that remaining fractions consisted of both the intermediate and the starting material. As ferrocene carboxylic acid had already been removed from the column as the first fraction this implied that the intermediate was being hydrolysed on the column by the silica and therefore converting back to its precursor. Thus, it was decided to adhere to the original synthetic procedure.

2.5.3 Disubstituted Ferrocene Hybrid Monomers



6 **17** **20**

n = 3, 5 and 7

Scheme 2.8

A range of disubstituted monomers were prepared following the serendipitous discovery of the ferrocenyldiamidopropylpyrrole complex. This discovery occurred whilst attempting to synthesis the asymmetric derivative, **22**. The endeavour to prepare this species involved the reaction ferrocenedicarboxylic acid with one equivalent of 1,1'-carbonyldiimmdazole,**19** , and the N-aminoalkylpyrrole moiety, **17**. The end product of this initial experiment was a disubstituted pyrrole complex in a yield of 34%. Consequently, it was decided to prepare disubstituted compounds, **20**, according to the reaction scheme shown in scheme 2.8. Hence two equivalents of the coupling reagent and the aminoalkylpyrrole were utilized. The resultant residue was not extracted into DCM as the disubstituted ferrocene was more soluble in water than its monosubstituted counterpart. Purfication was achieved solely through column chromatography. The yields of the coupling reactions are shown in table 2.21 and are based on ferrocene dicarboxylic acid as the limiting reagent. Tables 2.22-2.24 describe the spectroscopic data obtained for these compounds.

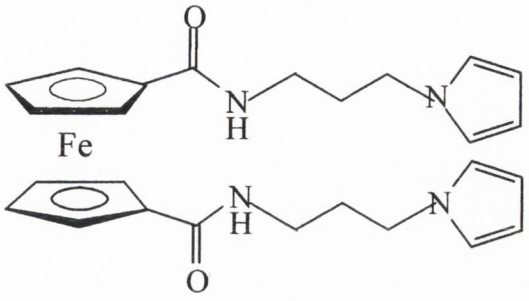
Table 2.21

Yields of disubstituted monomer species

Monomer		Yield (%)
1,1'-Bis-[3-(Pyrrol-1-yl)propyl]ferrocene-1,1'-dicarboxamide,	**20 n =3**	68
1,1'-Bis-[3-(Pyrrol-1-yl)pentyl]ferrocene-1,1'-dicarboxamide,	**20 n = 5**	63
1,1'-Bis-[3-(Pyrrol-1-yl)heptyl]ferrocene-1,1'-dicarboxamide,	**20 n = 7**	66

Table 2.22

NMR Spectroscopic details for 1,1'-Bis-[3-(Pyrrol-1-yl)propyl]ferrocene-1,1'-dicarboxamide



20 n=3

^{13}C (ppm)	^{1}H (ppm)	Multiplicity (^{1}H NMR)	Assignment
CH_2 31.1	2.09- 2.15	m	2 x $CH_2CH_2CH_2$
CH_2 37.2	3.43- 3.48	dd, J = 6.0, 6.5	2 x CH_2NH
CH_2 47.4	4.05- 4.08	t, J = 6.5Hz	2 x pyrroleNCH_2
CH 70.3	4.36	s	2 x 2(H_β-Cp-amide)
CH 70.8	4.41	s	2 x 2(H_α-Cp-amide)
	6.56	bs	N*H*
CH 108.1	6.21	s	s, pyrrole CH_α
CH 120.0	6.76	s	s, pyrrole CH_β
C=O 170.0			

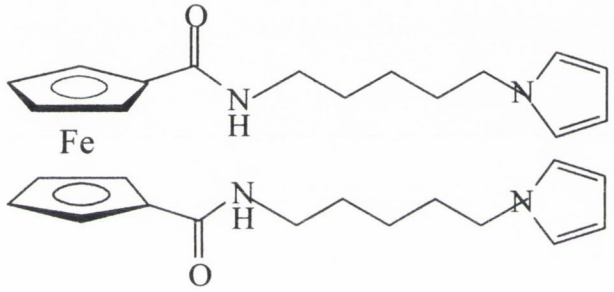
The NMR spectroscopic data obtained for **20 n=3** are summarised in Table 2.22. Key resonances in the ^{1}H NMR spectrum included a multiplet in the range δ_H 2.09-2.15ppm, which was assigned to 2 x $CH_2CH_2CH_2$ group split by the two adjacent CH_2 protons. These adjacent protons are observed as a doublet of doublets and a triplet in the spectrum at δ_H 3.43-3.48 and 4.05-4.08ppm. The former was assigned to 2 x CH_2NH protons and the latter to 2 x pyrroleNCH_2 protons. Integration of all of the aforementioned peaks showed the presence of four protons and was indicative of the disubstituted species. The presence of a broad singlet at δ_H 6.56ppm was attributed to the two amide protons. Other significant signals included two singlets at δ_H 4.36 and 4.41ppm. The two signals were assigned in accordance with their proximity to the CC=O group. The protons closest to this group are shifted more downfield to 4.41ppm whereas the remaining two protons have an are

atributed to the peak at δ_H 4.36. Signals for the C*H* protons of the pyrrole group are apparent at δ_H 6.21 and 6.76ppm. These peaks when integrated showed the presence of four protons. The absence of an unsubstituted cyclopentadienyl ring signal should be noted as this further indicated the presence of the disubstituted species.

The carbon resonances were assigned with the aid of ^{13}C DEPT and ^{13}C-^{1}H COSY experiments and are described in Table 2.22. A significant signal was evident at δ_C 170.0ppm in the ^{13}C and was attributed to the presence of the quaternary carboxyl carbon, this was supported by the disappearance of the peak in ^{13}C DEPT experiments.

Table 2.23

NMR Spectroscopic details for 1,1'-Bis-[5-(Pyrrol-1-yl)pentyl]ferrocene-1,1'-dicarboxamide



20 n=5

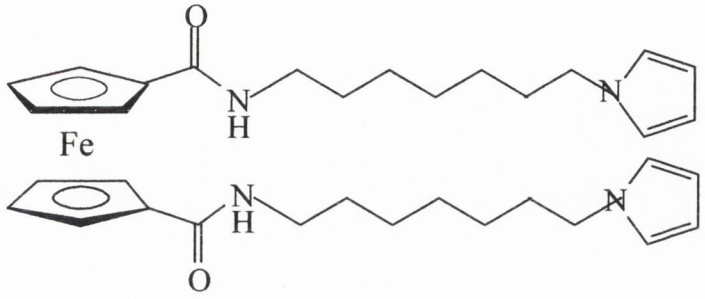
^{13}C (ppm)	^{1}H (ppm)	Multiplicity (^{1}H NMR)	Assignment
CH_2 23.6	1.39-1.43	m	2 x CH_2(CH$_2$)$_2$NH
CH_2 28.8	1.63-1.79	m	2 x CH_2CH$_2$NH
CH_2 30.7	1.82-1.89	m	2 x CH_2(CH$_2$)$_3$NH
CH_2 39.1	3.37-3.4	Dd, 6.5,7.0Hz	2 x CH_2NH
CH_2 49.0	3.90-3.94	t, J = 7.0Hz	2 x pyrroleNCH_2
CH 69.8	4.38	s	2 x 2(H_β-Cp-amide)
CH 70.3	4.46	s	2 x 2(H_α-Cp-amide)
	6.73	bs	N*H*
CH 107.5	6.15	s	s, pyrrole CH_α
CH 120.0	6.67	s	s, pyrrole CH_β
C=O 169.8			

The NMR spectroscopic data obtained for **20 n=5** are summarised in Table 2.23. Key resonances in the ^{1}H NMR spectrum included a multiplet in the range δ_H 1.39-1.43ppm which was assigned to the protons in the most aliphatic environment, 2 x $CH_2(CH_2)_2NH$. The multiplet at δ_H 1.63-1.79 was assigned to the 2 x CH_2CH_2NH group and the final multiplet at δ_H 1.82-1.89 to $CH_2(CH_2)_3NH$. This is in agreement with the previously assigned peaks of [5-(Pyrrol-1-yl)pentyl]ferrocene-carboxamide, **18** n = 5. The 2 x CH_2NH protons are observed as a doublet of doublets at δ_H 3.37-3.40ppm and the 2 x pyrroleNCH_2 protons as a triplet in the spectrum at δ_H 3.90-3.94ppm. Integration of all of the aforementioned peaks showed the presence of four protons and is indicative of the disubstituted species. The presence of a broad singlet at δ_H 6.73ppm was attributed to the two amide group protons. The absence of an unsubstituted cyclopentadienyl ring signal should be noted as this further indicates the presence of the disubstituted species.

The carbon resonances were assigned with the aid of ^{13}C DEPT and ^{13}C-^{1}H COSY experiments and are described in Table 2.23. A significant signal was evident at δ_C 169.8ppm in the ^{13}C and was attributed to the presence of the quaternary carboxyl carbon, this was supported by the disappearance of the peak in ^{13}C DEPT experiments. There was no evidence of a peak for the carbons of an unsubstituted cyclopentadienyl ring.

Table 2.24

NMR Spectroscopic details for 1,1'-Bis-[7-(Pyrrol-1-yl)heptyl]ferrocene-1,1'-dicarboxamide



20 n=7

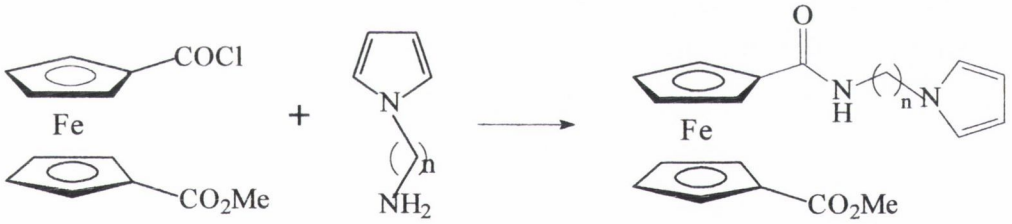
^{13}C (ppm)	^{1}H (ppm)	Multiplicity (^{1}H NMR)	Assignment
26.3, 26.5, 28.5,	1.39-1.41	m	2 x $(CH_2)_3(CH_2)_2NH$
29.2,	1.60-1.62	m	2 x CH_2CH_2NH
31.1	1.79-1.83	m	2 x $CH_2(CH_2)_4NH$
CH_2 49.1	3.37-3.42	dd, 6.0, 7.0Hz	2 x CH_2NH
CH_2 39.3	3.87-3.91	t, 7.0Hz,	2 x pyrroleNCH_2
CH 69.8	4.38	s	2 x 2(H_β-Cp-amide)
CH 67.5	4.49	s	2 x 2(H_α-Cp-amide)
	6.76	bs	N*H*
CH 107.3	6.15	s	s, pyrrole CH_α
CH 120.0	6.65	s	s, pyrrole CH_β
C=O 169.8			

The NMR spectroscopic data obtained for **20 n=7** are summarised in Table 2.24. Key resonances in the ^{1}H NMR spectrum included a multiplet in the range δ_H 1.39-1.41ppm which was assigned to the protons in the most aliphatic environment, 2 x $(CH_2)_3(CH_2)_2NH$. The multiplet at δ_H 1.60-1.62 was assigned to the 2 x CH_2CH_2NH group and the final multiplet at δ_H 1.78-1.83 to $CH_2(CH_2)_4NH$. This is in agreement with the previously assigned peaks of [7-(Pyrrol-1-yl)heptyl]ferrocene-carboxamide, **18** n = 7. The 2 x CH_2NH protons are observed as a doublet of doublets at δ_H 3.37-3.42ppm and the 2 x pyrroleNCH_2 protons as a triplet in the spectrum at δ_H 3.87-3.91ppm. The carbon resonances were assigned with the aid of ^{13}C DEPT and ^{13}C-^{1}H

COSY experiments and are described in Table 2.24. As in the assignment of the previous two disubsituted ferrocene species integration of all of the aforementioned peaks showed the presence of four protons and is indicative of the disubstituted species. The presence of a broad singlet at δ_H 6.76ppm was attributed to the two amide group protons. Once more, the absence of an unsubstituted cyclopentadienyl ring signal should be noted as this further indicated the presence of the disubstituted species.

The carbon resonances were assigned with the aid of ^{13}C DEPT and ^{13}C-^{1}H COSY experiments and are described in Table 2.22. A significant signal was evident at δ_C 169.8ppm in the ^{13}C and was attributed to the presence of the quaternary carboxyl carbon, this was supported by the disappearance of the peak in ^{13}C DEPT experiments. There was no evidence of a peak for the carbons of an unsubstituted cyclopentadienyl ring.

2.5.4 Asymmetrically Substituted Ferrocenes



9 **17** **21**

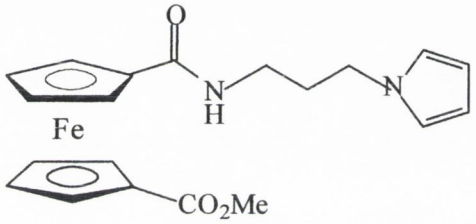
Scheme 2.9

The asymmetric ester derivative, **21**, was synthesized using a different coupling technique than previously and is illustrated in Scheme 2.9. The N-(aminoalkyl)pyrrole was dissolved in dry pyridine with one equivalent of triethylamine present to act as base and coordinate to the hydrogen chloride produced as a result of the condensation reaction. To this solution the ferrocene derivative, methyl-1,1'-chloroformylferrocenecarboxylate **9**, was added slowly. The solution was stirred under nitrogen for 12 hours. Filtration of the resultant trielthylaminehydrochloride salt and evaporation of the solvent from the filtrate resulted in a red residue being produced. Subsequent purification using column chromatography techniques produced the required hybrid monomer as an orange

powder in a 32% yield. It was envisaged that hydrolyses of this compound would produce the carboxylic acid derivative. However, with a limited amount of compound available and a limiting factor of time this ambition was not achieved. It is hoped that future work will allow for the synthesis of this compound for comparison purposes. Furthermore, covalent attachment of glucose oxidase to the polymer may be achieved through coupling of the amino residues on the enzyme to the carboxylic acid group on the second cyclopentadienyl ring of the ferrocene derivative.

Table 2.25

NMR Spectroscopic details for *[3-(Pyrrol-1-yl)propyl]ferrocene-carboxamide*



21 n=3

^{13}C (ppm)	^{1}H (ppm)	Multiplicity (^{1}H NMR)	Assignment
CH_2 30.9	2.07- 2.16	m	$CH_2CH_2CH_2$
CH_2 39.2	3.44- 3.48	dd, J = 6.0, 6.5	CH_2NH
CH_3 51.4	3.86	s	OCH_3
CH_2 49.1	4.05- 4.09	t, J = 6.5Hz	pyrroleNCH_2
CH 69.6, 70.9, 714, 72.3	4.37	s	2 x Cp-*H*
CH 69.6, 70.9, 714, 72.3	4.45	s	2 x Cp-*H*
CH 69.6, 70.9, 714, 72.3	4.53	s	2 x Cp-*H*
CH 69.6, 70.9, 714, 72.3	4.75	s	2 x Cp-*H*
	5.95	bs	N*H*
CH 108.3	6.23	s	s, pyrrole CH_α
CH 120.0	6.78	s	s, pyrrole CH_β
C=O 169.8			

The NMR spectroscopic data obtained for **21 n=3** are summarised in Table 2.25. Key resonances in the ^{1}H NMR spectrum included a multiplet in the range δ_H 2.07-2.16ppm, which was assigned to $CH_2CH_2CH_2$ group split by the two adjacent CH_2 protons. These adjacent protons are observed as a doublet of doublets and a triplet in the spectrum at δ_H 3.43-3.48 and 4.05-4.08ppm respectively. The former was assigned to CH_2NH protons and the latter to pyrroleNCH_2 protons. Other significant signals included a included a singlet at δ_H 3.86ppm, which was assigned to CH_3 group The presence of a broad singlet at δ_H 5.95ppm was attributed to the amide proton. Other significant signals included four singlets at δ_H 4.37, 4.45, 4.53 and 4.45ppm, these were assigned to the cyclopentadienyl protons, however differentiation between the protons on the different rings was not possible. Signals for the C*H* protons of the pyrrole group are apparent at δ_H 6.23 and 6.78ppm. The absence of an unsubstituted cyclopentadienyl ring signal should be noted as this further indicated the presence of the disubstituted species.

The carbon resonances were assigned with the aid of ^{13}C DEPT and ^{13}C-^{1}H COSY experiments and are described in Table 2.22. A significant signal was evident at δ_C 170.0ppm in the ^{13}C and was attributed to the presence of the quaternary carboxyl carbon, this was supported by the disappearance of the peak in ^{13}C DEPT experiments.

2.6 CONCLUSIONS

During the course of this work, the preparation of eight new N-substituted pyrrole moieties was realized using synthetic strategies already in place. To the best of our knowledge the following compounds are novel: N-(4-aminobutylpyrrole), N-(5-aminopentyl)pyrrole, N-(5-chloropentyl)pyrrole), N-(5-cyanopentyl)pyrrole, N-(6-aminohexyl)pyrrole, N-(6-chlorohexyl)pyrrole), N-(6-cyanohexyl)pyrrole and N-(7-aminoheptly)pyrrole.

The synthesis of seven novel hybrid monomers was successfully completed. [4-(Pyrrol-1-yl)butyl]ferrocene-carboxamide, [5-(Pyrrol-1-yl)pentyl]ferrocene-carboxamide, [6-(Pyrrol-1-yl)hexyl]ferrocene-carboxamide, [7-(Pyrrol-1-yl)heptyl]ferrocene-carboxamide, 1,1'-Bis-[5-(Pyrrol-1-yl)pentyl]ferrocene-1,1'-dicarboxamide, 1,1'-Bis-[7-(Pyrrol-1-yl)heptyl]ferrocene-1,1'-dicarboxamide and complex **21** were all prepared according to the facile, high yielding reaction schemes as outlined within this chapter. [3-(Pyrrol-1-yl)propyl]ferrocene-carboxamide,[14] and 1,1'-Bis-[3-(Pyrrol-1-yl)propyl]ferrocene-1,1'-dicarboxamide[15] were also prepared and their yields optimised by up to 60% to that of previous literature methods.

During the course of this work a number of different approaches were adopted in order to achieve the preparation of redox substituted pyrrole monomers. At first compounds shown in scheme 2.4 were produced and these may in due time be investigated for other purposes. However, despite the failure of these initial attempts to yield the desired complexes ultimately a facile synthetic scheme was devised for the preparation of hybrid monomers.

In summary, a total of fifteen novel compounds were successfully synthesised and characterized and with the novel pyrrole ligands in hand it may be possible to functionalise other metallocenes in a similar fashion. Alternatively, electropolymerization of these novel N-subsitituted pyrroles may be investigated in the future. N-(2-cyanoethyl)pyrrole has been previously investigated as a matrix for the immobilization of antibodies for the creation of biosensors.[16] These novel compounds could be investigated for similar purposes.

2.7 EXPERIMENTAL

2.7.1 General Experimental

All reagents were obtained from commercial suppliers and used without further purification unless otherwise stated. Tetrahydrofuran, THF, diethyl ether, petroleum ether (40 - 60 ^{0}C), hexane, toluene were pre-dried over potassium hydroxide, KOH and then dried by refluxing over sodium wire, benzophenone being used as indicator, and then distilled under nitrogen. Dichloromethane and dimethoxyethane were dried by refluxing over calcium hydride, followed by distillation under nitrogen. Flash chromatography was carried out using alumina (basic) and ethyl acetate: hexane, (2:1), as eluant. Proton and carbon NMR spectra were obtained on a 400 MHz Bruker WM 400 spectrometer. Microanalysis was carried out at the University of College Dublin.

2.7.2 Ferrocene Carboxylic Acids Formation

2.7.2.1 Preparation of ferrocene carboxylic acid,[1] **4**

i) Preparation of (2-Chlorobenzoyl)ferrocene

A thoroughly dried round bottom flask was charged under nitrogen with ferrocene, (10.8g, 0.058mol), (2- chlorobenzoyl) chloride, (7.35ml, 0.058mol) and dry dichloromethane, DCM (120ml). Anhydrous aluminium chloride (7.75g, 0.058mol) was added over a period of 15 min with the temperature being kept below 5 ^{o}C. The mixture was stirred for 30 min with cooling and for a further 2 h at r.t., during which time the reaction mixture turned blue. Once again the mixture was cooled, and water (100ml) added cautiously. The resulting two-phase mixture was stirred vigorously for 30 min. The mixture was transferred to a separating funnel and the aqueous layer extracted using DCM (2 x 30ml). The combined DCM portions were washed with water and 10% NaOH (2 x 30ml) before being dried over anhydrous magnesium sulfate. Filtration and evaporation to dryness under reduced pressure produced the required product as a red crystalline substance (18.075g, 96%).

ii) Preparation of Ferrocene Carboxylic Acid, **4**

Potassium tertiary butoxide (17.175g, 0.153mol) was dissolved in dry 1,2-dimethoxyethane, DME (150ml) and stirred under nitrogen for 10min. Water (0.92ml, 0.051mol) was added producing a slurry. (2-Chlorobenzoyl)ferrocene (16.611g, 0.051mol) was added and the mixture refluxed for 1h. The reaction was accompanied by a colour change from red to tan. Once the solution had cooled down to r.t. it was poured into water. This solution was then washed with ether (3 x 150ml). The ether portions were combined and washed with 10% NaOH (2 x 50ml). The aqueous phases were combined, acidified with conc. HCl, and the resulting precipitate collected by filtration. The required product was air dried to yield a yellow powder in a 90% yield.

^{1}H NMR (400MHz, $CDCl_3$):δ 4.28 (s, Cp, 5H), 4.49 (s, 2(H_β-Cp-acid), 2H), 4.88ppm (s, 2(H_α-Cp-acid), 2H).
^{13}C NMR (100MHz, $CDCl_3$): δ 70.1 (Cp), 70.6 (2x *C*HCHCCO), 72.0 (2x *C*HCCO), 177.1ppm (C=O).

2.7.2.2 Preparation of Ferrocene-1,1'-Dicarboxylic Acid,[2] **6**

n- Butyllithium (47ml, 1.6M, 0.075mol) in hexane was added to ferrocene (5.01g, 0.027mol) under nitrogen, this was followed by dropwise addition of N,N,N',N'-tetramethylethlenediamine, TMEDA, (11.3ml, 0.075mol). The mixture was allowed stir overnight. Next the supernatant was removed from the dilithiated ferrocene, this was then washed with dry pet. ether (30ml) and the supernatant removed once more. Finally dry diethyl ether (70ml) was added and the mixture poured into a flask of finely divided dry CO_2 in diethyl ether (70ml). The mixture was acidified with a small volume of conc. HCl resulting in the formation of a precipitate, which was collected by filtration and air-dried overnight. The required product was isolated as an orange powder (4.973, 67%). Proton and Carbon NMR was carried out in dimethylformamide, DMF, as the compound was insoluble in $CDCl_3$.

^{1}H NMR (400MHz, DMF): δ 4.49 (s, 4(H_{β}-Cp-acid), 4H), 4.79ppm (s, 4(H_{α}-Cp-acid), 4H).
^{13}C NMR (100MHz,DMF): δ 72.1 4(C_{β}-Cp-acid), 73.3 4(C_{α}-Cp-acid), 171.6ppm (C=O).

2.7.2.3 Preparation of Ferrocene 1,1'-Dimethyl Ester,[3] **7**

To a solution of ferrocene 1, 1'-dicarboxylic acid (2.2g) in methanol (30ml) conc. sulfuric acid (0.15ml) was added. The mixture was refluxed under nitrogen for 25h. and then allowed cool to r.t., this resulted in the formation of brown crystals. The crystals were recrystallised from methanol to yield the required product in a 83% yield.

^{1}H NMR (400MHz, $CDCl_3$): δ 3.84 (s, (2 x CH_3), 6H), 4.50 (s, 4(H_{β}-Cp-ester), 4H), 4.89ppm (s, 4(H_{α}-Cp-ester), 4H).
^{13}C NMR (100MHz, $CDCl_3$): δ 51.3 (CH_3), 71.2 (4x C_{α}-Cp-ester), 72.9 (4x C_{β}-Cp-ester), 170.2ppm (C=O)

2.7.2.4 Preparation of Ferrocene 1,1'-Methyl Ester, Acid,[3] **8**

Ferrocene 1,1'-dimethyl ester (1.8g) was dissolved in methanol (9ml) and allowed reach reflux before adding a solution of NaOH (0.24g) in water (0.8ml) and methanol (9ml) dropwise. The resultant mixture was allowed reflux under nitrogen for 75min. Water (20ml) was added to the cooled reaction mixture, and the unreacted dimethyl ester extracted with ether (3x35ml). The aqueous phase was acidified using 2M HCl, and the product extracted with ether (2x25ml). The ether phase was washed with water to neutrality and dried over magnesium sulfate. Solvent was removed *in vacuo* to afford the required product in a 42% yield.
^{1}H NMR (400MHz, $CDCl_3$): δ 3.86 (s, CH_3, 3H), 4.49 (t, (4 x H_{β}-Cp), 4H), 4.91ppm (t, (4 x H_{α}-Cp), 4H).

27.2.5 Preparation of methyl 1,1'-chloroformylferrocenecarboxylate,[3] **9**

To a solution of ferrocene 1,1'-methyl ester acid (0.72g) in dry, freshly dstilled DCM (10ml) a solution of oxalyl chloride (0.7ml) in dry DCM (5ml) was dopped over a period of 20min. The reaction mixture was allowed stand at r.t. for 7min and then stirred at 45-50°C for a further 75min, under nitrogen. The solvent was removed *in vacuo* and the remaining solid residue washed with dry hexane (10ml) at 50°C. The hot solution was filtered under nitrogen, the filtrate collected and then cooled to 0°C. Removal of solvent afforded the product as red crystals in a 71% yeld.

^{1}H NMR (400MHz, $CDCl_3$): δ 3.86 (s, CH_3, 3H), 4.55, 4.66 (s, (4 x H_β-Cp), 4H), 4.96ppm (s, (4 x H_α-Cp), 4H).

27.3 Preparation of Ferrocene Species 12

27.3.1 Preparation of **12**

Ferrocene carboxylic acid (0.88g, 3.8mmol) was dissolved in extremely dry THF (10ml). 1,1'-Carbonyldiimidazole (0.62g, 3.9mmol) was added and the mixture alowed stir under nitrogen overnight. 1,6 hexadiamine (0.44g, 3.8mmol) was added tothe solution and stirring continued for a further 24h. The solvent was removed *in vacuo*. The product was extracted into DCM (30ml) and washed with water (2x20ml). The organic layer was dried over anhydrous magnesium sulfate and the solvent removed *in vacuo* to give an orange powder which was applied to a cloumn of alumina (eluant: ethyl acetate/hexane, 2:1) The appropriate fractions were combined to give the product as a yellow powder, (0.5g, 0.91mmol), in a 48% yield.

^{1}H NMR (400MHz, $CDCl_3$):δ 1.28-1.32, 1.64-1.69 (2 x m, $(CH_2)_4CH_2NH$, 4H), 3.41-3.43 (t, 7.0Hz, CH_2NH, 4H), 4.23 (s, Cp, 10H), 4.35 (s, 2 x H_β-Cp-amide, 4H), 4.74ppm (s, H_α-Cp-amide, 4H), 6.01 (bs, N*H*, 2H).

2.7.4 Preparation of N-Substituted Pyrroles

2.7.4.1 *Preparation of N- (3-Aminopropyl)pyrrole,*[8] **17** n=3

Lithium aluminium hydride (2.3g, 60mmol) was dissolved in anhydrous diethyl ether (150ml). The solution was cooled in an ice bath. N- (2-cyanoethyl)pyrrole (6ml, 52mmol), dissolved in dry diethyl ether (20ml), was added over a period of 25 min with the temperature being kept below 5 °C. The mixture was allowed stir overnight under nitrogen. The mixture was cooled again to 5 °C and water (20ml) was added with care. The ether fraction was collected and washed with diethyl ether (3x20ml). The ether portions were combined, dried over anhydrous magnesium sulfate and filtered. The solvent was removed *in vacuo* to yield the required product as a pale yellow oil, (5.63g, 45mmol), in an 87% yield.

^{1}H NMR (400MHz, $CDCl_3$):δ 1.89-1.96 (m, $CH_2CH_2NH_2$, 2H), 2.71-2.74 (t, J = 6.5Hz, CH_2NH_2, 2H), 3.97-4.01 (t, J = 6.0Hz, pyrroleNCH_2, 2H), 6.16 (s, 2 x pyrrole CH_α, 2H), 6.69ppm (s, 2 x pyrrole CH_β, 2H).
^{13}C NMR (100MHz, $CDCl_3$):δ 34.6 ($CH_2CH_2NH_2$), 38.9 (CH_2NH_2) 46.7 (pyrroleNCH_2) 107.6 (2 x pyrrole *C's*), 120.1ppm (2 x pyrrole *C's*)

2.7.4.2 Preparation of N- (3-Chloropropyl)pyrrole, **15** n=3

Potassium tertiary butoxide (5.85g, 52mmol) was added to a solution of 18-crown-6 (1.2g, 4.5mmol) in dry diethyl ether (75ml). The mixture was stirred under nitrogen while pyrrole (3.12ml, 45mmol) was added. Stirring was continued for 15min. 1-Bromo-3-chloro-propane (5.16ml, 52mmol) was dissolved in diethyl ether (30ml) and added dropwise. The mixture was stirred for a further 18h before adding water (30ml). The product was extracted with ether (2x30ml), washed with a saturated NaCl solution before drying over anhydrous magnesium sulfate. Solvent was removed *in vacuo* to afford the required product as a pale yellow oil, (5.92g, 41.2mmol), in a 92% yield

^{1}H NMR (400MHz, $CDCl_3$): δ 2.26-2.29 (m, CH_2CH_2Cl, 2H), 3.53-3.57 (t, 6.0Hz, CH_2Cl, 2H), 4.15-4.19 (t, 6.5Hz, pyrroleNCH_2, *2H*), 6.28 (s, 2 x pyrrole CH_α, 2H), 6.78ppm (s, 2 x pyrrole CH_β, 2H).

^{13}C NMR (100MHz, $CDCl_3$): δ 32.1 (CH_2CH_2Cl), 41.3 (CH_2Cl), 45.6 (pyrroleNCH_2), 108.1 (2 x pyrrole *C's*), 120.3ppm (2 x pyrrole *C's*).

2.7.4.3 Preparation of N- (3-Cyanopropyl) pyrrole, **16** n=3

To a slurry of potassium cyanide (3g, 45mmol) in dimethyl sulfoxide (12ml) N-(3-chloropropyl)pyrrole (5.92g, 41.2mmol) was added and refluxed under nitrogen for 4h. The mixture was allowed cool to r.t. before being poured into water (50ml). The product was extracted into ether (3x15ml), dried over magnesium sulfate and filtered. The solvent was removed *in vacuo* to afford the required product as a yellow oil, (5.247g, 39mmol) in a 95%yield.

^{1}H NMR (400MHz, $CDCl_3$): δ 2.06-2.09(m, CH_2CH_2CN, 2H), 2.20-2.24 (t, 6.5Hz, CH_2CN, 2H), 4.01-4.05 (t, 6.5Hz, pyrroleNCH_2, 2H), 6.24 (s, 2 x pyrrole CH_α, 2H), 6.70ppm (s, 2 x pyrrole CH_β, 2H).

^{13}C NMR (100MHz, $CDCl_3$): δ 13.8 (CH_2CN), 26.9 (CH_2CH_2CN), 47.0 (pyrroleNCH_2), 108.4 (2 x pyrrole *C's*), 118.5 *C*N, 120.1ppm (2 x pyrrole *C's*),

2.7.4.4 Preparation of N- (4-Aminobutyl)pyrrole, **17** n=4

Lithium aluminium hydride (1.546g, 40.7mmol) was dissolved in anhydrous diethyl ether (100ml). The solution was cooled in an ice bath. N-(3-cyanopropyl)pyrrole (5.465g, 40.7mmol), dissolved in dry diethyl ether (20ml), was added over a period of 25 min with the temperature being kept below 5 °C. The mixture was allowed stir overnight under nitrogen. The mixture was cooled again to 5 °C and water (20ml) was added with care. The ether fraction was collected and the washed with diethyl ether (3x20ml). The ether portions were combined, dried over anhydrous magnesium sulfate and filtered. The solvent was removed *in vacuo* to yield the required product as a pale yellow oil, (4.64g, 33.6mmol), in an 88% yield.

^{1}H NMR (400MHz, $CDCl_3$): δ 1.44-1.49 (m, $CH_2CH_2NH_2$, 2H), 1.80-1.86 (m, $CH_2CH_2CH_2NH_2$, 2H), 2.72-2.75 (t, 7.0Hz, CH_2NH_2, 2H), 3.91-3.95 (t, 7.0Hz, pyrroleNCH_2, *2H*), 6.19(s, 2 x pyrrole CH_α, 2H), 6.70ppm (s, 2 x pyrrole CH_β, 2H). ^{13}C NMR (100MHz, $CDCl_3$): δ 28.5 ($CH_2CH_2NH_2$), 30.5 ($CH_2CH_2CH_2NH_2$), 41.3(CH_2NH_2), 49.0 (pyrroleNCH_2), 107.5 (2 x pyrrole *C's*), 120.0ppm (2 x pyrrole *C's*).

Preparation of N- (4-Chlorobutyl)pyrrole, **15** n=4

Potassium tertiary butoxide (5.85g, 52mmol) was added to a solution of 18-crown-6 (1.2g, 4.5mmol) in dry diethyl ether (75ml). The mixture was stirred under nitrogen while pyrrole (3.12ml, 45mol) was added. Stirring was continued for 15min. 1-Bromo-4-chloro-butane (5.99ml, 52mmol) was dissolved in diethyl ether (30ml) and added dropwise. The mixture was stirred for a further 18h before adding water (30ml). The product was extracted with ether (2x30ml), washed with a saturated NaCl solution before drying over anhydrous magnesium sulfate. Solvent was removed *in vacuo* to afford the required product as a pale yellow oil, (6.46g, 41mol), in a 91% yield

^{1}H NMR (400MHz, $CDCl_3$): δ 1.80-1.84 (m, CH_2CH_2Cl, 2H), 1.98-2.02 (m, $CH_2CH_2CH_2Cl$, 2H), 3.56-3.59 (t, 6.5Hz, CH_2Cl, 2H), 3.97-4.00(t, 7.0Hz, pyrroleNCH_2, 2H), 6.23 (s, 2 x pyrrole CH_α, 2H), 6.72ppm (s, 2 x pyrrole CH_β, 2H). ^{13}C NMR (100MHz, $CDCl_3$): δ 28.4 ($CH_2CH_2CH_2Cl$), 29.3 (CH_2CH_2Cl), 44.0 (CH_2Cl), 48.4 (pyrroleNCH_2), 107.8 (2 x pyrrole *C's*), 120.00ppm (2 x pyrrole *C's*).

2.7.4.5 Preparation of N- (4-Cyanobutyl)pyrrole, **16** n=4

To a slurry of potassium cyanide (3.56g, 54.7mmol) in dimethyl sulfoxide (12ml) N- (4-chlorobutyl)pyrrole (6.643g, 42.1mmol) was added and refluxed under nitrogen for 4h. The mixture was allowed cool to r.t. before being poured into water (70ml). The product was extracted into ether (3x20ml), dried over magnesium sulfate and filtered. The solvent was removed *in vacuo* to afford the required product as a yellow oil, (5.465g, 36.9mmol) in an 88%yield.

^{1}H NMR (400MHz, $CDCl_3$): δ 1.62-1.66 (m, CH_2CH_2CN, 2H), 1.92-1.96 (m, $CH_2CH_2CH_2CN$, 2H), 2.30-2.31 (t, 7.0Hz, CH_2CN, 2H), 3.80-3.97 (t, 6.5Hz, pyrroleNCH_2, *2H*), 6.17(s, 2 x pyrrole CH_α, 2H), 6.65ppm (s, 2 x pyrrole CH_β, 2H).
^{13}C NMR (100MHz, $CDCl_3$): δ 16.7(CH_2CN), 22.3 (CH_2CH_2CN), 29.92 ($CH_2CH_2CH_2CN$), 48.2 (pyrroleNCH_2), 108.0 (2 x pyrrole *C's*), 118.8 *C*N, 119.9ppm (2 x pyrrole *C's*).

2.7.4.6 Preparation of N- (5-Aminopentyl)pyrrole, **17** n=5

Lithium aluminium hydride (1.539g, 40.6mmol) was dissolved in anhydrous diethyl ether (150ml). The solution was cooled in an ice bath. N- (4-cyanobutyl)pyrrole (5.465g, 36.9mmol), dissolved in dry diethyl ether (20ml), was added over a period of 25 min with the temperature being kept below 5 °C. The mixture was allowed stir overnight under nitrogen. The mixture was cooled again to 5 °C and water (20ml) was added with care. The ether fraction was collected and the residue washed with diethyl ether (3x20ml). The ether portions were combined, dried over anhydrous magnesium sulfate and filtered. The solvent was removed *in vacuo* to yield the required product as a pale yellow oil, (4.64g, 30.5mmol), in an 83% yield.

^{1}H NMR (400MHz, $CDCl_3$): δ 1.32-1.45 (m, $CH_2CH_2NH_2$ or $CH_2CH_2CH_2NH_2$, 2H), 1.44-1.48 (m, $CH_2CH_2NH_2$ or $CH_2CH_2CH_2NH_2$, 2H), 1.79-1.82 (m, $CH_2(CH_2)_3NH_2$, 2H), 2.68-2.72 (t, 7.0Hz, CH_2NH_2, 2H), 3.88-3.91 (t, 7.0Hz, pyrroleNCH_2, *2H*), 6.15 (s, 2 x pyrrole CH_α, 2H), 6.66ppm (s, 2 x pyrrole CH_β, 2H).
^{13}C NMR (100MHz, $CDCl_3$): δ 26.7 ($CH_2CH_2CH_2$ NH_2), 30.9 ($CH_2(CH_2)_3NH_2$) 32.8 (CH_2CH_2 NH_2), 41.5 (CH_2 NH_2), 49.5 (pyrroleNCH_2), 107.4 (2 x pyrrole *C's*), 120.0ppm (2 x pyrrole *C's*).

2.7.4.7 Preparation of N- (5-Chloropentyl)pyrrole, **15** n=5

Potassium tertiary butoxide (5.85g, 52mmol) was added to a solution of 18-crown-6 (1.2g, 4.5mmol) in dry diethyl ether (75ml). The mixture was stirred under nitrogen while pyrrole (3.12ml, 45mmol) was added and stirring continued for

15min. 1-Bromo-5- chloro-pentane (6.85ml, 52mmol) was dissolved in diethyl ether (30ml) and added dropwise. The mixture was stirred for a further 18h before adding water (30ml). The product was extracted with ether (2x30ml), washed with a saturated NaCl solution before drying over anhydrous magnesium sulfate. Solvent was removed *in vacuo* to afford the required product as a pale yellow oil, (7.105g, 41.4mmol), in a 92% yield.

^{1}H NMR (400MHz, $CDCl_3$): δ 1.50-1.52 (m, C*H*$_2$CH$_2$CH$_2$Cl, 2H), 1.82-1.87 (m, C*H*$_2$CH$_2$C*H*$_2$CH$_2$Cl, 4H), 3.55-3.58 (t, 7.0Hz, C*H*$_2$Cl, 2H), 3.92-3.96 (t, 7.0Hz, pyrroleNC*H*$_2$, 2H), 6.20 (s, 2 x pyrrole C*H*$_\alpha$, 2H), 6.70ppm (s, 2 x pyrrole C*H*$_\beta$, 2H).
^{13}C NMR (100MHz, $CDCl_3$): δ 23.7 (*C*H$_2$CH$_2$CH$_2$Cl), 30.5, 31.7 (*C*H$_2$(CH$_2$)$_3$Cl), (*C*H$_2$CH$_2$Cl), 44.3 (*C*H$_2$ Cl), 48.9 (pyrroleN*C*H$_2$), 107.6 (2 x pyrrole *C's*), 120.0ppm (2 x pyrrole *C's*).

2.7.4.8 Preparation of N- (5-Cyanopentyl)pyrrole, **16** n=5

To a slurry of potassium cyanide (3g, 45mmol) in dimethyl sulfoxide (12ml) N- (5-chloropentyl)pyrrole (5.92g, 41.2mmol) was added and refluxed under nitrogen for 4h. The mixture was allowed cool to r.t.before being poured into water (50ml). The product was extracted into ether (3x15ml), dried over magnesium sulfate and filtered. The solvent was removed *in vacuo* to afford the required product as a yellow oil, (5.247g, 39mmol) in a 95%yield.

^{1}H NMR (400MHz, $CDCl_3$): δ 1.47-1.48 (m, *CH*$_2$CH$_2$CH$_2$CN, 2H), 1.66-1.68 (m, C*H*$_2$CH$_2$CN, 2H), 1.81-1.85 (m, *CH*$_2$(CH$_2$)$_3$CN, 2H), 2.32-2.35(t, 7.0Hz, C*H*$_2$CN, 2H), 3.91-3.94 (t, 7.0Hz, pyrroleNC*H*$_2$, 2H), 6.17(s, 2 x pyrrole C*H*$_\alpha$, 2H), 6.67ppm (s, 2 x pyrrole C*H*$_\beta$, 2H).
^{13}C NMR (100MHz, $CDCl_3$): δ 16.6 (*C*H$_2$CN), 25.5 (*C*H$_2$CH$_2$CN), 27.3 (*C*H$_2$CH$_2$CH$_2$CN), 30.3 (*C*H$_2$(CH$_2$)$_3$CN), 48.7 (pyrroleN*C*H$_2$), 107.7 (2 x pyrrole *C's*), *C*N 118.8, 120.0ppm (2 x pyrrole *C's*).

2.4.9 Preparation of N- (6-Aminohexyl)pyrrole, **17** n=6

Lithium aluminium hydride (3.06g, 8.1mmol) was dissolved in anhydrous diethyl ether (40ml). The solution was cooled in an ice bath. N- (5-cyanopentyl)pyrrole (1.30g, 8.1mmol), dissolved in dry diethyl ether (20ml), was added over a period of 25 min with the temperature being kept below 5 °C. The mixture was allowed stir overnight under nitrogen. The mixture was cooled again to 5 °C and water (20ml) was added with care. The ether solution was collected and the residue washed with diethyl ether (3x20ml). The ether portions were combined, dried over anhydrous magnesium sulfate and filtered. The solvent was removed *in vacuo* to yield the required product as a pale yellow oil, (0.771g, 4.6mmol), in a 58% yield.

^{1}H NMR (400MHz, $CDCl_3$): δ 1.31-1.38 (m, $CH_2CH_2CH_2CH_2NH_2$, 4H), 1.43-1.47 (m, $CH_2CH_2CH_2CH_2NH_2$, 2H), 1.77-1.81 (m, $CH_2(CH_2)_4NH_2$, 2H), 2.68-2.71(t, 7.0 Hz, CH_2NH_2, 2H), 3.87-3.91 (t, 7.0Hz, pyrroleNCH_2, *2H*), 6.17 (s, 2 x pyrrole CH_α, 2H), 6.67ppm (s, 2 x pyrrole CH_β, 2H).

^{13}C NMR (100MHz, $CDCl_3$): δ 26.0, 26.1 (CH_2)$_2$(CH_2)$_2$$NH_2$, 31.0 $CH_2(CH_2)_4NH_2$, 332 $CH_2CH_2NH_2$, 41.6 (CH_2NH_2), 49.1(pyrroleNCH_2), 107.4 (2 x pyrrole *C*)., 120.0ppm (2 x pyrrole *C*).

2.4.10 Preparation of N- (6-Chlorohexyl)pyrrole, **15** n=6

Potassium tertiary butoxide (5.85g, 52mmol) was added to a solution of 18-crown-6 (1.2g, 4.5mmol) in dry, diethyl ether (75ml). The mixture was stirred under nitrogen while pyrrole (3.12ml, 45mmol) was added. Stirring continued for 15min. 1-Bromo-6-chloro-hexane (7.76ml, 52mmol) was dissolved in diethyl ether (30ml) and added dropwise. The mixture was stirred for a further 18h before adding water (30ml). The product was extracted with ether (2x30ml), washed with a saturated NaCl solution before drying over anhydrous magnesium sulfate. Solvent was removed *in vacuo* to afford the required product as a pale yellow oil, (7.943g, 427mol), in a 95% yield.

^{1}H NMR (400MHz, $CDCl_3$): δ 1.30-1.35 (m, $CH_2CH_2CH_2Cl$ or $CH_2(CH_2)_3Cl$, 2H), 1.49-1.53 (m, $CH_2CH_2CH_2Cl$ or $CH_2(CH_2)_3Cl$, 2H), 1.81-1.92 (m, $CH_2(CH_2)_2CH_2CH_2Cl$, 4H), 3.45-3.57 (t, 7.0Hz, CH_2Cl, 2H), 3.92-3.94 (t, 7.0Hz, pyrroleNCH_2, *2H*), 6.18 (s, 2 x pyrrole CH_α, 2H), 6.68ppm (s, 2 x pyrrole CH_β, 2H).
^{13}C NMR (100MHz, $CDCl_3$): δ 24.8 ($CH_2CH_2CH_2Cl$), 25.2 ($CH_2(CH_2)_3Cl$), 30.8, 31.2 ($CH_2(CH_2)_2CH_2CH_2Cl$), (CH_2CH_2Cl), 44.2 (CH_2Cl), 49.1 (pyrroleNCH_2), 107.6 (2 x pyrrole *C's*), 120.0ppm (2 x pyrrole *C's*).

2.7.4.12 Preparation of N- (6-Cyanohexyl)pyrrole, **16** n=6

To a slurry of potassium cyanide (3g, 45mmol) in dimethyl sulfoxide (12ml) N-(6-chlorohexyl)pyrrole (7.943g, 42.7mmol) was added and refluxed under nitrogen for 4h. The mixture was allowed cool to r.t before being poured into water (50ml). The product was extracted into ether (3x15ml), dried over magnesium sulfate and filtered. The solvent was removed in vacuo to afford the required product as a yellow oil, (7.524g, 40mol) in a 95%yield.

^{1}H NMR (400MHz, $CDCl_3$): δ 1.31-1.47 (m, $CH_2(CH_2)_2CN$ or $CH_2(CH_2)_3CN$, 2H), 1.47-1.53 (m, $CH_2(CH_2)_2CN$ or $CH_2(CH_2)_3CN$, 2H), 1.66-1.70 (m, CH_2CH_2CN, 2H), 1.77-1.81 (m, $CH_2(CH_2)_4CN$, 2H), 2.35-2.41 (t, 7.0 Hz, CH_2CN, 2H), 3.87-3.91 (t, 7.0Hz, pyrroleNCH_2, *2H*), 6.17 (s, 2 x pyrrole CH_α, 2H), 6.67ppm (s, 2 x pyrrole CH_β, 2H).
^{13}C NMR (100MHz, $CDCl_3$): δ 16.8 (CH_2CN), 26.3 $CH_2(CH_2)_2CN$, 27.1 $CH_2(CH_2)_3CN$, 31.0 CH_2CH_2CN, 33.2 $CH_2(CH_2)_4CN$, 49.1(pyrroleNCH_2), 107.4 (2 x pyrrole *C*), 118.7 *C*N, 120.0ppm (2 x pyrrole *C*).

2.7.4.13 Preparation of N- (7-Aminoheptyl)pyrrole, **17** n=7

Lithium aluminium hydride (0.277g, 7.3mmol) was dissolved in anhydrous diethyl ether (40ml). The solution was cooled in an ice bath. N- (6-cyanohexyl)pyrrole (1.286g, 7.3mmol), dissolved in dry diethyl ether (20ml), was added over a period of 25 min with the temperature being kept below 5 °C. The mixture was allowed stir overnight under nitrogen. The mixture was cooled again to

5 °C and water (20ml) was added with care. The ether solution was collected and the residue washed with diethyl ether (3x20ml). The ether portions were combined, dried over anhydrous magnesium sulfate and filtered. The solvent was removed *in vacuo* to yield the required product as a pale yellow oil, (0.671g, 3.7mmol), in a 51% yield.

^{1}H NMR (400MHz, $CDCl_3$): δ 1.21-1.25, 1.43-1.46 (m, $(CH_2)_4NH_2$, 4H), (m, $(CH_2)_4NH_2$, 4H), 1.76-1.80 (m, $CH_2(CH_2)_5NH_2$, 8H),, 2H), 2.67-2.70(t, 6.5,7.0 Hz, CH_2NH_2, 2H), 3.86-3.90 (t, 7.0,7.5Hz, pyrroleNCH_2, *2H*), 6.15 (s, 2 x pyrrole CH_α, 2H), 6.66ppm (s, 2 x pyrrole CH_β, 2H).

^{13}C NMR (100MHz, $CDCl_3$): δ 26.2, 26.3, $(CH_2)_2(CH_2)_2NH_2$) 28.5, 33.3 ($CH_2(CH_2)_2CH_2CH_2NH_2$) 41.7 (CH_2NH_2), 49.1(pyrroleNCH_2), 107.3, 199.9ppm (2 x pyrrole C's).

2.7.5 Preparation of [N-(Pyrrol-1-yl)alkyl]ferrocene-carboxamide

2.7.5.1 Preparation of [3-(Pyrrol-1-yl)propyl]ferrocene-carboxamide, **18** n=3

Ferrocene carboxylic acid (2.5g, 10.8mmol) was dissolved in extremely dry THF (15ml). 1,1'-Carbonyldiimidazole (1.75g, 10.8mmol) was added and the mixture allowed stir under nitrogen overnight. N-(3-aminopropyl)pyrrole (1.35g, 109mmol) was added to the solution and stirring continued for a further 24h. The solvent was removed *in vacuo*. The product was extracted into DCM (30ml) and washed with water (2x20ml). Flash chromatography produced the required product as a yellow powder, (3.15g, 9.4mmol), in a 87% yield.

FTIR1660 (C=O), 2300cm^{-1} (NH)

^{1}H NMR (400MHz, $CDCl_3$):δ 2.04- 2.10 (m, $CH_2CH_2CH_2$, 2H), 3.42- 3.47 (dd, 6.0,6.5Hz, CH_2NH, 2H), 4.02- 4.05 (t, 6.5Hz, pyrroleNCH_2, 2H), 4.19 (s, Cp, 5H), 4.33 (s, 2 x H_β-Cp-amide, 2H), 4.60ppm (s, H_α-Cp-amide, 2H), 5.44 (bs, N*H*, 1H), 6.25 (s, 2 x pyrrole CH_α, 2H) and 6.75ppm (s, 2 x pyrrole CH_β, 2H).

^{13}C NMR (100MHz, $CDCl_3$): δ 31.2 ($CH_2CH_2CH_2$), 37.0 (*C*NH), 47.6 (NCH_2), 67.6 (2x C_α-Cp-amide), 69.2 (C_P), 69.8(2x C_β-Cp-amide), 108.3 (2 x pyrrole *C*), 120.0 (2 x pyrrole *C*), 169.8ppm (C=O).

Microanalysis: $C_{18}H_{20}N_2OFe$ Found: C: 64.27%, H: 6.00%, N:8.33%

Requires: C: 64.10%, H: 6.00%, N:8.31%

2.7.5.2 Preparation of [4-(Pyrrol-1-yl)butyl]ferrocene-carboxamide, **18** n=4

Ferrocene carboxylic acid (2.5g, 10.8mmol) was dissolved in extremely dry THF (15ml). 1,1'-Carbonyldiimidazole (1.75g, 10.8mmol) was added and the mixture allowed stir under nitrogen overnight. N-(4-aminobutyl)pyrrole (1.5g, 10.9mmol) was added to the solution and stirring continued for a further 24h. The solvent was removed *in vacuo*. The product was extracted into DCM (30ml) and washed with water (2x20ml). Flash chromatography produced the required product as a yellow powder, (3.03g, 8.6mmol), in an 80% yield.

FTIR 1660 (C=O), 2300cm^{-1} (NH)

^{1}H NMR (400MHz, $CDCl_3$):δ 1.55-1.62 (m, CH_2CH_2NH, 2H), 1.84-1.91 (m, CH_2CH_2CH_2NH, 2H), 3.34-3.42, (dd, 6.5,7.0Hz, CH_2NH, 2H) 3.95-3.98 (t, 6.5,7.0Hz, pyrroleNCH_2, 2H), 4.19 (s, Cp, 5H), 4.33 (s, H_β-Cp-amide, 2H), 4.60ppm (s, H_α-Cp-amide, 2H), 5.68 (bs, N*H*, 1H), 6.17 (s, 2 x pyrrole CH_α, 2H) and 6.67 (s, 2 x pyrrole CH_β, 2H).

^{13}C NMR (100MHz, $CDCl_3$): δ 26.8 (*C*H_2CH_2NH) , 28.4 (CH_2CH_2CH_2NH), 38.5 (*C*NH), 44.3 (NCH_2), 67.6 (2x C_α-Cp-amide), 69.2 (C_P), 69.8(2x C_β-Cp-amide), 108.3 (2 x pyrrole *C*), 120.0 (2 x pyrrole *C*), 169.8ppm (C=O).

Microanalysis: $C_{19}H_{22}N_2OFe$ Found: C: 64.88%, H: 6.33%, N:7.88%

Requires: C: 65.16%, H: 6.21%, N:8.00%

2.7.5.3 Preparation of [5-(Pyrrol-1-yl)pentyl]ferrocene-carboxamide, **18** n=5

Ferrocene carboxylic acid (2.5g, 10.8mmol) was dissolved in extremely dry THF (15ml). 1,1'-Carbonyldiimidazole (1.75g, 10.8mmol) was added and the mixture allowed stir under nitrogen overnight. N-(5-aminopentyl)pyrrole (1.65g, 10.8mmol) was added to the solution and stirring continued for a further 24h. The solvent was removed *in vacuo*. The product was extracted into DCM (30ml) and washed with water (2x20ml). Flash chromatography produced the required product as a yellow powder, (3.19g, 8.1mmol), in an 75% yield.

FTIR 1660 (C=O), 2300cm^{-1} (NH)

^{1}H NMR (400MHz, $CDCl_3$):δ 1.35-1.43 (m, CH_2(CH_2)$_2$NH, 2H), 1.58-1.65 (m, CH_2CH_2NH, 2H), 1.82-1.89 (m, CH_2(CH_2)$_3$NH, 2H), 3.35-3.40, (dd, 6.5, 7.0Hz,

CH_2NH, 2H) 3.91-3.94 (t, 7.0Hz, pyrroleNCH_2, 2H), 4.20 (s, Cp, 5H), 4.35 (s, H_β-Cp-amide, 2H), 4.66ppm (s, H_α-Cp-amide, 2H), 5.64 (bs, N*H*, 1H), 6.17 (s, 2 x pyrrole CH_α, 2H), 6.68ppm (s, 2 x pyrrole CH_β, 2H).

^{13}C NMR (100MHz, $CDCl_3$): δ 23.6 (*C*H_2(CH_2)$_2$NH), 29.1 (*C*$H_2$$CH_2$NH), 30.6 (*C*$H_2$($CH_2$)$_3$NH), 38.8 (*C*NH), 48.9 (N*C*H_2), 67.6 (2x C_α-Cp-amide), 69.2 (C_P), 69.8 (2x C_β-Cp-amide) 107.5 (2 x pyrrole *C*) 120.0 (2 x pyrrole *C*), 169.7ppm (C=O).

Microanalysis: $C_{20}H_{24}N_2OFe$ Found: C: 65.66%, H: 6.50%, N:7.45%

Requires: C: 65.94%, H: 6.64%, N:7.69%

2.7.5.4 Preparation of [6-(Pyrrol-1-yl)hexyl]ferrocene-carboxamide, **18** n=6

Ferrocene carboxylic acid (2.5g, 10.8mmol) was dissolved in extremely dry THF (15ml). 1,1'-Carbonyldiimidazole (1.75g, 10.8mmol) was added and the mixture allowed stir under nitrogen overnight. N-(6-aminohexyl)pyrrole (1.82g, 10.9mmol) was added to the solution and stirring continued for a further 24h. The solvent was removed *in vacuo*. The product was extracted into DCM (30ml) and washed with water (2x20ml). Flash chromatography produced the required product as a yellow powder, (3.07g, 8.8mmol), in a 81% yield.

FTIR 1660 (C=O), 2300cm^{-1} (NH)

^{1}H NMR (400MHz, $CDCl_3$):δ 1.39-1.42 (m, (CH_2)$_2$(CH_2)$_2$NH, 4H), 1.54-1.60 (m, C$H_2$$CH_2$NH, 2H), 1.79-1.83 (m, C$H_2$($CH_2$)$_4$NH, 2H), 3.35-3.40, (dd, 6.0, 7.0Hz, CH_2NH, 2H) 3.88-3.91 (t, 7.0Hz, pyrroleNCH_2, 2H), 4.21 (s, Cp, 5H), 4.35 (s, 2 x H_β-Cp-amide, 2H), 4.66ppm (s, H_α-Cp-amide, 2H), 5.64 (bs, N*H*, 1H), 6.16 (s, 2 x pyrrole CH_α, 2H) and 6.66ppm (s, 2 x pyrrole CH_β, 2H).

^{13}CNMR(100MHz,$CDCl_3$): δ 26.0, 26.1 (*C*H_2)$_2$(CH_2)$_2$NH, 29.5 *C*$H_2$$CH_2$NH, 31.0 *C*$H_2$($CH_2$)$_4$NH, 38.9 (*C*NH), 49.0 (pyrroleN*C*H_2), 67.6 (2x C_α-Cp-amide), 69.2 (C_P), 69.8 (2x C_β-Cp-amide), 107.4 (2 x pyrrole *C*), 120.0 (2 x pyrrole *C*), 169.6ppm (C=O).

Microanalysis:$C_{21}H_{26}N_2OFe$ Found: C: 66.97%, H: 6.92%, N: 7.61 %

Requires: C: 66.68%, H: 6.93%, N:7.41%

*2.7.5.5 Preparation of [7-(Pyrrol-1-yl)heptyl]ferrocene-carbo*xamide, **18** n=7

Ferrocene carboxylic acid (2.5g, 10.8mmol) was dissolved in extremely dry THF (15ml). 1,1'-Carbonyldiimidazole (1.75g, 10.8mmol) was added and the mixture allowed stir under nitrogen overnight. N-(7-Aminoheptyl)pyrrole (2.0g, 11mmol) was added to the solution and stirring continued for a further 24h. The solvent was removed *in vacuo*. The product was extracted into DCM (30ml) and washed with water (2x20ml). Flash chromatography produced the required product as a yellow powder, (3.49g, 8.9mmol), in a 82% yield.

FTIR: 1660 (C=O), 2300cm^{-1} (NH)

^{1}H NMR (400MHz, $CDCl_3$):δ 1.28-1.39 (m, $(CH_2)_3(CH_2)_2NH$, 6H), 1.59-1.60 (m, CH_2CH_2NH, 2H), 1.75-1.83 (m, $CH_2(CH_2)_5NH$, 2H), 3.35-3.40, (dd, 6.0, 7.0Hz, CH_2NH, 2H) 3.87-3.91 (t, 7.0Hz, pyrroleNCH_2, 2H), 4.21 (s, Cp, 5H), 4.36(s, 2 x H_β-Cp-amide, 2H), 4.66ppm (s, H_α-Cp-amide, 2H), 5.65 (bs, N*H*, 1H), 6.15 (s, 2 x pyrrole CH_α, 2H) and 6.66ppm (s, 2 x pyrrole CH_β, 2H).

^{13}CNMR(100MHz,$CDCl_3$): δ 26.2, 26.4, 28.4, $(CH_2)_3(CH_2)_2NH$ 29.5, CH_2CH_2NH 31.0 $CH_2(CH_2)_5NH$ CNH), 49.1 (pyrroleNCH_2), 67.5(2x C_α-Cp-amide), 69.2(C_P), 69.8 (2x C_β-Cp-amide),107.4 (2 x pyrrole *C*), 120.0 (2 x pyrrole *C*), 169.6ppm (C=O).

Microanalysis:	$C_{20}H_{24}N_2OFe$	Found:	C: 67.60%, H: 7.46%, N:6.85%
		Requires:	C: 67.35%, H: 7.19%, N:7.14%

2.7.6 Preparation of Disubstituted Hybrids

2.7.6.1 Synthesis of 1,1'-Bis-[3-(Pyrrol-1-yl)propyl]ferrocene-1,1'-dicarboxamide, **20** n=3

1,1'-Ferrocene dicarboxylic acid (1.0g, 3.65mmol) was dissolved in extremely dry THF (15ml). 1,1'-Carbonyldiimidazole (1.18g, 7.3mmol) was added and the mixture allowed stir under nitrogen overnight. N-(3-aminopropyl)pyrrole (092g, 7.38mmol) was added to the solution and stirring continued for a further 24h. The solvent was removed *in vacuo*. Flash chromatography produced the required product as a yellow powder, (1.23g, 2.5mmol), in a 68% yield.

^{1}H NMR (400MHz, $CDCl_3$):δ 2.09- 2.15 (m, 2 x $CH_2CH_2CH_2$, 4H), 3.43- 3.48 (dd, 6.0,6.5Hz, 2 x CH_2NH, 4H), 4.05- 4.08 (s, 6.5Hz, 2 x pyrroleNCH_2, 4H), 4.36-4.37 (s, 4 x H_β-Cp-amide, 4H), 4.41-4.42 (s, 4 x H_α-Cp-amide), 4H), 6.21-6.22 (s, 4 x pyroleCH_α, 4H), 6.56 (bs, 2 x N*H*, 2H), 6.76 (s, 4 x pyrrole CH_β, 4H).

^{13}C NMR (100MHz, $CDCl_3$): δ 31.1 (2 x $CH_2CH_2CH_2$), 37.2 (2 x *C*NH), 47.4 (2 x pyroleNCH_2), 70.3 (4 x C_β-Cp-amide), 70.8 (4 x C_α-Cp-amide), 108.1 (2 x pyrrole *C*), 120.0 (2 x pyrrole *C*), 170ppm (2 x C=O).

Microanalysis: $C_{26}H_{30}N_4O_2Fe$ Found: C: 64.54%, H: 6.39%, N:10.75%

Requires: C: 64.20%, H: 6.22%, N:11.52%

2.7.6.2 Synthesis of 1,1'-Bis-[5-(Pyrrol-1-yl)pentyl]ferrocene-1,1'-dicarboxamide, **20**n=5

1,1'-Ferrocene dicarboxylic acid (1.0g, 3.65mmol) was dissolved in exremely dry THF (15ml). 1,1'-Carbonyldiimidazole (1.18g, 7.3mmol) was added and the mixture allowed stir under nitrogen overnight. N-(5-aminopentyl)pyrrole (112g, 7.36mmol) was added to the solution and stirring continued for a further 24h. The solvent was removed *in vacuo*. Flash chromatography produced the required product as a yellow powder, (1.25g, mmol), in a 63% yield.

^{1}HNMR (400MHz, $CDCl_3$):δ 1.39-1.43 (m, 2 x $CH_2(CH_2)_2NH$, 4H), 1.63-1.79 (m, 2 x CH_2CH_2NH, 4H), 1.82-1.89 (m, 2 x $CH_2(CH_2)_3NH$, 4H), 3.37-3.42, (dd, 6.5,

7.0Hz, 2 x CH_2NH, 4H) 3.90-3.94 (t, 7.0,6.5Hz, 2 x pyrroleNCH_2, 4H), 4.38 (s, 4 x H_β-Cp-amide, 4H), 4.46ppm (s, 4 x H_α-Cp-amide, 2H), 6.15 (s, 4 x pyrroleCH_α, 4H), 6.67ppm (s, 4 x pyrrole CH_β, 4H), 6.73 (bs, 2 xNH, 1H).

^{13}C NMR (100MHz, $CDCl_3$): δ 23.6 (2 x $CH_2(CH_2)_2$NH), 28.8 (2 x CH_2CH_2NH) 30.7 (2 x $CH_2(CH_2)_3$NH), 39.1 (2 x CH_2NH), 49.0 (2 x pyrroleNCH_2) 69.8 (2 x 2x C_β-Cp-amide) 70.3 (2x C_α-Cp-amide), 107.5 (4 x pyrrole C) 120.0 (4 x pyrrole C), 169.8ppm (2 x C=O).

Microanalysis: $C_{30}H_{38}N_4O_2Fe$ Found: C: 66.03%, H: 7.10%, N:10.00%

Requires: C: 66.42%, H: 7.06%, N:10.33%

2.7.6.3 Synthesis of 1,1'-Bis-[7-(Pyrrol-1-yl)heptyl]ferrocene-1,1'-dicarboxamide, **20** n=7

1,1'-Ferrocene dicarboxylic acid (1.0, 3.65mmol) was dissolved in extremely dry THF (15ml). 1,1'-Carbonyldiimidazole (1.18g, 7.3mmol) was added and the mixture allowed stir under nitrogen overnight N-(7-aminoheptyl)pyrrole (1.36g, 7.6mmol) was added to the solution and stirring continued for a further 24h. The solvent was removed *in vacuo*. The product was extracted into DCM (30ml) and washed with water (2x20ml). Flash chromatography produced the required product as a yellow powder, (1.44g, 5.6mmol), in a 66% yield.

^{1}H NMR (400MHz, $CDCl_3$):δ 1.39-1.41 (m, 2 x $(CH_2)_3(CH_2)_2$NH, 6H), 1.60-1.62 (m, 2 x CH_2CH_2NH, 4H), 1.79-1.83 (m, 2 x $CH_2(CH_2)_4$NH, 2H), 3.37-3.42, (dd, 6.0, 7.0Hz, 2 x CH_2NH, 4H) 3.87-3.91 (t, 7.0Hz, 2 x pyrroleCH_2, 4H), 4.38 (s, 2 x (2 x CHCHCO), 4H), 4.49ppm (s, 2 x CHCO, 4H), 6.15 (s, 4 x pyrrole CH_α, 4H) and 6.66 (s, 4 x pyrrole CH_β, 4H) 6.76 (bs, NH, 1H),.

^{13}CNMR(100MHz,$CDCl_3$): δ 26.3, 26.5, 28.5 (2 x$(CH_2)_3(CH_2)_2$NH), 29.2 (2 x CH_2CH_2NH), 31.1 (2 x $CH_2(CH_2)_4$NH) 39.3 (2 x pyrrole-C), 49.1 (2 x CNH), 70.3 (2 x C_P), 107.3, 120.0 (pyrrole C's), 169.8ppm (C=O).

Microanalysis:$C_{34}H_{46}N_4O_2Fe$ Found: C: 67.80%, H: 7.68%, N:9.05%

Requires: C: 68.22%, H: 7.75%, N:9.36%

27.6.5 Preparation of **21**

N-(3-aminopropyl)pyrrole (0.38g, 3mmol) was dissolved in dry DCM. Triethylamine (0.22ml, 3mmol) was added and the solution cooled to 0°C, before the dropwise addition of a solution of methyl,1'-chloroformylferrocenecarboxylate (0.65, 2.5mmol) in DCM (10ml). The reaction mixture was allowed warm to room temperature and stirred for 1 hour. The solvent was removed *in vacuo* and the residue dissolved in dry THF (20ml). This allowed the insoluble triethylaminehydrochloride to be removed via filtration. The solvent was evaporated from the filtrate and the residue purified via flash chromatography. This process afforded the required product as an orange powder, (0.32g, mmol), in a 32% yield.

^{1}H NMR (400MHz, $CDCl_3$):δ 2.07- 2.16 (m, $CH_2CH_2CH_2$, 2H), 3.44- 3.48 (dd, 6.0, 6.5Hz, CH_2NH, 2H), 3.86 (s, OCH_3, 3H) 4.05- 4.09 (t, 6.5Hz, pyrroleNCH_2, 2H), 4.37, 4.45, 4.53, 4.75ppm (4 x s, 8 x *H*-Cp, 8H), 5.95 (bs, N*H*, 1H), 6.23 (s, 2 x pyrroleCH_α, 2H), and 6.78ppm (s, 2 x pyrroleCH_β, 2H),

^{13}C NMR (100MHz, $CDCl_3$): δ 30.9 ($CH_2CH_2CH_2$), 39.2 (CH_2NH), 47.6 (pyrroleNCH_2) 51.4 (OCH_3), 69.8 (4 x C_β-Cp-amide) 67.6 (4x C_α-Cp-amide), 108.3 (2x pyrrole *C*) 120.0 (2 x pyrrole *C*), 169.8ppm (2 x C=O).

Mcroanalysis: $C_{20}H_{22}N_2O_3Fe$ Found: C: 60.39%, H: 5.69%, N:6.84%

Requires: C: 60.93%, H: 5.62%, N:7.11%

28 REFERENCES

1 P.C. Reeves, *Org. Synth.*, **56**, 28, (1969).

2 M. D. Rausch, *J. Organomet. Chem.*, **10**, 127, (1967).

3 H. J. Lorkowski, R. Pannier, *J. Prakt. Chem.*, **311**, 958, (1969).

4 N. Elming, N. Clauson-Kaas, *Acta Chem. Scand.*, **6**, 867, (1952).

5 P. G. Gassau, J. T. Lumb, F. V. Zalar, *J. Am. Chem. Soc.*, **89**, 946, (1967).

6 W.C. Guida, D.J. Mathre, *J. Org. Chem.*, **45**, 3172, (1980).

7 J.M. Patterson, J. Brasch, P.Drenchko, *J. Am. Chem. Soc.*, **27**, 1652, (1962).

8 L. H. Amundsen, L. S. Nelson, *J. Am. Chem. Soc.*, **73**, 242, (1951).

9 Rajesh, Takashima, Kaneto, *Sens. And Actuators B.*, **in press** 2004.

10 H.A. Stabb,, M. Luking, F.A. Darr, *Chem Ber.*, **95**, 1275, *(*1962).

11 M.J. Brooks, R.C. Morton, *J. Am. Chem. Soc.*, **1958**, *80*, 4423

12 M.L. Hudson, *J. Am. Chem. Soc.*, **1960**, *82*, 4596

13 K.Lau, F.Hart, *J. Org. Chem.*, **1962**, *27*, 2094

14 N.C. Foulds, C.R. Lowe, *Anal. Chem.*, **60**, 2473, (1988).

15 J.G. Eaves, R. Mirrazei, D. Parker, H.S. Munro, *J. Chem. Soc., Perkin Trans. 2*, 475, (1989).

16 O.Ouerghi, A.Senillou, N. Jaffrezic-Renault, C. Martelet, H. Ben Ouada, S. Cosnier, *J. Electroanal. Chem.*, **501**, 62, (2001).

CHAPTER THREE
EXPERIMENTAL ELECTROCHEMICAL METHODOLOGIES AND GENERAL THEORY

3.1 INTRODUCTION

In this chapter the instrumentation and experimental techniques employed during the course of this study shall be described. The discussion will include a description of the instrumentation used for electrochemical experimentation. Subsequent to this, the electrochemical cell and its components, pre-treatment of the electrode surface and also a description of the electrode modification techniques used shall be outlined. These are based on electronic apparatus designed to control and measure the potential, the current and the charge passed in an electrochemical cell. Finally, the experimental applications and the relevant theoretical foundations of the principle techniques used in this study, (cyclic voltammetry, potential step voltammetry) will be outlined.

3.2 INSTRUMENTATION

3.2.1 BAS 100B Workstation

Experimental work was carried out using the BAS 100B/W electrochemical workstation. The experimental set-up is illustrated in Figure 3.1, with the three main components of the workstation are the electrochemical cell, the potentiostat and the PC. All the experimental parameters are entered through the BAS/Windows interface; either general machine suggested parameter values or specific user defined parameters may be set. The experiment may be run directly via keyboard entry. The experimental data are collected digitally in real time and are displayed on the PC monitor. The data may be subsequently manipulated, analyzed and transformed using software based protocols.

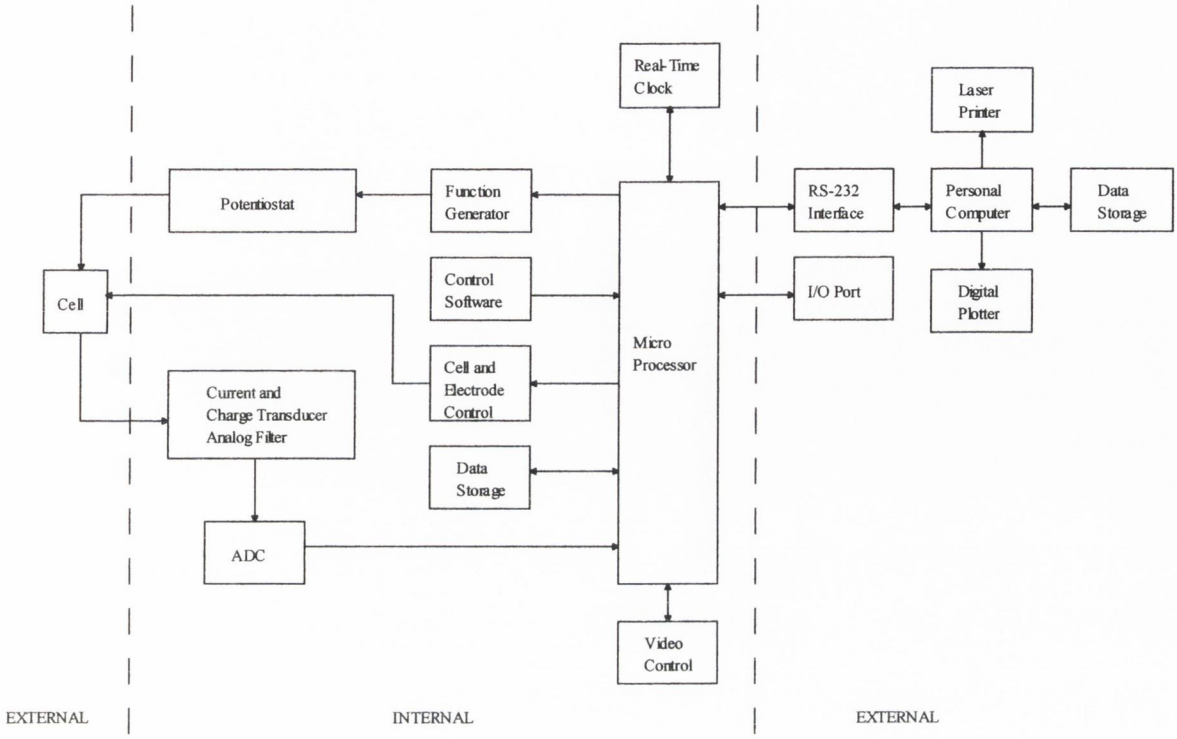


Figure 3.1 Block diagram of the BAS 100B/W Electrochemical Workstation.[1]

3.2.2 The Potentiostat

Potentiostatic control and measurement are required to carry out voltammetric experimentation. The potential at the working electrode is monitored and controlled with respect to the reference electrode via the potentiostat. The basic component in the construction of a potentiostat is an operational amplifier. This unit comes in the form of an integrated circuit, often with varying characteristics, depending on its designated application or requirement. A brief description of its operation and incorporation into a potentiostat circuitry is now outlined. However, a more comprehensive account may be found in many electrochemical texts.[1-3]

As previously mentioned, the basic building block of the potentiostat is the operational amplifier, which is depicted schematically in Figure 3.2. The fundamental property of the amplifier is that the output, e_0, is the inverted, amplified voltage

difference, e_s, where e_s is the voltage of the inverting input with respect to the non-inverting input, i.e.

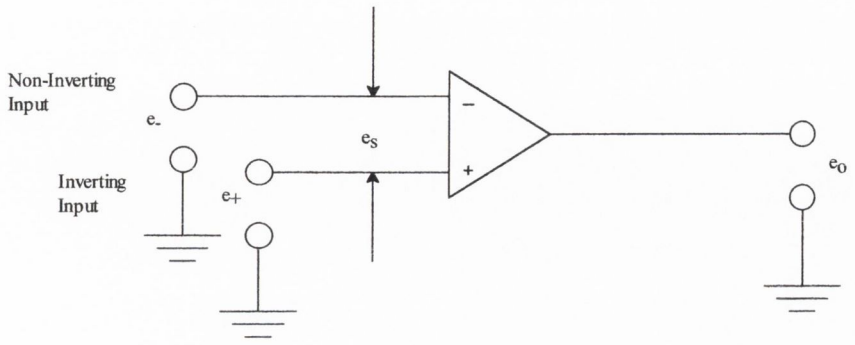


Figure 3.2. Schematic diagram of an operational amplifier.

$$e_o = -Ae_s \tag{3.1}$$

where A is the open loop gain.

The operational amplifier possesses certain important properties. Firstly, the open loop gain is effectively infinite so that the smallest input, e_s, will drive the output to reach the limit transferable by the power supply. In addition, the device should have infinite input impedance, thereby accepting input voltages without drawing any current from the voltage sources. The amplifier should also have zero output impedance, thereby supplying any desired current to its load. Finally, the amplifier should respond to signals of any frequency, ensuring an infinite bandwidth.

As was stated the operational amplifier is the backbone unit of a potentiostat, however a number of alterations and additions must be made to the basic circuitry before this device is fully operational. Figure 3.3 is a schematic diagram of how an operational amplifier may be used in controlling a voltage at a fixed point. The input voltage is applied so that the top terminal is at e_i, with respect to the bottom one. However the inverting input is a virtual ground resulting in the lower terminal and the point A on the diagram being at $-e_i$ versus ground. The amplifier will adjust its output to control the

currents through the resistors so that this condition is maintained therefore facilitating the means to control the potential at a fixed point in the network of resistances. This implicitly is the task of a potentiostat during voltammetric studies and figure 3.4 shows how the circuit is used in operating a basic potentiostat. The current that flows through the cell is controlled by the amplifier so that the reference electrode is $-e_i$ versus ground as was stated earlier. Since the working electrode is grounded irrespective of the fluctuations in the interfacial impedances at the counter and working electrodes.

$$e_{wk}\ (\text{vs, ref}) = e_I \tag{3.2}$$

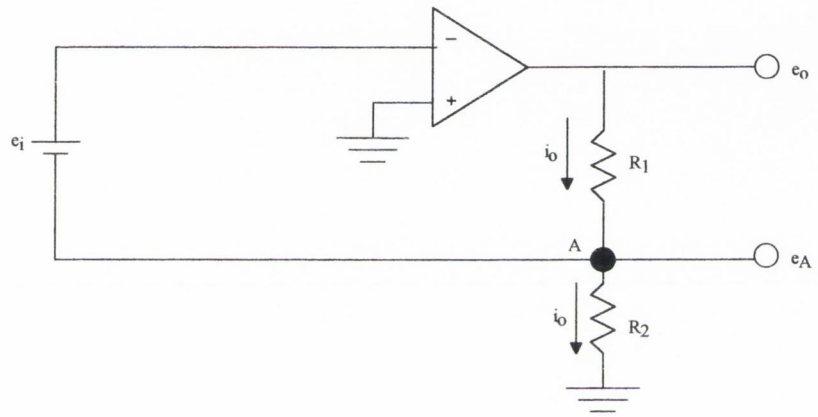


Figure 3.3 Schematic diagram of a circuit for controlling the potential at a fixed point, A. The potential may be controlled independently of the changes in the two resistors R_1 and R_2.

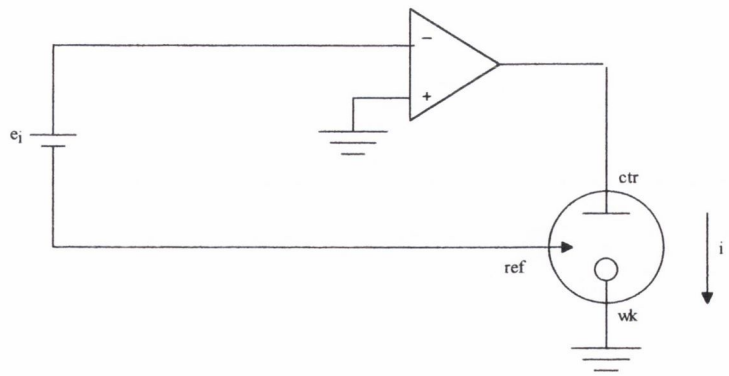


Figure 3.4 Schematic diagram of a simple potentiostat based on a control circuit

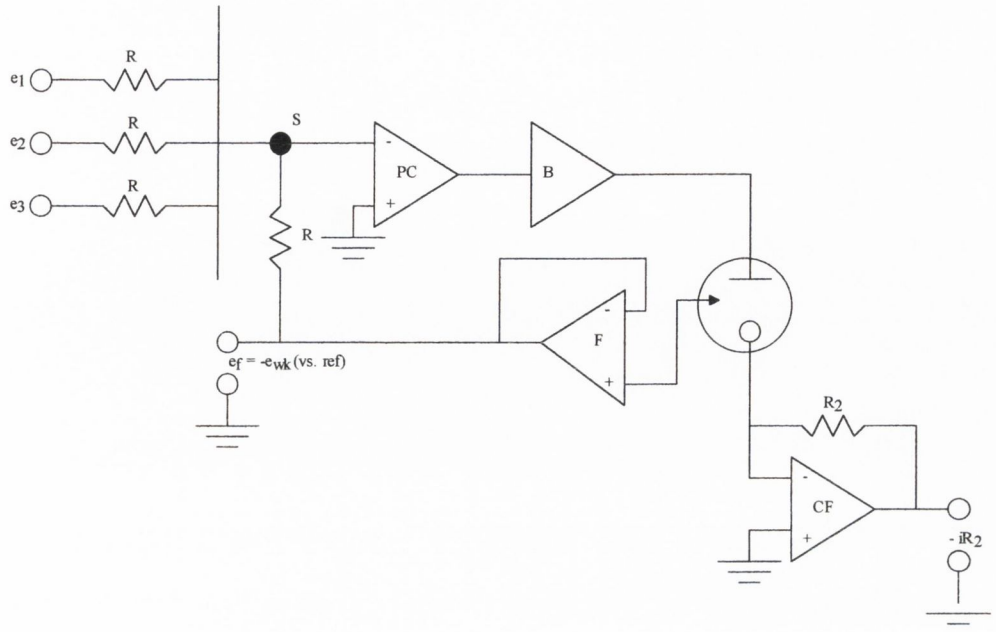


Figure 3.5 Schematic diagram of a full potentiostat based on an adder control amplifier (PC)

The potentiostat described so far will accomplish the basic tasks required however there are a few drawbacks which must be considered. First it should be noted that neither input terminal is a true ground therefore the function generator supplying the waveform for potential control has to possess a differential floating output. Another factor which must be taken into account is that there is no facility for inputting complicated waveforms at e_i, a necessity needed when conducting ac voltammetric experiments. However the application of more than one input, a device known as the adder potentiostat, solves both of the drawbacks considered *i.e.* all the inputs are true grounds and the requirement of producing complex waveforms achieved simply by the addition of the input signals. Nevertheless, more modifications to the basic adder potentiostats circuit are needed before it can be successfully used as a operational potentiostat. These modifications include inserting a voltage follower into the feedback loop of the reference electrode therefore ensuring that the electrode supplies a significant current to the summing point. Another change in the circuitry includes adding a current

follower, which the working electrode supplies, therefore making the measurement of current in the cell possible. Finally a booster(non-inverting amplifier) is placed in series with the operational amplifier, therefore increasing the power available at the cell. The final product, a full potentiostatic system based on an operational amplifier is illustrated in figure 3.5. The potentiostat used as the control element in this body of work was incorporated into the BAS 100B electrochemical analyser. The potentiostat was connected to the electrochemical cell as shown in figure 3.6.

3.2.3 C2 Cell Stand

The C2 cell, figure 3.6, stand is used for isolating the electrochemical cell completely during experimentation. The cell is composed of a Faraday cage in order to shield the cell from external electrical interference, this being an important factor when working with microelectrodes were the measured currents are at submicroampere level. Another advantage of the cell stand is that the cell during experimentation is completely isolated from light therefore facilitating work with light sensitive chemicals. The cell also features manual or computer controlled gas purging and stirring of solutions.

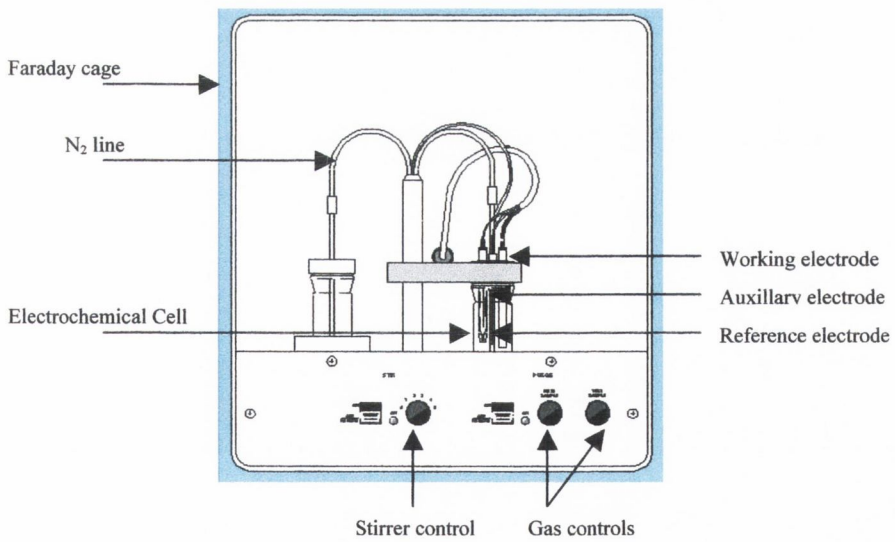


Figure 3.6 Schematic diagram of BAS 100B/W C2 cell stand

3.2.4 Low Current Module

The low current module is used in conjunction with the C2 cell stand when the working electrodes radius is of the order of micrometers. Because of their small size typically nA or pA currents are generated in studies involving microelectrodes and since the workstation is designed to measure currents from conventional electrodes (100nA – 100mA) a low current module is required. The signal to noise ratio is maximised during low current measurement by separating the electronics into two separate boxes figure 3.7. One box contains the potentiostat and the current to voltage transducer, while the other contains a second gain stage, filters, power supply and control circuitry. It should also be noted that since the electronics of the first box are close to the cell, the leads are short therefore minimising stray capacitance and increasing frequency response. The signal from the transducer is then transferred into the second box where it is filtered through a second-order, low-pass, Bessel filter and further amplified is necessary.

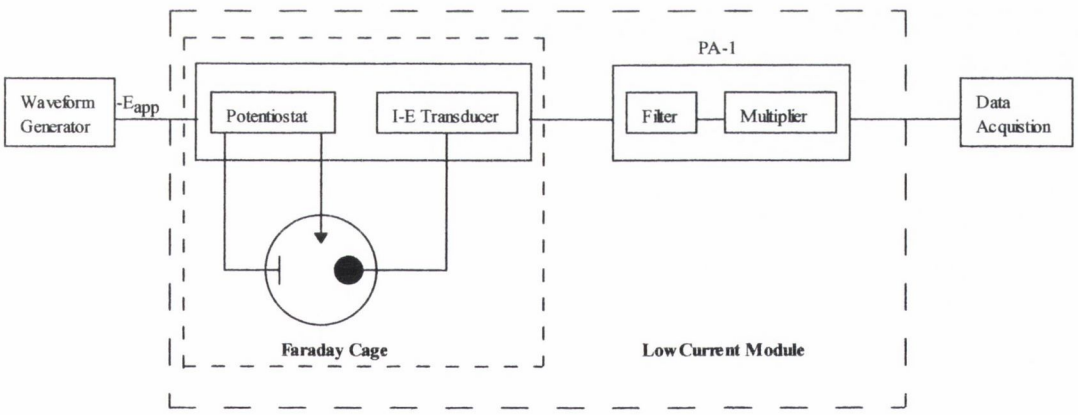


Figure 3.7 Block diagram of the Low Current Module(LCM) set up

3.3 THE ELECTROCHEMICAL CELL

The electrochemical cell consists of a working vessel, electrodes and an electrolyte solution. The working vessel is sealed (to prevent the entrance of air), with inlets for the electrodes and gas purger. Solutions were purged with nitrogen gas for 15 minutes to ensure deoxygenation before experimentation. In addition, a blanket of the inert gas was maintained during experimentation above the solution. A standard three electrode cell was used, which consisted of a working electrode, which defines the interface under study, a reference electrode, which maintains a constant reference potential, and an auxiliary (counter) electrode, which allows passage of current. The cell volume was $15cm^3$ cell for the C2 cell stand work. All work was conducted at 25°C ±1°C. Figure 3.8 illustrates the experimental set-up.

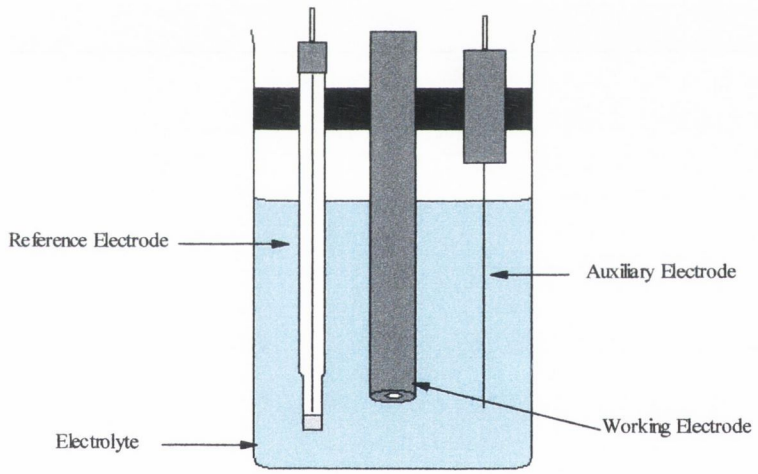


Figure 3.8 Schematic diagram of the electrochemical cell

3.3.1 The Working Electrode

In electrochemical experiments, the reactions of interest occur at the surface of the working electrode. The working electrode material used is usually pre-determined by the requirements of the experiment. A fundamental feature is that the electrode should not react chemically with the solvent or solution constituents. An additional requirement is that the electrode works correctly within the desired potential range. This accessible potential range of a particular working electrode may be limited due to a number of processes such as electrolyte and solvent decomposition, gas evolution and oxide formation on the electrode surface. Many different solid materials such as platinum, carbon, gold and mercury have all been put to use as working electrodes in order to minimise the effects of such phenomena and to maximise electrode reliability. Finally, it is necessary that the area of the working electrode is smaller than the area of the auxiliary electrode, in order to ensure even current distribution.

During the course of this work, both glassy carbon and platinum electrodes were used. The stationary glassy carbon electrode had a surface area of $0.071cm^2$ (radius = 0.0036cm), while the stationary platinum electrode had an area of $0.02cm^2$ (radius = 0.056cm). All electrodes were constructed by embedding the disc of glassy carbon or platinum into a PTFE plastic rod. All electrodes were polished to a mirror finish, as outlined in section 3.4.1, to ensure that a reproducible state of oxidation, surface morphology and absence of adsorbed impurities was achieved.

Included in this work was experimentation with five platinum micro-disc electrodes of respective areas $1.25 \times 10^{-7}cm^2$, $7.85 \times 10^{-7}cm^2$, $3.141 \times 10^{-6}cm^2$, $1.96 \times 10^{-5}cn^2$ and $7.85 \times 10^{-5}cm^2$. Their respective radii were as follows: 1.41×10^{-4}cm, 3.53cm x 10^{-4}cm, 7.07×10^{-4}cm, 9.96×10^{-4}cmand 3.53×10^{-3}cm. A factor worth mentioning when discussing microelectrodes is their construction. Although in our case no construction was required due to the presence of a viable commercial source namely BAS electrochemical, it should be noted that the construction of microelectrodes requires skill and extremely accurate equipment. Two practical considerations which must be kept in mind when working with small wires and fibres are their resistivity and their delicacy. The former consideration requires that only short sections of the

microwire be used for electrode construction, while the latter mainly represents a significant source of frustration for the novice electrode maker. For the microelectrode used during this experimentation the platinum wire is sealed directly in soft glass. The reason for using soft glass is because it has a lower stiffening temperature than other glasses and its thermal expansion and contraction behaviour is well matched to that of the microwire. A short section of the wire is then attached to a hook-up wire, the connection being made by silver epoxy. The hook-up wire is then mounted in the lumen of a soft glass tube. The hook-up wire is then secured to the glass tube with a drop of fast-setting epoxy before the tube is sealed. Finally the end of the tube is melted to form a seal around the microwire. Once all this has been completed the sealed end of the glass tube is ground flat and polished to form the microdisk.

3.3.2 The Auxillary Electrode (Counter Electrode)

The auxiliary or counter electrode supplies the required current to the working electrode, thereby preventing the polarization of the reference electrode due to the passage of current. The properties of the auxiliary electrode must be such that they do not impose its characteristics upon the measured cell response, i.e. it should be insoluble and inert in the supporting electrolyte. Properties such as size, shape and position of the auxiliary electrode are important considerations since it is these properties that decide whether the working electrode is an equipotential surface. During the course of this work a platinum wire (area= 1.3cm^2) was used as counter electrode. This was placed close to the working electrode in an attempt to minimise overall cell resistance. Finally, the surface area of the counter electrode is kept high to minimise polarization on the electrode, thus avoiding unwanted contributions to the cell response.

3.3.3 The Reference Electrode

The function of the reference electrode is to provide a fixed potential, which is uniform with respect to time during experimentation. This fixed potential is then related to another scale, for example, to the normal hydrogen electrode (NHE). Therefore, any

fluctuation in applied potential in the cell arises at the working electrode/solution interface. Ideally, if a small current passes through the reference electrode, the potential change should be negligible and should return to its initial value following cessation of the current. The most common reference electrodes capable of meeting the aforementioned criteria are the silver/ silver chloride electrodes (Ag/AgCl) and the mercury/ mercurous chloride (calomel) electrodes. The reference potential depends on the chloride concentration in the electrolyte in addition to the standard redox potential of the electrochemical reaction. In the instance of the Ag/AgCl electrode the electrolyte is generally saturated KCl or NaCl. In order to maintain a virtually constant concentration of chloride ion in the electrolyte a porous barrier is normally placed between the internal filling solution and the surrounding external solution. This allows contact between the solutions whilst minimizing their mixing. Accordingly the main reason for failure of reference electrodes is dehydration of the electrode, hence the electrode must be immersed in a saturated solution of KCl or NaCl when not in use. During the course of the microelectrode work a silver/silver chloride electrode (E= 0.197V vs NHE, E = -0.045 vs SCE)[2] was used and is represented as follows, Ag/AgCl, KCl (sat.).

However, there has been considerable debate over the use of aqueous reference electrodes such as the silver/silver chloride electrode with non-aqueous solvent systems. Among these concerns are the problems associated with the precipitation of the electrolyte and the contamination of the sample solution. The electrolytes normally used in reference electrodes (sodium and potassium) are not very soluble in organic solvents, and prolonged immersion of aqueous reference electrodes in organic solvents can lead to precipitation of these electrolytes in the Vycor frit. The precipitation of these salts results in increasing the reference electrode impedance and changes the liquid junction potential, which in turn causes the reference electrode potential to change with time. Tetrabutylammonium perchlorate, TBAP, may be used to overcome this problem, as it is soluble in both aqueous and non-aqueous solvents. The electrode was constructed using the BAS non-aqueous reference electrode kit, which must be prepared fresh each day prior to experimentation due to the photoreactivity of the electrolyte. The electrode consists of a silver wire immersed in a solution of 0.01M silver nitrate and 0.1M TBAP in acetonitrile, MeCN. The potential for this electrode is E= 0.3V vs SCE. For the

reasons described, the decision was taken to use a non-aqueous reference electrode during work involving organic solvent systems. However, in some early work the aqueous electrode was employed as the reference electrode. Direct comparison of the results obtained using these two reference electrodes is achievable as both potentials are known with respect to the NHE and can therefore be compared. Overall there is a difference of 0.345V (vs SCE) between the two reference electrode systems.

3.3.4 Electrolyte Solutions

All electrode reactions are conducted in solutions containing a high concentration of inert electrolyte, or supporting electrolyte. The purpose of an electrolyte solution is to increase the conductivity of the solution and also to minimise migration of the electroactive species caused by the electric field and to confine the interfacial potential difference to the distance of closest approach of solvated ions to the electrode. Typically, the electrolyte solution is a concentrated solution of ionised salt in a suitable solvent, which has a concentration of at least 100 times that of the electroactive species, normally varying between 0.1M and 1.0M. The supporting electrolyte must not react chemically with the electroactive species, electrodes or with the electrode products under investigation. Electrolyte reagents must be of high purification standards for this reason also. Contradictory to this experimental technique investigations into the experimental behaviour of multicharged species through cyclic voltammetry in the absence of supporting electrolyte have been carried out recently by Bond *et al.*[4] In this instance voltammetry of the highly charged electroactive species, without electrolyte addition, is achieved due to the electroreactant and its counterion providing the means for the current to be transported through the cell.

A number of different electrolytes were used throughout the course of this work for both aqueous and organic solvents. The aqueous electrolytes were prepared from ultra-pure water from a Millipore water purification system. Organic solvent work was carried out using HPLC grade acetonitrile. The electrolytes tetraethylammonium perchlorate (TEAP), tetrabutylammonium perchlorate (TBAP), lithium perchlorate

($LiClO_4$), potassium perchlorate ($KClO_4$) and sodium perchlorate ($NaClO_4$) were obtained from Aldrich.

In order to minimise the undesirable effects caused by dissolved oxygen the electrolyte solutions were deoxygenated thoroughly with a fine stream of nitrogen before every experiment for at least 15minutes. Some problems which might be encountered if oxygen were present include: oxygen reduction at cathodic potentials, oxide formation on electrode surface and reaction with intermediates formed during the electrode reactions. More specifically, reduced polypyrrole may be slowly oxidised in an oxygen environment. [5]

3.3.5 Reagents

All solutions were thoroughly deoxygenated prior to electrochemical measurements. Standard solutions of electroactive species were prepared fresh daily. Pyrrole was freshly distilled prior to use. The monomer materials were all purified by column chromatography to ensure a high level of purity (95-99%). NMR analysis and microanalysis or mass spectrometry verified their high degree of purity.

3.4 ELECTRODE MODIFICATION TECHNIQUES

3.4.1 Electrode pre-treatment

All electrodes were polished prior to use to ensure a reproducible electrode surface morphology and freedom from any adsorbed impurities. The technique employed to pre-treat the electrode was dependent on the electrode material. The platinum electrodes were polished using alumina oxide (0.3μm) and distilled water on a fine grit pad. Glassy carbon electrodes were, however, initially polished on a cloth pad with diamond lapping compounds of 15, 3 and 1μm dimensions. This was then followed by polishing with alumina oxide paste on the fine grit pad. In all cases a reproducible, uniform electrode surfaces were obtained. Finally, the electrode was washed thoroughly with Millipore water to remove any trace of the solid polishing residues. The result was

a reproducible, uniform electrode surface onto which the polymer film readily adhered onto.

3.4.2 Polymer Film Synthesis

Electronically conducting copolymers are deposited as thin films onto a platinum electrode through anodic oxidation of equimolar amounts (50mM) of the redox active monomer and pyrrole in a solution of 0.1M tetraethylammonium perchlorate in acetonitrile. Cyclic voltammagrams of the copolymers were obtained by sweeping the potential from 0 to 1.2V at a scan rate of $50mV/s^{-1}$ vs a Ag/AgCl reference electrode. Previous attempts at polymerizing the monomer (i.e monomers **18** n=3-7) in the absence of pyrrole resulted in a passivating polymeric layer being formed. The pyrrole monomer (Aldrich) was distilled prior to use, ensuring that a fresh monomer solution was used daily. The working solution was deoxygenated by passing a fine stream of nitrogen through the solution for 15 minutes before each experiment and additionally a blanket of nitrogen was maintained over the solution throughout experimentation.

Electropolymerization of the disubstituted ferrocenyl monomers was directly achieved through the application of a sweep potential over the potential range 0 to 0.9V to a solution of monomer (10mM) Continued cycling between these limits led to the growth of a conducting polymer film. The electopolymerization conditions included using a solution of 0.1M TBAP/CH_3CN as electrolyte and employing a scan rate of $50mV/s^{-1}$. In this case an Ag/$AgNO_3$ reference electrode was used. Once more the working solution was deoxygenated by passing a fine stream of nitrogen through the solution for 15 minutes before each experiment.

3.5 EXPERIMENTAL TECHNIQUES

3.5.1 Potential Sweep Techniques

Potential sweep techniques include two fundamental areas, linear sweep voltammetry, LSV, and cyclic voltammetry, CV. Both techniques involve applying a time dependent potential to a working electrode in a solution of interest, possibly containing an electroactive substrate, an excess of electrolyte, a reference, and a counter electrode. The potential may be swept linearly to a predetermined voltage limit (LSV) or cyclically (CV). Cyclic voltammetry basically involves the potential being swept linearly between two predetermined voltage limits, E_1 and E_2 with the sweep direction reversed at a chosen potential, E_2, also known as the switching potential, and continued in the opposite direction at a known scan rate, υ where $\upsilon = dE/dt$. The resulting triangular waveform is represented in figure 3.9. Ordinarily, the starting working electrode potential is chosen where a substrate is electroinactive. Subsequently, the potential is changed at a constant scan rate through a potential window where the redox reaction of interest takes place until the switching potential is reached. The resulting voltammogram displays the measured cell current as a function of the applied potential and is indicative of specific electrode reactions or mechanism. In addition, the determination of the potentials where these reactions occur (i.e. standard redox potential, E^0) may be achieved.

Cyclic voltammetry has become one of the most important electroanalytical techniques in recent years.[6-10] This may be attributed to the fact that invaluable information on the presence of electroactive moieties in the solution or at the electrode interface may be ascertained *via* such techniques. Identification of the roles of adsorption, diffusion, and coupled homogeneous chemical reactions may be identified from the sweep rate dependence of the observed peaks. In addition elucidation of kinetic parameters may also be achieved. These factors have ensured an increase in popularity for such techniques and also rendered it one of the first techniques to be employed whilst researching a novel electrochemical system.

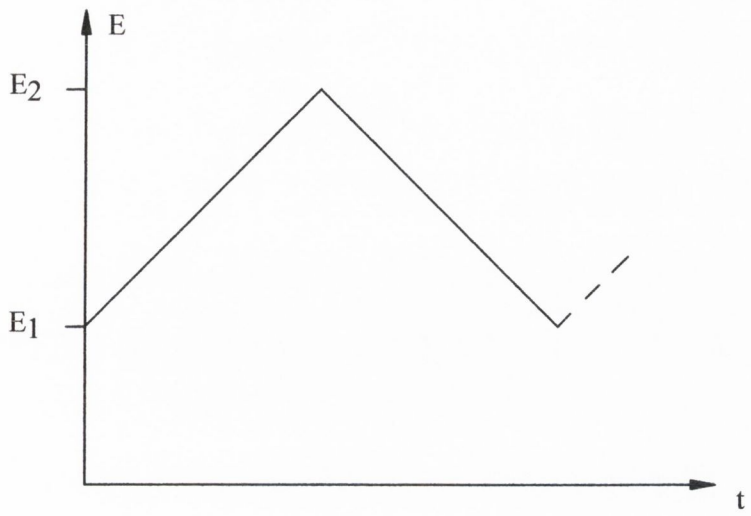


Figure 3.9 Illustration of the linear potential sweep with a triangular waveform, which is applied to the working electrode. This excitation signal scans the electrode between two potentials E_1 and E_2

Generally, electrochemical systems are classified into three categories; reversible, irreversible and quasi-reversible systems. In essence, the magnitude of the electrode transfer rate constant for a particular system determines the subsequent allocation of type. Furthermore, redox reactions may involve either solution phase or immobilized couples. The observed current response is dependent mainly on two steps, the transport of electroactive species from the bulk solution to the electrode surface and secondly, the electron transfer reaction between the species and the electrode surface. To elaborate further, a reversible system occurs when the oxidised and reduced species are in equilibrium at the electrode surface, in this situation the Nernst equation (equation 3.1) can be applied. The electrode reaction is known as reversible since it obeys the condition of thermodynamic reversibility. The application of the Nernst equation, and therefore the criteria for reversibility, is related to the time it takes the electrode reaction to reach equilibrium. The concentration of the electroactive species at the interface depends on the mass transport of these moieties from bulk solution and is governed by the mass transfer coefficient, k_d. The rate constant when $E = E_0$ is known as the standard rate constant, k_o. In the case of a reversible reaction the kinetics of the electrode reaction

is mush faster than the transport. Conversely, an irreversible reaction is one where the rate of electron transfer is insufficient to maintain Nernstian equilibrium. The shape of the voltammogram in this instance is reliant on the sweep rate applied. At low potential sweep rates the rate of electron transfer is greater than that of mass transfer, and a reversible cyclic voltammogram is observed. However, as the sweep rate is increased the rate of mass transport increases and becomes comparable to the rate of electron transfer. The most observable manifestation of this is the increase in peak separation. As previously mentioned, certain systems may be reversible at low sweep rates and become irreversible at higher ones, this occurs after passing through a region known as quasi-reversible at intermediate values. Figure 3.10 illustrates the transition from reversible to quasi-reversible and finally to irreversible behaviour as observed through a plot of Ip *vs* $\upsilon^{1/2}$.

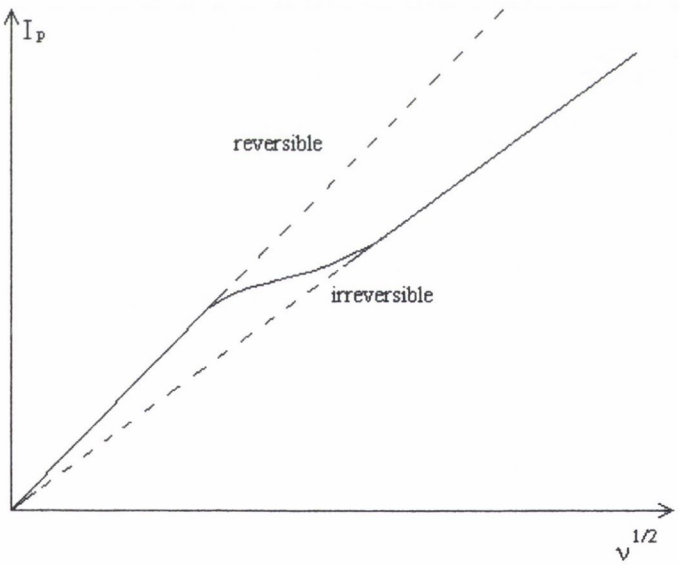


Figure 3.10 Transition from reversible to irreversible behaviour of the redox couple due to change of scan rate.

In order to comprehend the shape of a typical cyclic voltammogram let us examine the sitaution for a reversible system. If the electrochemical kinetics of the overall process are so fast that the rate determining step is the transport of the substrate to the interface, then the reaction is said to be mass transport controlled. Under such circumstances the electron transfer process obeys the Nernst equation. The following equation may explain the electrochemical process of a simple *n* electron reversible electrode reaction.

$$R \Leftrightarrow O + ne^-$$

where *R* and *O* represent the reduced and oxidised forms of the electroactive species respectively.

Figure 3.11 illustrates the expected cyclic voltammetric response for this simple n electron reaction. The shape of this voltammogram may be quantitatively explained as follows. For a reversible redox process, the ratio of the concentration of the oxidised form to reduced form, C_o/C_R, within the region next to the electrode surface follows the applied potential in a Nernstian manner,

$$E = E^0 + 2.303\left(\frac{RT}{nF}\right) ln\left(\frac{C_0}{C_R}\right) \tag{3.3}$$

where the potential, E, can be related to the formal potential of the redox couple, E^0, using equation (3.3). T is the absolute temperature and R and F represent the gas and Faraday's constants respectively. The experimentally measured response is the current, which passes between the working electrode and the counter electrode. This current i, is proportional to the concentration gradient near the electrode surface according to Fick's first law

$$I = nFAD\left(\frac{dC_0}{dx}\right) \tag{3.4}$$

where D is the diffusion coefficient, F is the Faraday constant and A is the geometric area of the electrode.

The shape of the cyclic voltammogram may be explained in terms of the concentration profiles shown in figure 3.12. The working electrode may be considered as a "reagent" of adjustable oxidising and reducing strength. This is purely a theoretical image as the electrochemical processes are occurring at the interface of the two different phases and is therefore heterogeneous in nature. In order for electron transfer to occur, the molecules in solution have to approach the electrode. As the solution is unstirred, mass transport in this situation can only occur by diffusion due to the concentration gradients created around the electrode surface. Such concentration distance profiles are illustrated in Figure 3.12 and are representative of the different steps of a cyclic voltammogram scan shown in figure 3.11. Initially at potentials prior to the commencement of an electrode reaction there is no cell current produced. However as the potential is swept anodically towards the potential where the electrode reaction occurs, E^0 the electrode becomes a sufficiently strong oxidant transforming R to O, hence the surface concentration of the reduced species, R, decreases progressively (point c). This results in a small anodic current flowing. At E^0, the redox potential of the redox couple, the ratio of concentrations, C_o/C_R, is always unity. Continuation of the potential sweep, past E^0 causes the concentration gradient to reach a maximum, this correlates to the peak current, i_{pa}. The increasing of the potential leads to the consumption of the reduced form of the electroactive species at the electrode surface resulting in the depletion of the R species concentration to almost zero, (point d). In unstirred solutions the mass transport of R reaches a maximum rate, which then decreases as the consumption of R, further and further from the electrode surface occurs. This is evident in the decay of the current (point e and f). On reverse scanning the series of events described is repeated for the generation of O, the oxidised form of the electroactive species, which now predominates at the electrode surface. This process eventuates in the generation of a reduction peak on the reverse scan, the net process producing a current/potential trace similar to that illustrated in figure.3.11, (pointsg-k)

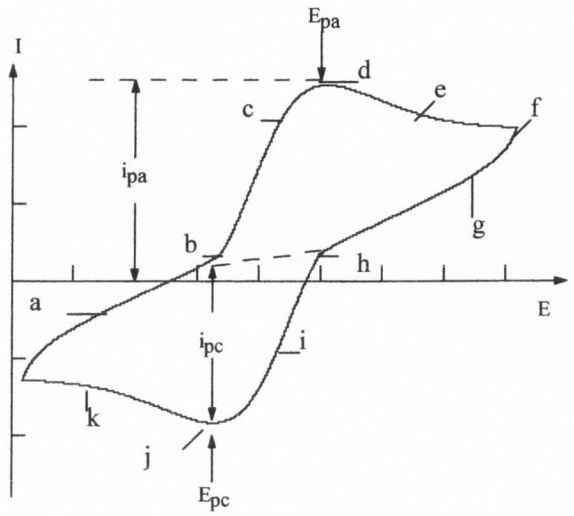


Figure 3.11 Cyclic Voltammogram for a model reversible process, $R \Leftrightarrow O + ne^-$.

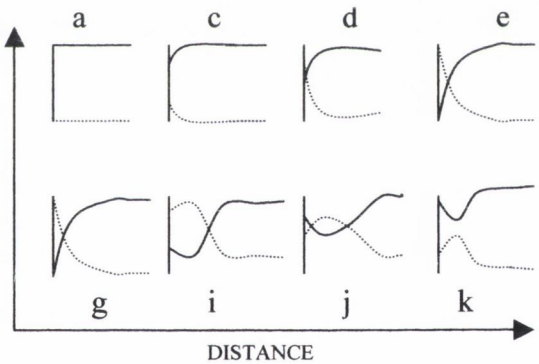


Figure 3.12 The concentration-distance profiles for an electroactive species, R, during various stages of cyclic sweep voltammetry as illustrated in figure 3.11; the solid lines correspond to the oxidising species and the dotted lines to the reducing species. The overall reaction sequence is $R \Leftrightarrow O + ne^-$. The curves correspond to the following approximate potentials; (a) E^0 –90mV; (b) E^0 –50mV; (c) E^0; (d) E^0 +30mV; (e) E^0 +130mV; (f) E^0 +280mV, (g)-(k) represent the reverse sweep potentials.

The mass transport of the redox species reaches a maximum through its diffusional transport to the electrode surface which arises as a result of the generation of an interfacial concentration gradient. Elimination of migration effects is achieved through the presence of an excess of electroinactive ions, while convection currents are avoided through the use of unstirred solutions. The shape of the resultant cyclic voltammograms is then a function of experimental parameters such as the applied potential, E, the scan rate, υ, electron transfer rate parameters, concentration of redox species, diffusion coefficients, and finally the nature and geometry of the working electrode.

Under the conditions of semi-infinite linear diffusion and reversible electron transfer kinetics, the peak current i_p, is given by[11-13]:

$$i_p = 0.4663nFA\left(\frac{nF}{RT}\right)^{1/2} C_0^{\infty} D^{1/2}\upsilon^{1/2} \qquad (3.5)$$

where D is the diffusion coefficient, υ is the scan rate, and C_0 is the concentration of the bulk solution of electroactive species. This is known as the Randles-Sevcik equation and shows that the peak current is proportional to the square root of the scan rate. It should be noted, however, that the diffusion characteristics of the system may only hold for a short time, as thermal and concentration gradients may induce random convection processes, resulting in fluctuations of the resulting current. For this reason, only data obtained from analysis of the first sweep is normally used to deduce kinetic parameters.

As previously discussed, in the case of irreversible systems, the electron transfer rates at all potentials are significantly less than the rate of mass transfer. As a result, Nernstian equilibrium is not maintained at the electrode surface. When the rate of electron transfer is insufficient to maintain this surface equilibrium, then a modification of the shape of the cyclic voltammogram is observed. Probably the most marked feature of a cyclic voltammogram recorded for a totally irreversible system, is total absence of a reverse peak, however this alone is not conclusive evidence of an irreversible system and other diagnostic tests are necessary for verification.[14] A description of the various

diagnostic tests for irreversible and reversible systems may be found in work carried out by Nicholson and Shain.[13]

Frequently, processes under cyclic voltammetric examination appear reversible at low values of scan rate, but appear to become irreversible at higher values of sweep rate. This scan dependence is illustrated in figure 3.10. Generally, if the extent of irreversibility increases with increasing scan rate, the system is said to be quasi-reversible. This type of system is mathematically complex as it necessitates simultaneous consideration of the kinetics of both the oxidation and the reduction reactions at the electrode surface and the rate of material transport to the electrode surface. These kinetics are described by the Butler-Volmer equation. Here the observed current is proportional to the difference between the rate of the oxidation and reduction reactions at the electrode surface and is given by:

$$I = nFA(k_a[C_R] - k_c[C_O])$$

Where k_a and k_c are the anodic and cathodic rate constants respectively.

3.5.2 Cyclic Voltammetry at Microelectrodes

Cyclic voltammetry at microelectrodes is conducted in the exact same media as at macroelectrodes except that the working electrode has a characteristic length typically less than 50 μm. Several advantages exist for the employment of microelectrodes in place of macroelectrodes. These include:

At microelectrodes the rates of mass transport to and from the working electrode are significantly greater than that for macroelectrodes.

Steady-state (time–independent) rates of mass transport are readily and rapidly established at microelectrodes. If we consider the simple n electron reversible electrode reaction ;

$$R \Leftrightarrow O + ne^-$$

With a working electrode upon electrolysis, the reduced species is consumed at the surface of the electrode and so a concentration gradient is formed between the electrode and the bulk solution. A consequence of this is that the R molecules diffuse towards the working electrode in order to replace those being consumed by the electrochemical reaction. The domain perturbed by the electrolysis region is called the diffusion layer. Equations for both planar and non-planar (spherical) diffusion to the electrode surface predict that at the onset of electrolysis the diffusion layer will keep growing into the solution as a function of time [15-18]. It has also been established that at small electrodes the growth of the diffusion layer is initially similar to that observed at larger electrodes. However the difference occurs at much longer times where growth slows down considerably. That is, the size of the diffusion layer at $t>>0$ is smaller for small electrodes and consequently the concentration gradient (rate of mass transport) is notably greater. This occurrence is easily explained. At short times, the size of the diffusion layer is smaller than that of the electrode and as with macroelectrodes planar diffusion dominates, thus explaining why at short times a microelectrode will exhibit macroelectrode like behaviour, figure 3.13 (a) and (c). However at longer times the dimensions of the diffusion layer exceed those of the microelectrode and the diffusion profile becomes hemispherical and steady state (sigmoidal-shaped) voltammograms comparable to those obtained at rotating disc electrodes are obtained, figure 3.13 (b). The change in the diffusion profile at a microelectrode over long times means many more electroactive particles per unit time reach the electrode than in the case of pure planar diffusion at macroelectrodes. On the other hand the particle flux in and out of the volume eventually become stationary and the diffusion layer stops growing.

Comprehensive theoretical studies completed by Oldham [19-21] et al. have shown that the stationary limiting current at microelectrodes of different dimensions is given by

$$i = 2nFc^{*}Dd \tag{3.6}$$

where d is the surface diameter. For an embedded disk microelectrode d is equal to $2r_0$, for a sphere $d = 2\pi r_0$ and for a hemisphere $d = \pi r_0$.

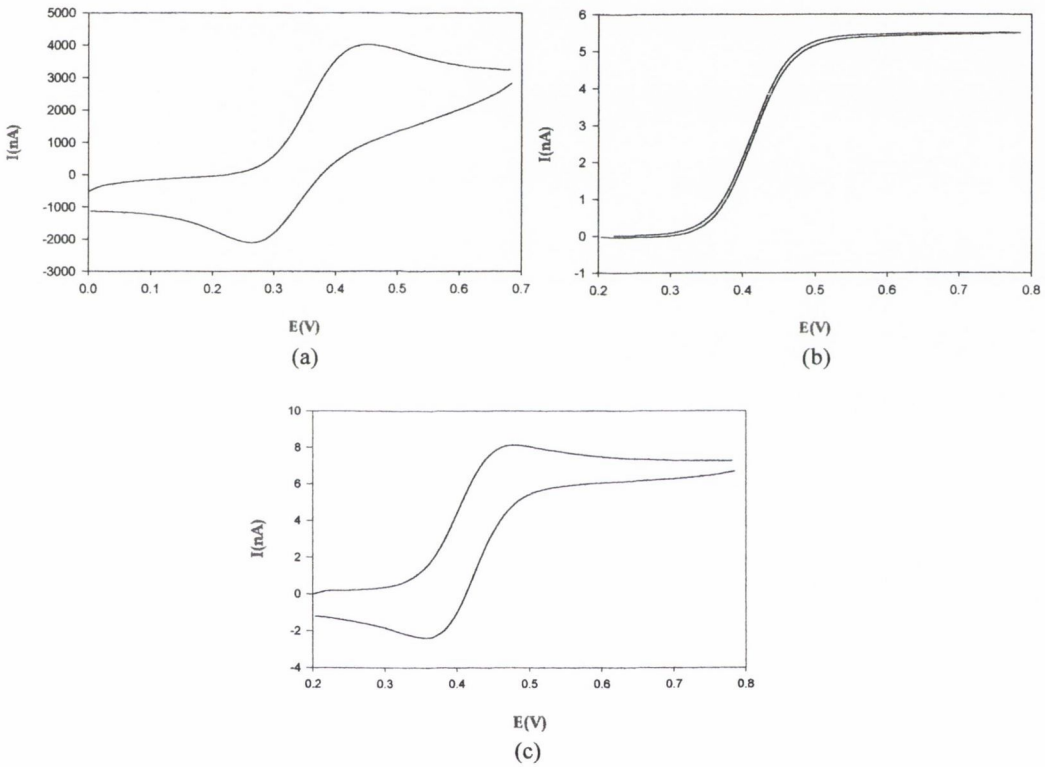


Figure 3.13 Voltammetric responses at (a) a macroelectrode (b) a microelectrode at long time and (c) a microelectrode at short time.

3.5.3 Potential Step Techniques

Chronoamperometric experiments involve an instantaneous change in the applied potential to the working electrode and the resulting current-time response recorded as the system relaxes towards its new steady state. If we consider the simple n electron reversible electrode reaction;

$$R \Leftrightarrow O + ne^-$$

A potential-time profile as shown in figure 2.18(a), is applied to the working electrode. E_1 is chosen so that initially only species R is present in solution. At t=0, the potential is instantaneously changed from E_1 to E_2, where oxidation of the R species occurs at a diffusion controlled rate. The resulting current-time transient is shown in figure 3.14 (b). The current will be the sum of the electrochemical double layer charging current and the Faradaic current. The double layer charging current is due to a reorganisation of the species in the double layer as a result of changing the potential and manifests itself as a sharp spike in the current at short times with a typical lifetime of a few hundred microseconds. The Faradaic current is due to electron transfer to R species in solution.

Concentration profiles develop near the electrode surface with time. At t=0, the surface concentration of R, C_R changes from its initial value C_R^{∞}, to zero. This occurs at points very close to the electrode surface and consequently the concentration profile will be steep. With increasing time, diffusion causes the concentration profiles to relax towards their steady state by extending into solution and becoming less steep. Fick's second law of diffusion (eqn. 3.7), describing the change in C_R with time, may be solved to obtain more detailed knowledge of the current-time transient,

$$\frac{\partial C_R}{\partial t} = D_0\left(\frac{\partial^2 C_R}{\partial x^2}\right) \tag{3.7}$$

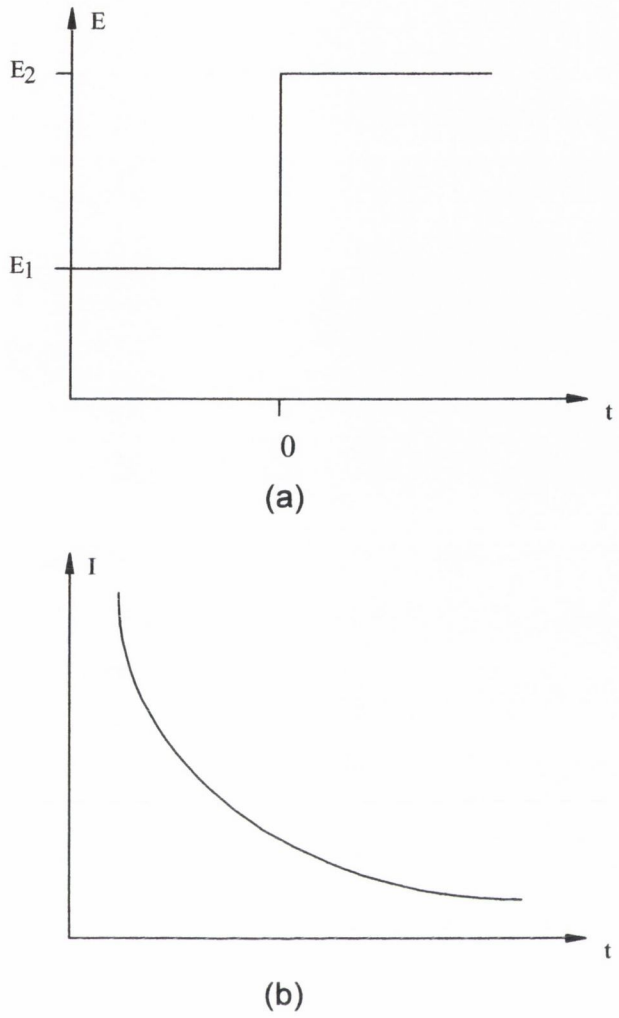


Figure 3.14 (a) The potential-time profile for a single potential step chronoamperometric experiment, (b) The resulting current-time transient for the reaction $O + ne^- \Leftrightarrow R$

subject to the boundary conditions appropriate for semi-infinite diffusion:

At t=0 and for all x, $C_R = C_R^{\infty}$,

For t>0, at x=0, $C_R = 0$,

At x= ∞, $C_R = C_R^{\infty}$.

Typically for purely planar diffusion to the electrode, solution of the differential equation (3.7) yields the Cottrell equation[22]

$$i = \frac{nFAD_0^{1/2} C_R^{\infty}}{\pi^{1/2} t^{1/2}} \tag{3.8}$$

where n is the number of electrons transferred, D is the diffusion coefficient, F is the Faraday constant and A is the geometric area of the electrode. Therefore if the reaction is diffusion controlled a plot of I *versus* $t_{1/2}$ should be linear and pass through the origin. However when diffusion is not purely planar and consideration of spherical diffusion is needed (in the case of microelectrodes) the Cottrell equation for a disc electrode is modified to

$$\frac{it^{1/2}}{nFAD^{1/2} C_R^{\infty}} = \frac{1}{\pi^{1/2}} \left(1 + b \left(\frac{Dt}{r_0^2} \right)^{1/2} \right) \tag{3.9}$$

where the value of the prefactor b is $\pi^{1/2} \leq b \leq 4\pi^{1/2}$.

3.6 CONCLUSIONS

A detailed account of the instrumentation employed during the course of this work was described. In addition the various experimental techniques applied during experimentation were outlined. Finally, an account of the basic three-electrode electrochemical cell was described. This account included an outline of the working, auxiliary and reference electrodes as well as the electrolyte solutions and reagents employed during the course of this work.

3.7 REFERENCES

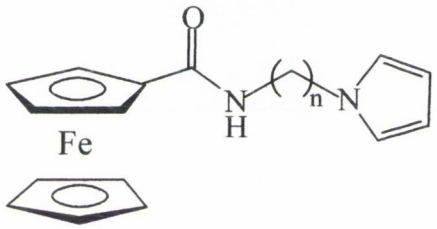
1. A. Von Fraunhofer, C.H. Banks, Potentiostat and its applications, Butterworth & Co. Ltd., 1st Edition, (1972).
2. A.J. Bard, L.R. Faulkner, Electrochemical Methods, Fundamentals and Applications. J. Wiley & Sons, (1980).
3. C.M.A. Brett, A.M.O Brett, Electrochemistry-Principles, Methods and Applications, Oxford Science Publications, (1993).
4. A.M. Bond, D.C. Coomber, S.W, Feldberg, K.B. Oldham, T. Vu, *Anal. Chem.*, 73, 352, (2001)
5. A.F. Diaz, Chemica. Scr., **17**, 145, (1981).
6. K. Aoki , K. Tokuda and H. Matsuda, *J. Electroanal. Chem.*, **146**, 417, (1983).
7. G.A. Mabbott, *J. Chem. Edu.*, **60**, 697-706, (1983).
8. R.S. Nicholson, *Anal. Chem.*, **37**, 1351, (1965).
9. P.T. Kissinger, W.R. Heineman, *J. Chem. Educ.*, **60**, 702, (1983).
10. J. Heinze, *Angew. Chem. Int. Ed. Engl.*, **23**, 831, (1984).
11. J.E.B. Randels, *Trans. Faraday Soc.*, **44**, 327, (1948).
12. A. Sevcik, *Coll. Czech. Chem. Commun.*, **13**, 349, (1958).
13. R.S. Nicholoson, I. Shain, *Anal. Chem.*, **36,** 706, (1964).
14. Southampton Electrochemistry Group, "*Instrumental Methods in Electrochemistry*", ed. T.J. Kemp, Ellis Hardwood, Chichester, (1985).
15. M.S. Wightman, *Anal. Chem.*, **53**, 9, (1981).
16. S. Pons and M. Fleischman, *Anal. Chem.*, **59**, 24, (1987).
17. K. Aoki, *Electroanalysis*, **5**, 627, (1993).
18. J. Heinze, *Angew. Chem. Int. Ed. Engl.*, **32**, 1268, (1993).
19. K.B. Oldham, *J. Electroanal. Chem.*, **122**, 1, (1981).
20. K.B. Oldham, C.G. Zoski, *J. Electroanal. Chem.*, **256**, 1, (1988).
21. C.G. Zoski, A.M. Bond, E.T. Alinson, K.B. Oldham, *Anal. Chem.*, **62**, 37, (1990).
22. F.G. Cottrell, *Z. Physik. Chem.*, **42**, 385, (1902).

CHAPTER FOUR

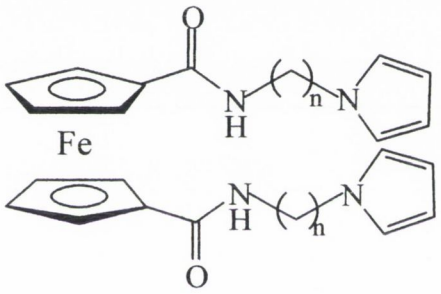
ELECTROCHEMICAL PROPERTIES OF HYBRID MONOMER AND POLYMER SPECIES

4.1 INTRODUCTION

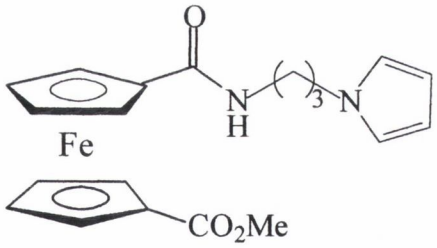
The syntheses of ferrocene-pyrrole derivatives of the given formula **18**, **20** and **21** as shown in Scheme 4.1, were presented in detail in chapter 2. This chapter shall discuss the electrochemical properties of these novel materials. In addition, the ability of the monomer groups to be electropolymerized, or copolymerized in cases where appropriate, is considered. For the purpose of distinctness the novel monomers are divided into two groups, mono-substituted ferrocene species, **18**, and disubstituted ferrocene moieties, **20** and **21**. The latter group is sub-divided into symmetrically, **20**, and asymmetrically, **21**, substituted subgroups. Electrochemical characterization and polymerization investigations into these groups of compounds shall be dealt with individually before discussing any overall difference that occurs between these groups.



18 n = 3, 4, 5, 6 and 7



20 n = 3, 5 and 7



21

Scheme 4.1

4.2 ELECTROCHEMICAL PROPERTIES OF FERROCENE-PYRROLE HYBRID COMPOUNDS.

4.2.1 Electrochemical behaviour of compounds of structure 18

The electrochemical behaviour of the ferrocene modified pyrrole monomer, of the structure **18** n = 3, was investigated using cyclic voltammetry. The voltammogram of a 1mM solution of monomer in acetonitrile, using tetrabutylammonium perchlorate (TBAP) as supporting electrolyte, is presented in figure 4.1. The sweep rates employed were in the range of 0.005-0.2Vs^{-1}. The scan was recorded between the voltage limits of 0-0.6V against a $Ag/AgNO_3$ reference electrode. Experimental results showed that this behaviour was similar for both platinum and glassy carbon working electrodes. In addition this behaviour was found to typify the four remaining monomers, **18** n= 4, 5, 6 and 7, see figures 4.2 to 4.5 respectively.

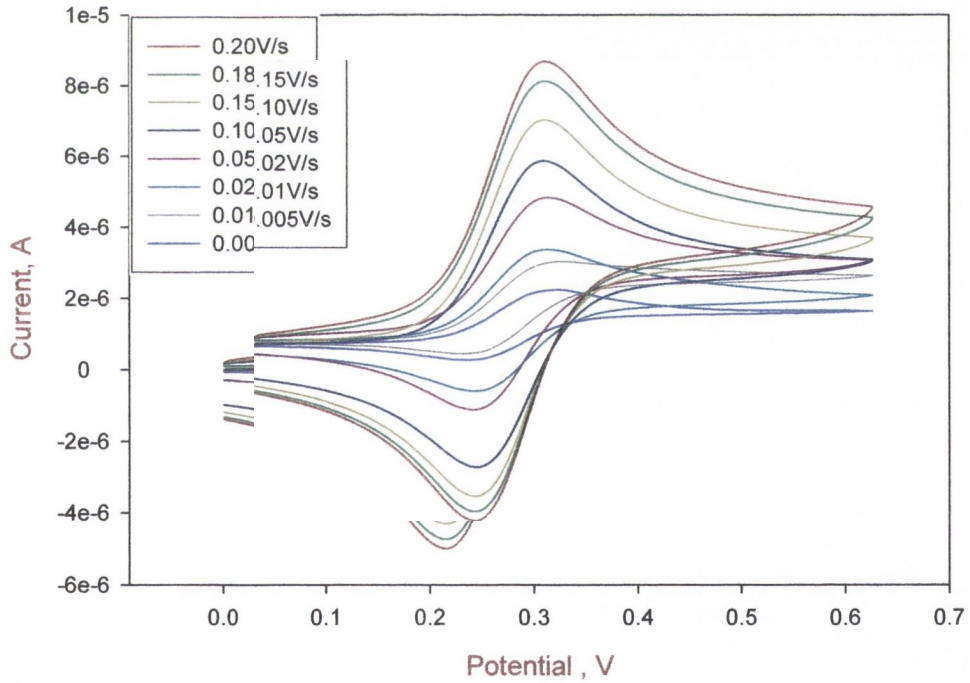


Figure 4.1 Cyclic voltammogram of **18** n=3 (1mM) at varying scan rates in 0.1M TBAP/ CH_3CN at a Pt disk electrode at 25°C vs $Ag/AgNO_3$ reference electrode.

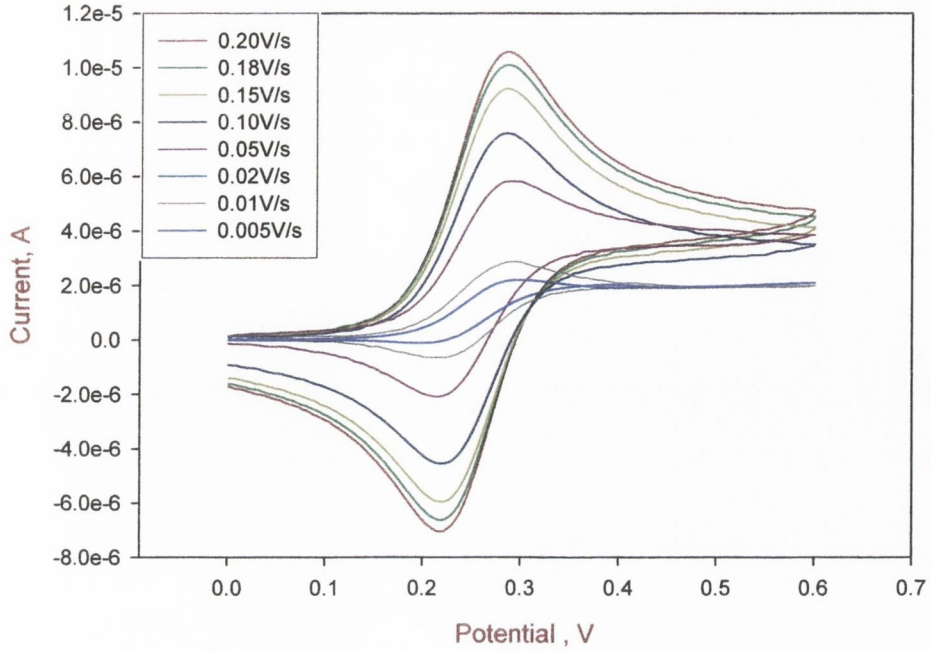


Figure 4.2: Cyclic voltammogram of **18** n=4 (1mM) at varying scan rates in 0.1M TBAP/ CH_3CN at a Pt disk electrode at 25°C vs $Ag/AgNO_3$ reference electrode.

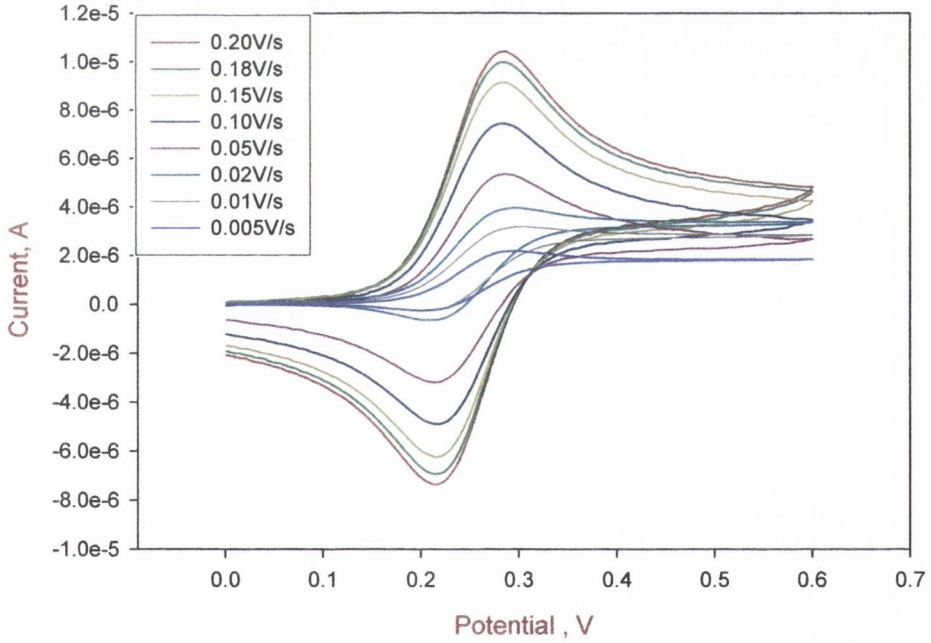


Figure 4.3: Cyclic voltammogram of **18** n=5 (1mM) at varying scan rates in 0.1M TBAP/ CH_3CN at a Pt disk electrode at 25°C vs $Ag/AgNO_3$ reference electrode.

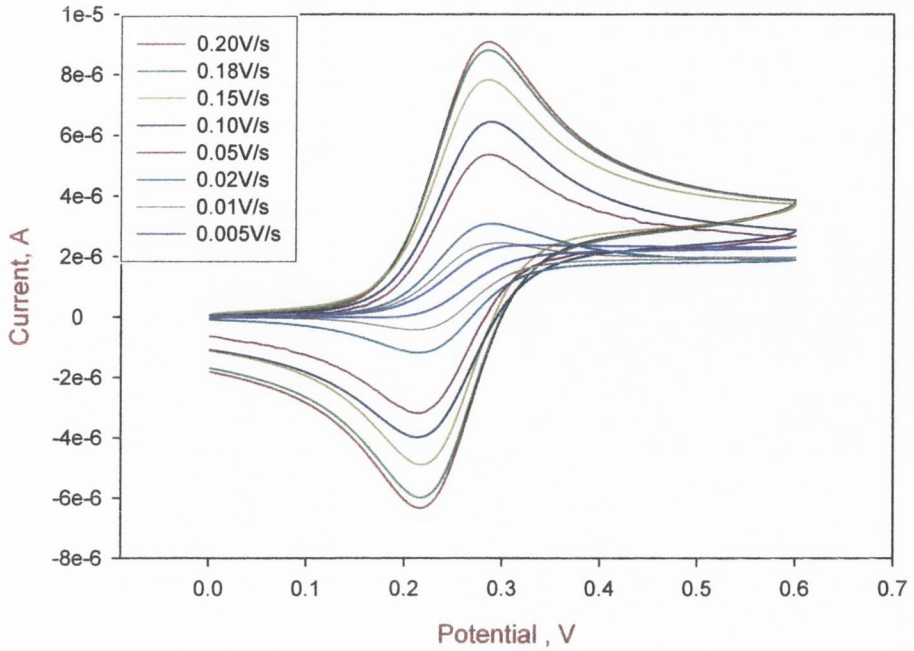


Figure 4.4: Cyclic voltammogram of **18** n=6 (1mM) at varying scan rates in 0.1M TBAP/ CH_3CN at a Pt disk electrode at 25°C vs $Ag/AgNO_3$ reference electrode.

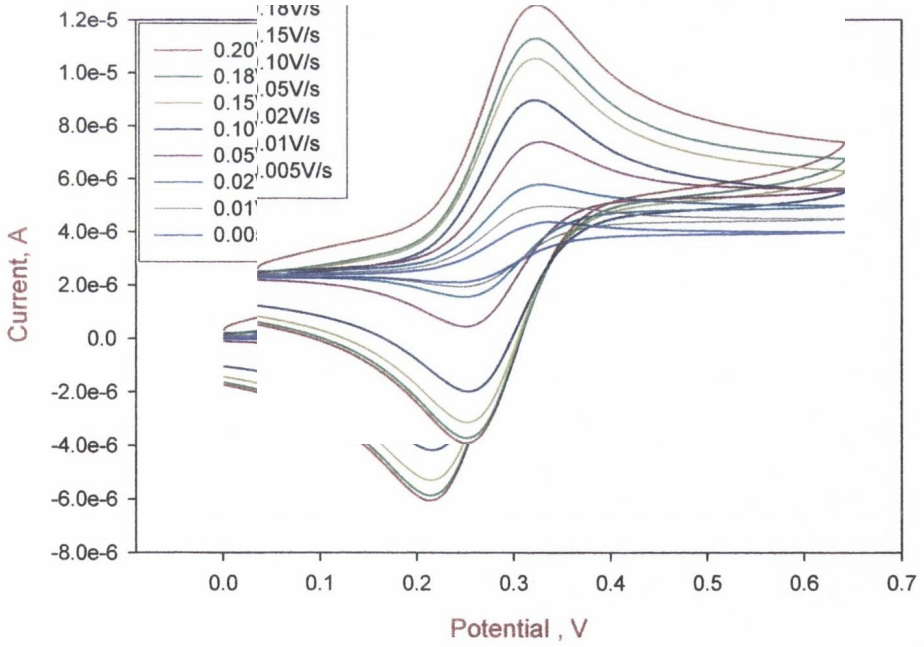


Figure 4.5: Cyclic voltammogram of **18** n=7 (1mM) at varying scan rates in 0.1M TBAP/ CH_3CN at a Pt disk electrode at 25°C vs $Ag/AgNO_3$ reference electrode.

The formal potential values taken as an average of anodic and cathodic peak potentials at a scan rate of $0.1Vs^{-1}$ were $E^{0'} = 0.251$, 0.253, 0.251, 0.252, and 0.250V for **18** n= 3, **4**, 5, 6 and 7 respectively. The confidence limit is ±5mV in each case. These values are in good accordance with the redox potentials reported for ferrocene and other substituted ferrocene derivatives.[1-5] Literature values for the standard formal potential for a range of ferrocene derivatives are outlined in table 4.1, the structure of these compounds is also depicted.

In the case of other amide ferrocene-pyrrole derivatives the mono-substituted ferrocene, N-[2-(pyrrole-1yl)ethyl]-N-ethylferrocene-1-carboxamide, **23**, has a formal potential of 0.22V in 0.1M TBAP/MeCN versus a $Ag/AgNO_3$ reference electrode.[3] Similarly, the potential for a ferrocene moiety with a mono- amide linked pyridine group, **31**, is 0.24V [5]. Furthermore, a mono-substituted amide linked 2,2'-bipyridine ferrocene, **25**, was found to have a formal potential of 0.26V under identical conditions[2]. All these compounds have a mono-substituted ferrocene with an amide linkage and are in good agreement with the results found for the compounds synthesised during the course of this work. The corresponding ferrocene substituted with a carboxylic ester linked 2,2'bipyridine group, **27**, was found to have formal potential of 0.34V, again under identical conditions[2], which suggests the ester linkage renders the oxidation process of the ferrocene more difficult. However, the formal potential of a ferrocene compound with an alkyl chain directly attached, N-[3-(pyrrole-1yl)propyl]-ferrocene[4], **29**, is 0.35V. This suggests that the amide linkage results in a lower formal potential for the ferrocene group as compared to those with direct or ester linkages, this is an important factor when considering the synthesis of future redox active monomers of this type. It may be useful in the design of conducting electrocactive polymers with a specific redox potential range. This deduction will be discussed further on examination of the disubsituted ferrocene-pyrrole monomers.

Table 4.1: Estimated Standard Potentials and Diffusion Coefficients for a range of Ferrocene derivatives in 0.1M TBAP/MeCN vs $Ag/AgNO_3$ reference electrode

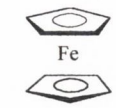
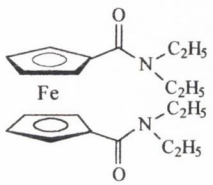
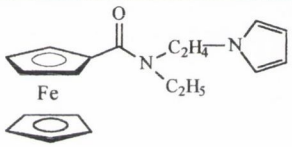
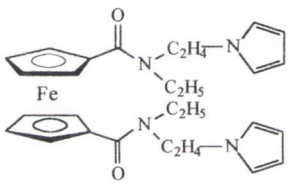
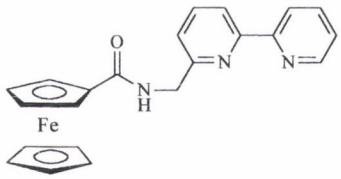
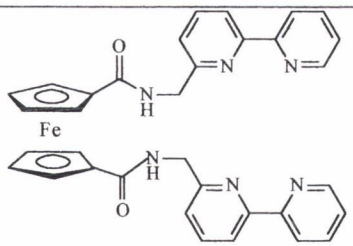
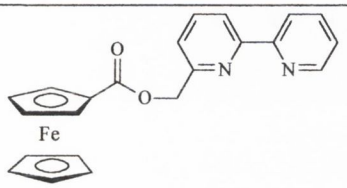
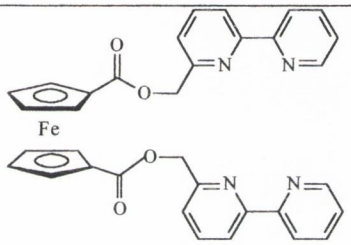
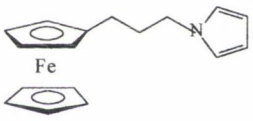
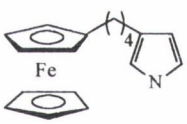
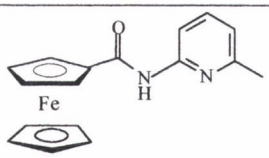
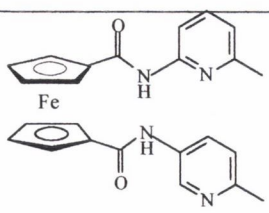
Ferrocene derivative	No.	E V	$10^5D/$ cm^2s^{-1}	Reference
	**1**	0.085	2.4	1,2
	**22**	0.300	0.21	3
	**23**	0.22	0.77	3
	**24**	0.31	0.93	3
	**25**	0.263	N/A	2
	**26**	0.510	N/A	2

Table 4.1: continued

Estimated Standard Potentials and Diffusion Coefficients for a range of Ferrocene derivatives in 0.1M TBAP/MeCN vs $Ag/AgNO_3$ reference electrode

Ferrocene derivative	No.	E	10^5D/ cm^2s^{-1}	Reference
	**27**	0.343	N/A	2
	**28**	0.575	N/A	2
	**29**	0.35	N/A	4
	**30**	0.33	N/A	4
	**31**	0.24	N/A	5
	**32**	0.44	N/A	5

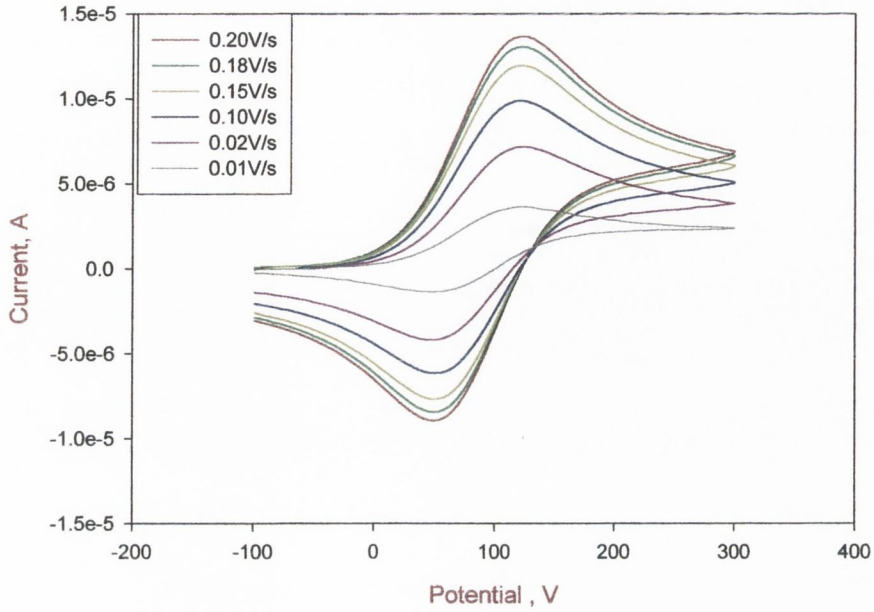


Figure 4.6: Cyclic voltammogram of ferrocene at varying scan rates in 0.1M TBAP/ CH_3CN at a Pt disk electrode at 25°C vs $Ag/AgNO_3$ reference electrode.

Electrochemical investigations into the unsubstituted ferrocene system were carried out in order to determine both the formal potential and the diffusion coefficient of the system for comparative purposes with previous literature values. Successive cyclic voltammograms at various scan rates are illustrated in figure 4.6. The unsusbsituted ferrocene was found to have a formal potential, $E^{0'} = 0.088 \pm 0.004V$. The value is in accordance with those previously reported for ferrocene[2], **1**, in a 0.1M TBAP/MeCN versus a $Ag/AgNO_3$ reference electrode, i.e. $E^{0'} = 0.085V$, see table 4.1. This experiment provided proof of the cleanliness of the working electrode in addition to testing the reliability of the experimental processes used during the course of this work. Compared to the simple unsubstituted ferrocene all the compounds are shifted towards more positive potentials this is due to the substitution of the Cp rings with electron-withdrawing groups. The formal potential of the substituted ferrocenes are closer to that found for ferrocene carboxylic acid vs a $Ag/AgNO_3$ reference electrode , $E^{0'} = 0.365V$.

The electrochemical reversibility of the hybrid moieties, **18** n = 3, 4, 5, 6 and 7, was studied over the range of 0-0.6V; these limits were chosen in order to prevent the oxidation of the pyrrole group. Electrochemical reversibility was decided on the basis of two criteria. Firstly, the anodic and cathodic peak separation values, ΔE_p, and secondly the ratio of anodic to cathodic peak current, $i_{p,a}/i_{p,c}$. A pair of well-defined, stable redox peaks was observed for each of the monomers **18** n = 3-7 in solution as shown in figures 4.1-4.5 respectively. It can be seen that the charge recorded for the anodic and cathodic sweeps are approximately equal.

Examination of the cyclic voltammograms with varying sweep rate shows symmetrical redox waves for all five monomers with the ratio of the anodic and cathodic peak current, $i_{p,a}/i_{p,c}$, being almost unity and independent of scan rate.

The value of ΔE_p for all compounds was in the range of 63-85mV in the 10-200mVs^{-1} range of scan rate. These values are in good agreement with the theoretical value for a one-electron Nernstian system and with values previoulsy obtained for substituted ferrocenes.[3] For example, the values obtained for mono- and 1,1'-bis amide-linked 2,2' bipyridine substituted ferrocenyl ligands was 60-85mV. Further evidence of a reversible reaction was found through the analysis of the variation of the magnitude of the voltammetric peak current with the square root of the applied sweep rate shows a linear dependency and is indicative of a reversible electrochemical process occurring, figure 4.7.

The diffusion coefficients were computed using the Randels Sevcik equation[6]:

$$i_p = 0.4663nFA\left(\frac{nF}{RT}\right)^{1/2} C_0^{\infty} D^{1/2} \upsilon^{1/2} \qquad (4.1)$$

where n is the number of electrons transferred, D is the diffusion coefficient, F is the Faraday constant and A is the geometric area of the electrode, (0.2 cm^2). Thus, the slope of the plot of peak current versus the square root of the sweep rate, which displays a (0,0) intercept, is directly proportional to the diffusion coefficient.

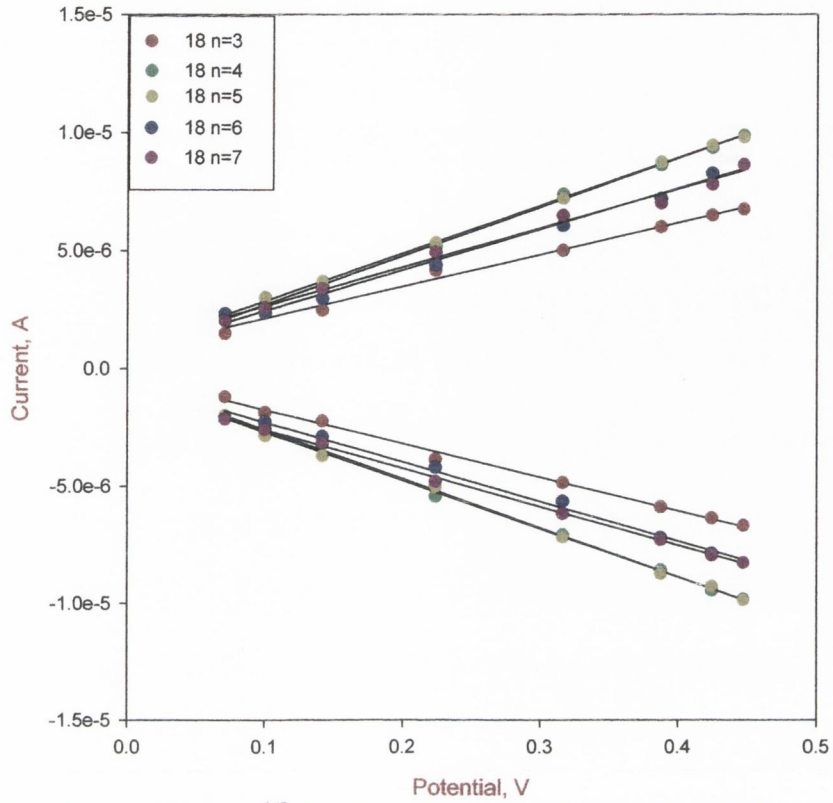


Figure 4.7 Graph of i_p vs $v^{1/2}$ for the oxidation and reduction of the monomers of the structure **18** n=3-7 (1mM) in 0.1M TBAP/ CH_3CN at a Pt disk electrode at 25°C vs $Ag/AgNO_3$ reference electrode.

The graph of i_p vs $v^{1/2}$ is shown in Figures 4.7, data points for each scan rate was plotted and a linear regression applied to these data points in order to determine the least-squares fit for the data. The standard deviation of the slopes of the linear regressions was used to calculate the confidence intervals of the diffusion coefficients and are reported in Table 4.2.

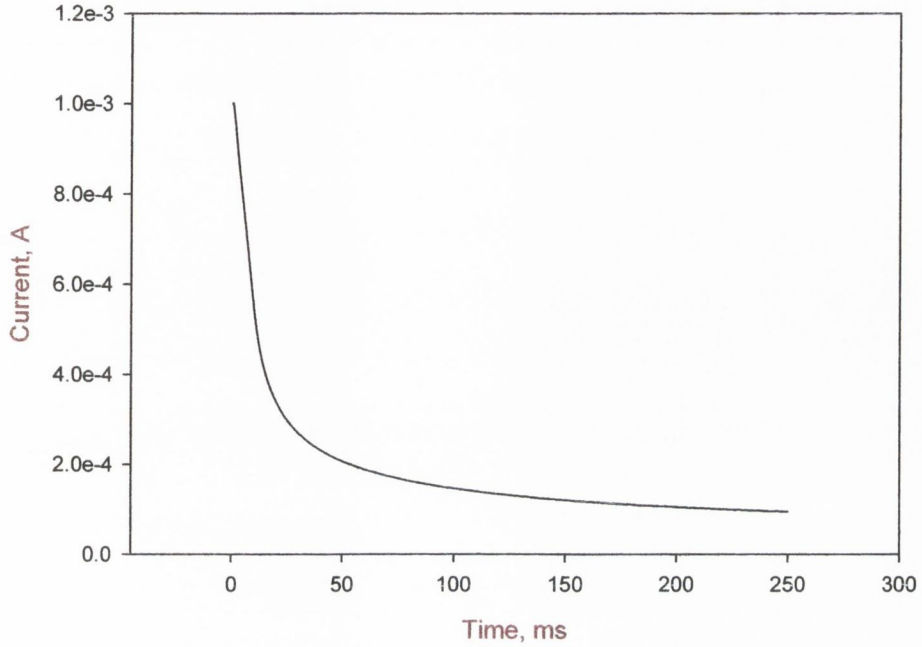


Figure 4.8: Graph of the variation of current with time of **18** n=5 (1mM) in 0.1M TBAP/ CH_3CN at a Pt disk electrode at 25°C vs $Ag/AgNO_3$ reference electrode

i_p vs $t^{-1/2}$

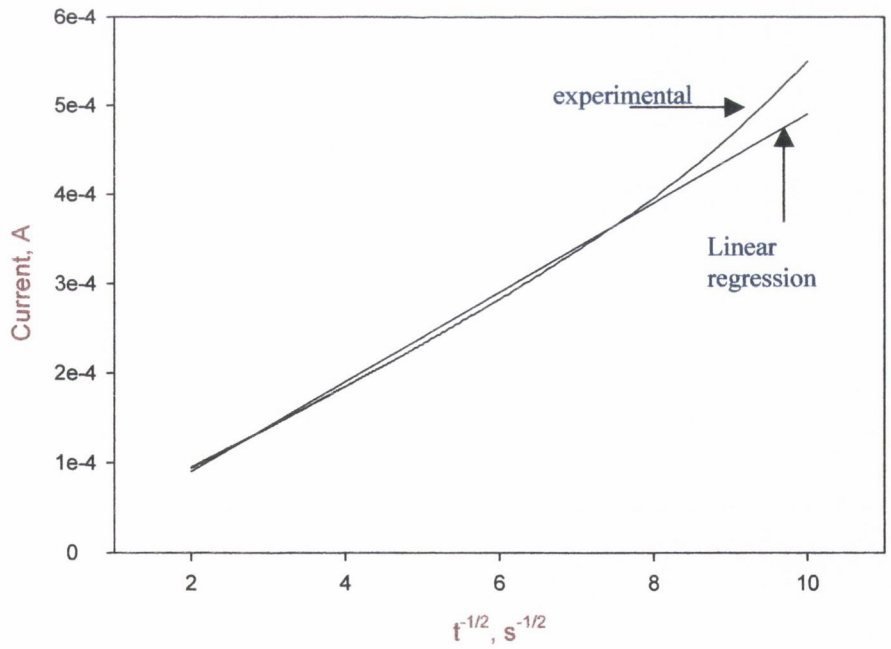


Figure 4.9: Graph of i vs $t^{-1/2}$ of **18** n=5 (1mM) in 0.1M TBAP/ CH_3CN at a Pt disk elecrode at 25°C vs $Ag/AgNO_3$ reference electrode

Chronoamperometric techniques were also employed to investigate the reversibility of the novel monomers and to test the reliability of the diffusion coefficients for these systems. Experiments were carried out by stepping the potential from 0 to 0.6V which is in the range where the anodic current on the cyclic voltammograms were diffusion controlled. The relationship between i and $t^{-1/2}$ was examined using the Cottrell equation[7]:

$$i = \frac{nFAD_0^{1/2}C_R^{\infty}}{\pi^{1/2}t^{1/2}} \qquad (4.2)$$

Therefore if the reaction is diffusion controlled a plot of i *vs* $t^{-1/2}$ should be linear and pass through the origin.

The diffusion coefficients were obtained through applying the Randels Sevcik[6] amd Cottrell[7] relationships and are displayed in Table 4.2. In a similar manner to the i_p vs $v^{1/2}$ graph a linear regression was applied to the data points in Figure 4.9. The standard deviation of these slopes was used to calculate the confidence intervals of the diffusion coefficients and are reported in Table 4.2.

Table 4.2: Cyclic voltammetry and chronoamperometry data corresponding to the redox behaviour of **18** n= 3, 4, 5, 6, and 7 in 0.1M TBAP/CH_3CN

Monomer	**Cyclic Voltammetry Diffusion coefficient, 10^5 D/cm^{2}s^{-1}**	**Chronoamperometry Diffusion coefficient, 10^5 D/cm^{2}s^{-1}**
[3-(Pyrrol-1-yl)propyl]ferrocene-carboxamide, **18 n= 3**	0.63 ± 0.05	0.69 ± 0.08
[4-(Pyrrol-1-yl)butyl]ferrocene-carboxamide, **18 n=4**	1.48 ± 0.04	1.42 ± 0.04
[5-(Pyrrol-1-yl)pentyl]ferrocene-carboxamide, **18 n=5**	1.41 ± 0.04	1.42 ± 0.06
[6-(Pyrrol-1-yl)hexyl]ferrocene-carboxamide, **18 n=6**	1.04 ± 0.08	1.14 ± 0.10
[7-(Pyrrol-1-yl)heptyl]ferrocene-carboxamide, **18 n=7**	0.94 ± 0.08	0.98 ± 0.08

The diffusion coefficient for ferrocene in 0.1M TBAP/ MeCN was calculated from the cyclic voltammograms in figure 4.6 by obtaining the slope of the corresponding i_p vs $v^{1/2}$ plot. The value obtained was 2.56 ± 1.01 x 10^{-5} cm^2s^{-1}, this was in agreement with the literature value of 2.4 x 10^{-5} cm^2s^{-1} and demonstrated the cleanliness of the working electrode and the repeatability of the electrochemical measurements that were carried out.

In the case of other amide ferrocene-pyrrole derivatives the mono-substituted ferrocene N-[2-(pyrrole-1yl)ethyl]-N-ethylferrocene-1-carboxamide had a diffusion coefficient of 0.77 x 10^{-5} cm^2s^{-1} in 0.1M TBAP/MeCN versus a $Ag/AgNO_3$ reference electrode[3]. The diffusion coefficient of the analogous disubstituted ferrocene species, NN'-bis-[2-(pyrrole-1-yl)ethyl]-N,N'-bisethylferrocene)-1,1'-dicarboxamide[3], was 0.93 x 10^{-5} cm^2s^{-1} and that of bis-(N,N'-bisethyl)ferrocene 1,1'-dicarboxamide[3] is reported as was 0.21 x 10^{-5} cm^2s^{-1} under identical conditions. There is good agreement between the diffusion coefficient values obtained by both methods and they are close to data reported for ferrocene and the aforementioned ferrocene derivatives[1-5]. The range for the mono-substituted ferrocenes reported in this work is 0.63 ± 0.05 to 1.48 ± 0.04 x 10^{-5} cm^2s^{-1}, previous data reported for a mono-substituted ferrocene with a similar alkylpyrrole, (N-[2-(pyrrole-1yl)ethyl]-N-ethylferrocene-1-carboxamide), is 0.77 x 110^{-5} cm^2s^{-1} and lies within the range reported. However, both the butyl and pentyl derivatives have a diffusion coefficient of approximately 1.4 x 10^{-5} cm^2 s^{-1}, which is larger than any values previously reported for either the mono- or disubstituted species.

No effect was observed for the increasing alkyl chain length in the monomeric species on the formal electrode potentials, the [(Pyrrol-1-yl)alkyl]ferrocene-carboxamides monomers had a formal potential in the range $E^{0'}$ = 0.250-0.253. However, the potential was higher than that for unsubstituted ferrocene and indicated that the effect of the substitution was to render the ferrocene more difficult to oxidise. The data reported for the diffusion coefficients of the mono-substituted hybrid monomers showed a range of values form 0.63 ± 0.05 to 1.48 ± 0.04 x 10^{-5} cm^2s^{-1}, that smallest coefficient pertaining to the propyl monomer whilst the butyl and pentyl derivatives have the largest diffusion coefficients.

4.2.2 Electrochemical behaviour of compounds of structure 20 and 21

Investigations into the electrochemical reversibility of the monomers **20** n = 3, 5, and 7 and **21** were carried out in a similar manner to those examining the mono-substituted monomers. The limits of 0-0.6V were chosen once more to prevent the oxidation of the pyrrole group. The electrochemical behaviour of compounds of the structure **20**, n = 3, using tetrabutylammonium perchlorate (TBAP) as supporting electrolyte is presented in figure 4.10. The sweep rates employed were in the range of 0.01 to $0.2Vs^{-1}$ and the scan was recorded between the voltage limits of 0-0.6V against a $Ag/AgNO_3$ reference electrode. Experimental results showed that this behaviour was similar for both platinum and glassy carbon working electrodes. In addition this behaviour was found to typify the remaining three monomers, **20** n= 5 and 7 and **21** as shown in figures 4.11 to 4.13

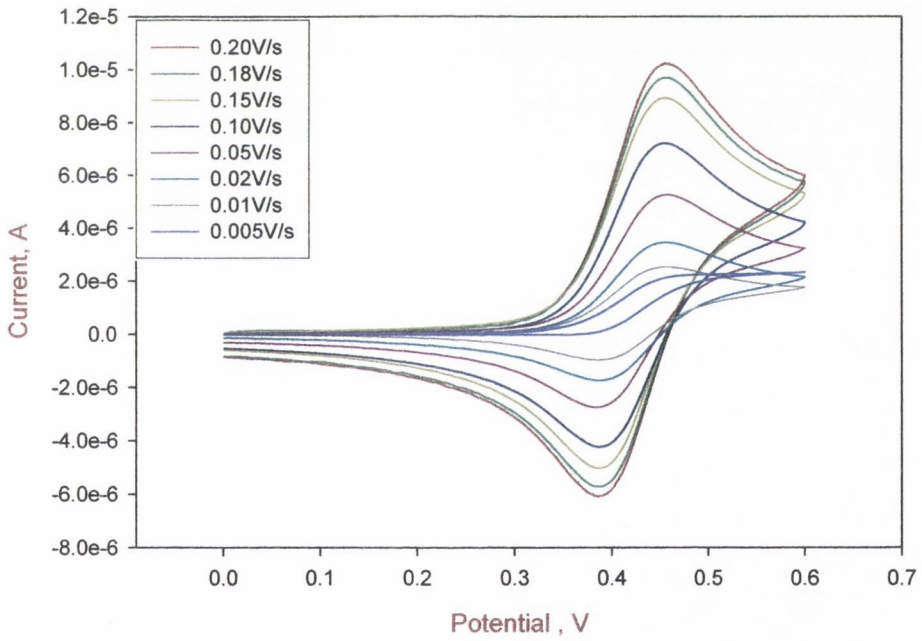


Figure 4.10 Cyclic voltammogram of **20** n=3 (1mM) at varying scan rates in 0.1M TBAP/ CH_3CN at a Pt disk electrode at 25°C vs $Ag/AgNO_3$ reference electrode.

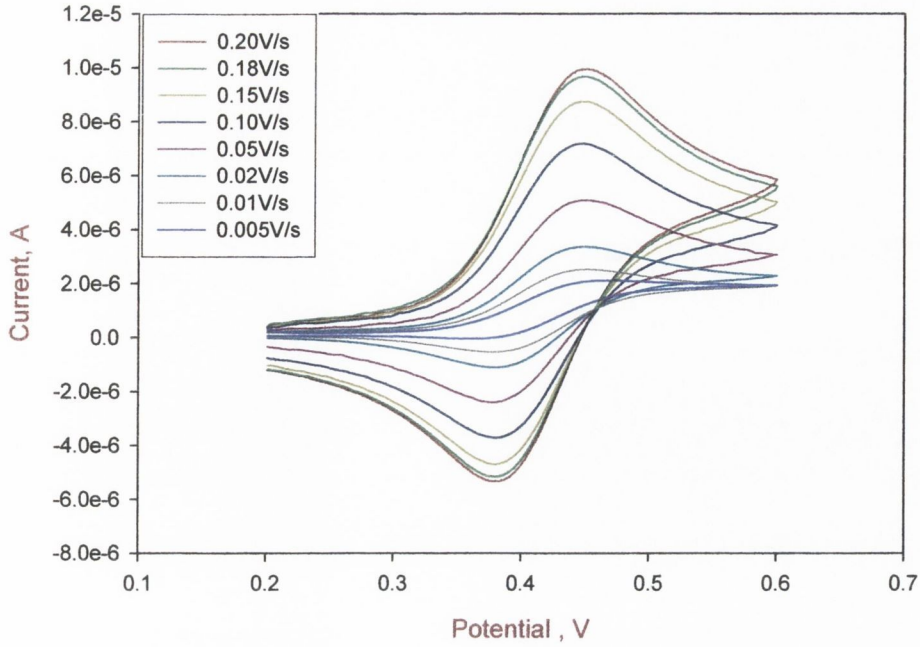


Figure 4.11 Cyclic voltammogram of **20** n=5 (1mM) at varying scan rates in 0.1M TBAP/ CH_3CN at a Pt disk electrode at 25°C vs $Ag/AgNO_3$ reference electrode.

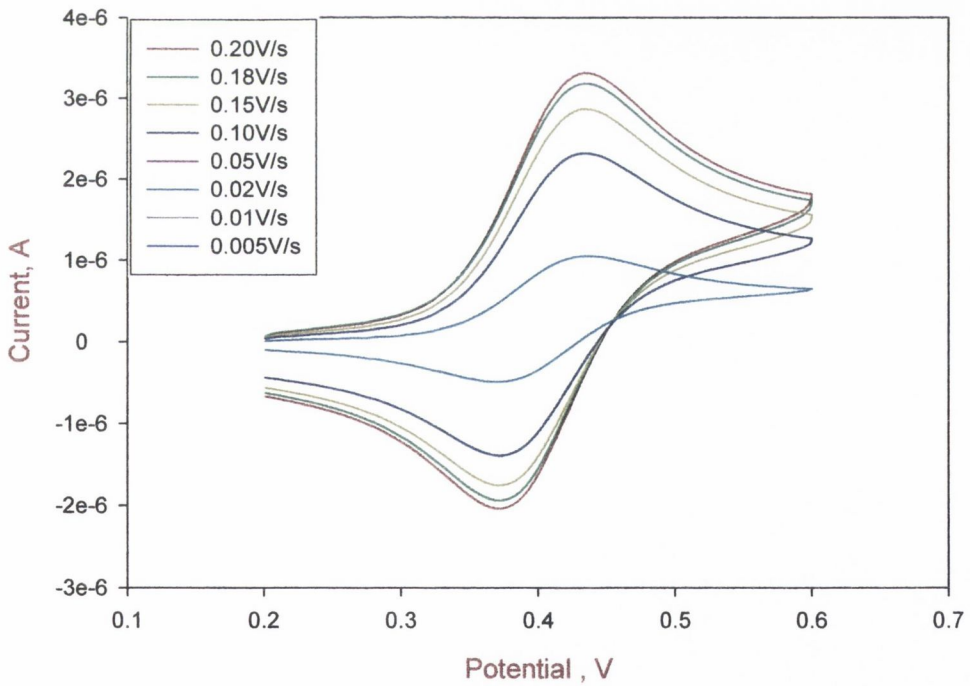


Figure 4.12 Cyclic voltammogram of **20** n=7 (1mM) at varying scan rates in 0.1M TBAP/ CH_3CN at a Pt disk electrode at 25°C vs $Ag/AgNO_3$ reference electrode.

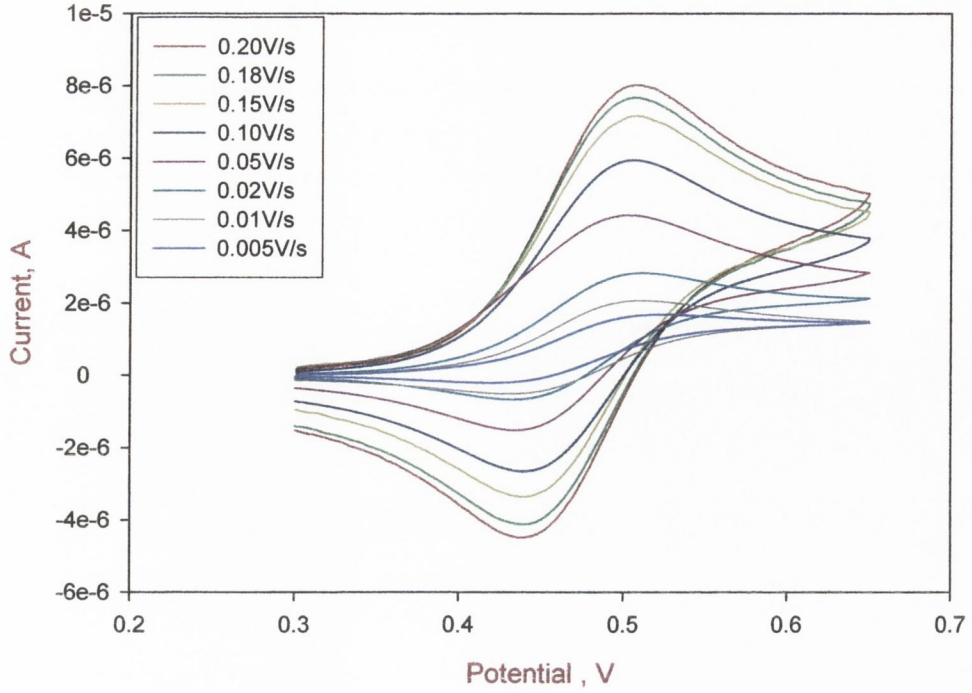


Figure 4.13 Cyclic voltammogram of **21** (1mM) at varying scan rates in 0.1M TBAP/ CH_3CN at a Pt disk electrode at 25°C vs $Ag/AgNO_3$ reference electrode.

The cyclic voltammograms observed for the disubstituted species, 1,1'-bis-[(Pyrrol-1-yl)alkyl]ferrocene-1,1'-dicarboxamides, **20**, are shown in figures 4.10-4.12, and that of 1,1'-[3-(Pyrrol-1-yl)propyl]ferrocene-dicarboxamide, methylester, **21**, in Figure 4.13. Examination of the cyclic voltammograms with varying sweep rate shows symmetrical redox waves for all four disubstituted monomers with the ratio of the anodic and cathodic peak current, $i_{p,a}/i_{p,c}$, being almost unity and independent of scan. The value of ΔE_p was in the range of 60-70mV for the symmetrically derivatized moieties and 62-68mV for compound **21**. Analysis of the variation of the magnitude of the voltammetric peak current with the square root of the applied sweep rate shows a linear dependency and is indicative of a reversible electrochemical process occurring, figure 4.13.

The formal potential values taken as an average of anodic and cathodic peak potentials at a scan rate of $0.1Vs^{-1}$ were $E^{0'}$ = 0.421, 0.413, 0.405 and 0.475V for **20** n= 3, 5, 7 and **21** respectively. The confidence limit is ±5mV in each case. These values are in good accordance with the redox potentials for other disubstituted ferrocene

species[2,3,5]. In the case of other amide ferrocene-pyrrole derivatives the disubstituted ferrocenes, N,N'-bis-[2-(pyrrole-1yl)ethyl]-N,N'-bisethylferrocene-1,1'-dicarboxamide[3], **24**, and bis-(N,N'-bisethyl)ferrocene-1,1'-dicarboxamide[3], **22**, had a formal potential of 0.31V and 0.30V respectively in 0.1M TBAP/MeCN versus a $Ag/AgNO_3$ reference electrode.Under identical conditions a disubstituted ferrocene with an amide linked 2,2'-bipyridine[2] has a formal potential of 0.51V whereas the corresponding disubstituted ferrocene with a carborboxylic ester linked 2,2'bipyridine[2], **28**, 0.575V. Finally, a disubstituted ferrocene with an amide linked pyridine[5], **32**, has a potential of 0.44V. On examination of the literature values it is apparent that the ester linkages result in a higher formal potential than those with the amide linkages, this was also reported for the mono-substituted hybrid monomers. On comparison of the potential for **21**, $E^{0'} = 0.475V$ with the other N- (3-aminopropyl)pyrrole substituted ferrocene monomers it is evident that the formal potential is higher than both the mono-and bis-species ($E^{0'} = 0.251$ and 0.421V respectively). The formal potentials of the disubstituted hybrid monomers are greater than those for the mono-substituted species, this may be due to the substitution of both Cp rings with electron-withdrawing groups, thereby increasing the limits required by the ferrocene to be oxidised.

In a similar manner to the mono-substituted hybrid monomers, the electrochemical reversibility of the hybrid moieties, **20** n = 3, 5, 7 and **21** was studied over the range of 0-0.6V; once more these limits were chosen in order to prevent the oxidation of the pyrrole group. Electrochemical reversibility was decided on the basis of two criteria. Firstly, the anodic and cathodic peak separation values, ΔE_p, and secondly the ratio of anodic to cathodic peak current, $i_{p,a}/i_{p,c}$. A pair of well-defined, stable redox peaks was observed for each of the monomers **20** n = 3, 5, 7 and **21** in solution as shown in figures 4.10-4.13 respectively. It can be seen that the charge recorded for the anodic and cathodic sweeps are approximately equal. Examination of the cyclic voltammograms with varying sweep rate shows symmetrical redox waves for all three monomers with the ratio of the anodic and cathodic peak current, $i_{p,a}/i_{p,c}$, being almost unity and independent of scan rate.

The value of ΔE_p for all disubstituted compounds, **20** and **21**, was in the range of 61-80mV in the 10-200mVs^{-1} range of scan rate. These values are in good agreement with the theoretical value for a one-electron Nernstian system and with values previoulsy obtained for substituted ferrocenes[1,2]. For example, the values obtained for mono- and 1,1'-bis amide-linked 2,2' bipyridine substituted ferrocenyl ligands was 60-85mV. Further evidence of a reversible reaction was found through the analysis of the variation of the magnitude of the voltammetric peak current with the square root of the applied sweep rate shows a linear dependency and is indicative of a reversible electrochemical process occurring, figure 4.14.

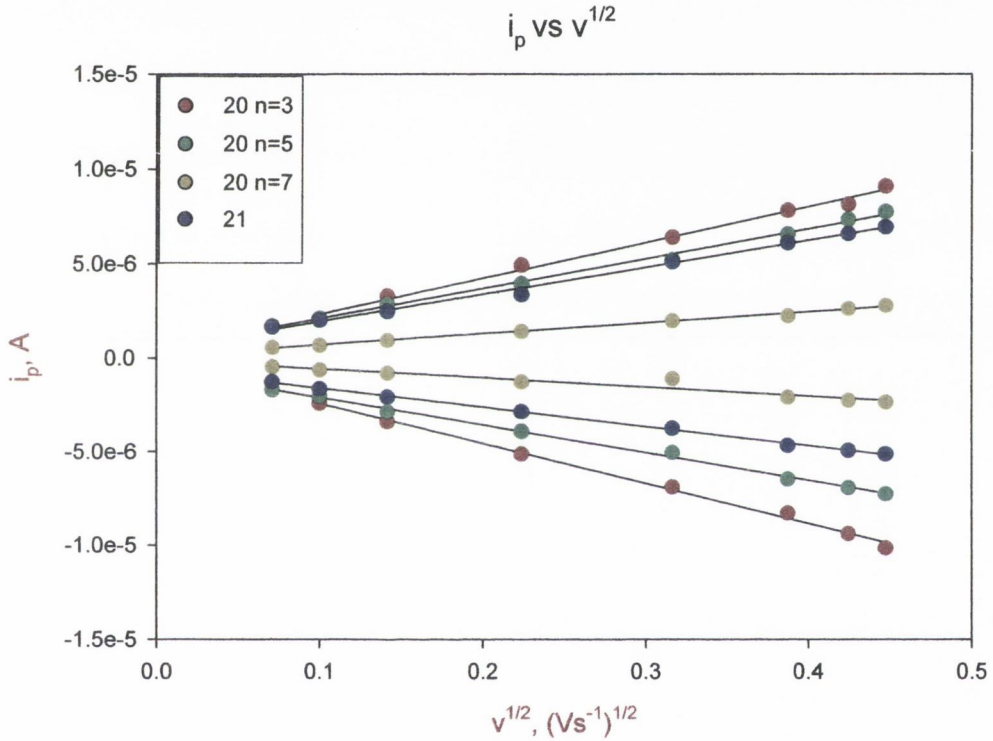


Figure 4.14 Graph of i_p vs $v^{1/2}$ for the oxidation and reduction of the monomers of the structure **20** n=3, 5, 7.and structure **21**.

The diffusion coefficients were obtained through applying the Randels Sevcik[3] (4.1) and Cottrell[4] (4.2) relationships and are displayed in Table 4.3.

A linear regression was applied to the resultant data points for the i_p vs $v^{1/2}$ and i_p vs $t^{-1/2}$ graphs. The standard deviation of the slopes obtained was used in the determination of the confidence intervals of the diffusion coefficients reported.

Table 4.3: Cyclic voltammetry and chronoamperometry data corresponding to the redox behaviour of **20** n= 3, 5, and 7 and **21** in 0.1M TBAP/CH_3CN

Monomer	**Cyclic Voltammetry Diffusion coefficient, 10^5 D/cm^2s^{-1}**	**Chronoamperometry Diffusion coefficient, 10^5 D/cm^2s^{-1}**
1,1'-Bis-[3-(Pyrrol-1-yl)propyl]ferrocene-1,1'-dicarboxamide, **20 n=3**	1.25 ± 0.10	1.20 ± 0.10
1,1'-Bis-[5-(Pyrrol-1-yl)pentyl]ferrocene-1,1'-dicarboxamide, **20 n=5**	1.20 ± 0.10	1.18 ± 0.10
1,1'-Bis-[7-(Pyrrol-1-yl)heptyl]ferrocene-1,1'-dicarboxamide, **20 n=7**	1.30 ± 0.08	1.20 ± 0.08
1,1'-[3-(Pyrrol-1-yl)propyl]ferrocene-dicarboxamide, methylester, **21**	0.71 ± 0.04	0.77 ± 0.04

The diffusion coefficients for the disubstituted monomers lie in the range of 0.71 ± 0.04 to 1.30 ± 0.08 x 10^{-5} cm^2s^{-1}. Those reported previously for disubstituted ferrocene moieties are 0.21 and 0.93 x 10^{-5} cm^2s^{-1} for bis-(N,N'-bisethyl)ferrocene-1,1'-dicarboxamide[3], **22**, and N,N'-bis-[2-(pyrrole-1yl)ethyl]-N,N'-bisethylferrocene-1,1'-dicarboxamide[3], **24**, respectively. The values for the symmetrically substituted hybrid monomers (approximately 1.25 ± 0.1 x 10^{-5} cm^2s^{-1}) are close to that found for the symmetrically disubstituted monomer, **24**, and are all within the stated range of error. However, the value for the asymmetrically disubstituted 1,1'-[3-(Pyrrol-1-yl)propyl]ferrocene-dicarboxamide, methylester, **21**, is considerably less than that found for the other disubstituted compounds. At this time there is no obvious explanation for this dissimilar behaviour.

4.3 ELECTROPOLYMERIZATION OF HYBRID MONOMERS

4.3.1 Electropolymerization of compounds of structure 18

It has been previously reported that the properties of the polypyrrole film should be influenced by substitution at the N- atom[9,10]. In order to modify the electrochemical properties of the polypyrrole film it is best to incorporate the redox active substituents with redox potentials within the conductivity region of the polymer. The monomers prepared with the structure **18** n= 3-7 were examined for their ability to be electropolymerized. The cyclic voltammogram of the monomer **18** n=4, is illustrated in figure 4.15 , shows a reversible oxidation of the ferrocene redox system at 0.25V and an irreversible oxidation peak of the pyrrole moiety at 1.0V.

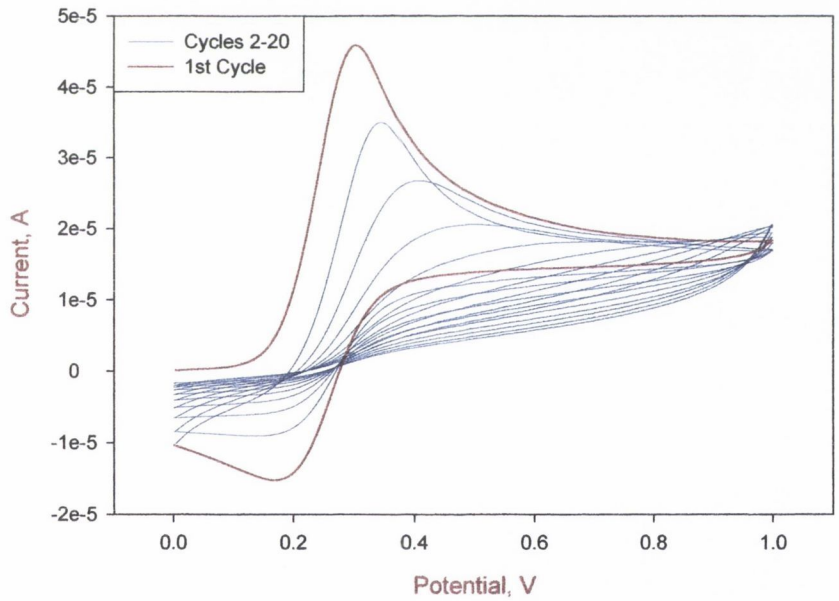


Figure 4.15: Cyclic voltammogram of repeated cycling of **18** n=4 (10mM) in 0.1M TBAP/ CH_3CN at a Pt disk electrode at 25°C vs $Ag/AgNO_3$ reference electrode.

There may be several explanations for the inability of the monomer to be polymerized. Firstly, the pyrrole radical cation of the monomer may be too stable and diffuse away from the electrode forming insoluble by-products. Secondly, the loss of an electron from the monomer may produce a species that is so unstable that it reacts with solvent or electrolyte molecules forming insoluble products before reacting with another monomer molecule. Scheme 4.2 outlines one proposed mechanism for the situation involved for monomers with the structure **18**. It is proposed that the electron loss occurs from the ferrocene component of the monomer (case A). It is believed that the ease with which the ferrocene may be oxidised in some way hinders the oxidation of the pyrrole group (case B). The absence of a second anodic wave in the cyclic voltammogram even at potentials of 1.0 V (vs $Ag/AgNO_3$ reference electrode) is consistent with the cationic species being more difficult to oxidise. Subsequent cycles results in a reduced current in the cathodic peak and suggests the monomer reacts in some manner that leads to a species which passivates at the electrode. Figure 4.16 depicts the potentiodynamic growth of polypyrrole under comparable conditions, and negates the possibility of experimental error.

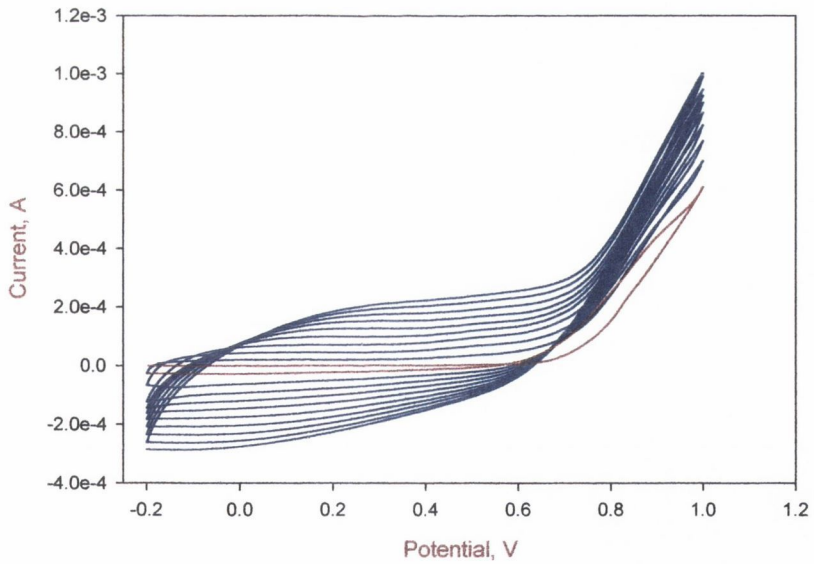
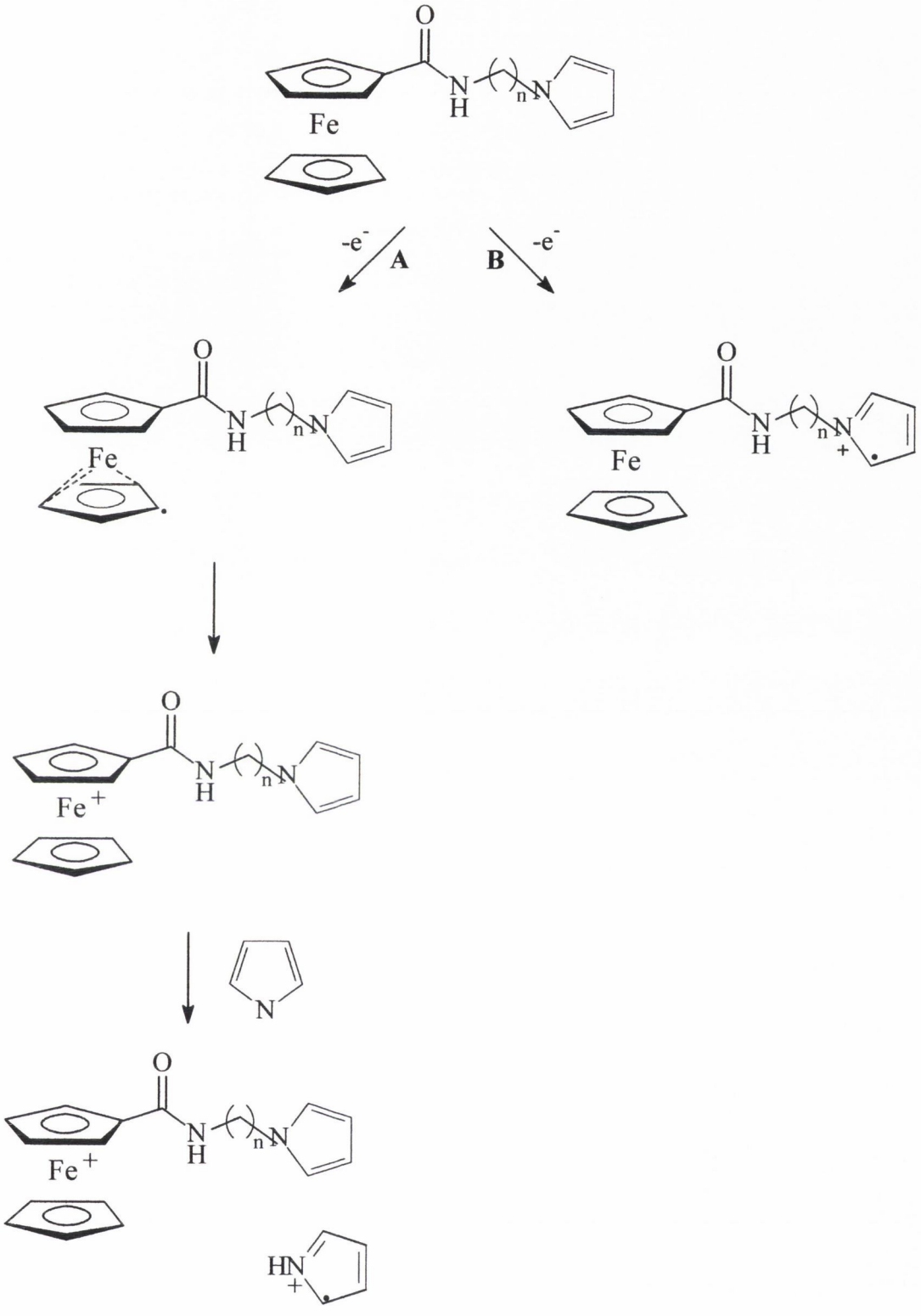


Figure 4.16: Cyclic voltammogram of repeated cycling of pyrrole (10mM) in 0.1M TBAP/ CH_3CN at a Pt disk electrode at 25°C vs Ag/AgCl reference electrode.



Scheme 4.2

The attempted potentiodynamic growth of the mono-substituted ferrocene hybrid monomers are depicted in figures 4.15 and 4.17 to 4.20. The initial cyclic sweep is shown in red with subsequent cycles depicted in blue. It is evident from examination of these scans that in each case there is a decrease in both the anodic and cathodic peaks corresponding to the ferrocene group, and that there is no clear oxidation peak of the pyrrole moiety.

Figure 4.16 clearly shows the presence of a polypyrrole oxidation peak at approximately 0.8V, which increases in intenisty with increasing scan number. This is not the case for the hybrid monomer species. Figure 4.15 shows that on repeated scanning of [4-(Pyrrol-1-yl)butyl]ferrocene-carboxamide, **18** n=4, within potential limits of 0 to 1.0V, the current produced by the ferrocene/ferricinium redox system decreased and the reversible oxidation peak of the ferrocene redox couple is shifted 012V to 0.37V on examination of the second scan. This is indicative of the formation of a layer on the support surface which served to block interfacial electron transfer, see scheme 4.2. In addition, the oxidation of the ferrocene group in this environment is more difficult and may also be attributed to a passivating layer on the electrode surface blocking electron transfer. Likewise, electropolymerization of the monomers of the structure **18** was not achieved by potential step methods, for similar reasons.

The electrochemical reponse for monomer [3-(Pyrrol-1-yl)propyl]ferrocene-carboxamide, **18** n=3, is illustrated in figure 4.17 and is similar to the response exhibited by [4-(Pyrrol-1-yl)butyl]ferrocene-carboxamide, **18** n=4, [6-(Pyrrol-1-yl)hexyl]ferrocene-carboxamide, **18** n=6, and [7-(Pyrrol-1-yl)heptyl]ferrocene-carboxamide, **18** n=7, see figures 4.15, 4.19 and 4.20 respectively. In these cyclic voltammograms there is a modest current response between 0.8 and 1.0V which may be atirbuted to the irreversible oxidation of the pyrrole moiety. This is not the case for the [5-(Pyrrol-1-yl)pentyl]ferrocene-carboxamide, **18** n=5, species, see figure 4.18. There is no indication that a pyrrole group is present in solution, there is no apparent explanation for this behaviour at this time.

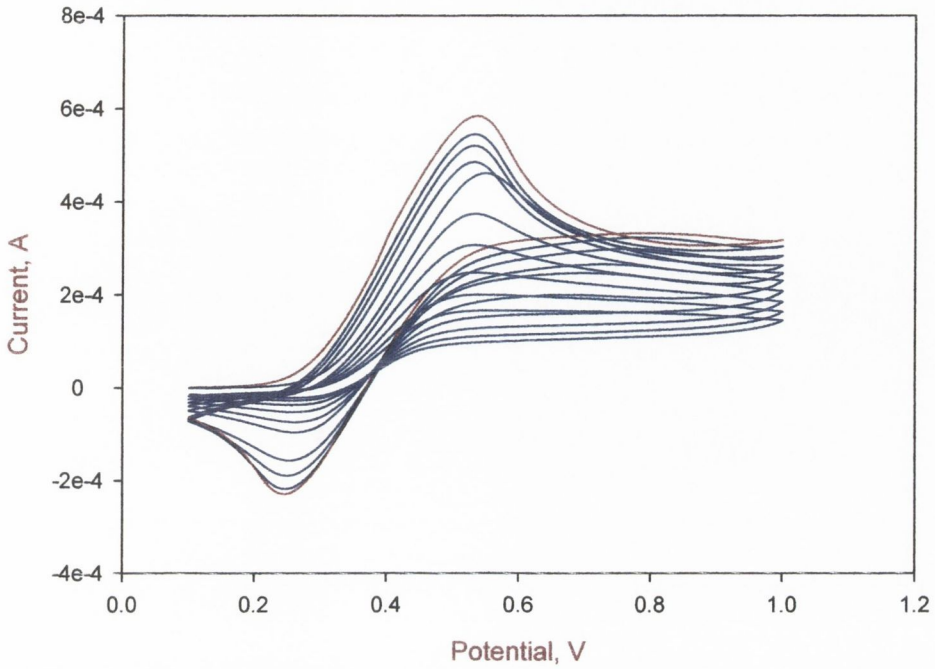


Figure 4.17: Cyclic voltammogram of repeated cycling of **18** n=3 (10mM) in 0.1M T3AP/ CH_3CN at a Pt disk electrode at 25°C vs Ag/AgCl reference electrode.

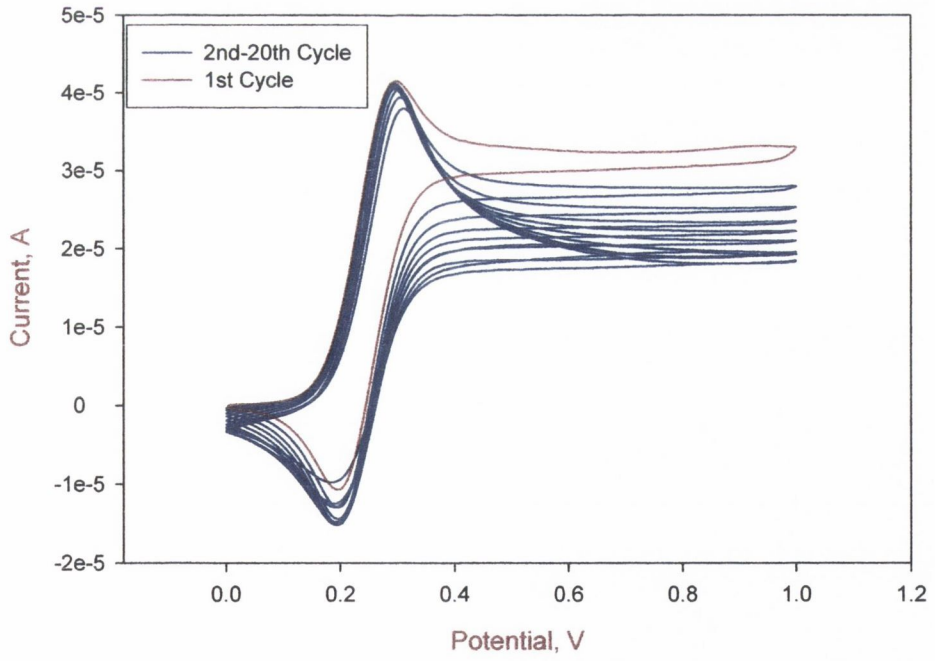


Figure 4.18: Cyclic voltammogram of repeated cycling of **18** n=5 (10mM) in 0.1M T3AP/ CH_3CN at a Pt disk electrode at 25°C vs Ag/$AgNO_3$ reference electrode.

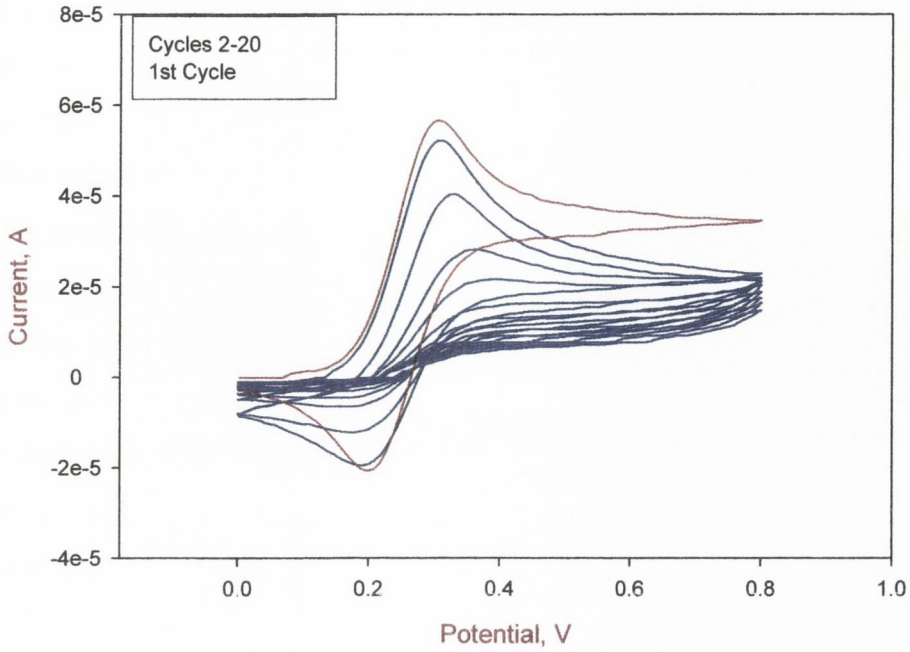


Figure 4.19: Cyclic voltammogram of repeated cycling of **18** n=6 (10mM) in 0.1M TBAP/ CH_3CN at a Pt disk electrode at 25°C vs $Ag/AgNO_3$ reference electrode.

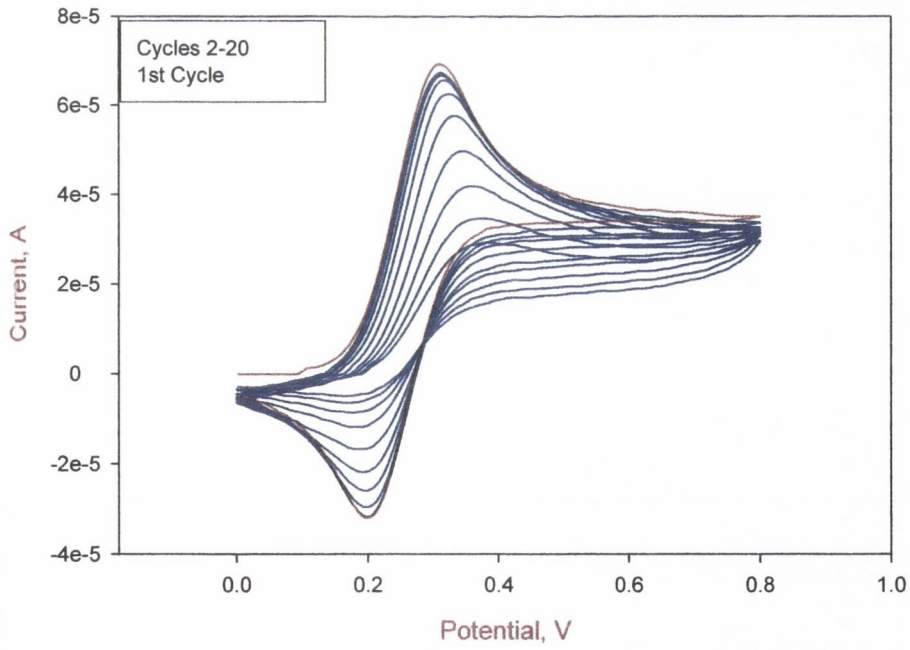


Figure 4.20: Cyclic voltammogram of repeated cycling of **18** n=7 (10mM) in 0.1M TBAP/ CH_3CN at a Pt disk electrode at 25°C vs $Ag/AgNO_3$ reference electrode.

It was decided to attempt to copolymerize the mono-substituted hybrid monomers with pyrrole. According to the mechanism proposed in Scheme 2.4 if an initiator was added to the solution a copolymer of the hybrid could be readily accomplished. The copolymerization of a solution of 1:1; pyrrole: **18** n=4 was successful and the results are illustrated in figure 4.21. Apparently, the radical cation of the N-substituted pyrroles cannot function as initiators[11], so the pyrrole radical cation formed in the initial cycle serves as a polymerization initiator.[12,13] This outcome has been reported before with similar systems. However, contrary findings have also been reported with direct anodic polymerization of two N-substituted pyrrole derivatives occurring with even more bulky substituents. In this instance, coopolymerization was also achieved from a solution of 1:10; pyrrole: **18** n=4, this suggests that the pyrrole may function as the initiator species.

The formation of the copolymer of the hybrid monosubstituted monomer and pyrrole was achieved by scanning the potential from 0 to 1.2V vs a Ag/AgCl reference electrode over a period of 20 successive scans, a sweep rate of $50mVs^{-1}$. figures 4.21, 4.23, 4.25, 4.27 and 4.29 illustrates the growth of the copolymer with increasing number of scans for the range of mono-substituted hybrid monomers. For the purpose of clarity, the initial cycle is depicted in red with subsequent cycles denoted in blue. The increasing current with increasing number of scans is indicative of potentiodynamic growth of a conducting electroactive polymer. The electrochemical activity of the copolymer film was investigated using cyclic voltammetry. The film was placed in a solution of background electrolyte (0.1M TBAP/MeCN) and the potential was scanned from –0.6V to 0.9V at $50mVs^{-1}$ vs a Ag/AgCl reference electrode. Figures 4.22, 4.24, 4.26, 4.28 and 4.30 shows the continuous voltammogram of the seventh cycle of the copolymer film. Steady state peaks can be observed for both ferrocene (0.5-0.7V) and pyrrole (0.4V) moieties indicating that the formation of a modified polypyrrole film has indeed been achieved. The redox couples for all copolymers are denoted using identifiers A/B for the copolymer backbone which typically is present at 0.4V and C/D for the ferrocene redox couple which is apparent at 0.7V. It should be noted that these potentials are referenced against a Ag/AgCl reference eletrode, when adjusted for a $Ag/AgNO_3$ reference eletrode the potentials would be approximately 0.1V for the A/B couple and 0.4V for the C/D couple.

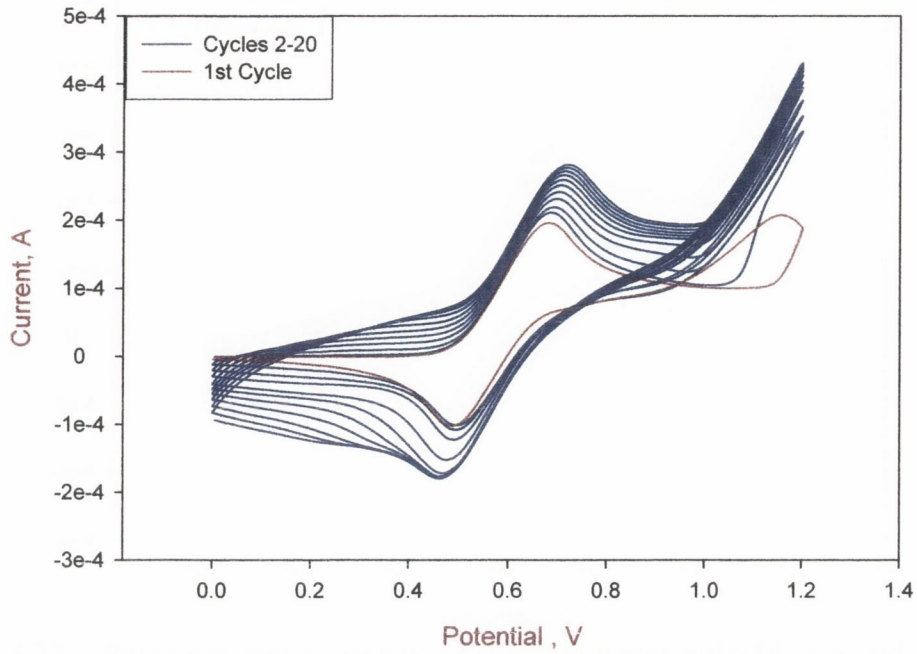


Figure 4.21: Potentiodynamic growth of the copolymer poly(**18** n=3 and pyrrole) in 0.1M TBAP/ CH_3CN, at a Pt disk electrode at 25°C vs Ag/AgCl reference electrode. Scan rate $50mVs^{-1}$

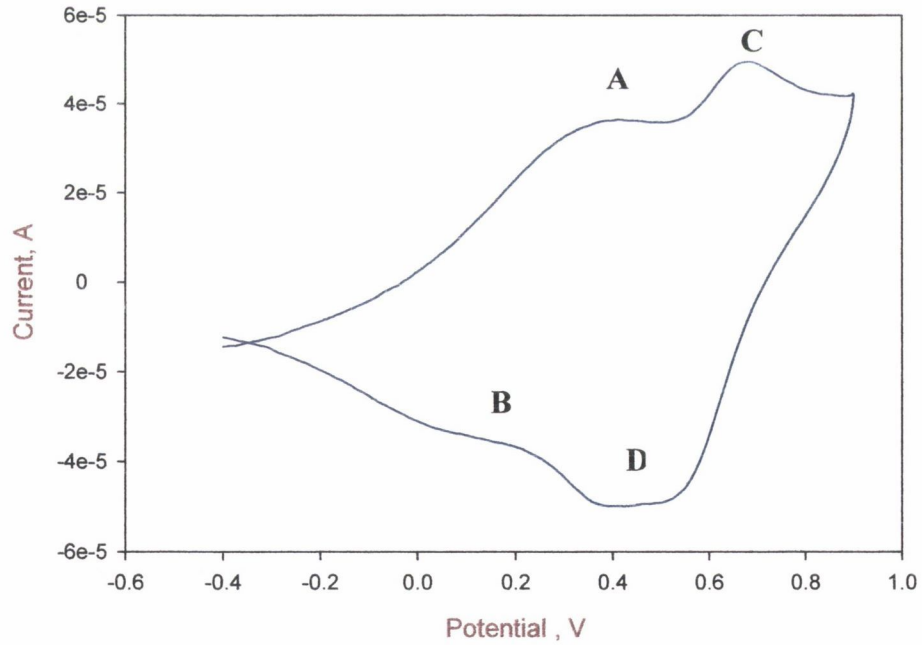


Figure 4.22: Cyclic voltammogram of 7th cycle of the copolymer of poly(**18** n=3 and pyrrole) in background electrolyte, 0.1M TBAP/ CH_3CN, at a Pt disk electrode at 25°C vs Ag/AgCl reference electrode

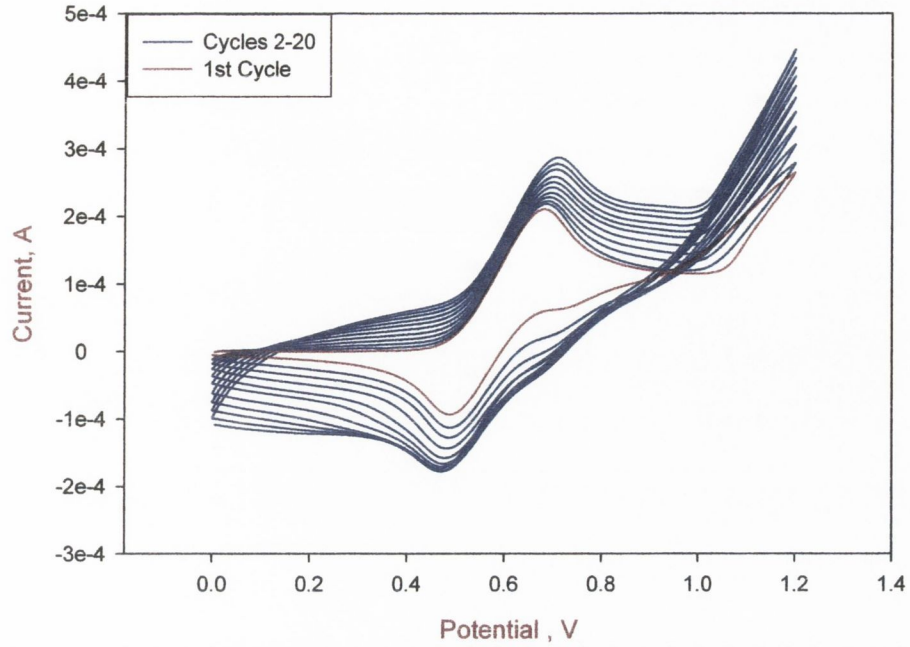


Figure 4.23: Potentiodynamic growth of the copolymer poly(**18** n=4 and pyrrole) in 0.1M TBAP/ CH_3CN, at a Pt disk electrode at 25°C vs Ag/AgCl reference electrode. Scan rate $50mVs^{-1}$

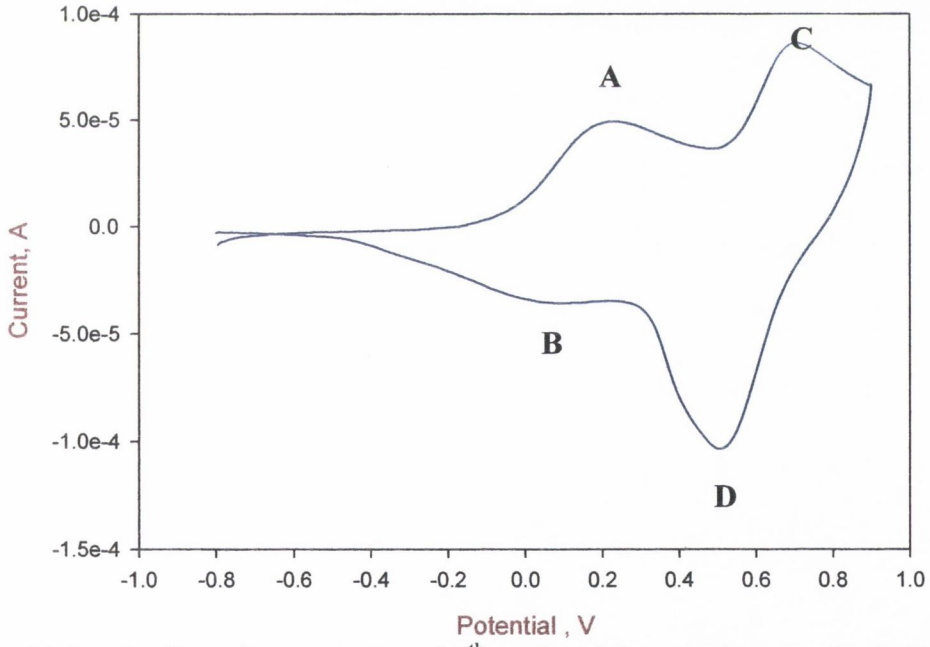


Figure 4.24: Cyclic voltammogram of 7th cycle of the copolymer of poly(**18** n=4 and pyrrole) in background electrolyte, 0.1M TBAP/ CH_3CN, at a Pt disk electrode at 25°C vs Ag/AgCl reference electrode

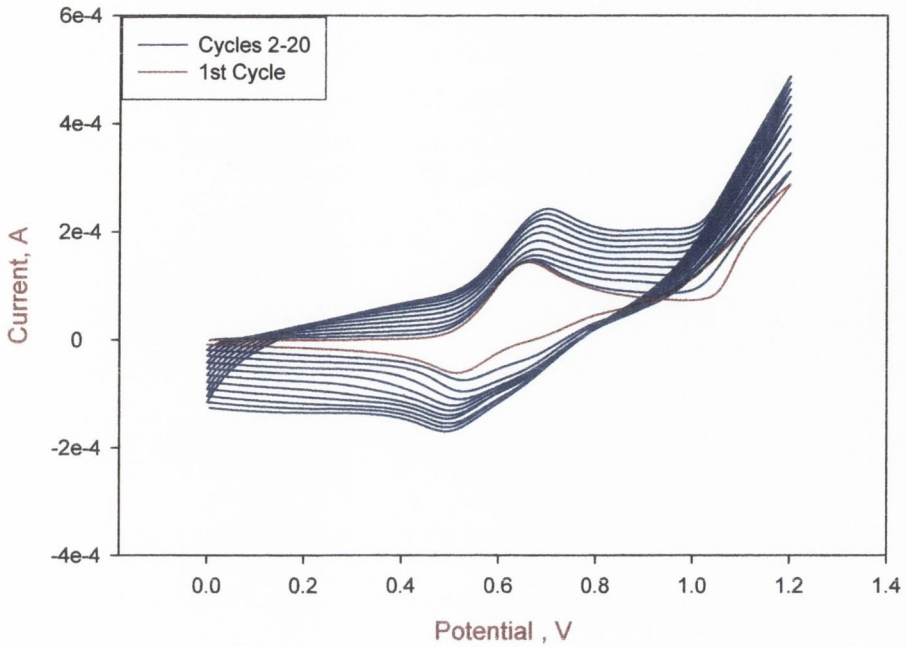


Figure 4.25: Potentiodynamic growth of the copolymer poly(**18** n=5 and pyrrole) in 0.1M TBAP/ CH_3CN, at a Pt disk electrode at 25°C vs Ag/AgCl reference electrode. Scan rate $50mVs^{-1}$.

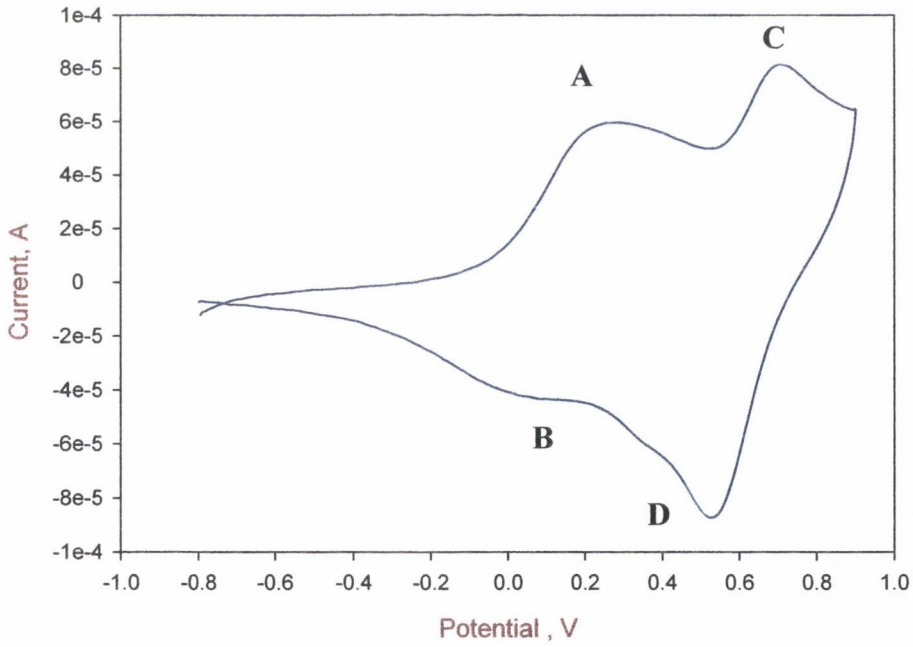


Figure 4.26: Cyclic voltammogram of 7th cycle of the copolymer of poly(**18** n=5 and pyrrole) in background electrolyte, 0.1M TBAP/ CH_3CN, at a Pt disk electrode at 25°C vs Ag/AgCl reference electrode

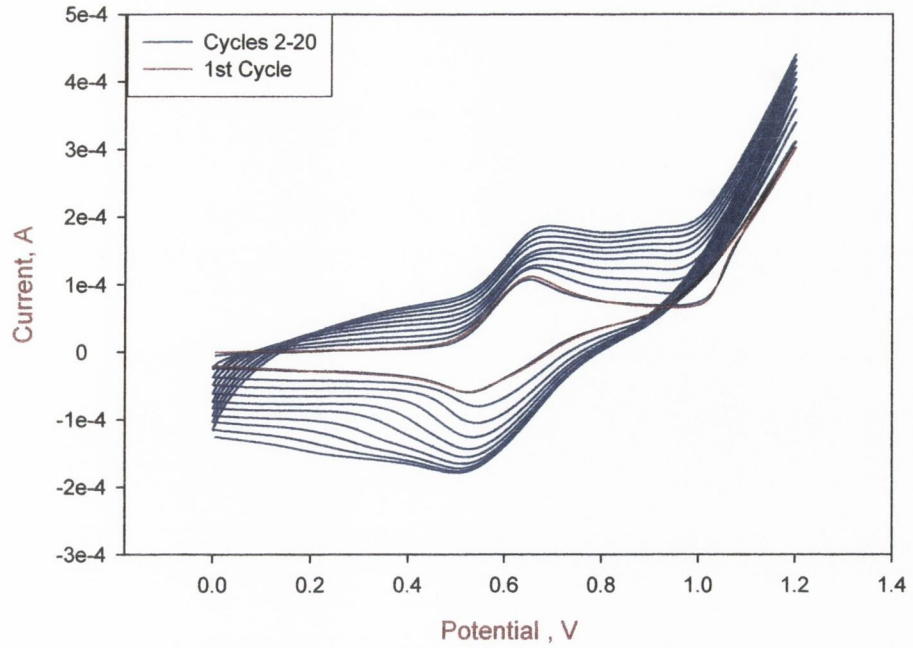


Figure 4.27: Potentiodynamic growth of the copolymer poly(**18** n=6 and pyrrole) in 0.1M TBAP/ CH_3CN, at a Pt disk electrode at 25°C vs Ag/AgCl reference electrode

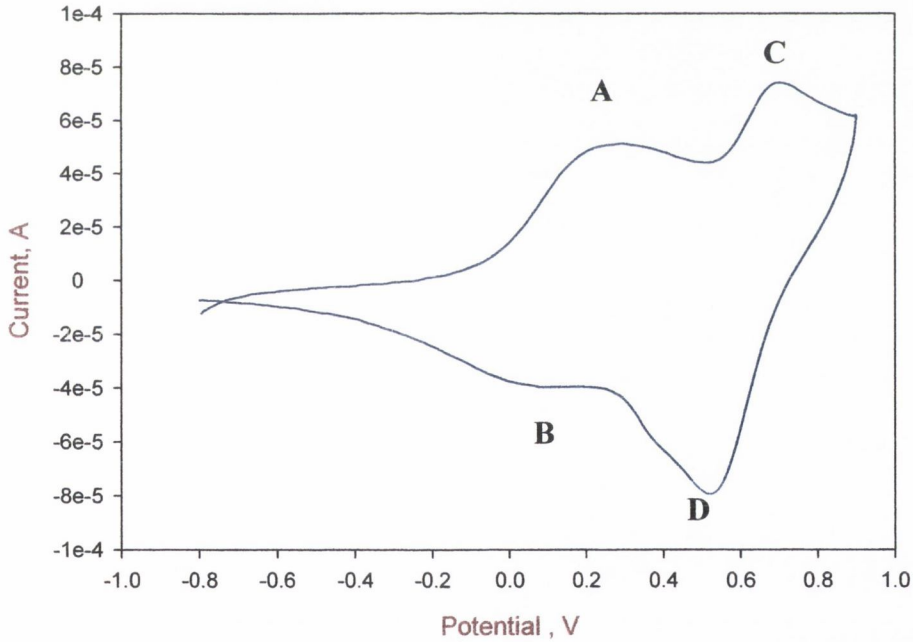


Figure 4.28: Cyclic voltammogram of 7th cycle of the copolymer of poly(**18** n=6 and pyrrole) in background electrolyte, 0.1M TBAP/ CH_3CN, at a Pt disk electrode at 25°C vs Ag/AgCl reference electrode

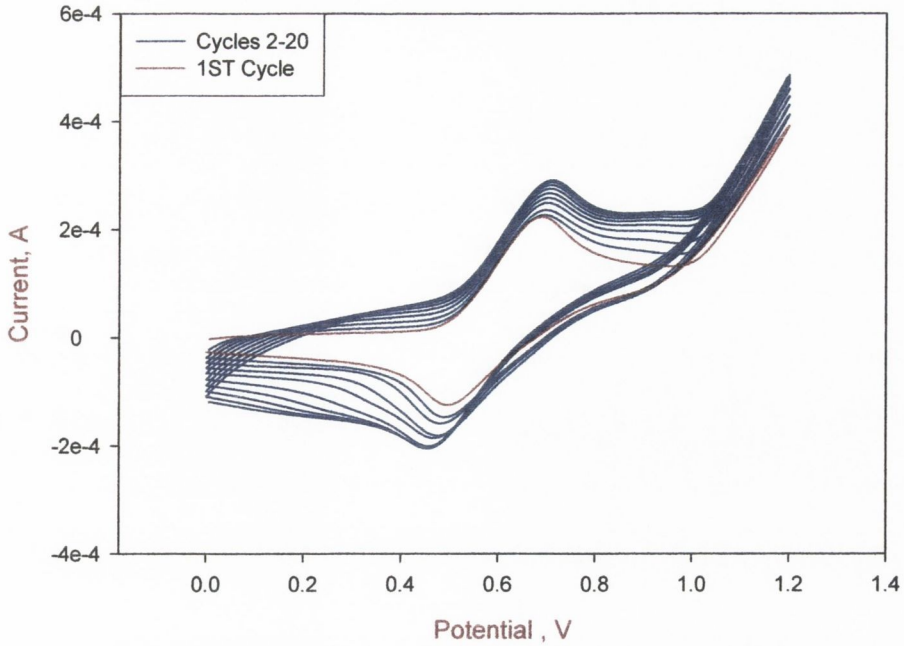


Figure 4.29: Potentiodynamic growth of the copolymer poly(**18** n=7 and pyrrole) in 0.1M TBAP/ CH_3CN, at a Pt disk electrode at 25°C vs Ag/AgCl reference electrode. Scan rate $50mVs^{-1}$

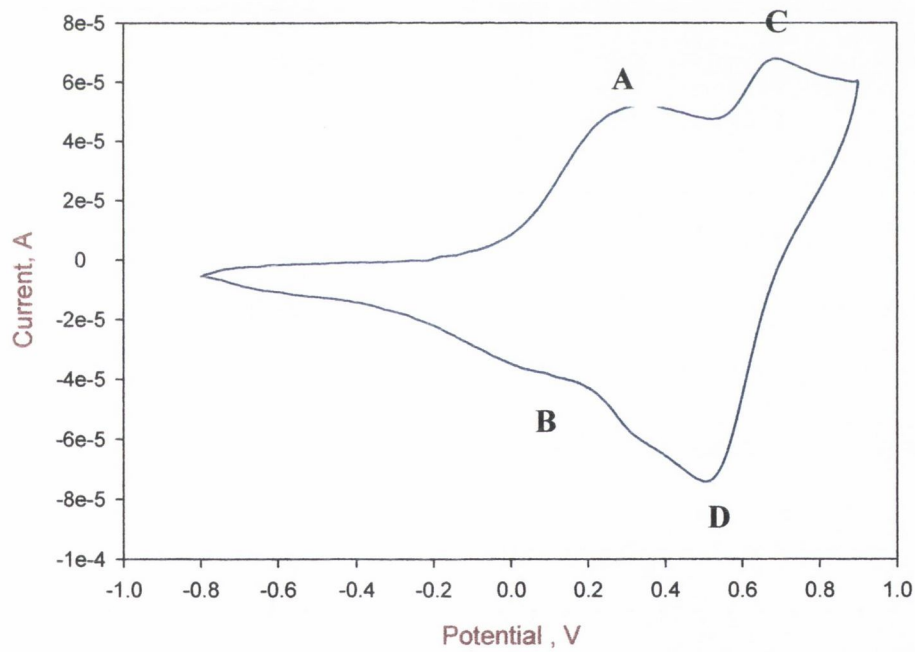


Figure 4.30: Cyclic voltammogram of 7th cycle of the copolymer of poly(**18** n=7 and pyrrole) in background electrolyte, 0.1M TBAP/ CH_3CN, at a Pt disk electrode at 25°C vs Ag/AgCl reference electrode

The determination of the surface coverage, Γ, of the redox-active moiety that was immobilized on the electrode surface was established through the integration of the anodic peak between approx. 0 and 0.5V for the pyrrole moiety and between approx. 0.6 and 0.8V for the ferrocene group of the post-polymerization scans in background electrolyte solution (0.1M TBAP/MeCN). This was then divided by the number of moles of electrons transferred by the pyrrole or ferrocene unit when oxidised, 0.33 and 1 respectively. The values for the apparent surface coverage, Γ_{app} are shown in Table 4.3.

Table 4.4: Surface coverage values for polypyrrole unit and the ferrocene hybrid unit

Copolymer	**D_{CV} 10^5 D/cm^{2}s^{-1}**	**Polypyrrole Surface Coverage, Γ_{app} 10^9 /molcm^{-2}**	**Ferrocene hybrid Surface Coverage, Γ_{app} 10^9 /molcm^{-2}**
PPy- co-([3-(Pyrrol-1-yl)propyl] ferrocene-carboxamide, **18 n= 3)**	0.63 ± 0.05	2.7	0.5
PPy- co-([4-(Pyrrol-1-yl)butyl] ferrocene-carboxamide, **18 n=4**	1.48 ± 0.04	3.1	1.3
PPy- co-([5-(Pyrrol-1-yl) pentyl] ferrocene-carboxamide, **18 n=5**	1.41 ± 0.04	3.5	1.1
PPy- co-([6-(Pyrrol-1-yl)hexyl] ferrocene-carboxamide, **18 n=6**	1.04 ± 0.08	3.1	1.0
PPy- co-([7-(Pyrrol-1-yl)heptyl] ferrocene-carboxamide, **18 n=7**	0.94 ± 0.08	3.9	0.9

It is evident from the surface coverage values that [3-(Pyrrol-1-yl)propyl] ferrocene-carboxamide, **18 n= 3**, has the least moles immobilised on the electrode surface. This may be due to the fact that it has the lowest diffusion coefficient value (D = 0.63 x 10^{-5}cm^{2}s^{-1}) of the range of monomers. There also seems to be a correlation between the amount of hybrid monomer deposited on the electrode surface with their diffusion coefficients. The order of the smallest to largest diffusion coefficient and the least to most moles deposited on the surface appears to be

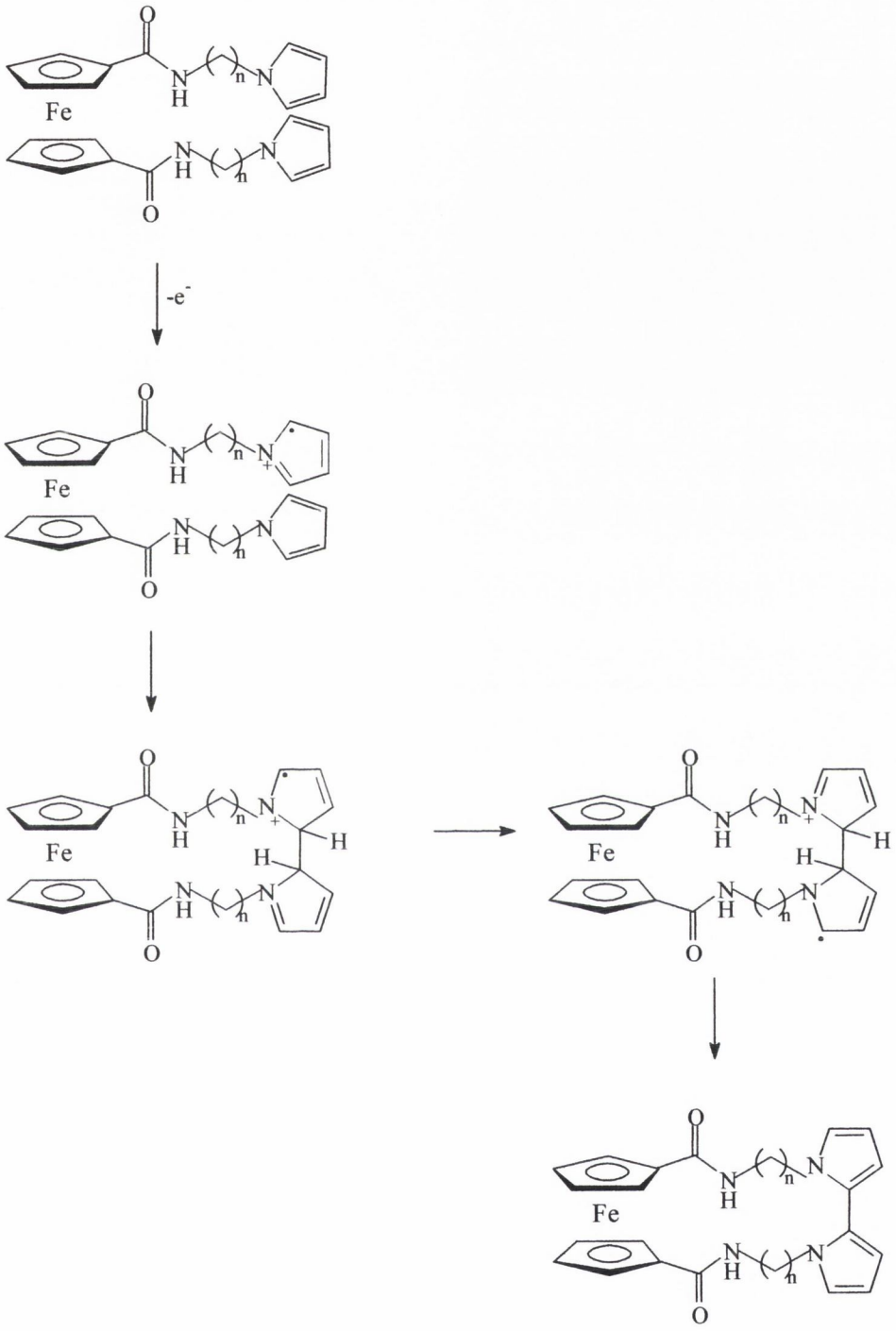
Butyl > Pentyl> Hexyl > Heptyl > Propyl

4.3.2 Electropolymerization of compounds of structure 20

Successive scans over the potential range 0 to 0.9V led to the growth of a yellow, conducting polymer film. Figure 4.31 illustrates the continuous increase in the peak intensity of the ferrocene/ferricinium system (approximately 0.45V). However, there is a decrease in the polypyrrole wave (approx. 0.85V) and is indicative of the increased difficulty experienced by the polypyrrole backbone in the electron transfer process with the electrode interface. The process of electropolymerization is similar to that previously reported for other pyrrole substituted ferrocene dicarboxamides[3]. However, it should be noted that the potential of the ferrocene/ferricinium redox couple is shifted to a more positive potential by 100mV form the first scan. This indicates that the ferrocene/ferricinium redox couple is quite different in homogeneous solution than in the polymer phase. Subsequent cycles show no change in the potential of the ferrocene/ferricinium system.

This behaviour has been observed with previous systems and one explanation may be that the formation of an intramolecular bond between the two pyrrole units upon polymerization results in the formation of a bridge between the two cyclopentadienyl rings[3]. Scheme 4.3 illustrates the mechanism involved. Ferrocenes with different bridges between the two cyclopentadienyl rings have been reported to lack coplanarity and this causes the rings to shift to more positive potentials for the ferrocene/ferricinium redox couple. This hypothesis is examined further through the electropolymerization of compound **21** in section 4.3.

The conductivity of the polymer film was found to deteriorate when the potential limit was extended to 1.0V. In this case the peak currents of the ferrocene/ferricinium redox couple decrease considerably during cycling of the film, this may be attributed to the irreversible oxidation of the polymer film. Cyclic voltammograms were carried out in background electrolyte to determine the surface coverage of the immobilised ferrocene species and to characterise the electrochemical behaviour of the polymer.



Scheme 4.3

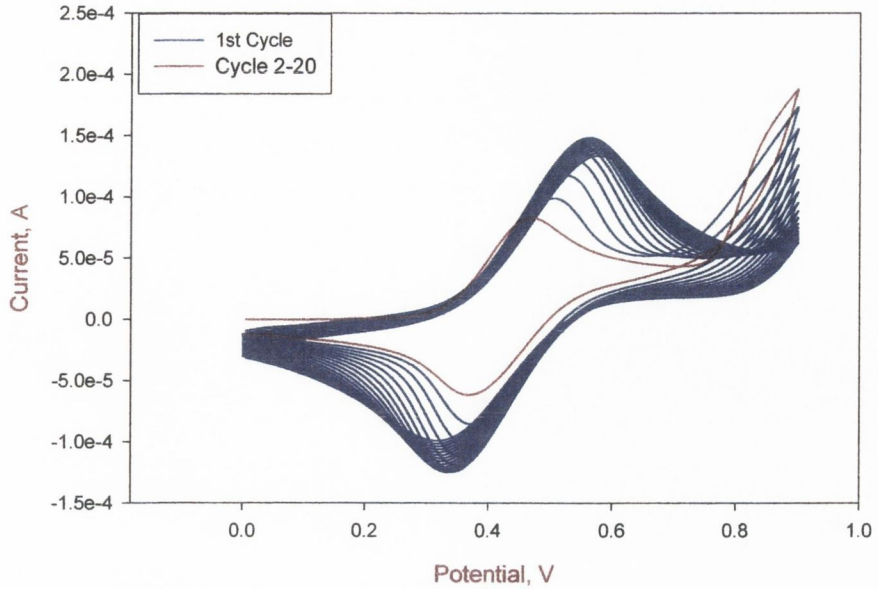


Figure 4.31 Electropolymerization upon repeated cycling of **20** n=3 (10mM) in 0.1M TBAP/ CH_3CN at a Pt disk electrode at 25°C vs $Ag/AgNO_3$ reference electrode; 20 successive scans between 0 and 0.9V.

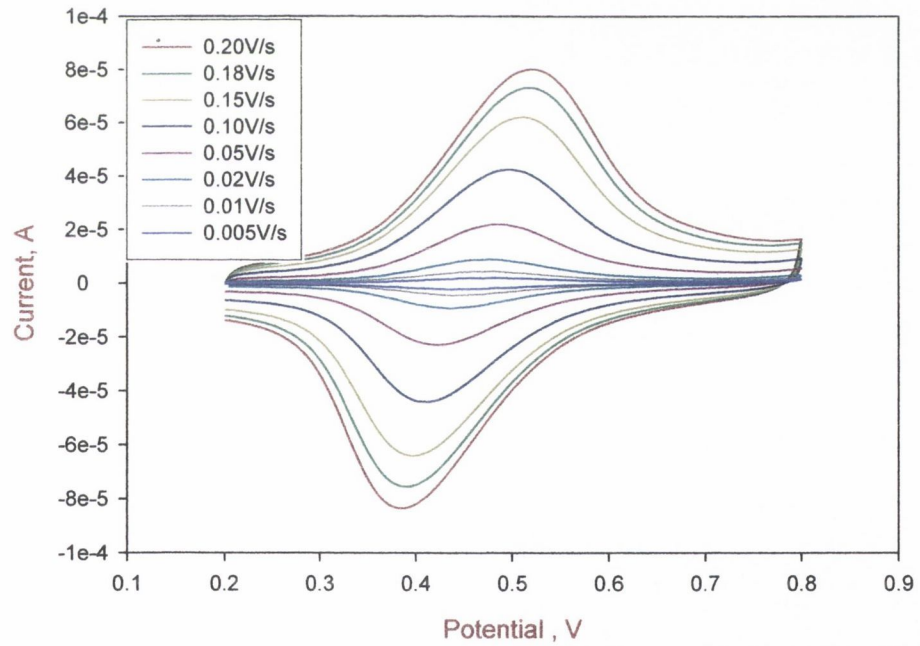


Figure 4.32: Cyclic voltammogram of poly(**20** n=3) at varying scan rates in 0.1M TBAP/ CH_3CN at a Pt disk electrode at 25°C vs $Ag/AgNO_3$ reference electrode.

After the production poly(**18** n=3), the modified polymer film was transferred to a solution of background electrolyte consisting of 0.1M TBAP/ CH_3CN. The cyclic voltammogram shown in figure 4.32 displays the current response of the modified electrode due to the ferrocene/ferricinium redox couple at $E_{1/2}$ = 0.45V. Following six cycles between the limits of 0 to 0.9V a steady state was observed. The determination of the surface coverage, Γ, of the redox-active moiety immobilized on the electrode surface was established through the integration of the anodic peak between approx. 0 and 0.9V for the for all disubstituted ferrocene hybrids of the post-polymerization scans in background electrolyte solution. Unlike the mono-substituted ferrocene copolymers there was no obvious peak that may be attributed to the polypyrrole backbone, however, the electrochemical response is expected at approximately 0.4V and may be hidden under the peaks corresponding to the pendant ferrocene group. The number of moles of electrons transferred by the disubstituted pyrrole polymers was calculated at 1.66, (2 x 0.33 for the oxidation of the pyrrole unit plus one for the oxidation of the ferrocene unit). The values for the apparent surface coverage, Γ_{app} are shown in Table 4.5.

Table 4.5: Surface coverage values for disubstituted ferrocene hybrids.

Monomer	**D_{CV}** **10^5 D/cm^{2}s^{-1}**	**Ferrocene hybrid** **Γ_{app}, 10^{10} /molcm^{-2}**
1,1'-Bis-[3-(Pyrrol-1-yl)propyl]ferrocene-1,1'-dicarboxamide, **20 n=3**	1.25 ± 0.10	8.0
1,1'-Bis-[5-(Pyrrol-1-yl)pentyl]ferrocene-1,1'-dicarboxamide, **20 n=5**	1.20 ± 0.10	5.8
1,1'-Bis-[7-(Pyrrol-1-yl)heptyl]ferrocene-1,1'-dicarboxamide, **20 n=7**	1.30 ± 0.08	5.3
1,1'-[3-(Pyrrol-1-yl)propyl]ferrocene-dicarboxamide, methylester, **21**	0.71 ± 0.04	3.2

In a similar fashion, the electropolymerization of poly(**20** n=5) and poly(**20** n=7) were achieved as shown in figures 4.33 and 4.35 respectively.

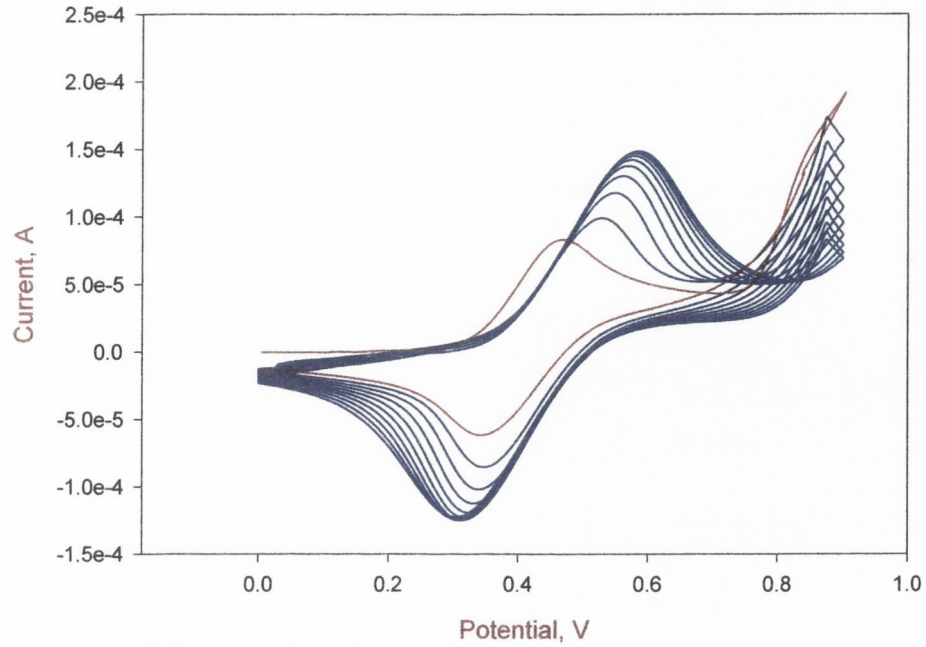


Figure 4.33 Electropolymerization upon repeated cycling of **20** n=5 (10mM) in 0.1M TBAP/ CH_3CN at a Pt disk electrode at 25°C vs $Ag/AgNO_3$ reference electrode; 20 successive scans between 0 and 0.9V.

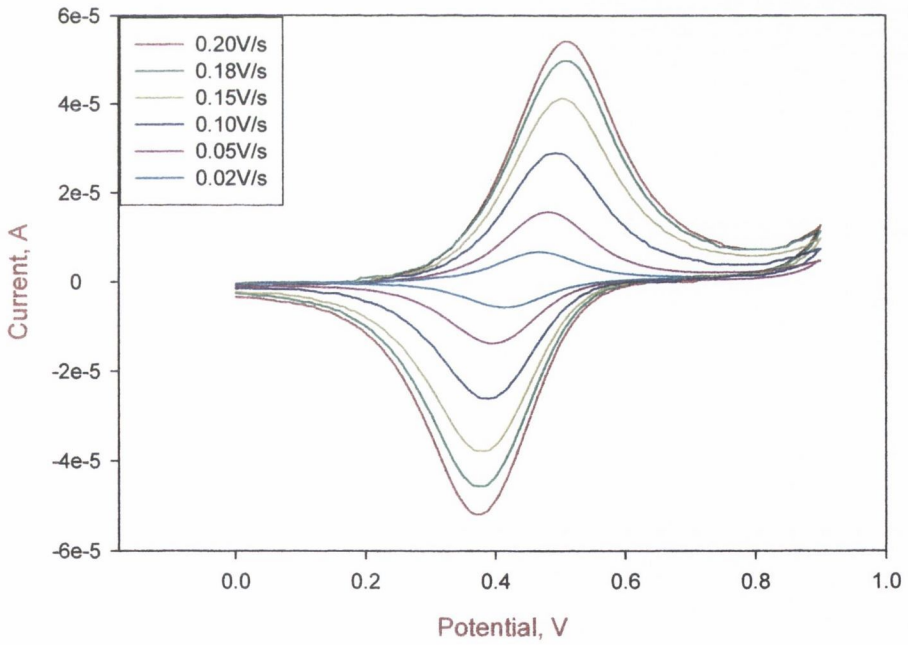


Figure 4.34: Cyclic voltammogram of poly(**20** n=5) at varying scan rates in 0.1M TBAP/ CH_3CN at a Pt disk electrode at 25°C vs $Ag/AgNO_3$ reference electrode.

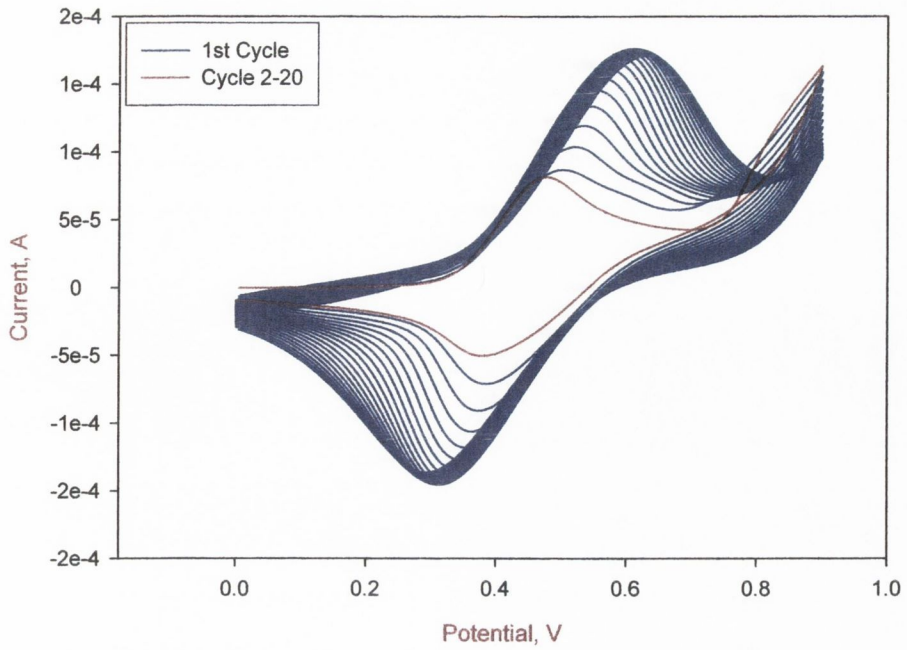


Figure 4.35: Electropolymerization upon repeated cycling of **20** n=7 (10mM) in 0.1M TBAP/ CH_3CN at a Pt disk electrode at 25°C vs $Ag/AgNO_3$ reference electrode; 20 successive scans between 0 and 0.9V.

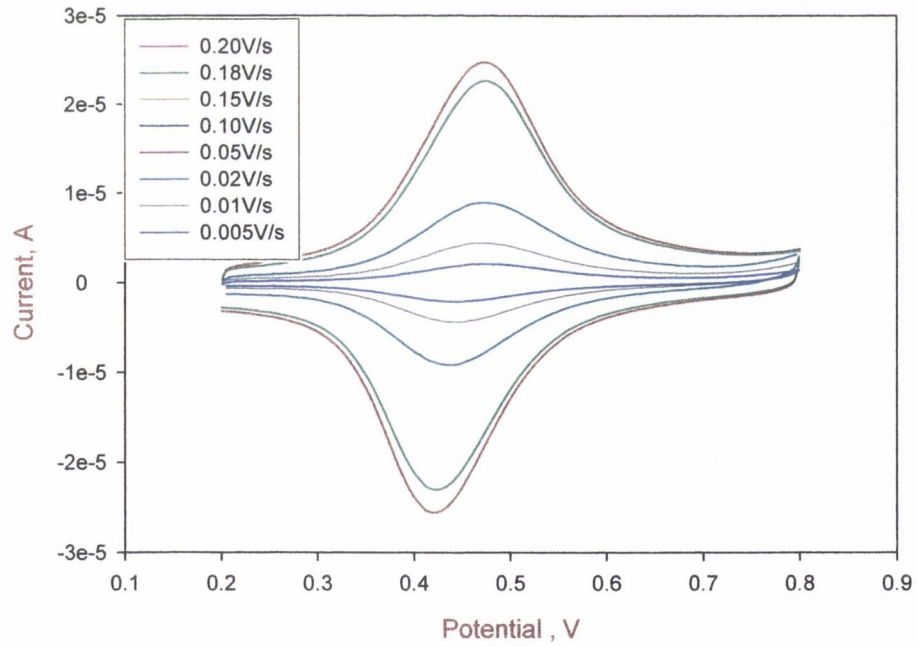


Figure 4.36: Cyclic voltammogram of poly(**20** n=7) at varying scan rates in 0.1M TBAP/ CH_3CN at a Pt disk electrode at 25°C vs $Ag/AgNO_3$ reference electrode.

The electrochemical behaviour of the electroactive polymers was studied by cyclic voltammetry. Figures 4.32, 4.34 and 4.36 depict the cyclic voltammograms of poly(**20** n=3), poly(**20** n=5) and poly(**20** n=7), repectively, in 0.1M TBAP/MeCN solution at different scan rates. The reversible cyclic voltammogram in acetonitrile shows approximately symmetrical anodic and cathodic peaks that have a ΔE_p of 30mV. Examination of the dependence of the peak current to scan rate discovered a linear relationship between these two parameters, as illustrated in figure 4.37. This suggests that there is a reversible redox process occurring within the polymer layer and is indicative of a thin film being formed. This is supported by the surface coverage values determined earlier, see table 4.4. The reversible mechanism of switching is of great significance in the design of a redox active conducting polymer whose application may lie in the oxidative regeneration of an enzymatic species within a biosensor. Hence, a range of polymers has been produced with the desired characteristics for the creation of a reagentless biosensing electrode.

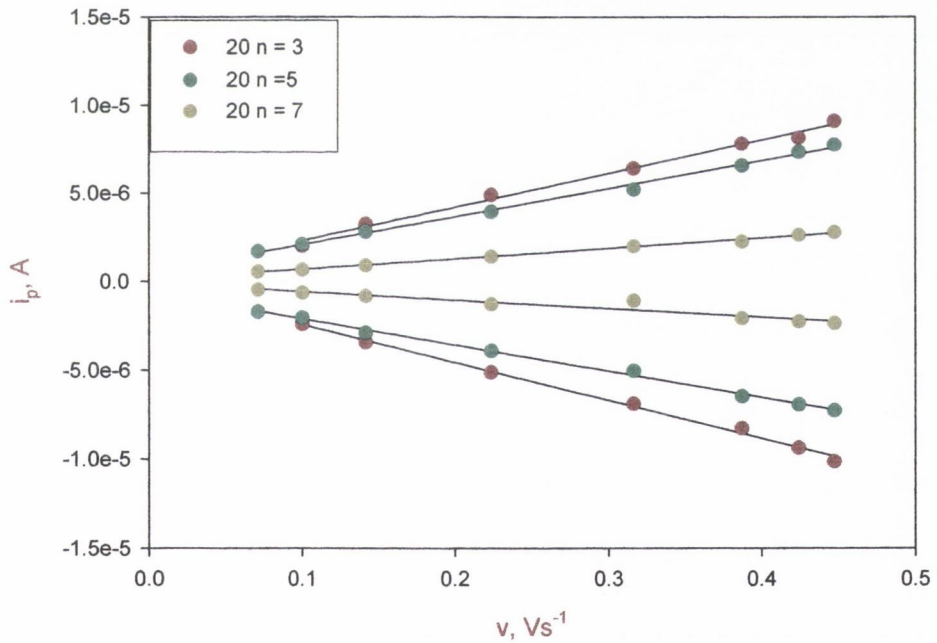


Figure 4.37 Graph of i_p vs v for the oxidation and reduction of poly(**20** n=3, 5, 7) in 0.1M TBAP/ CH_3CN at a Pt disk electrode at 25°C vs $Ag/AgNO_3$ reference electrode.

4.3.3 Electropolymerization of compounds of structure 21

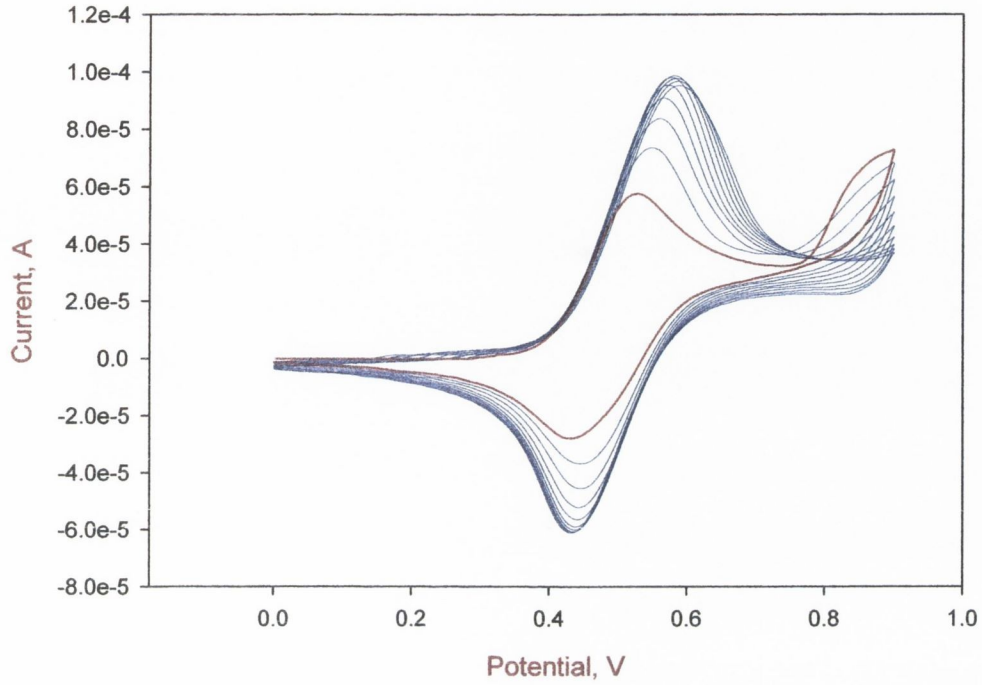
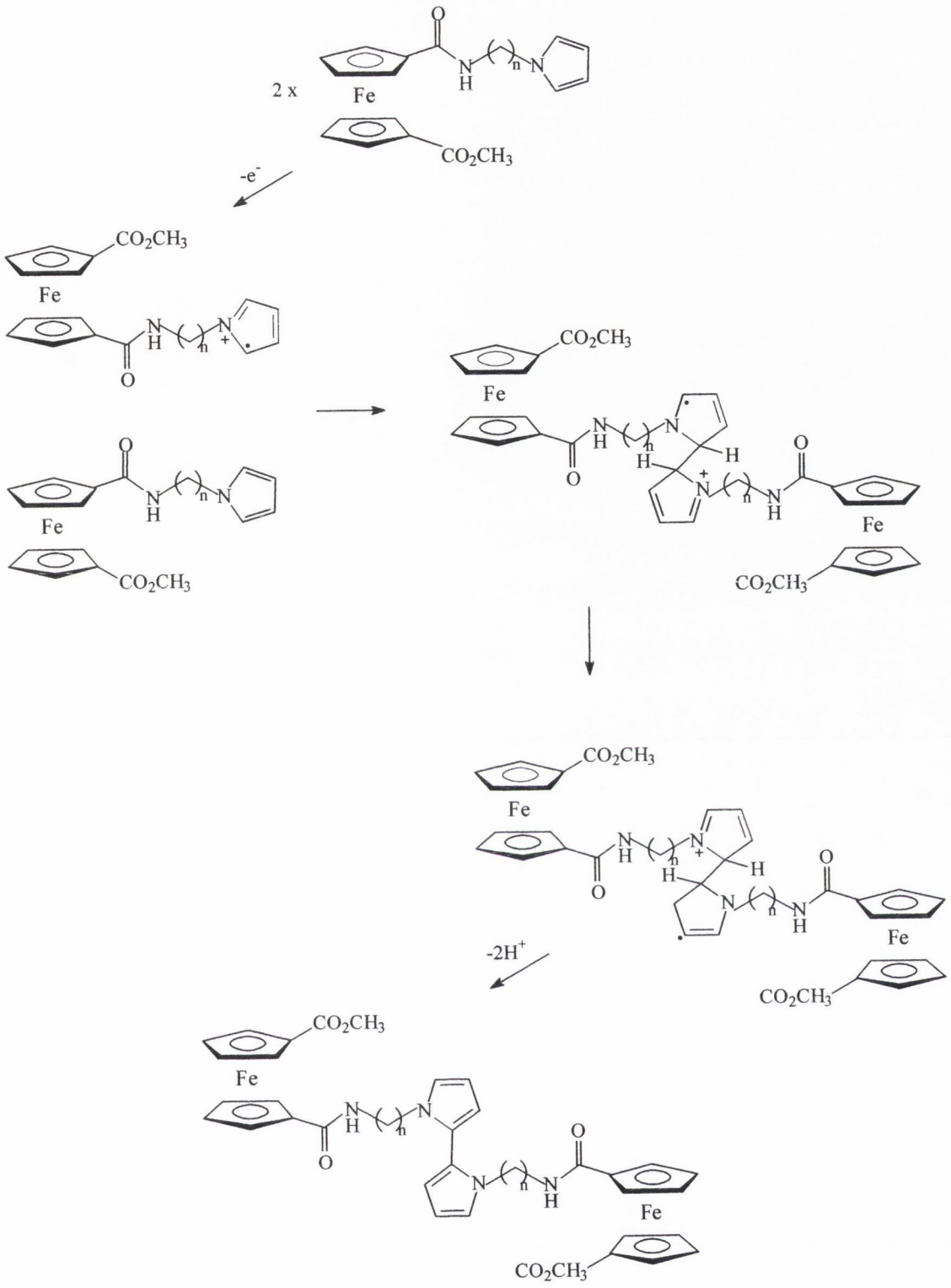


Figure 4.38: Electropolymerization upon repeated cycling of **21** (10mM) in 0.1M TBAP/ CH_3CN at a Pt disk electrode at 25°C vs $Ag/AgNO_3$ reference electrode; 20 successive scans between 0 and 0.9V.

The growth of a conducting polymer film was achieved through continuous cycling of the potential over the range 0 to 0.9V. Figure 4.38 illustrates the continuous increase in the peak intensity of the ferrocene/ferricinium system and the polypyrrole wave (approximately 0.85V). The process of electropolymerization is similar to that previously reported for the symmetrically, disubstituted monomer, **20** n=5, in section 4.3. However, in this case the compound contains only one pyrrole functionality and is incapable of forming an intramolecular bridge. Figure 4.38 shows that the electropolymerization of this moiety only induced a weak and continuous change (less than 30mV) in the potential of the ferrocene/ferricinium redox couple. The mechanism proposed is shown in scheme 4.4, where the lack of an intramolecular bridge may be noted.



Scheme 4.4

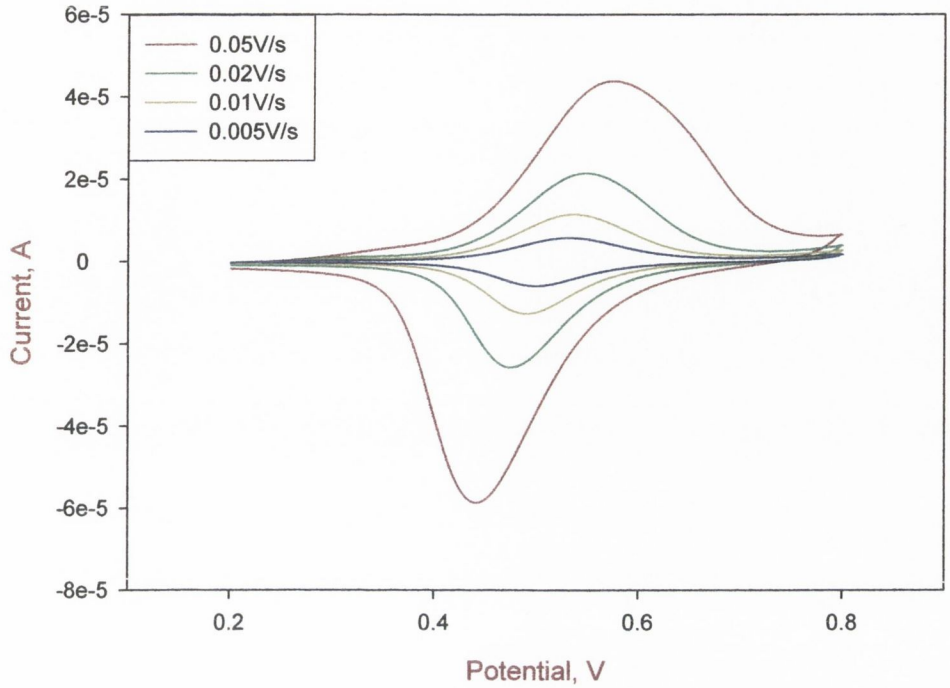


Figure 4.39: Cyclic voltammogram of poly(**21**) at varying scan rates in 0.1M TBAP/ CH_3CN at a Pt disk electrode at 25°C vs $Ag/AgNO_3$ reference electrode.

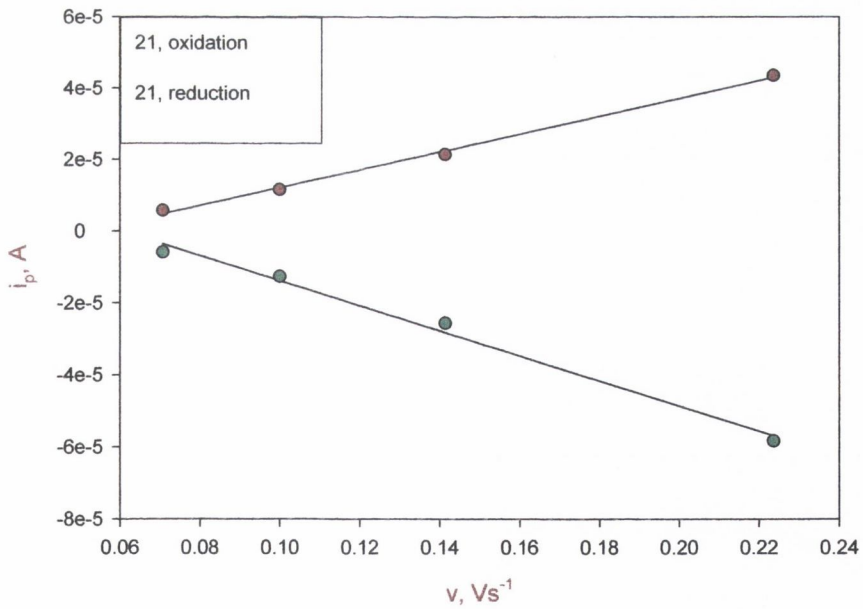


Figure 4.40: Graph of i_p vs v for the oxidation and reduction of the polymer poly(**21**) in 0.1M TBAP/ CH_3CN at a Pt disk electrode at 25°C vs $Ag/AgNO_3$ reference electrode.

The procedure described in section 4.3.2 was repeated for the analysis of the redox conducting polymer, poly(**21**). The modified polymer film was transferred to a solution of background electrolyte consisting of 0.1M TBAP/ CH_3CN. The cyclic voltammogram shown in figure 4.39 displays the current response of the modified electrode due to the ferrocene/ferricinium redox couple at $E_{1/2}$ = 0.5V. Following six cycles between the limits of 0 to 0.6V a steady state was observed. Cyclic voltammograms were carried out at various scan rates and a linear relationship between the variation of the magnitude of the voltammetric peak current with the applied sweep rate was observed, figure 4.40. It is therefore concluded that a reversible mechanism of switching of the incorporated ferrocene species to the oxidised and reduced form inside the polymer is occurring, which is thought to be an essential characteristic for the creation of polymers capable of immobilizing and regenerating enzyme species.

4.4 GLUCOSE OXIDASE IMMOBILIZATION

With the encouraging electropolymerization results of the redox conducting polymers in hand, preliminary studies to undertake the immobilization of the enzyme, glucose oxidase, were carried out. Adsorption of the enzyme (200U) onto a pre-formed copolymer or polymer layer was attempted by cycling the potential between 0 and 1.0V at $50mVs^{-1}$ in 0.1M TBAP/CH_3CN. The interaction between the overall positive charge of the polypyrrole backbone and the negatively charged active site of glucose oxidase produces an electrostatic interaction that allows for overall electroneutrality to be achieved and consequently immobilization of the enzyme onto the polymer film. However the electrostatic interaction proved too weak, subsequent cycling of the in background electrolyte (0.1M TBAP/CH_3CN or McIlvane buffer solution ph7) resulted in the decay of the film after 2 cycles. Copolymerization of the mono-substituted monomers (10mmol) with pyrrole (10mmol) and glucose oxidase (200U) and direct electropolymerization of the disubstituted monomers (5mmol) with glucose oxidase (200U), resulted in the production of an electroactive thin film. The electrochemical

response of the copolymer film of PPy- co-([5-(Py rrol-1-yl) pentyl] ferrocene-carboxamide, **18 n=5** film in 0.1M TBAP/CH_3CN at a sweep rate of 50 mVs^{-1} is depicted in figure 4.41, where there is an apparent redox peak for the ferrocene/ ferrocenium redox couple at 0.25V and a large current at 0.8V corresponding to the oxidation of the glucose oxidase molecules. This indicates that immobilization of an enzyme species can be achieved within the novel polymer and copolymer films.

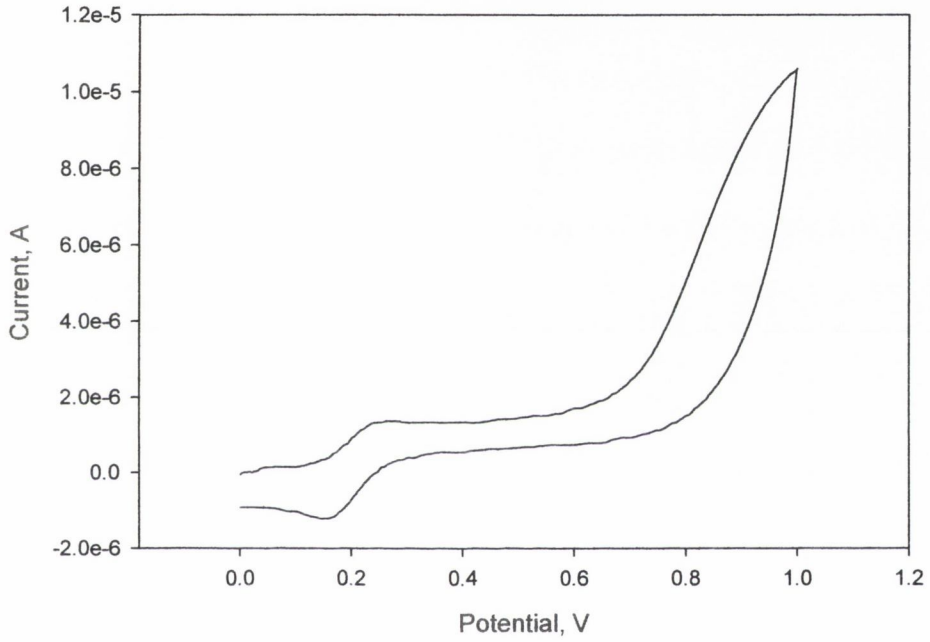


Figure 4.41: Cyclic voltammogram of a thin film of PPy- co-([5-(Pyrrol-1-yl) pentyl] ferrocene-carboxamide, **18 n=5** and 200U glucose oxidase] in 0.1M TBAP/ CH_3CN at a Pt disk electrode at 25°C vs $Ag/AgNO_3$ reference electrode

However, during the course of this work full characterisation of the enzyme films was not accomplished as cycling of the polymer film in background electrolyte (0.1M TBAP/CH_3CN) proved detrimental to the enzymatic activity of the layer, resulting in the decay of the electrochemical response of the film. This may be due to the fact that the

film was cycled to 1.0V vs $Ag/AgNO_3$ and may have caused the non-reversible oxidation of the polymer backbone. It should be noted that these were preliminary studies and should not be considered as disappointing. Further work is required to develop a satisfactory methodology for the immobilization of the enzyme within the polymer layer. This should include the examination of the enzymatic response at redefined potential limits, in different electrolyte and buffer solutions in addition to the quantification of the number of enzyme molecules immobilized in the film.

4.5 CONCLUSIONS

In conclusion, a series of novel, reproducible polymers and copolymers have been successfully produced. The electrochemical behaviour of the monomer species has been investigated and insights into the effect of substitution of the cyclopentadienyl rings on the formal potential of the ferrocene/ferrocenium redox couple have been elucidated. The effect of the substituent on the cyclopentadienyl ring on the formal potential of the ferrocene/ ferrocenium redox couple was defined. On comparison of the hybrid monomers investigated during the course of this work and also those that have been previously reported the formal potential of mono-substituted ferrocene-pyrrole species is lower (approx 0.2V) than that of the disubstituted ferrocene-pyrrole species. The covalent linkage between the pyrrole and ferrocene molecules also causes a shift in the formal potential of the hybrid monomer. Lower formal potentials are observed for those with amide linkages when compared to those with ester linkages (approx 0.05V). There was no observable effect on the formal potential of the redox couple on increasing the alkyl chain length between the ferrocene and the pyrrole groups. The diffusion coefficients for all monomers are reported in tables 4.2 and 4.3.

The successful coplolymerization and electropolymerization of the mono-substituted and disubstituted hybrid ferrocene-pyrrole species respectively was achieved. In the case of the disubstituted species thin films of poly(**20**) and poly(**21**) which exhibited a reversible mechanism of electron switching in background electrolyte were

produced. The surface coverage values for all the films produced were in the range 0.5 to 1.3 x 10^9 molcm^{-2} and are of the magnitude found for monolayers. The effect of the length of the alkyl chain on both the magnitude of the diffusion coefficient and the surface coverage of the hybrid species within the copolymer film was as follows:
(i.e. smallest, propyl, to largest, butyl, diffusion coefficient and the least to most moles deposited on the surface)

Butyl > Pentyl> Hexyl > Heptyl > Propyl

The electrochemical behaviour of the polymers has been shown to include the reversible redox reaction of the ferrocene group in addition to the conducting matrix of the polypyrrole. Investigations into the mechanism of electropolymerization of this group of redox conducting polymers have shown that by appropriately functionalizing the second cyclopentadienyl ring of the ferrocene moiety, monomers that are directly electropolymerizable may be created. It is believed that the electronic effect of the second substituent on the cyclopentadienyl ring allows the pyrrole fragment of the hybrid monomer to form a radical cation upon the application of the appropriate potential. With the design of reagentless electrodes for the purpose of biosensing in mind, this has given us a methodology of creating a conducting polymer with an incorporated redox active group which may be further manipulated to allow the covalent attachment of the enzyme material. For example, the acidification of the ester group on compound **21** would allow for the covalent attachment of the enzyme through the coupling of amino residues using a similar strategy to the one in place in this study. The problem of leaching of substances out of the conducting polymer film may be truly eliminated in these circumstances.

Future work should include the investigation of the ability of the novel pyrrole ligands to be electropolymerized with an immobilised biological species and their examination as potential biosensors.

4.6 REFERENCES

1. A.J. Bard. L.R. Faulkner, *Electrochemical Methods-Fundamentals and Applications,* J. Wiley & Sons, (1980).
2. M. Buda, A. Ion. J.-C. Moutet, E. Saint-Aman, R. Ziessel, *J. Electroanal. Chem.*, **469**, 132, (1999).
3. E. Saint-Aman, M. Ungureanu, T. Visan, J.-C. Moutet, , *Electrochim. Acta*, **42**, 1829 (1997)
4. J. Chen, C.O. Too, G.G. Wallace, G. F. Swiegers, B. W. Skelton, A.H. White, , *Electrochim. Acta*, **47**, 4227 (2002).
5. J.D. Tucker, L. Lambert, D.E. Hibbs, M.B. Hursthouse, K.M.A. Malik, J.H.R. Tucker, *Chem. Commun*, 1649, (1997).
6. J.E.B. Randels, *Trans. Faraday Soc.*, 44, 327, 1948
7. F.G. Cottrell, *Z. Physik. Chem.*, **42**, 385, (1902).
8. H. Scholl, K.Sochaj, *Electrochim. Acta,* **36**, 689, (1991).
9. A.F. Diaz, J.I. Castillo, J.A. Logan, W.Y.J. Lee, *J. Electroanal.Chem.*, **129**, 115. (1981).
10. A. Merz, R. Schwartz, R. Schroop, *Adv. Mater*, **6**, 409, (1992).
11. G. Bidan, A. Deronzier, J.C. Moutet, *J. Chem. Soc. Chem. Commun.*, 1185 (1984)
12. T. Lee, US Pat 4487667, *Chem Abs.*, **129**, 174999, (1985).
13. A. Haimerl, A. Merz, *Angew. Chem. Int. Ed. Engl.*, **25**, 180, (1986).

CHAPTER 5

HETEROGENEOUS REDOX CATALYSIS AT CONDUCTING POLYMER MICROELECTRODES

5.1 INTRODUCTION

In electrochemistry much research over the last fifteen years has focused on two major areas. Firstly the examination and development of chemically modified electrodes (CME) for areas such as chemical sensing, energy storage/conversion and electrocatalysis[1-3] has been the subject of intense investigations. Secondly, the need for miniaturization has come to the forefront of developing chemical devices and with this microelectronic devices have been created. Microelectrodes (0.5 – 50μm)[4-6] are been heavily researched in order to achieve such goals. By attempting to marry the two areas one may be capable of designing sensing and electrocatalytic microelectrodes. This chapter shall investigate a model for mediated electron transfer at conducting polymer microelectrodes and thereby prove its legitimacy.

5.2 MEDIATED ELECTRON TRANSFER AT CONDUCTING POLYMER MICROELECTRODES.[7]

5.2.1 Preliminary Comments

Rational design of microelectronic devices requires knowledge of the physical processes occurring during their operation. These processes, while generally complex, may be described by simple mathematical models. These models require suitable differential equations for coupled diffusion and chemical reaction and reasonable boundary conditions. Previous work carried out by Lyons et al describes a model for mediated electron transfer at conducting polymer ultramicroelectrodes[7]. This theoretical model takes into account the catalytic reaction, the diffusion of substrate and electron percolation occurring within the polymer film. In addition it also includes the possibility of "spill-over" which occurs when the polymer layer extends onto and covers part of the insulating sheath which surrounds the inlaid disc. In order to appreciate the strategy employed when investigating the governing kinetics of the catalytic reaction it is necessary to discuss the model in some detail.

5.2.2 Assumptions

The theoretical description of mediated electron transfer at electroactive polymer films deposited on macroelectrodes has been elucidated by Albery and Hillman[8] and by Andrieux and Saveant[9-12]. While these theories differ in their approaches their conclusions are equivalent. Both theories consider planar diffusion of the substrate in the polymer matrix as the predominant behavior of diffusion. Despite the fact that these theories were developed for macro sized electrodes, many of the assumptions used still stands when dealing with microelectrodes. For instance, the assumptions that substrate diffusion occurs through pores in the polymer matrix, charge percolation occurs along or between strands of polymer and bimolecular reaction between the immobilized redox group and substrate contribute to the net current response will apply. It has been noted previously by Lyons et al[7, 13] that the prediction of the exact geometrical pattern adopted by the deposited layer proves difficult. Therefore, this model allows for the absence/ occurrence of "spill-over", as can be seen in the boundary conditions set. Finally, diffusion is assumed to be radial, for the sake of simplicity.

Boundary Conditions

The reaction/ diffusion equations are given in non-dimensional form under steady state conditions by general differential equations and are valid for any value of the electronic conductivity of the layer, and so may be used for redox conducting and electronically conducting polymer films alike.

$$\begin{aligned} \frac{d^2u}{d\xi^2} + \frac{2}{\xi}\frac{du}{d\xi} - \gamma_S uv = 0 \\ \frac{d^2v}{d\xi^2} + \frac{2}{\xi}\frac{dv}{d\xi} - \gamma_E uv = 0 \end{aligned} \qquad (5.1)$$

where v, u denote the normalized concentrations of oxidized mediator and substrate species within the polymer matrix respectively, they may be defined further as follows:

$$u = \frac{s}{\kappa s^{\infty}} \quad v = \frac{b}{c_{\Sigma}} \quad \xi = \frac{r}{L} \qquad (5.2)$$

where $c_\Sigma = a + b$, represents the total concentration of reduced and oxidized mediator species in the polymer layer of layer thickness L. κ signifies the substrate partition coefficient. In addition, the reaction/ diffusion parameters, γ_E and γ_S, may be defined as:

$$\gamma_E = \frac{k\kappa s^\infty L^2}{D_E} = \frac{f_R}{f_E} = \frac{\lambda}{\rho\sigma^2}$$
$$\gamma_S = \frac{kc_\Sigma L^2}{D_S} = \frac{f_R}{f_S} = \frac{\lambda}{\sigma^2} \qquad (5.3)$$

these parameters serve to quantify the ratio of the rates of chemical reaction (defined via the bimolecular rate constant, k) to that of charge percolation (defined by the electron diffusion coefficient, D_E), or the ratio of the rate of chemical reaction to the rate of substrate diffusion in the polymer matrix (defined by the substrate diffusion coefficient, D_S).

f_i denoting the relevant flux factor (R, S and E signifying the rate determining catalytic reaction, substrate diffusion within the film and charge percolation respectively) and k is the bimolecular rate constant for the mediator/substrate reaction. Also the Andrieux and Saveant[10] parameters σ, λ and ρ, have been introduced and may be defined as:

$$\sigma = \frac{\kappa D_S \delta}{D'_S L} = \frac{f_S}{f_D} \qquad (5.4)$$

The parameter σ compares the diffusion of substrate in the film (defined by diffusion flux f_S) with the substrate diffusion in solution (defined either by diffusion flux f_D or diffusion coefficient D'_S). The diffusion layer thickness, δ, is taken as $\delta = \frac{\pi a}{4}$, for ultramicroelectrodes, where a represents the radius of the disc.

Conversely, the parameter λ expresses the efficiency of the chemical reaction of the substrate with the mediator as related to the diffusion of the substrate in the solution, thereby giving an expression for λ as follows:

$$\lambda = \frac{\kappa^2 k c_\Sigma D_S \delta^2}{D'^2_S} = \frac{f_R f_S}{f_D^2} \qquad (5.5)$$

Finally, ρ compares electron diffusion flux in the polymer matrix with substrate diffusion flux within it.

$$\rho = \frac{D_E c_\Sigma}{\kappa D_S s^\infty} = \frac{f_E}{f_S} \tag{5.6}$$

Considering equation (3) once more it may be shown that:

$$\sqrt{\gamma_S} = \frac{L}{\mu_S}$$
$$\sqrt{\gamma_E} = \frac{L}{\mu_E} \tag{5.7}$$

where $\mu_S = \sqrt{\frac{D_S}{kc_\Sigma}}$ and defines a characteristic layer thickness, this is of particular importance when electrons transverse rapidly across the polymer layer and react with substrate before the substrate can diffuse through polymer film. $\mu_E = \sqrt{\frac{D_E}{\kappa k s^\infty}}$ defines a reaction layer thickness, however, this is important when the converse is true, i.e. the substrate diffuses readily through the polymer matrix and reacts with the mediator before the mediator has diffused radially from the support electrode.

5.2.3 "Spill-Over"

If we examine radial reaction/diffusion in a polymer film of thickness L between r = a and r = a + L (see Dong and Che[15,16]), then any spillover is adequately accounted for.

The boundary conditions defining the problem are:

$$\xi = \frac{a}{L} = \zeta \quad \frac{du}{d\xi} = 0, \quad v = 1$$
$$\xi = \frac{a+L}{L} = 1 + \zeta \quad \frac{dv}{d\xi} = 0, \quad 1 - u = \sigma\left(\frac{du}{d\xi}\right) \tag{5.8}$$

this allows for the incorporation of the substrate diffusion in the solution adjacent to the polymer film into the analysis.

In accordance with Andrieux and Saveant[10], a normalized current density is introduced:

$$\Psi = \frac{j_{cat}}{j_D} \tag{5.9}$$

where j_{cat} indicates the catalytic current density at the chemically modified microelectrode and j_D denotes the diffusion limited current density at an unmodified microelectrode and may be further defined as:

$$j_D = \frac{nFD'_S s^{\infty}}{\delta} = \frac{4nFD'_S s^{\infty}}{\pi a} \tag{5.10}$$

Finally, the normalized current density is given by:

$$\Psi = 1 - u_{1+\zeta} = \sigma\left(\frac{du}{d\xi}\right)_{1+\zeta} = -\rho\sigma\left(\frac{dv}{d\xi}\right)_{\zeta} \tag{5.11}$$

5.2.4 Development of u- and v- master equations

Equation (1) presents the set of general reaction/diffusion equations in mixed uv terms. The boundary conditions may be used to relate u and v and thereby rearrange the differential equations into a form containing a single normalized concentration variable, i.e. either u or v.

This results in the development of equation (12):

$$v = \frac{u - u_{\zeta}}{\rho} + \frac{(1+\zeta)^2\Psi}{\rho\sigma}\left\{\frac{1}{\xi} - \frac{1}{\zeta}\right\} + 1$$

$$u = \rho\left\{(v - v_{1+\zeta}) + \frac{(1+\zeta)\Psi}{\rho\sigma}\left[1 - \frac{1+\zeta}{\xi}\right]\right\} + 1 - \Psi \tag{5.12}$$

Consequently, when equation (12) is substituted into equation (1) we obtain the set of master equations required to define the transport and kinetics within the polymer layer. The u-master defines the transport and kinetic properties of the substrate within the film, while the v-master describes those of the mediator.

$$\frac{d^2u}{d\xi^2} + \frac{2}{\xi}\frac{du}{d\xi} - \frac{\lambda}{\sigma^2}\left\{\frac{u - u_{\zeta}}{\rho} + \frac{(1+\zeta)^2\Psi}{\rho\sigma}\left(\frac{1}{\xi} - \frac{1}{\zeta}\right) + 1\right\}u = 0 \tag{5.13}$$

$$\frac{d^2v}{d\xi^2} + \frac{2}{\xi}\frac{dv}{d\xi} - \frac{\lambda}{\rho\sigma^2}\left\{\rho\left[(v - v_{1+\zeta}) + \frac{(1+\zeta)\Psi}{\rho\sigma}\left(1 - \frac{1+\zeta}{\xi}\right)\right] + 1 - \Psi\right\}v = 0 \tag{5.14}$$

These equations while similar in style to those reported by Dong and Che[16], differ in some respects to those reported previously. It is the contention of the author that this model is to be preferred over the original work.

5.2.5 Case by case kinetic analysis

Electron diffusion through the polymer layer more rapid than substrate diffusion

R + S case

When electron diffusion through the polymer film is very fast compared to substrate transport through the same, i.e. when $\rho \to \infty$ and $\frac{1}{\rho} \to 0$ equation (13) may be reduced to:

$$\frac{d^2u}{d\xi^2} + \frac{2}{\xi}\frac{du}{d\xi} - \frac{\lambda}{\sigma^2}\left\{\frac{(1+\zeta)^2\Psi}{\rho\sigma}\left(\frac{1}{\xi} - \frac{1}{\zeta}\right) + 1\right\}u = 0 \qquad (5.15)$$

If it is also assumed that the diffusion of electrons in the polymer layer is fast compared to that of the substrate in solution then it may be said that $\rho\sigma \to \infty$ and therefore $\frac{1}{\rho\sigma} \to 0$, this further reduces equation (15) to:

$$\frac{d^2u}{d\xi^2} + \frac{2}{\xi}\frac{du}{d\xi} - \left(\frac{\lambda}{\sigma^2}\right)u = 0 \qquad (5.16)$$

Using the Andrieux and Saveant notation[10], this case scenario would be the equivalent of the R + S kinetic case, which corresponds to slow bimolecular reaction and slow substrate diffusion in the polymer layer. The normalized amperometric response for this case is:

$$\Psi = \frac{1 + \left\{\frac{F_2 - 1}{F_1 - 1}\right\}G\exp\left[-2\sqrt{\frac{\lambda}{\sigma^2}}\right]}{\frac{F_1}{F_1 - 1} + \frac{F_2 G}{F_1 - 1}\exp\left[-2\sqrt{\frac{\lambda}{\sigma^2}}\right]} \qquad (5.17)$$

where:

$$F_1 = 1 + \sigma\left\{\sqrt{\frac{\lambda}{\sigma^2}} - \frac{1}{1+\zeta}\right\}$$

$$F_2 = 1 - \sigma\left\{\sqrt{\frac{\lambda}{\sigma^2}} - \frac{1}{1+\zeta}\right\} \qquad (5.18)$$

$$G = \frac{\sqrt{\frac{\lambda}{\sigma^2}} - \frac{1}{\zeta}}{\sqrt{\frac{\lambda}{\sigma^2}} + \frac{1}{\zeta}}$$

If the polymer layer is thin in comparison with the radius of the ultramicroelectrode then $\zeta >> 1$ and so $\zeta \to 0$. This approximation is reasonable as the polymer films on support electrodes attain a nominal thickness of ca. 3μm and the radius of the inlaid microdisc lie in the range of 2-50μm. This allows equations (17) and (18) may be simplified to the following:

$$F_1 \cong 1 + \sqrt{\lambda}$$

$$F_2 \cong 1 - \sqrt{\lambda} \qquad (5.19)$$

$$G \cong 1$$

and

$$\frac{F_2 - 1}{F_1 - 1} \cong -1$$

$$\frac{F_1}{F_1 - 1} \cong \frac{1 + \sqrt{\lambda}}{\sqrt{\lambda}} \qquad (5.20)$$

$$\frac{F_2}{F_1 - 1} \cong \frac{1 - \sqrt{\lambda}}{\sqrt{\lambda}}$$

The normalized amperometric current response now becomes:

$$\Psi \cong \frac{1}{1 + \frac{1}{\sqrt{\lambda}\tanh\left[\sqrt{\frac{\lambda}{\sigma^2}}\right]}} = \frac{\sqrt{\lambda}\tanh\left[\sqrt{\frac{\lambda}{\sigma^2}}\right]}{1 + \sqrt{\lambda}\tanh\left[\sqrt{\frac{\lambda}{\sigma^2}}\right]} \qquad (5.21)$$

SR Case

When $\sqrt{\frac{\lambda}{\sigma^2}} = \sqrt{\gamma_S} \to \infty$ the flux due to the bimolecular catalytic reaction will be much greater than the flux of substrate diffusion through the polymer matrix.

In this situation $f_R >> f_S$, and substrate diffusion is rate limiting. This is equivalent to the SR kinetic case[10], where in such circumstances the catalytic reaction between B and S will be limited to a reaction layer near the film/solution interface.

Here $\tanh\left[\sqrt{\frac{\lambda}{\sigma^2}}\right] \cong 1$ and equation (21) reduces to:

$$\Psi \cong \frac{\sqrt{\lambda}}{1+\sqrt{\lambda}} \tag{5.22}$$

If the latter expression is inverted, the result is as follows:

$$\frac{1}{\Psi} = 1 + \frac{1}{\sqrt{\lambda}} \tag{5.23}$$

In addition it has been shown that equation (23) may be put in terms of current density as follows:

$$\frac{1}{j_{cat}} = \frac{\pi a}{4nFD'_S s^{\infty}} + \frac{1}{nF\kappa\sqrt{kc_{\Sigma}D_S s^{\infty}}} \tag{5.24}$$

this equation is analogous to that derived by Koutecky-Levich[17] which describes transport and kinetics at a rotating disc electrode.

R Case

The kinetic case R pertains when $\sqrt{\frac{\lambda}{\sigma^2}} = \sqrt{\gamma_S} \to 0$, i.e. when substrate diffusion is faster than the bimolecular chemical reaction, $f_R << f_S$.

Here $\tanh\left[\sqrt{\frac{\lambda}{\sigma^2}}\right] \cong \sqrt{\frac{\lambda}{\sigma^2}}$ and equation (21) now becomes:

$$\Psi \cong \frac{\lambda\sigma^{-1}}{1+\lambda\sigma^{-1}} \tag{5.25}$$

or

$$\frac{1}{\Psi} = 1 + \frac{\sigma}{\lambda} \tag{5.26}$$

Once again, this expression may be translated into terms of current density as below:

$$\frac{1}{j_{cat}} = \frac{\pi a}{4nFD'_S s^{\infty}} + \frac{1}{nF\kappa k c_{\Sigma} L s^{\infty}} \tag{5.27}$$

When the SR + E case is examined, the situation where $\sqrt{\frac{\lambda}{\sigma^2}} = \sqrt{\gamma_S}$ is still very large occurs, but the condition that $\rho\sigma \to \infty$ is not applicable. Hence $\frac{f_E}{f_D}$ is finite. This implies that the bimolecular catalytic reaction is still confined to a reaction layer close to the film/solution interface. The boundary conditions in this case (for the u-master equation) is $\xi = 1 + \zeta$ and that $\rho^{-1} \to 0$:

$$\frac{d^2u}{d\xi^2} + \frac{2}{\xi}\frac{du}{d\xi} - \frac{\lambda}{\sigma^2}\left\{\frac{(1+\zeta)^2\Psi}{\rho\sigma}\left(\frac{1}{1+\zeta} - \frac{1}{\zeta}\right) + 1\right\}u = 0 \tag{5.28}$$

By introducing a new parameter ω as:

$$\begin{aligned}\omega &= \frac{\lambda}{\sigma^2}\left\{\frac{(1+\zeta)^2\Psi}{\rho\sigma}\left(\frac{1}{1+\zeta} - \frac{1}{\zeta}\right) + 1\right\} \\ &= \frac{\lambda}{\sigma^2}\left\{1 - \frac{(1+\zeta^{-1})\Psi}{\rho\sigma}\right\}\end{aligned} \tag{5.29}$$

equation (28) reduces to:

$$\frac{d^2u}{d\xi^2} + \frac{2}{\xi}\frac{du}{d\xi} - \omega u = 0 \tag{5.30}$$

The normalized amperometric response now becomes:

$$\Psi = 1 - \frac{1}{1 + \sigma\left(\sqrt{\omega} - \frac{1}{1+\zeta}\right)} = \frac{\sigma\left(\sqrt{\omega} - \frac{1}{1+\zeta}\right)}{1 + \sigma\left(\sqrt{\omega} - \frac{1}{1+\zeta}\right)} \tag{5.31}$$

When the parameter $\zeta >> 1$ then equation (31) becomes:

$$\Psi \cong \frac{\sigma\sqrt{\omega}}{1 + \sigma\sqrt{\omega}} \tag{5.32}$$

This applies for the case SR + E for the condition where a >> L. Two subcases may be derived from this expression depending on the vale of the product $\rho\sigma$. When ζ is large equation (29) now becomes:

$$\omega \cong \frac{\lambda}{\sigma^2}\left\{1-\frac{\Psi}{\rho\sigma}\right\} \tag{5.33}$$

However, if $\rho\sigma \to \infty$ then $\omega \cong \frac{\lambda}{\sigma^2}$ and equation (32) reduces to $\Psi \cong \frac{\sqrt{\lambda}}{1+\sqrt{\lambda}}$ which is definitive of the SR subcase (see equation (22)). When ζ is finite the corresponding equation is given by $\Psi = \frac{\sqrt{\lambda} - \frac{\sigma}{1+\zeta}}{1+\sqrt{\lambda} - \frac{\sigma}{1+\zeta}}$.

E Case

Alternatively, if the product $\rho\sigma \to 0$ the subcase E is achieved. Case E concurs with the situation where the catalytic current is controlled completely by electron diffusion in the polymer layer. The bimolecular reaction takes place in a very thin surface region near the film/solution interface. The substrate does not penetrate the layer to any great extent. The limiting expression for case E is:

$$\Psi \cong \frac{\rho}{1+\sigma^{-1}\left(1+\frac{1}{\zeta}\right)} \xrightarrow{\zeta \text{ large}} \frac{\rho}{1+\sigma^{-1}} \tag{5.34}$$

This equation shall reappear for the kinetic case S + E under suitable limiting conditions.

Substrate diffusion through the polymer layer more rapid than electron diffusion

When substrate diffusion through the polymer matrix is faster than electron diffusion through the layer the parameter $\rho \to 0$. This situation arises when electronic conductivity of the layer is low.

R + E Case

In this situation the v-master equation is utilized. In the R + E case the parameter $\sigma \to \infty$ to indicate the more rapid diffusion of the substrate through the film in comparison to the diffusion of the same through the solution. Hence, it may

be assumed that the normalized substrate concentration u is constant within the film and that $u = 1 - \Psi$. If the parameter $\rho \to 0$ is set in equation (14) the following is obtained:

$$\frac{d^2v}{d\xi^2} + \frac{2}{\xi}\frac{dv}{d\xi} - \frac{\lambda}{\rho\sigma^2}\{1-\Psi\}v = 0 \tag{5.35}$$

The normalized amperometric response is given by:

$$\Psi = \frac{\rho\sigma\left\{\left(\sqrt{\beta}+\frac{1}{\zeta}\right)\theta\exp\left[2\sqrt{\beta}\right] - \left(\sqrt{\beta}-\frac{1}{\zeta}\right)\right\}}{1+\theta\exp\left[2\sqrt{\beta}\right]} \tag{5.36}$$

where

$$\beta = \frac{\lambda}{\rho\sigma^2}(1-\Psi) = \gamma_E(1-\Psi) \tag{5.37}$$

and

$$\theta(\beta,\zeta) = \frac{\sqrt{\beta} - \frac{1}{1+\zeta}}{\sqrt{\beta} + \frac{1}{1+\zeta}} \tag{5.38}$$

When ζ is large $(1+\zeta)^{-1} \cong \zeta^{-1} \to 0$ and also $\theta(\beta,\zeta) \cong 1$. Under these circumstances equation (36) reduces to:

$$\begin{aligned}\Psi &\cong \rho\sigma\sqrt{\beta}\left\{\frac{\exp\left[2\sqrt{\beta}\right]-1}{1+\exp\left[2\sqrt{\beta}\right]}\right\} = \rho\sigma\sqrt{\beta}\tanh\left[\sqrt{\beta}\right] \\ &= \sqrt{\rho\lambda(1-\Psi)}\tanh\left[\sqrt{\frac{\lambda}{\rho\sigma^2}}(1-\Psi)\right]\end{aligned} \tag{5.39}$$

R Case

Two subcases may be achieved from this equation depending on the value of the parameter $\sqrt{\gamma_E} = \sqrt{\frac{\lambda}{\rho\sigma^2}}$.. When $\sqrt{\frac{\lambda}{\rho\sigma^2}} \to 0$ the subcase R is obtained. This case corresponds to the rate determining bimolecular catalytic reaction. Here

$\tanh\left[\sqrt{\frac{\lambda}{\rho\sigma^2}(1-\Psi)}\right] \cong \sqrt{\frac{\lambda}{\rho\sigma^2}(1-\Psi)}$ and equation (41) reduces to:

$\Psi \cong \frac{\lambda\sigma^{-1}}{1+\lambda\sigma^{-1}}$ which has been obtained previously in equation (25).

When ζ is not very large the corresponding equation is $\Psi = \frac{1}{1+\frac{1}{\lambda\sigma^{-1}+\zeta^{-1}\sigma}}$.

ER Case

Alternatively, when $\sigma \to \infty$ and also $\sqrt{\frac{\lambda}{\rho\sigma^2}} \to \infty$ the subclass ER is achieved. In this case $\tanh\left[\sqrt{\frac{\lambda}{\rho\sigma^2}(1-\Psi)}\right] \cong 1$ and so equation (39) is reduced to:

$$\frac{\Psi}{\sqrt{1-\Psi}} = \sqrt{\rho\lambda} \tag{5.40}$$

Equation (40) corresponds to a quadratic equation in Ψ:

$$\Psi^2 + \rho\lambda\Psi - \rho\lambda = 0 \tag{5.41}$$

and therefore

$$\Psi = \frac{\rho\lambda}{2}\left\{\sqrt{1+\frac{4}{\rho\lambda}} - 1\right\} \tag{5.42}$$

In terms of current density equation (40) takes the form:

$$j_{cat}\left\{1-\frac{j_{cat}}{j_D}\right\}^{-1/2} = nF\sqrt{\kappa k D_E}\sqrt{s^{\infty}c_{\Sigma}} \tag{5.43}$$

It should be noted that in the ER case the diffusion of the substrate to the polymer film and the catalytic processes occurring within the said layer are not distinctly separated. For this reason, the limiting situation is different to that for the SR case. In regards to the ER case a plot of current density function $J = {}_{cat}\left\{1-\frac{j_{cat}}{j_D}\right\}^{-1/2}$ vs electrode radius, a should result in a horizontal line. In addition, the modified current density function J should vary in a first order fashion

with respect to the mediator concentration c_Σ and show a half order variation with respect to changes in bulk substrate concentration s^∞. Determination of the slope of either of these plots enables the parameter $\sqrt{\kappa k D_E}$ to be elucidated. Symmetry between the ER and SR cases may be observed.

ER + S Case

Following the assumption that $\rho \to 0$ and that σ is not very large and so $1/\sigma$ need not approach zero leads to the ER + S case. The pertaining reaction/diffusion equations in such circumstances may be achieved by setting $\xi \to \zeta$ in the v-master equation and noting that $\rho \to 0$. In this situation the v-master equation reduces to:

$$\frac{d^2v}{d\xi^2} + \frac{2}{\xi}\frac{dv}{d\xi} - \frac{\lambda}{\rho\sigma^2}\left\{1 - \Psi\left(1 - \frac{\left(1+\zeta^{-1}\right)}{\sigma}\right)\right\}v = 0 \tag{5.44}$$

If α is defined as:

$$\alpha = \frac{\lambda}{\rho\sigma^2}\left\{1 - \Psi\left(1 + \frac{\left(1+\zeta^{-1}\right)}{\sigma}\right)\right\} \tag{5.45}$$

then the equation (44) defining the ER + S case reduces to:

$$\frac{d^2v}{d\xi^2} + \frac{2}{\xi}\frac{dv}{d\xi} - \alpha v = 0 \tag{5.46}$$

This equation may be integrated using the boundary conditions $\xi = \zeta, v = 1$ and $\xi = 1 + \zeta, \frac{dv}{d\xi} = 0$ to obtain the normalized amperometric response:

$$\Psi = \frac{\rho\sigma\left\{\left(\sqrt{\alpha} + \frac{1}{\zeta}\right)\phi\exp\left[2\sqrt{\alpha}\right] - \left(\sqrt{\alpha} - \frac{1}{\zeta}\right)\right\}}{1 + \phi\exp\left[2\sqrt{\alpha}\right]} \tag{5.47}$$

where

$$\phi(\alpha,\zeta) = \frac{\sqrt{\alpha} - \frac{1}{1+\zeta}}{\sqrt{\alpha} + \frac{1}{1+\zeta}} \tag{5.48}$$

When ζ is large then equation (47) reduces to:

$$\Psi \cong \rho\sigma\sqrt{\alpha}\tanh\left[\sqrt{\alpha}\right] \tag{5.49}$$

where

$$\alpha \cong \frac{\lambda}{\rho\sigma^2}\left\{1-\Psi\left(1+\frac{1}{\sigma}\right)\right\} \tag{5.50}$$

Once again equation 50 agrees with previous results obtained by Andrieux and Saveant.

This equation may be further reduced since $\frac{\lambda}{\rho\sigma^2} \to \infty$ then α will be large and so $\tanh\sqrt{\alpha} \cong 1$ and therefore:

$$\Psi \cong \rho\sigma\sqrt{\alpha} = \sqrt{\rho\lambda\left\{1-\Psi\left(1+\frac{1}{\sigma}\right)\right\}} \tag{5.51}$$

This is the normalized amperometric response for the ER + S case where the polymer layer thickness is smaller than the radius of the ultramicroelectrode.

S Case

When $\sigma \to 0$ the catalytic reaction between mediator and substrate takes place in a reaction layer very close to the electrode surface. The kinetics are then governed by the transport of substrate to said region. Also substrate diffusion within the polymer matrix will be much slower than substrate diffusion in the solution. The expression for the normalized amperometric response corresponding to the S case is as follows:

$$\Psi \cong \frac{1}{1+\frac{1}{\sigma}\left(1+\frac{1}{\zeta}\right)} \tag{5.52}$$

S + E Case

When $\rho \cong 1$ diffusion of electrons and substrate through the polymer layer occur at similar rates. Therefore $\frac{\lambda}{\rho\sigma^2} = \gamma_E$ and $\frac{\lambda}{\sigma^2} = \gamma_S$ are both large. The normalized amperometric current response may be determined using either u or v-master equations.

$$u\left\{\frac{u-u_{\zeta}}{\rho}+\frac{(1+\zeta)^2\Psi}{\rho\sigma}\left(\frac{1}{\xi}-\frac{1}{\zeta}\right)+1\right\}=0$$
$$v\left\{\rho\left[(v-v_{1+\zeta})+\frac{(1+\zeta)\Psi}{\rho\sigma}\left(1-\frac{1+\zeta}{\xi}\right)\right]+1-\Psi\right\}=0 \qquad (5.53)$$

and noting that $u_{\zeta}=0$, $u_{1+\zeta}=1-\Psi$, $v_{\zeta}=1$, $v_{1+\zeta}=0$ to obtain:

$$\Psi \cong \frac{1+\rho}{1+\sigma^{-1}\left\{1+\frac{1}{\zeta}\right\}} \qquad (5.54)$$

In this situation the catalytic reaction is so fast that rate control is assigned to the transport of substrate and electrons within the polymer matrix. When $\rho \rightarrow 0$ case S is achieved as shown in equation (52). If ζ is large then equation (52) reduces to:

$$\Psi \cong \frac{1}{1+\sigma^{-1}} \qquad (5.55)$$

In terms of catalytic current density equation (55) becomes:

$$\frac{1}{j_{cat}}=\frac{\pi a}{4nFD'_S s^{\infty}}+\frac{1}{nF\kappa D_S s^{\infty}} \qquad (5.56)$$

Thus spherical diffusion within the solution and transport processes within the polymer matrix are cleanly separated. The catalytic current density in this case is inversely proportional to the radius of the inlaid microdisc, and to the polymer film thickness. In addition the catalytic current density is independent of mediator concentration, and directly proportional to the substrate concentration.

Case E

When $\rho >> 1$ case E is achieved as shown in equation (34). Again if ζ is large then equation (54) reduces to:

$$\Psi \cong \frac{\rho}{1+\sigma^{-1}\left\{1+\frac{1}{\zeta}\right\}} \xrightarrow[\zeta \text{ large}]{} \frac{\rho}{1+\sigma^{-1}} \cong \rho\sigma \qquad (5.57)$$

In terms of catalytic current density, equation (57) becomes:

$$\frac{1}{j_{cat}} = \left\{ \frac{\pi\kappa D_S}{4nFD'_S D_E c_\Sigma} \right\} a + \frac{1}{nFD_E c_\Sigma} \qquad (5.58)$$

Once more a linear relationship is established between j_{cat}^{-1} and the microdisc radius a. However, a clear separation between spherical diffusion in solution and transport processes within the polymer layer is not obtained. In addition, the catalytic current density will vary in a first order fashion with mediator concentration, c_Σ, and will be independent of the substrate concentration, s^∞. Also the catalytic current density will vary inversely with polymer film thickness.

5.2.6 Summary of the pertinent rate limiting cases

Six limiting kinetic situations have been identified. The terminology devised by Andrieux and Saveant[9-12] has been adopted in order to define the various situations. These include rapid electron and substrate transport and rate determining bimolecular chemical reaction; R. Rapid electron percolation, slow substrate diffusion and chemical reaction; SR. Rapid substrate diffusion and slow electron percolation and chemical reaction; ER. Rapid chemical reaction with the rate being controlled by electron and substrate transport; S + E. Case 4 can be further delineated into two subcases. Firstly fast chemical reaction, slow substrate transport and more rapid electron percolation; S. Secondly, the converse of case 5, fast chemical reaction, slow electron percolation and more rapid substrate transport; E

Another important feature of these kinetic situations is that the specific reaction locations vary with each case. Case R, the entire polymer layer is utilized. Case SR, the reaction occurs in a thin layer near the film/solution interface. Case ER, the reaction occurs in a thin layer near the electrode/film interface. Case S + E occurs in a thin layer within the film. Case S takes place within a thin layer near the polymer/electrode interface. Case E takes place within a thin layer near the polymer/solution interface. The kinetic case diagram is presented in Figure 5.1.

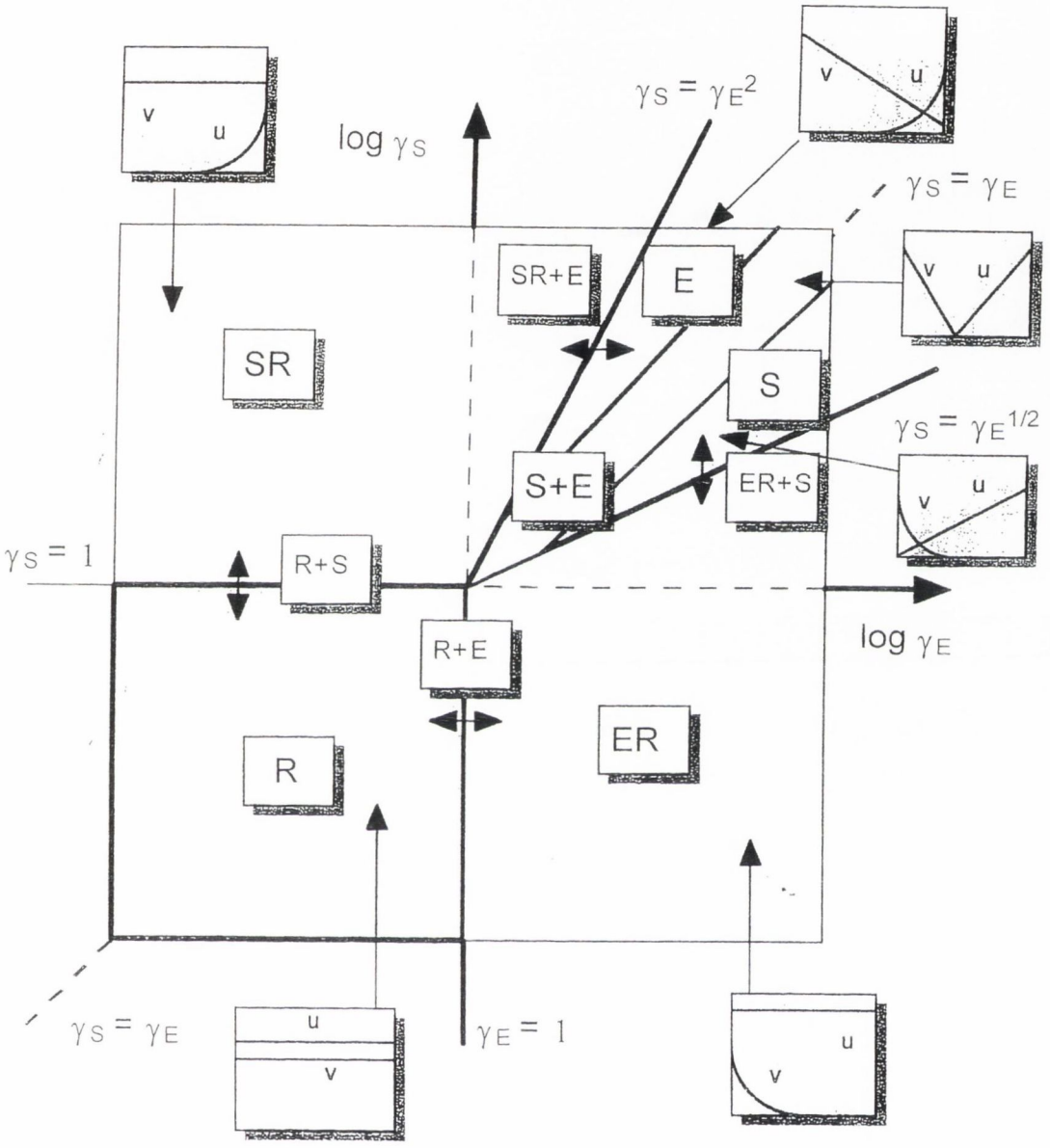


Figure 5.1 Kinetic Case Diagram

5.2.7 Experimental strategy for determination of specific kinetic case

The following conclusions may be determined from the model described:

A plot of j_{cat}^{-1} vs a will be linear for cases SR, R, S+E, S and E.

A plot of j_{cat}^{-1} vs a will be non-linear for case ER, instead a function $J = \frac{j_{cat}}{\sqrt{1 - \frac{j_{cat}}{j_D}}}$ vs a will result in a horizontal line, and a plot of J vs $\sqrt{s^{\infty}}$ will be linear. The slope of the latter plot will vary inversely with layer thickness.

Both the slope and intercept of the j_{cat}^{-1} vs a plots will be inversely proportional to the substrate concentrations for SR, R, S+E and S, whereas both will be independent of concentration for case E.

The slope of j_{cat}^{-1} vs a recorded at the polymer-modified electrode will be equal in magnitude to that obtained for an unmodified electrode for cases SR, R, and S.

Finally, the variation of the intercept of j_{cat}^{-1} vs a provides a method of distinguishing between cases SR, R, S, and E.

5.3 VOLTAMMETRIC BEHAVIOUR OF THE FERROCYANIDE/ FERRICYANIDE REDOX COUPLE AT PPy/DBS$^-$ MODIFIED MICROELECTRODES

5.3.1 Determination of the validity of the model for mediated electron transfer at polymer modified ultramicroelectrodes.

In accordance with the strategy developed by Lyons et al[14] in their recent model investigations were carried out in order to determine the validity of this theoretical model for the heterogenous catalysis at conducting polymer ultramicroelectrodes, as set out in section 5.2. The electrode kinetics of the model redox couple, potassium hexacyanoferrate (II) trihydrate/ hexacyanoferrate (III), (potassium ferrocyanide/ potassium ferricyanide or $K_4Fe(CN)_6.3H_2O$/ $K_3Fe(CN)_6$) were to be examined at a conducting polymer film. A series of polypyrrole/ dodecylbenzoylsulphonate, PPy/DBS, coated micro disc electrodes of various radii in the region of 2-50μm were used. The effect of varying the substrate concentration and the layer thickness on the reciprocal catalytic current density with respect to the electrode radii were examined.

We now consider the voltammetric response at disc electrodes of the redox couple ferrocyanide/ ferricyanide within a concentration range of 0.5 – 10mM. These responses were obtained for a microelectrode of radius of 25μm modified with a polymer layer of 0.03μm thickness. Figure 5.2 shows the voltammetric responses obtained for the electro-oxidation/ reduction of these various concentrations of ferrocyanide/ ferricyanide at a scan rate of $0.02Vs^{-1}$. Experimental work was carried out using 0.1M potassium chloride, KCl, as the electrolyte and a Ag/AgCl reference electrode. The potential was swept continuously between 0.1 and 0.6 V.

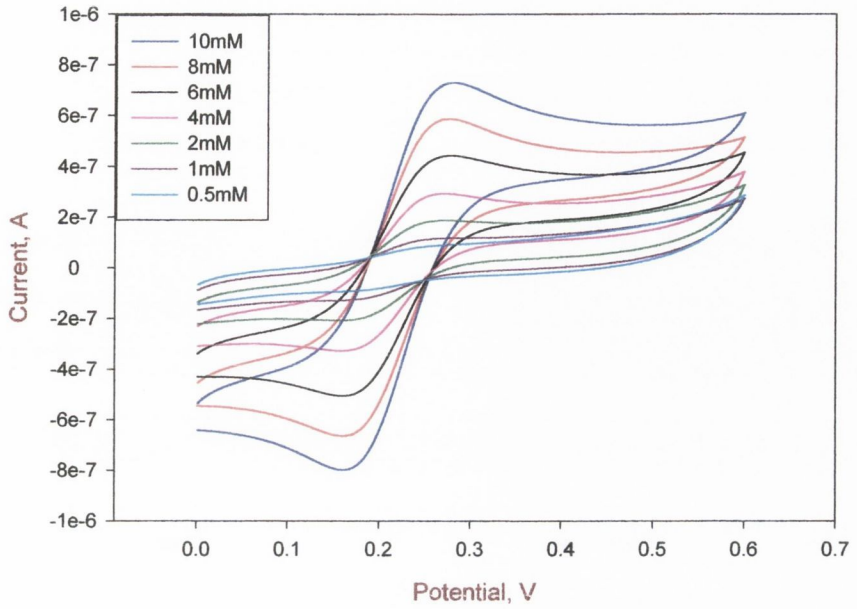


Figure 5.2 Graph of j_{cat}^{-1} vs a of PPy/DBS^- layer of 0.03μm thickness in aqueous solutions of various concentrations of $K_4Fe(CN)_6.3H_2O$ and $K_3Fe(CN)_6$.

j_{cat}^{-1} Vs a

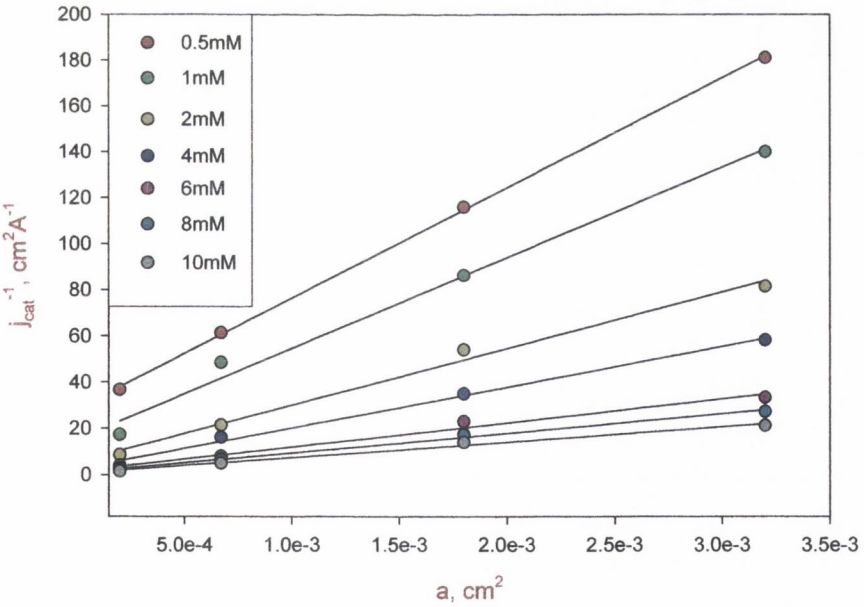


Figure 5.3: Graph of j_{cat}^{-1} vs a of PPy/DBS^- layer of 0.03μm thickness in aqueous solutions of various concentrations of $K_4Fe(CN)_6.3H_2O$.

Figure 5.3 shows the linear dependence established when the relationship between the reciprocal catalytic current density and the electrode area was examined for four different microelectrodes in the range of 2-50μm for electro-oxidation/ reduction of the redox couple $K_4Fe(CN)_6.3H_2O$/ $K_3Fe(CN)_6$ of concentration in the range of 0.5 – 10mM. According to the conclusions elucidated by the Lyons model for mediated electron transfer at conducting polymer ultramicroelectrodes this is indicative for the kinetic cases SR, R, S + E, S and E. In the ER case a non-linear relationship is expected, with a linear dependence between the function $J = \frac{j_{cat}}{\sqrt{1 - \frac{j_{cat}}{j_D}}}$ vs a being the governing criteria, for this reason the ER case is eliminated in this instance.

With the graph of j_{cat}^{-1} vs a in hand, and in accordance with the strategy previously described, investigations into the relationship between the slope and intercept of the graphs of the inverse catalytic current density vs the area of the ultramicroelectrode and the substrate concentration were carried out. Figure 5.4 illustrates the inversely proportional relationship between the slope of the j_{cat}^{-1} vs a plots and the substrate concentration. Similarly, the intercept of the aformentioned plots is inversely proportional to the concentration of substrate. This condition is required by the model for cases SR, R, S + E and S. However, case E is independent of substrate concentration, therefore a rate-limiting electron percolation mechanism may be dismissed as a possible mechanism of electrode kinetics from our study.

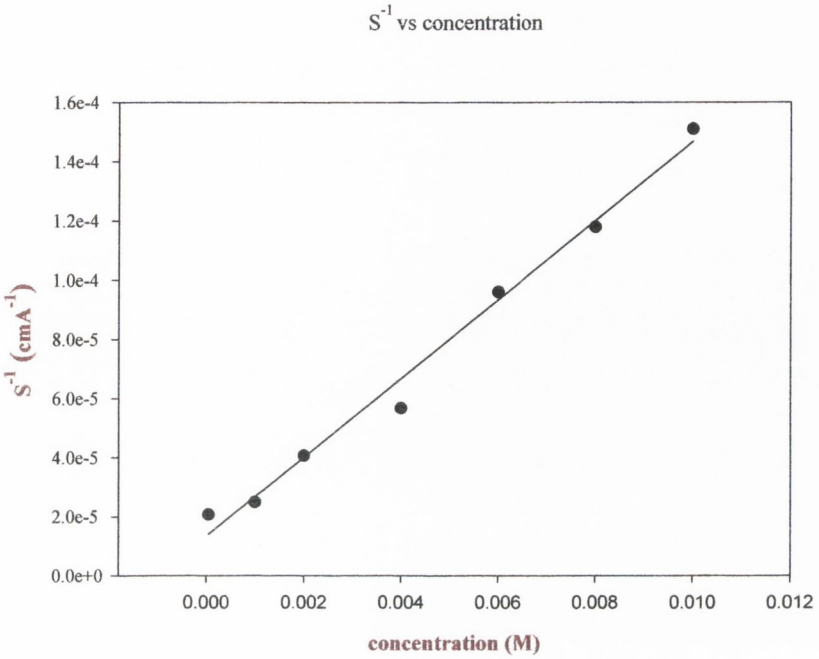


Figure 5.4 *Graph of S^{-1} of j_{cat}^{-1} vs a plotted versus concentration of $K_4Fe(CN)_6.3H_2O$.*

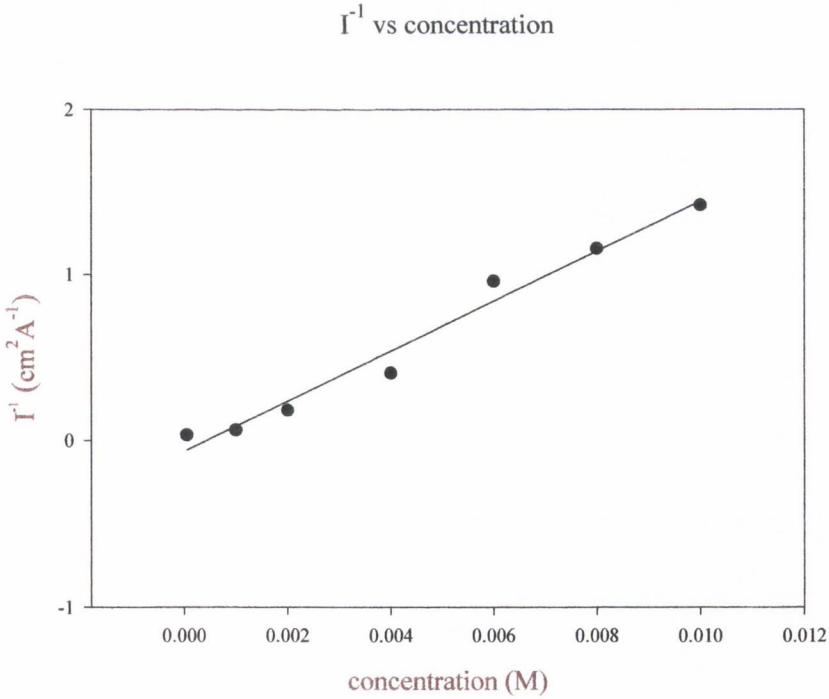


Figure 5.5 *Graph of I^{-1} of j_{cat}^{-1} vs a plotted versus concentration of $K_4Fe(CN)_6.3H_2O$.*

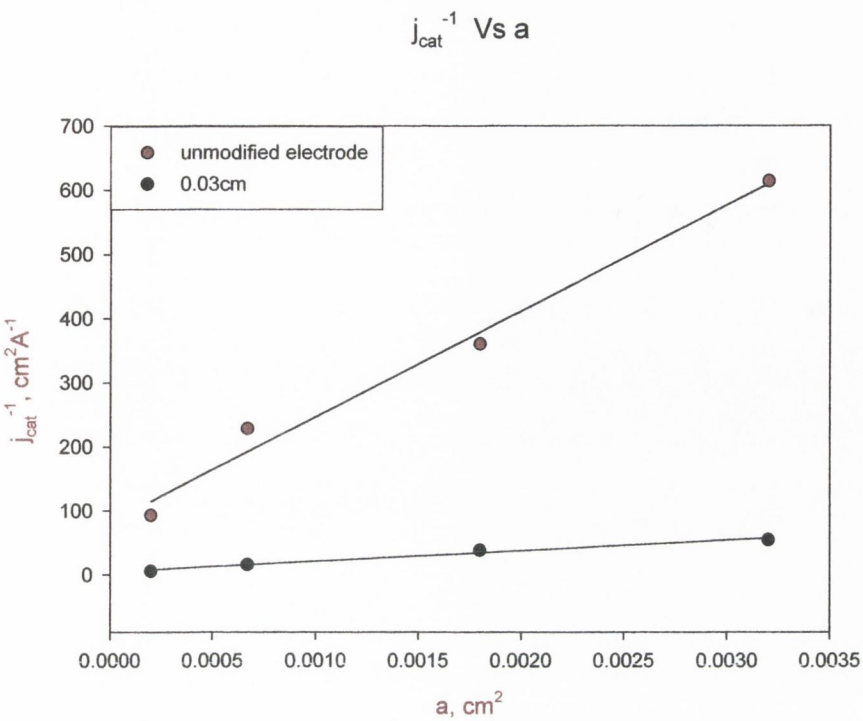


Figure 5.6: Graph of j_{cat}^{-1} vs a of 6mM $K_4Fe(CN)_6.3H_2O$ at bare platinum microelectrodes and at PPy/DBS^- layer of 0.03 thickness.

The experimental strategy outlined in section 5.2.6 dictates that when the former cases have been proven, investigations between the reciprocal catalytic current density and the electrode area for the ferrocyanide/ ferricyanide redox couple at both a polymer modified microelectrode and a bare electrode will further elucidate which kinetic case is applicable. This revealed a linear dependence in both cases.

Examinations into the relationship between the reciprocal catalytic current density and the electrode area for the ferrocyanide/ ferricyanide redox couple at both a polymer modified microelectrode and a bare electrode revealed a linear dependence. Both situations are shown in figure 5.6. The magnitude of the slopes were found to be not equal as illustrated in table 5.1. This suggests that the kinetic case applicable in this situation is S + E and not cases SR, R, or S.

Table 5.1: Table of the slopes of the j_{cat}^{-1} vs a for the ferrocyanide/ ferricyanide couple response at varying layer thickness of polymer film

A(cm^2)	Layer Thickness (μm)	Slope
1.8e-3	0	171275.15
1.8e-3	0.01	16459.86
1.8e-3	0.02	15319.18
1.8e-3	0.03	10372.98
1.8e-3	0.04	7027.01
1.8e-3	0.05	5965.90

The strategy employed for the kinetic analysis of the oxidation of $K_4Fe(CN)_6.3H_2O$ was also carried out for the reduction of $K_3Fe(CN)_6$.The kinetic analysis of the reduction of $K_3Fe(CN)_6$ at a PPy/DBS^- modified microelectrode reiterates the results found for the oxidation of $K_4Fe(CN)_6.3H_2O$, as shown in figures 5.7 – 5.10. This leads to the conclusion that this catalytic reduction also follows a S + E mechanism.

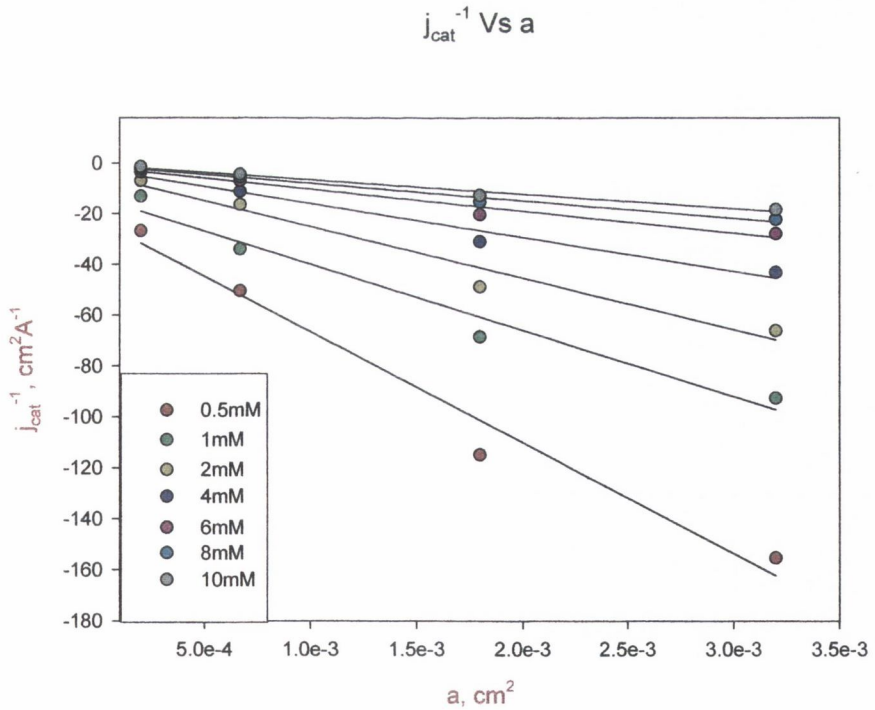


Figure 5.7: Graph of j_{cat}^{-1} vs a of PPy/DBS^- layer of 0.03μm thickness in aqueous solutions of various concentrations of $K_3Fe(CN)_6$.

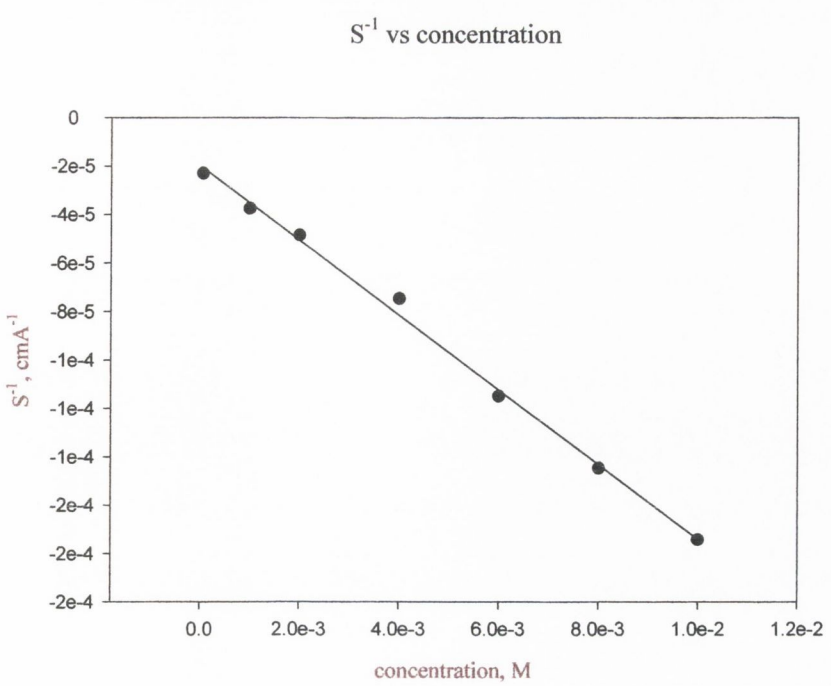


Figure 5.8: Graph of the inverse slope of (j_{cat}^{-1} vs a) Vs concentration of $_3Fe(CN)_6$.

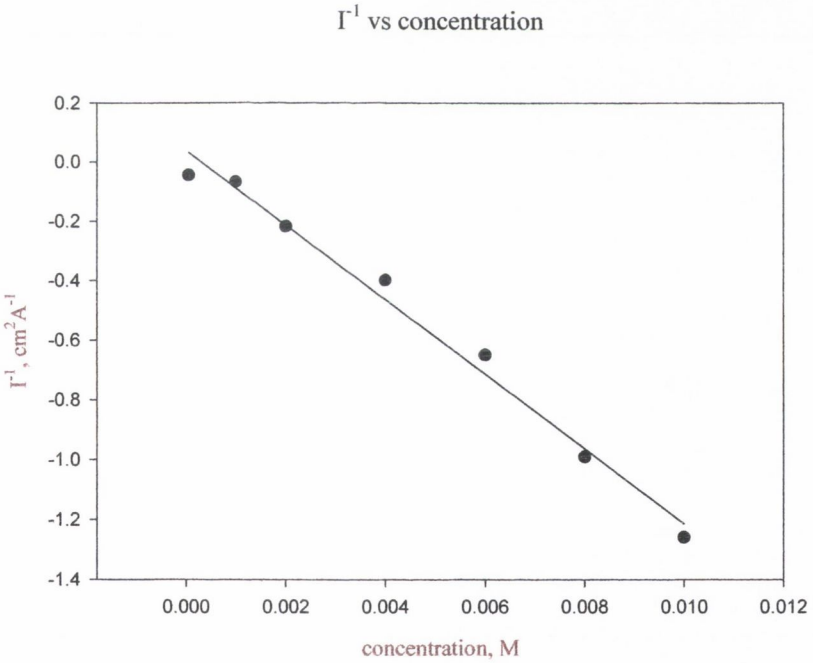


Figure 5.9: Graph of inverse intercept of (j_{cat}^{-1} vs a) Vs concentration of $K_3Fe(CN)_6$.

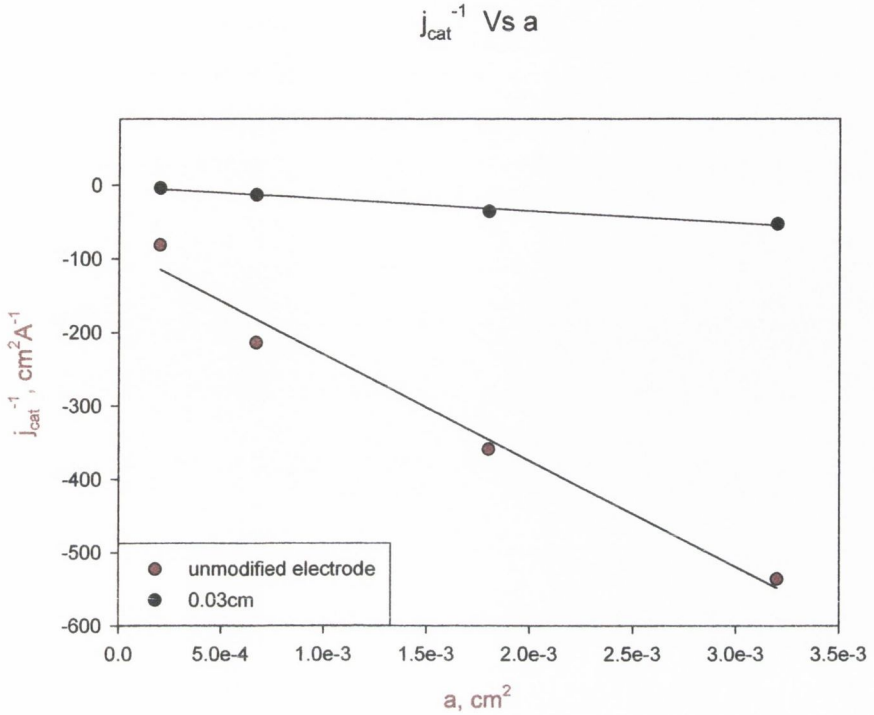


Figure 5.10: Graph of j_{cat}^{-1} vs a of 6mM $K_3Fe(CN)_6$ at bare platinum microelectrodes and at PPy/DBS^- layer of 0.03μm thickness.

5.4 Conclusions

The S + E mechanism of electrode kinetics was identified as the mechanism in operation for the oxidation of hexacyanoferrate (II) trihydrate or $K_4Fe(CN)_6.3H_2O$ and the reduction of hexacyanoferrate (III), $K_3Fe(CN)_6$). This case occurs when the catalytic reaction is so fast that the current is under the kinetic control of the rate of electron hopping occurring between the polymer strands and the rate of diffusion of the substrate into the pores of the polymer film. Hence, both the substrate and electron diffusional fluxes govern the kinetics of the process. In this instance, the catalytic current density is independent of the mediator concentration, in this case the polypyrrole/ DBS^- film.

It should also be noted that the validity of the Lyons model for the heterogeneous catalysis at conducting polymer ultramicroelectrodes has been confirmed experimentally. Hence, a model for the determination of possible rate determining kinetic situations may be used in practice.

5.5 REFERENCES

1. A.R. Hillman, *Electrochemical Science and Technology of Polymers*, ed R.G. Linford, Elsevier, Amsterdam, 103-291, (1987).
2. G.P. Evans, *Advances in Electrochemical Science and Engineering*, ed. H. Gerisher and C.W. Tobias, VCH, Weinheim, **vol.1**, 1-74, (1990).
3. M.E.G. Lyons, *Electroactive Polymer Electrohemistry: Part I, Fundamentals*, ed. M.E.G. Lyons, Plenum Press, New York, 1-374, (1994).
4. J.O. Howell, *Current Separations,* **8**, 2, (1987).
5. A.C. Michael, R.M. Wightman, *Laboratory Techniques in Electroanalytical Chemistry*, ed. P.T. Kissinger, W.R. Heineman, 2nd ed., Marcel Dekker, New York, 336-402, (1996).
6. J. Heinze, *Angew. Chem. Int. Ed. Engl.*, **32**, 1268, (1993).
7. M.E.G. Lyons, T. Bannon, S. Rebouillat, *Analyst*, **123**, 1961, (1998).
8. W.K. Albery, A.R. Hillman, *J. Electroanal. Chem.*, **170**, 27, (1984).
9. C.P. Andrieux, J.M. Dumas-Bouchiat, J.M. Saveant, *J. Electroanal. Chem.*, **87**, 39 (1978).
10. C.P. Andrieux, J.M. Dumas-Bouchiat, J.M. Saveant, *J. Electroanal. Chem.*, **131**, 1, (1982).
11. C.P. Andrieux, J.M. Dumas-Bouchiat, J.M. Saveant, *J. Electroanal. Chem.*, **169**, 9, (1984).
12. C.P. Andrieux, J.M. Saveant, *J. Electroanal. Chem.*, **171**, 65, (1984).
13. M.E.G. Lyons, T. Bannon, S. Rebouillat, *Analyst*, **125**, 345, (2000).
14. S. Rebouillat, M.E.G. Lyons, A. Flynn, *Analyst,* **124**, 1635, (1999).
15. S. Dong, G. Che, *J. Electroanal. Chem.*, **309**, 103, (1991).
16. G. Che, S. Dong, *Electrochim. Acta,* **38**, 581, (1992).

CHAPTER SIX

GENERAL CONCLUSIONS AND FUTURE PROSPECTS

6.1 GENERAL CONCLUSIONS

This thesis outlines the synthesis of novel redox substituted ferrocene-pyrrole monomers, as well as the study into their electrochemical behaviour as free monomers and as electropolymerized or copolymerised conducting electroactive polymers. Chapter two describes the methodology employed in the synthesis of the hybrid monomers. Fifteen novel compounds were synthesised, this included seven new monomer species: [4-(Pyrrol-1-yl)butyl]ferrocene-carboxamide, **18** n=4, [5-(Pyrrol-1-yl)pentyl]ferrocene-carboxamide, **18** n=5, [6-(Pyrrol-1-yl)hexyl]ferrocene-carboxamide, **18** n=6 [7-(Pyrrol-1-yl)heptyl]ferrocene-carboxamide, **18** n=7, 1,1'-Bis-[5-(Pyrrol-1-yl)pentyl]ferrocene-1,1'-dicarboxamide, **20** n = 5, 1,1'-Bis-[7-(Pyrrol-1-yl)heptyl]ferrocene-1,1'-dicarboxamide, **20** n=7, and complex **21** were all prepared according to facile, high yielding reaction schemes. In addition the novel pyrrole ligands that were synthesised, N- (4-Aminobutyl)pyrrole, **17** n=4, N- (5-Chloropentyl)pyrrole, **15** n=5, N- (5-Cyanopentyl)pyrrole, **16** n=5, N- (5-Aminopentyl)pyrrole, **17** n=5, N- (6-Chlorohexyl)pyrrole, **15** n=6, N- (6-Cyanohexyl)pyrrole, **16** n=6, N- (6-Aminohexyl)pyrrole, **17** n=6, N- (7-Aminoheptyl)pyrrole, **17** n=7, may be investigated in future as polymerisable species and may provide us with insight into the effect of the substitution on the polypyrrole conducting backbone. The methodology developed for the synthesis of all compounds is readily reproducible, high yielding and may be employed for the synthesis of a covalently linked ferrocene-pyrrole-enzyme moiety in the future.

Chapter Four outlines the electrochemical investigations into the reversibility of the ferrocene-pyrrole compounds. These included examination of the formal potential of both the monomer species and the ferrocene/ ferrocenium redox couple with the polymer film. Furthermore, the diffusion coefficient for all monomers is reported and the electrochemical reversibility of each system is confirmed. Results indicate that a one-electron reversible reaction occurs in each of the new hybrid monomer species. The attempted electropolymerization of the mono-substituted ferrocene-pyrrole species is outlined and a mechanism proposed for the passivation of the species at the electrode, whereby the inability of the modified pyrrole group to form an initiator species is described. The copolymerization of the mono-substituted ferrocene-pyrrole monomer

with pyrrole and the electropolymerization of the disubstituted ferrocene-species are outlined. It is postulated that the latter process involves the formation of an intramolecular bond between the two pyrrole units upon polymerization resulting in an intramolecular bridge being formed between the two cyclopentaideinyl rings. In addition, the surface coverage of the hybrid species with the copolymer or polymer films for the mono-substituted ferrocene-pyrrole and disubstituted ferrocene-pyrrole films respectively is reported.

Chapter five describes the examination of a model kinetic system. The validity of the model being investigated is confirmed experimentally. This involved the examination of the heterogeneous electrocatalysis processes at conducting polymer ultramicroelectrodes. The modified electrode studied was a conducting polypyrrole film, doped with the counter ion dodecylbenzene sulphonate. The mechanism of electrode kinetics for the oxidation of hexacyanoferrate (II) trihydrate and the reduction of hexacyanoferrate (III) was analysed. Results indicate that the kinetic process occurring was governed by an S+E mechanism.

6.2 FUTURE RECOMMENDATIONS

While the pyrrole tethered ferrocenes synthesis and electrochemically investigated during the course of this work display distinct possibilities for applications as biosensors, further research is required prior to their realistic achievement as such. There are a number of applications for conducting electroactive polymers of this type due to the ability of the (co)polymers to retain the ferrocene redox couple even after frequent cycling. Conducting polymers may be doped with ferrocene groups however, these are typically lost through diffusion during the cycling and the compounds described in this work offer the advantage of maintaining the ferrocene activity post-polymerization and cycling. The immobilization of glucose oxidase in these films and the quantification of the response of the resultant chemically modified electrode to glucose is warranted. In addition, the covalent attachment of glucose oxidase to the second cyclopentadienyl ring of the ferrocene-pyrrole polymers is achievable through the acidification of the ester group on compound **21**, and the subsequent electropolymerization of the species. Once the polymer is in hand the enzyme may be

covalently linked to the acid residue through the coupling technique employed in this work. Furthermore, these novel polymers may be used for the production of a range of different biosensors. Recent studies have investigated redox-active conducting polypyrrole films incorporating ferrocenes for the immoblization of the enzyme cytochrome C.[1] The ability of these films to quantitatively determine the amount of cyctochrome C present in solution is encouraging and the methodology employed may be readily used for the investigation of the polymers described within this work for similar purposes. In addition, the immobilisation of tyrosinase[2] onto an electrochemically polymerised copolymer poly(N-3-Aminopropyl pyrrole-co-pyrrole) film for the purpose of sensing phenolic compounds in solution has been achieved by Rajesh *et al.* The range of novel N-aminoalkyl pyrroles should be investigated in a similar manner in order to elucidate if the length of the alkyl chain affects the electron transfer between the enzyme and the polypyrrole backbone. Furthermore, the covalent immobilisation of tyrosinase onto the second cyclopentadienyl ring is also achievable through the acidification of monomer **21** and the subsequent coupling of the acid to the amino residues on the enzyme. This method would offer the advantade of having a covalently attached redox species capable of regenerating the enzyme once oxidised. Finally, the use of poly(2-cyanoethylpyrrole) as a matrix for the immobilization of Ig immunoglobulins through has also been achieved.[3] The range of novel N-cyanoalkylpyrroles should be examined for similar purposes. It is envisaged that once a suitable methodology for the incorporation of glucose oxidase within the polymer film is developed it will be applied to a range of different enzyme and immunoglobulin species, in order to produce an actual reagentless biosensing modified electrode.

6.3 REFERENCES

1. Chen, C.O. Too, G.G. Wallace, G. F. Swiegers, B. W. Skelton, A.H. White, , *Electrochim. Acta*, **47**, 4227 (2002).
2. Rajesh, Takashima, Kaneto, *Sens. And Actuators B.*, **in press** 2004.
3. O.Ouerghi, A.Senillou, N. Jaffrezic-Renault, C. Martelet, H. Ben Ouada, S. Cosnier, *J. Electroanal. Chem.*, **501**, 62, (2001).